A Novel Approach to Power Cable Performance Assessment using Perturbed Thermal Field Analysis

By

Mamdooh S. Al-Saud

A Thesis
Submitted to the School of Graduate Studies
in Partial Fulfillment of the Requirements
for the Degree
Doctor of Philosophy of Electrical Engineering

McMaster University
© Copyright by Mamdooh Al-Saud, July 2007

A Novel Approach to Power Cable Performance Assessment

Ph.D of Electrical Engineering (Power System)

McMaster University Hamilton, Ontario

TITLE: A Novel Approach to Power Cable Performance Assessment using Perturbed Thermal Field Analysis

AUTHOR: Mamdooh S. Al-Saud (B.Sc., M.Sc.)

SUPERVISOR: Professor R.D. Findlay (Ph.D., P.Eng., FIEEE, FEIC)

CO-SUPERVISOR: Professor M. A. El-Kady (B.Sc., M.Sc., Ph.D., P.Eng.)

NUMBER OF PAGES: xviii, 235

Abstract

This thesis reports on a novel approach to cable thermal field and ampacity computations using a newly proposed concept of perturbed finite-element analysis, which involves the use of derived sensitivity coefficients associated with various cable parameters of interest. It uses the sensitivity coefficients to achieve optimal cable performance. The proposed model provides a quick methodology, based on the finite element model, to assess the cable thermal performance subject to variations in the cable thermal circuit parameters. Furthermore, an optimization model for an underground power cable thermal circuit, based on generated gradients was developed, where subsequent utilization of the derived sensitivities as gradients of objective functions in a general framework of power cable performance optimization is presented. This comprehensive model uses the more accurate perturbed finite element method, which enables calculation of the objective function value and its gradients, without sacrificing the model accuracy. The algorithm developed was applied to various benchmark cable systems with their actual configurations, for different practical cable performance optimization objectives of interest to power utilities operators. The thermal field of an underground power cable sample directly buried in the soil was observed in the laboratory using a developed full size experimental setup. The investigation involves all parts of the thermal circuit parameters including cables composition, surrounding soil and boundaries phenomena. This experimental set was used to validate the developed simulation model by comparing the simulation results with the real laboratory measurements. Such experimental verification confirmed the accuracy of the newly introduced finite element sensitivity methodology.

To My Family

Acknowledgements

I would like to express my sincere appreciation of valuable help from my supervisor Dr. Raymond D. Findlay and my co-supervisor Dr. Mohamed A. El-kady. I would like to thank them for their patient guidance, continuous support, advice, thoughtful reviews and comments that have helped me in the preparation of this thesis. Their expert recommendation is reflected in the content organization of the presented work.

Table of Contents

List of Tables

List of Figures

List of symbols

Symbol	Description
ΔQ_{st}	Change of energy stored within the cable
ε	Emissivity radiation coefficient
ρ	Thermal resistivity
σ	Stefan-Boltzmann constant
φ	An unknown quantity
$\widetilde{\varphi}$	Trial function
Ω^e	Area of the element e
$\mathbf{A}$	Heat conductivity matrix
A	Surface area
$\boldsymbol{b}$	Heat load vector
c	Volumetric thermal capacity of the material
c_j	Constant coefficients
$\mathbf{D}^e$	Displacement matrix
E	Total number of sub-elements
f	An exciting function or forcing function
$\mathbf{g}$	Generation vector
h	Heat convection loss coefficient
I	Functional
i	Current
k	Thermal conductivity
$\mathbf{K}$	Conduction matrix
l	Numbers of inequality constraints
ℓ	Differential operator
M	Total number of nodes
m	Total number of variables (parameters)
N	An interpolation function
n_g	Number of parameters groups
n_z	Number of sensitivity coefficient zones

$\mathbf{p}$	Vector of thermal circuit parameters
$\mathbf{p_j}$	Vector of parameter group
Q	Heat generating rate
q	Heat flux
Q_{ent}	Rate of energy entering the cable
Q_{int}	Heat generated internally in the cable by joule or dielectric losses
Q_{out}	Energy dissipated by conduction, convection and radiation
r	Residual
R_t	Weight residual integral
T	Temperature
t	Time
T_a	Ambient temperature
$\mathbf{T_i}$	Vector of zonal temperatures
v	Numbers of equality constraints
v_j	Expansion function
w_t	Weighting function

List of Acronyms

Symbol	Description
AEIC	Association of Edison Illuminating Companies
AIEE	American Institute of Electrical Engineers
CEA	Canadian Electrical Association
CFE	Conventional Finite Element
CIGRE	Conseil International des Grands Réseaux Electriques
DTS	Distributed Temperature Sensor
EEI	Edison Electric Institute
EHV	Extra High Voltage
ERA	Electrical Research Association
FDM	Finite Difference Method
FEM	Finite Element Method
FTB	Fluidized Thermal Backfill
GRG	Generalized Reduced Gradient
GUI	Graphical User Interface
ICC	Insulated Conductor Committee
IEC	International Electrotechnical Commission
IEEE	Institute of Electrical and Electronics Engineers
IPCEA	Insulated Power Cable Engineering Associated
NEC	National Electrical Code
NELA	National Electrical Light Associated
NLP	Nonlinear Programming
OTDR	Optical Time Domain Reflectometer
PFE	Perturbed Finite Element
PVC	Polymers of Vinyl Chloride
QP	Quadratic Programming
SQP	Sequential Quadratic Programming
SWA,CU	Steel Wired Armoured, Cupper
XLPE	Crosslinked Polyethylene

CHAPTER 1

INTRODUCTION

1.1 OVERVIEW

The capital investment on underground transmission systems is often very high as compared with overhead transmission lines of similar capacity. The greater cost of underground installations reflects the high cost of equipment, labor and time necessary to manufacture the cable, to excavate and backfill the trench and install the cable. Because of the extra expense, most underground installations are constructed in congested urban areas, as leads from generating plants and as leads into and from substations. The large capital cost associated with cable installations also makes it necessary that particular care be applied in selecting the proper cable type and size to serve the load for the projected life of the installation.

Because of high capital expenditure, underground power cable systems are frequently operated at the maximum continuous current rating [1-2]. Therefore, one of the most important needs in power cable engineering and operation is to have information about the maximum current-carrying capacity that a cable can tolerate throughout its life without risking deterioration or damage. Ampacity values are required for every new cable installation as well as for cable systems in operation. With some underground transmission cable circuits approaching the end of their design life, the development of a systematic method for determining the feasibility of extending cable life and increasing current ratings is of paramount importance[3]. Determination of the thermal behaviour of underground power cable plays an important role in the design and manufacture processes of the cables, as the heat generated inside the cable may lead to cable breakdown.

Cable heating presents one of the major problems associated with underground lines. While it is relatively easy to dissipate the heat generated by the current through the conductor in overhead lines, the heat generated by losses in underground systems must pass through the electrical insulation system to the surrounding earth, where both the insulation and earth represent an obstacle to heat dissipation. The use of various materials in the composition of the cables and the backfill in contact with them, under certain conditions of use, can give rise to a temperature increase above levels that the cable insulation can withstand without deterioration. As a consequence, under normal use, these installations are used below their load capabilities. However, given the high cost of such installations, it would be useful to make better use of them so that the maximum possible current can circulate without exceeding the temperature limit for insulation deterioration. Consequently, it is necessary to know the temperature distribution around buried cables that can arise, during use, as accurately as possible. As insulation of the cable and soil are not good thermal conductors, the heat generated inside the cable may not be transferred away efficiently resulting in thermal breakdown of the cable, eventually. Therefore, transfer of the heat generated inside the cable to the surrounding atmosphere is a priority [4].

Because of tight economical constraints and limitations on space availability, public utilities and manufactures all around the world are striving to attain higher cable ampacity through improved designs. At the same time, it is desirable to achieve better accuracy of cable parameter values so that the simulated results match as closely as possible to the real-life situations. One effective way of offsetting the effect of over-conservativeness in the cable designs and, therefore achieving better cable utilization, is to improve the accuracy of the ampacity calculations via better modeling and solution methodologies. The traditional method of computing temperature distribution and cable ampacity is based on approximate formulas derived first by Neher and McGrath [5] in 1957 and adopted later by the International Electrotechnical Commission (IEC). The ampacity of a cable circuit is affected by many factors, such as the cable insulation and structure, thermal conductivity of the surrounding soil, ambient temperature and sheath bonding. Since the ambient temperature and the thermal properties of soil change with time depending on the weather, the ampacity of a cable circuit could change significantly from time to time. Numerical methods can conveniently deal with varying properties of the materials involved, the complexity of the system and the variability of the parameter with time. Different models have been presented that use finite element and finite difference methods. These methods represent the buried cable system by means of a discrete set of points and solve the heat diffusion equation using one of the discrete techniques mentioned [6].

The finite element method is well established as a technique for solving engineering problems, and this may be applied to model heat conduction in non-homogeneous media. The proposed research work will investigate a new approach to cable thermal field and ampacity computations using a proposed concept of perturbed finite element analysis, which involves the use of derived sensitivity coefficients associated with various cable parameters of interest, and using such sensitivity coefficients to achieve optimal cable performance. The proposed method for a perturbed finite element analysis of the general performance of buried power cable, and parameter evaluation procedures for the purpose of advanced thermal analysis and ampacity calculations, involves solving the thermal field of a cable system. The method can handle complex configurations, boundaries and heat sources. It can also be adapted to optimize cable performance and sensitivity analysis under varying loading and environmental conditions. The numerical technique used incorporates a general algorithm that simulates the real cable installation configuration.

1.2 HISTORICAL PERSPECTIVE

Practical calculation of the temperature distribution of underground power cables in the steady-state was presented in 1893 by Dr A.E. Kennelly, whose name is still attached to the hypothesis of the isothermal surface of the soil.

The first rating tables were issued in Britain in the early 1920s. A history of the calculation of the current rating in the United Kingdom can be traced through the reports of one company that is still active in the field of cable rating. This company is ERA Technology Ltd., formerly the Electrical Research Association.

The first report on the subject, published in 1923, set out a standard method of calculating current rating. It provided a tabulation of ratings. Work continued over the years, with calculation methods improved in many areas. Many papers were published by a number of workers, most notable is the work by Arnold on joule losses. A major U.K document was prepared by Whitehead and Hutchings and published in 1939. This report was limited to methods of calculation, with tabulated ratings being published in a separate document. In the following two decades, many reports were published which improved one aspect or another in the calculation of current ratings. These improvements were brought together by Goldenberg in a 1958 report. This was the last U.K document to give a comprehensive guide to current rating calculations before the publication of IEC 287 [7].

In the United States, The National Electrical Light Associated (NELA) adopted in 1931 a set of standard constants and reference conditions for the calculation of load capacities of cables. This in turn, resulted in the publication of the first set of current-carrying capacity tables for paper-insulated, lead-covered, cable in underground ducts or in air [8].

In 1933, the tables were expanded and republished by the Edison Electric Institute (EEI) [9]. These tables lasted for ten years. In 1943, after considerable improvements in cable insulation materials and growth in underground systems, the Insulated Power Cable Engineering Associated (IPCEA) published three documents for impregnated paper, rubber, and varnished cambric insulated cables respectively [10].

The National Electrical Code (NEC) in the United State has published ampacity tables for building wires since 1897. These ampacity tables have dealt primarily with low-voltage and below. The technical basis for the development of the tables issued by NEC was developed by a committee chaired by S. J. Rosch. The committee dealt primarily with low-voltage, code-grade, and rubber-insulation cables. The committee's final report was issued in June 1938.

In the 1930s, the field of heat transfer was in its infancy, and Rosch did not appear to be aware of some of the heat transfer studies conducted mostly in the United Kingdom. Lacking any heat transfer foundations and unaware of the other similar work, he and his committee resorted to a series of experimental tests to determine the relation between the current in a conductor and the conductor temperature. The committee's tests were limited to a relatively small number of all-copper conductors, insulated with code grade rubber and suspended horizontally in air. No buried cables were considered, and shield losses were not included. In 1938 he published a paper that detailed a series of experimental tests on cables in horizontal conduits. In 1951, W.A Del Mar of the Phelps Dodge Wire and Cable Company coined the word "ampacity" to replace "current-carrying capacity".

Ampacity work progressed steadily from the time of Rosch's final report until 1957 when Neher and McGrath published their paper, which successfully summarized most of the important ampacity work by extending an earlier comprehensive work of Simmons [11, 12]. Their paper actually introduced no new advancements in the area of ampacity, it simply and effectively put all of the ampacity principles into a single, all-encompassing paper. Due to Neher and McGrath's successful paper, most engineers in North America refer to that calculation procedure to determine ampacity values. Actually, the technique that they described is based on a simple model of energy balance in the conductor, and on an analogy between the electrical current and the flow heat. Both of these principles were well known long before 1957. Nonetheless, the Neher and McGrath paper is credited as the paper which forms the basis for modern ampacity standards.

The Neher-McGrath model, as opposed to the Rosch model, is based on a technically correct set of equations. It effectively accounts for a much greater diversity of cable designs and insulation geometries. It considers heat generated in the shield material resulting from induced shield current and it also accounts for dielectric heating which can become significant in high voltage cables. It uses more accurate and more technically correct heat transfer coefficients than the Rosch model. It described the equations that should be used for underground installation, as well as for a cable oriented vertically or horizontally in air. It describes a procedure that can be used to derate cables when the heat generated by one cable influences other cables. In other words, it permits ampacity calculations for multiple cable installation where mutual heating between cables can be significant. It also includes a technique for calculating the thermal resistance of a duct bank that may contain multiple cables.

Although the Neher-McGrath model is technically correct, it does have some weakness, mainly in dealing with a cable in air. Since the method is based on the analogy between the flow of heat and current, one must know the thermal resistances on the circuit before the ampacity value can be calculated. Unfortunately, heat transfer coefficients are temperature dependent, and therefore the temperature at local points in the thermal circuit must be known before the problem can be solved. Neher and McGrath use assumed temperature values to solve this dilemma. In some instances, these assigned temperatures can lead to unacceptable errors. Also, the Neher-McGrath model uses experimental constants to aid in the computation of the thermal resistance of the fluid layers in the thermal circuit. And finally, the model accounts for only a single value for the thermal resistance of the soil layer for buried installation. Changes in the soil resistivity can occur when the soil adjacent to the cable earth interface begins to dry. This change is known to be very influential in the cable ampacity because the soil thermal resistance is the largest single resistance in the composite circuit. Such change in the resistance of the soil can lead to thermal runaway of the cable temperature resulting from a phenomenon referred to as the thermal instability of the soil.

After several dissenting views were resolved at a symposium devoted to the subject, the electric power industry adopted the Neher-McGrath methods for the calculation of the power cable ampacity. In 1962, the American Institute of Electrical Engineers (AIEE) and IPCEA jointly published new ampacity tables based on the Neher-McGrath paper. These Tables were published in two volumes, one for copper and one for aluminum cables (AIEE S-135-1 and S-135-2), providing ratings for impregnated paper, varnished cloth, rubber, thermoplastic polyethylene and asbestos-insulated cables. Subsequently, these tables became known in industry circles as the black book. In 1967, the IPCEA published a revised version of ampacities for impregnated paper insulated cable (IPCEA#48-426) because the Association of Edison Illuminating Companies (AEIC) revised their specification upward for conductor operating temperatures.

After the publication of Goldenberg's [13, 14] report in the United Kingdom and the Neher-McGrath paper in the United States, it was felt that sufficient methodology had been developed to warrant the issuing of an international standard. Such a standard was prepared by the International Electrotechnical Commission (IEC287, 1969, 1982) [7]. The immediate predecessor of IEC 287 was a CIGRE report in 1964. The countries that participated in preparing the CIGRE document were the United Kingdom, the Netherlands, France, Germany, Italy, and the United States. The same countries, with the addition of Canada and Belgium, are active in the continued development of IEC 287. The CIGRE report was adopted by IEC in 1969 and after number of amendments, a second edition was published in 1982. For the third edition, IEC 287 is being divided into parts, each of which covers a different aspect of the calculation of cable ratings.

Meanwhile, in the United States after the publications of the IPCEA tables in 1967, the work on any new ampacity tables remained dormant for approximately ten years. In 1972, due to proliferation of shielded single conductor cables and the absence of ratings for cable with circulating currents in the shields, a working group was formed within the Insulated Conductor Committee (ICC).

During the late 1970s, the Insulated Conductor Committee requested and received a project authorization from Institute of Electrical and Electronics Engineers (IEEE) to revise the "black book". This project was necessitated by continued use of outdated parameters and cable constants, and by the major advance in heat transfer technology.

To accomplish this task, another working group was organized in ICC, and in 1981 it published a set of new parameters for new ampacities tables. The tables published in 1994 [15], addressed new issues such as cable-earth interface temperature and limiting heat flux, cable in vented and non-vented risers, and cable in open cover trays. Over 300 amapcity tables for extruded dielectric power cables rated though 138 kV and laminar dielectric power cables rated though 500 kV are provided.

The work on refining cable ampacity computation is being continued. It proceeds in two directions, experimental studies are being performed to fine-tune some of the computational formulas and adjust the values of constants, and numerical methods are being applied to overcome limitations inherent in the analytical approach.

1.3 PROBLEM DIFFICULTY AND TECHNICAL CHALLENGES

Unrealistic simplifications used for calculating the heat dissipation from underground cable limited the validity of the calculation to specific cable geometries. Consequently, the first challenge in this work was the development of a general reliable numerical procedure for the analysis of thermal field characteristic of underground cable systems of any system geometry, backfill and soil environment.

However, because of the added computation efforts, the task of optimizing cable performance under varying soil and environmental conditions would be extremely difficult and challenging. Unfortunately, the effect of the thermal circuit parameters variations was a main concern as it has a big influence on the cable thermal behaviour and it may result in a significant difference in the cable ampacity with the resultant cost of installation. In this regard, special attention was drawn to the development of a sensitivity methodology of thermal field with respect to the thermal parameter changes. The difficulties have arisen since the model developed here was based on the exact finite element implementation and did not involve any simplification for the thermal heat modeling.

Efficient cable design requires the selection of the best possible values for the thermal circuit parameters, taking into account the cost of criteria of different alternatives as well as other constraints. In this regard the real challenge was to develop an algorithm that searches for the solution based on the varying multiparameters at the same time using a reliable optimization strategy to handle all design variables simultaneously. Consequently, our model is designed to take these considerations into account, which, on the other hand, has added more difficulties as follows:

First, the ampacity evaluation was not based on approximated modeling; the developed finite element model was embedded to find the exact thermal field solution.

Second, the optimization model was developed based on the parameter gradient to ensure a reliable algorithm. The developed sensitivity model based on the finite element algorithm was embedded to supply accurate needed information for the search direction.

Third, one of the main goals was to preserve the generality of the thermal model to handle any configuration and incorporate this with flexibility to handle any general optimization objective and constraints. Designing such a global model was challenging.

1.4 THESIS OBJECTIVES

The main objectives of the present research work are as follows:

1. To study the general analytical and computational aspects of power cable performance and parameter evaluation procedures for the purpose of advanced thermal analysis and ampacity calculations.

2. To investigate and study available techniques and algorithms for cable thermal analysis using both traditional and field-based methods.

3. To developed a new methodology for optimized cable performance and sensitivity analysis under varying loading and environmental conditions using the concept of perturbed thermal field analysis using a modified finite element algorithms.

4. To demonstrate the applicability and usefulness of the developed methodology via applications to several test and actual cable systems under different loading, soil and atmospheric conditions.

1.5 KEY CONTRIBUTIONS

A novel methodology and associated algorithms were developed to study thermal characteristics of electrical cable systems, suited for implementation in the computer aided cable design program for a practical system implementation. The method was implemented for several actual cable systems including data taken from Saudi Electricity Company. Throughout the work of this thesis a number of publications have been produced and the basic achievements have been presented in [16-27].

Unlike the conventional methods of power cable thermal analysis based on the Neher/McGrath method and the subsequent more detailed methods that have appeared in the literature, including those using the traditional finite element technique, the work of this thesis takes the concept of finite elements one step further by deriving sensitivity coefficients directly from within the finite element numerical solution structure. Therefore, these sensitivities are both very fast in computations and general in nature as they encompass all known parameters of cable, soil, trench and atmospheric conditions representing complex boundaries and non-uniform media around the cable.

The successful derivation of the finite element sensitivities opened the door for the subsequent utilization of such sensitivities as gradients of an objective function in a general framework of power cable performance optimization. Therefore, based on the work of this thesis, it is now possible to perform non-linear optimization of cable performance indices using the more accurate finite element method, without sacrificing the modeling accuracy in order to suit other existing traditional methods.

Some computational and software programming aspects of the present work are also considered. For example, the derivation and use of the so-called zonal sensitivities allows lumping specific groups of media patches around the cable, that are of interest to the power cable engineer, for the derivation of the associated sensitivity information. Also, the linear nature of the sensitivity expressions allows very fast computations to predict the resulting impact on cable performance indices (including its ampacity) due to combined, relatively small, variations of several cable design and operating parameters without repeating the finite element analysis.

1.6 THESIS ORGANIZATION

This thesis contains eight chapters. Following the current introductory chapter, Chapter 2 reviews comprehensive literature of various approaches on the subject of power cable thermal analysis and ampacity calculations as well as estimation methodologies of power cable thermal parameters as adopted and implemented by power companies. The literature survey covers the issues relating to cable measurement techniques and the associated laboratory setup and implementation aspects of live cable systems. Subsequently, Chapter 3 includes a description of the technical background on finite element method formulation, various available techniques for solving finite element problems and specific feature related to power cable thermal analysis applications. The novel concept of perturbed thermal field analysis for power cable sensitivity analysis is described in Chapter 4, which also outlines the structure of the optimized design and performance of power cable thermal circuits based on finite element generated gradient. In Chapter 5, a description of the novel methodologies and computational algorithms developed for cable thermal field evaluation, including the simulation software, are presented. Chapter 6 includes the laboratory experimental setup used in the research work as well as the obtained laboratory results. Chapter 7 includes applications to practical cable samples, bench-mark and demonstrative case scenarios. Finally, chapter 8 summarizes the main finding of the work and outlines the main conclusions.

CHAPTER 2

SURVEY OF RELEVANT LITERATURE

2.1 INTRODUCTION

Considerable research efforts have been expended during the past two decades in developing techniques and criteria for thermal analysis and ampacity evaluation of practical power cable systems. Research and development efforts pertaining to cable thermal analysis have been documented in numerous publications. This chapter presents a literature survey and describes recent advances in thermal field calculation of underground cable. For convenience, the section is divided into five main categories: literature dealing with the aspects of power cable thermal analysis based on finite element, finite difference, other numerical algorithms based on thermal field calculations; on methods based on analytical algorithms; and laboratory measurements techniques on live cable systems. Table 2-1 summarizes and classifies the research publications.

TABLE 2-1: CLASSIFICATION OF REFERENCES

Topic	Reference
Methods and algorithms based on finite element thermal field calculations	[1-3], [6] & [28-52]
Methods and algorithms based on finite difference thermal field calculations	[4] & [53-57]
Methods and algorithms based on other numerical thermal field calculations	[58-61]
Methods and algorithms based on analytical methods and ladder network	[62-69]
Measurement, laboratory setup and live cable implementation	[70-80]

2.2 METHODS AND ALGORITHMS BASED ON FINITE ELEMENT THERMAL FIELD CALCULATIONS

The work on refining cable ampacity computation has been continued. Numerical methods were applied to overcome limitations inherent in the analytical approach. The implementation of the finite element method in the solution of the thermal transient problem has been presented in reference [28]. The analysis presented by the author included an evaluation of thermal transients in a 275 kV oil/paper insulated buried power cable system when the load current has a prescribed variation with time. The heat losses due to conductor current as well as dielectric losses were represented as heat sources. The shield losses were introduced as heat sources at the cable boundary, while the shield thickness and its materials thermal properties were ignored. In his implementation, the author has set the ground-air surface as convective surface and all other surfaces were considered non-conducting.

Reference [29] presented a finite element computer program HEAT to study both transient and steady-state temperature distributions both within the cable trench backfill and surrounding soil. Allowable heat input rate to limit cable sheath temperature to 60 ^{0}C and 90 ^{0}C were determined and the influences of varying weather and soil property conditions were studied. Furthermore, all other boundary conditions were treated as a constant temperature boundary (isothermal). With the implemented boundary conditions, the authors have varied the size of the discretized area so that the computed temperature distribution would not be significantly different from that obtained for a free field. The effects of different trench configurations, soil properties, geometrical factors, and ambient temperature on the amount of heat transfer away from the buried cable for the steady analysis were discussed. Instead of modeling air-ground surface as a convective boundary, the authors have used an approximated formula derived by Barber to find an effective air temperature. The transient heat flow analysis has been made in order to evaluate the times required to reach thermal equilibrium.

The steady-state temperature distribution within the cable trench backfill and surrounding soil has been calculated in reference [30] using the finite element procedure with a proposed integral equation (Green's identity) as a constraint, which was introduced to reduce the computation region and consequently, reduce the computation time and the required memory space. The authors have shown the simulated temperature distribution for different practical cable configurations of three cable systems.

The sensitivity of the cable temperature to the some thermal circuit parameters has been addressed in reference [31]. The author considered the effect of fluctuations in some cable circuit parameters on the cable ampacity and provided sensitivity indices of a cable ampacity. The technique used the finite element analysis to evaluate power cable performance. The technique has been applied to few practical cable systems including direct-buried and pipe-type cables as well as cable in duct banks. In reference [32] the authors described an efficient, finite element-based technique for calculating geometric factors for extending the range of height/width ratio of the duct bank or backfill that enabled the Neher-McGrath method to be applied to a wider range of cable configurations. However this technique was based on the assumption that the duct bank represents an isothermal boundary. This is not the case, and may result in some errors in the derived geometric factor values. However, the authors considered this point in reference [33]. The same technique was applied, taking into account the variation of the temperature along the duct bank or backfill. Results for selected cable configurations were presented. However, in spite of the duct bank surface modeling improvement, the representation of the earth surface as an isothermal boundary can be considered as a source of error. Furthermore, this method is applicable for the case of two-material soils, and can not be used for the solution of the more complex problem of multi-layer soils and non-isothermal boundary conditions.

The authors of reference [3] developed a computer program for power cable ampacity and temperature calculations under a contract to the Research and Development Division of the Canadian Electrical Association (CEA). The program is based on the IEC standard 278 and Neher-McGrath procedure with some modifications to account for the specific nature of distributed cables. Some modifications were incorporated in the program to permit computations for wider range of cable systems. Such of these modifications present in using the development of geometrical factor computations for a large duct bank described in references [32, 33], and allowance of analysis of special installation encountered in practice (i.e. submarine, and rise on pole cables). The proposed program contain an initial library of 47 distribution cables, included in the data base and has the ability to retain reference files of previous calculations and compare alternative solutions.

Under unfavorable conditions, the heat flux from the cable entering the soil may cause significant migration of the moisture away from the cable. Consequently, a dry-out zone may develop around the cable, for which the thermal conductivity is reduced. The effect of the moisture content on the thermal conductivity has been described in reference [34] using a finite element modeling coupled heat and moisture flow around power cables in steady state and time varying conditions. The authors compared the calculated results with the data from field experiments. They showed closer agreement to test results using moisture consideration in their modeling.

In reference [35] the author introduced a combined steady state finite element analysis of both electromagnetic and thermal fields effects on an underground cable system with structural steels constructed in a duct bank. Such techniques are used in underground cable systems to provide a high degree of mechanical protection for electrical cables. To consider the effect of eddy current losses induced in the steel, in addition to the effect of the total cable electrical losses, the author proposed an algorithm to evaluate the losses generated in the conductors and in the steels using the finite element analysis of electromagnetic fields, and consequently these were used as the heat sources for thermal analysis. However, the cable and steels were modeled as constant heat flux sources, the ground surface as a convective boundary, and others as isothermal boundaries. A duct bank of three cables with different structural steel configurations has been analyzed in order to show the effect of the steel arrangement on the duct bank and cable thermal field. Reference [36] describes the extensions of the previous works in [35] to investigate the effect of having an air gap between the external cable surface and the internal duct surface. Also the inclusion of radiation heat exchanges between the external cable surface and the internal duct surface was considered using an iterative procedure, adopted to deal with any nonlinearities introduced by such a boundary condition.

The transformation technique is used to limit the open region of the solution space, resulting in more accurate solutions with fewer mesh elements and less computing time than that required by an open boundary FE solution. A transformation technique in conjunction with coupled magneto-thermal FE field analysis has been described in reference [37] to obtain the temperature distribution profile of underground power cables. The proposed method was applied to the analysis of a single conductor cable and a three phase, gas-insulated power cable and the results were compared with those obtained by analytical and open boundary coupled field method.

The design problem of selecting the least cost parameter values associated with cable trench and thermal backfill were formulated as an optimization problem and solved using a multi-dimensional gradient optimization method as in reference [1]. The technique presented by the author considers all design parameters simultaneously and provides the desired solution which either minimizes the cost of backfill and trench production subject to an ampacity constraint or maximizes the cable ampacity subject to a cost constraint. In either formulation, upper and lower bounds on design parameters as well as other thermal and physical constraints were included. The author introduced the role of backfill parameters in reducing the effect of environmental fluctuations on cable ampacity in the optimization analysis via defining functional sensitivity profiles which may be used to ensure secure and reliable designs. However, he suggested some further extensions to the proposed work including, the use of advanced thermal analysis techniques in conjunction with the optimization routine to solve, more accurately, for the temperature distribution around the cable, and the use of sensitivity profiles with respect to more cable fluctuations including the backfill material itself.

The cable temperature is, in general, a function of the cable loading as well as other soil and ambient parameters which constitute the thermal circuit of the cable. In practice, these parameters are subject to random operating, geographical and seasonal variations that affect the cable temperature and, hence, the allowable loading level of any practical cable. A technique for calculating the temperature rise and load capabilities of power cables with provision for statistical variations of various soil, boundary and loading conditions has been described in reference [38]. The authors assigned a certain probability of occurrence with the nominal parameter values assumed in thermal analysis and, consequently, the value of the cable temperature is also subjected to certain probability. The ampacity sensitivity algorithm described in [31] was exploited in conjunction with statistical data gathered for a variety of soil materials, ambient parameters and load cycle characteristics in order to provide information concerning the expected values and confidence levels of ampacity and cable temperature rise as well as the probabilities associated with excessive temperature and thermal instability.

A probabilistic method of calculating cable rating was used in reference [39] to predict the allowable current carrying capabilities of the circuit under consideration based on probability distribution for the cable loading and ambient temperature as well as thermal resistivity of the backfill and native soil. The probability distribution of loading and ambient temperature for the circuit under consideration was obtained from historical records. Also, these derived statistical data of weather and cable loading was used combined with a soil moisture content survey to construct the probability distributions of backfill and native soil. The probability density function of cable temperature is obtained using a Monte Carlo simulation procedure combined with a finite element method.

The thermal behaviour of a directly buried line has been evaluated in reference [40]. The method considers the influence of climatic conditions and takes into account the mechanism of radiative and convective heat transfer at the soil-air interface. The thermal model, based on the finite element method, was proposed and used to study a three phase underground cable placed under a daily cyclic load, extracted from experimental observations made on a line with a cable of similar characteristics. The study evaluates the influence of the radiative heat transfer component on the thermal behaviour of the conductor. From the results, the authors deducted that ignoring the radiative heat transfer emitted implies that the temperatures can, in some cases, be noticeably different from ones obtained considering the complete boundary condition at the air-soil interface. On the other hand, in the same cases, they noted that avoiding radiative heat transfer completely could lead to a minor temperature difference. Finally, they came up with the final conclusion that the influence of the radiative heat exchange at the air-soil interface on the thermal behaviour of the cable can be neglected, allowing noticeably simplified modeling and computations.

In reference [6], transient heat transfer of medium voltage underground power cables was investigated numerically using finite element methods and validated experimentally using a developed laboratory model of PE installed power cable. In order to minimize the error arising from the modeling of the boundary conditions, the authors suggested to choose a distance such that the temperature distribution found by applying both isothermal and zero heat flux will would lead to improved results. Also, the correction factor for the cable carrying capacity was calculated for the XLPE cables to consider the effect of soil thermal conductivity at the chosen values.

The finite element method was employed to determine the temperature rise of a three phase underground cable system in reference [41]. The cable maximum current carrying capability was investigated for both the transient and the steady-state load conditions for cyclic daily load diagrams. The soil drying out phenomenon was considered using an iterative procedure. The developed finite element model and the procedures to determine the maximum current carrying capability were demonstrated for a 110 kV polyethylene insulated cable. Some experimental results were used to verify the presented model.

The influences of asymmetry, unbalance and nonlinearity on the cable temperature distribution were presented in [42]. The temperature distribution in the cable section was calculated considering the load conditions, and subsequently simulated using 2D finite element modeling by assuming maximum insulation temperature as a boundary condition. Subsequently, the authors of [43] investigated a sensitivity analysis in order to evaluate the influence of the different boundary conditions determining the cable temperature. Measurements of the cable temperature were performed to verify the simulation results.

In reference [44], a coupled finite element analysis technique was proposed to predict the temperature rise in the EHV bus bare. The finite element technique was used to solve the magnetic field governing equation, in order, to carry out the power losses due to the source current in the main conductor and the eddy current in the metallic tank, which containing the conductors and the SF gas fills in between them. The calculated power losses were used as input data for the thermal analysis. The heat transfer coefficient on the model boundaries, which was considered to include both convective and radiative effects, was calculated using an iterative scheme. At every step, the heat transfer coefficient is calculated and the temperature is compared to the previously calculated one.

One of the most important parameters in 3-core belted ampacity calculations is the internal thermal resistance between conductors and a common sheath. All 3-core cables require fillers to fill the space between insulated cores and the belt insulation or a sheath. The equations given in IEC 287 and in the Neher-McGrath paper (1957) for the internal thermal resistance of 3-core cables were developed for paper insulated cables. In the past, when impregnated paper was used to insulate the conductor, the resistivity of the filler material matched very closely that of paper. The majority of current materials used as fillers will have a higher thermal resistivity than the insulation. This may have a significant influence on the overall cable ampacity. The authors of references [45, 46] investigated the influence of the filler thermal resistivity on the internal thermal resistance and ampacity calculation using a finite element method. Furthermore, a new formula was developed to compute the value of the thermal resistance taking into account the thermal resistivity of the filler. The effect of filler resistivity on cable ampacity was also discussed.

In reference [47], the author proposed an inverse problem approach to estimate the unknown thermal parameters of the cable materials from the measured cable surface temperature and by using a gradient-base optimization technique in conjunction with the finite element method. The optimization procedure was designed to reduce the difference between the measured and estimated temperatures, which is a function of the cable thermal parameters. On the other hand finite elements were applied to the thermal field to obtain the variation of the estimated temperature with respect to thermal parameters and the gradient vector of the estimated parameter, which was implemented in the optimization algorithm. A practical case study was used to estimate the thermal parameters of the 6.6 kV cables and was used to calculate the transient temperature rise. Subsequently, in reference [48, 49] the author suggested the installation of a distributed temperature sensor (DTS) to monitor in real time the cable surface temperature. The technique developed of the previously mentioned reference [47] was used in these two papers to make full use of the DTS by calculating the conductor temperature and predict the cable rating from the cable surface temperature. This involved estimation of the soil parameters by matching the computed thermal field to that obtained from measurements. Also laboratory tests were carried out to predict cable rating under emergency overloading conditions. Subsequently the author continued working on application for this developed model. The local overheating of underground power cable referred to as hotspots was investigated in [50]. The hotspots of a 230 kV 500MVA underground cable circuit were located using fiber-optic temperature sensing. In conjunction with the measured temperatures at hotspots, a thermal model was used to find the thermal resistivity and ground temperature of individual hotspots for the purpose of cable dynamic rating determination.

In reference [51], the authors proposed an original nonlinear coupled electric-thermal model of underground cables with the solid sheaths. The proposed method provides a numerical evaluation of losses, heating and ampacity. The computation of the current dependent losses of cables with solid sheaths was computed by means of the filament method, where conductors and sheaths were replaced by a number of small sub-conductors or filaments, sufficiently small to assume uniform current density. The heat transfer was formulated and solved using a weighted residual finite element approach. The infinite domain beneath the ground surface was treated via a mapped infinite element. The iterative procedure starts with the evaluation of losses using arbitrarily chosen conductor and sheath temperatures which is used as input losses data for the thermal field model to calculate the later iteration temperatures values, and the losses are computed again at the new temperature values, the producer goes on repeatedly as long as the prescribed temperature discrepancy through successive iteration is achieved.

In reference [52], the authors developed a numerical stochastic technique for an optimization of an underground power cable which involves a finite element mesh generator, nonlinear coupled-thermal model, multi-quadric ampacity approximations including successive zooming steps and stochastic optimization method using a differential evaluation. The proposed technique determines the optimal geometrical parameters of a cable system in relation to either the maximum ampacity achieved with acceptable initial investment cost, or the minimal initial investment cost by which the required ampacity is reached. The optimization algorithm is based on radial basis function by interpolating a scattered ampacity data calculated by a computationally expensive numerical electrical-thermal model provided in [51] and associated with a chosen parameter sample, with the aim of reducing the required computation effort. This proposed method required large computational efforts due to a number of necessary objective function evaluations, which was overcome by multi-quadric ampacity approximation at the expense of accuracy. Also the proposed method deals with a geometrical parameter and does not take into consideration the variation effects of the thermal parameters values which were assumed to be fixed.

2.3 METHODS AND ALGORITHMS BASED ON FINITE DIFFERENCE THERMAL FIELD CALCULATIONS

The heat dissipation and temperature distribution in multilayered soil surrounding a buried cable using the finite difference method and the energy conservation principle have been described in reference [53, 54]. The problem of setting the boundary temperature of the area surrounding the cable in a trench was treated by introducing a constraint based on the energy conservation law, which state that the heat losses from the grid boundaries should be equal to the heat dissipated from the cable, consequently, the difference between the two heats was kept as small as possible by reducing the value of the absolute error for temperature converge. In this paper the authors developed the model and studied the parameters that influence the conversion and stability of the numerical solution. In reference [55], they continued to study the effect of the trench dimensions, cable location, trench thermal conductivity, and environmental conditions on the heat dissipation. They subsequently modified the proposed method to accommodate two cables with different diameters, randomly located in the trench, and three under ground cables in reference [56, 57] respectively.

A model based on the finite difference technique was introduced in reference [4] in order to calculate the ampacity and the heat distribution in a buried three cable system in both steady state and emergency situations. In addition to multilayered soil surrounding the system, they introduced a model that takes into account the inside elements constituting the cable (conductor, insulation, shield, armor, etc.). The heat diffusion equation is solved in cylindrical coordinates inside the cables and in Cartesian coordinates in the surrounding soil. The authors have introduced a variable step discretization which enables the model to focus on the interior of the cable and the area near, where the higher temperatures variation exist. The model includes the variability with temperature of such parameters as conductor resistivity, and thermal conductivities of the different materials in the cable and soil. Consequently, the simulation of the moisture migration is possible using a variable soil thermal conductivity as a function of the temperature.

2.4 METHODS AND ALGORITHMS BASED ON OTHER NUMERICAL THERMAL FIELD CALCULATIONS

The underground cable thermal field problem has been formulated and solved in reference [58] using the boundary element method. Based on the fact that the boundary element method focuses its attention on the region boundaries rather than on its interior, unlike in domain-type methods (FEM, FDM), the authors tried to introduce this method as an effective low computation method. However, this is not quite accurate in the case of a complex cable configurations consisting of several subregions where the boundaries between the subregions need to be included and, consequently, increases the computational effort. The authors carried out some applications of the BEM for the single and three phase cable in a homogeneous soil.

The author of reference [59] introduced an analytical technique based on the concept of thermal resistance/capacitance analogue, in order to study the transient temperature rise of a three core cable. The proposed algorithm based on discretizing the area of interest (cross section of the cable) as in FD or FE, but rather than dealing with partial differential equations, the energy flowing across all surfaces of a small finite cell added to gather with the heat absorbed and produced by the cell to carry out the energy balance equation for that cell. The heat flux between centers of two adjacent cells is considered as uniform flux and the thermal resistance, for a rectangle containing the common surface between the two cells and passing through their centers, is calculated. The energy flows across any cell surface can be written as functions of the thermal resistance with the adjacent cell and the difference of their center temperatures and substituted in the cell energy balance equation. Similar equations can be written for each cell, resulting in a set of simultaneous equations which can be solved to obtain unknown cell temperatures. The accuracy of the model will depend on how well the assumption of uniform flux was approximated in the rectangular region defined by the two center points and the boundary between two adjacent cells.

In reference [60], the authors presented a numerical methodology for thermal analysis of underground cables with constant and cyclic load in presence of moisture migration in the surrounding soil. The governing equations were solved using a finite volume methodology. They described the transfer of both heat and moisture content. Simulations were performed for a 138 kV installation considering a native soil as well as the backfill. Authors have indicated the role played by the moisture saturation degree of the native soil on the thermal stability of the soil. In case the native soil has moisture content below its critical value (the value in which the liquid in the soil becomes mobile), authors indicated that severe loads can cause thermal instability which can be prevented using artificial backfill. They have also indicated that although the presence of a backfill layer is of major importance for cable reliability, its thickness has a minor effect on the cable operating temperature as long as the cable is completely surrounded by at least one cable diameter of backfill. Furthermore, the investigated cases showed that an increase in the ambient temperature as well as in the soil temperature have a direct impact on the cable temperature as expected.

Reference [61] deals with the interval simulation of a finite difference power cable thermal model. In this approach the cable components are partitioned in several concentric cylindrical elements and the resulting thermal model takes the form of continuous dynamic system characterized by a set of state variables (temperatures of the conductors) and a set of ordinary differential equations provide the dynamics behaviour of the system. This model is based on the simplified thermal equivalent equations and relies on the availability of number of characteristic parameters (e.g. weather along the line route, thermo-physical properties of the soil, cable parameters). Because these parameters, often, are not precisely known, the authors proposed the use of non-probabilistic methods in thermal rating assessment of a complex transmission or distribution system, when sufficient information is not available to identify a probabilistic description of the uncertainty.

2.5 METHODS AND ALGORITHMS BASED ON ANALYTICAL METHODS AND LADDER NETWORK

A fundamental analytical method using a lumped parameter model for computation of transient ratings of buried power cables has been described in reference [62]. The mathematical model is based on the ladder network representation of the cable thermal circuit, in which the temperature rise of a cable component can be represented by the sum of the both temperature rise inside and outside the cable. The new contributions of the authors including additions and modifications to the techniques of (CIGRE 1972, IEC 287 1982), including the extension of the formulation for different and non equally loaded cables and provision of the possibility to take into account the effect of the backfill or duct bank.

In reference [63], the authors proposed an algorithm to calculate the short-time thermal capacity of duct-installed power cables. The proposed algorithm is based on the estimation of the thermal resistance and capacitance of the surrounding soil using continuously measured duct temperatures. In this algorithm, a genetic algorithm was employed to estimate this resistance and capacitance accurately. In addition, an optical fiber temperature sensor was developed to measure the duct temperature. The proposed work introduced a truncation algorithm of the variation of thermal resistance and capacitance of the surrounding soil with the time using the measured data, which results in improvement of the short-time thermal capacity calculations of duct-installed power cables.

In reference [64], the authors described the importance of optimization of cable ampacities through the use of controlled backfill. They showed the role of a thermal survey at the early stages of the project as soon as the route is selected, and the effect of testing during construction by some thermal property equipment. As well they examined the role of a laboratory analysis in evaluation of the thermal parameters of native soil and backfill when the soil temperature and moisture changes with depth as well as with the seasons. The authors stressed the importance of quality control and field inspection for both granular backfill and fluidized thermal backfill (FTB). They recommended that the designer keep a close contact with the installation of the backfill and adjust the backfill thickness if the native soil thermal resistivity is higher than the value assumed in the design, or if the cable buried depth is increased. While this is desirable it may not always be a practical arrangement. An upfront, trench and backfill optimization as a part of the cable thermal design is probably a more practical approach. The electrical analog of the cable thermal circuit in conjunction with Neher-McGrath thermal parameters procedure was used to perform the ampacity calculations.

The calculation of the external thermal resistance of a power cable buried in backfill has been formulated in reference [65] using a multiple reflection of a line heat source and its images at the boundary between media having different thermal resistivity. The multiple reflections of the line source and its images results in equations containing a few terms or the sum of many terms, depending on the configuration of the cable system. The formulas derived by the authors deal with the case of only one backfill layer and a single cable (single heat source); this reflects the limitation of proposed method in the case of complex configurations in which an additional images and reflection coefficients would be added, resulting in more complications.

An algorithm to calculate temperature of cable and pipe of an underground pipe type cable system has been described in reference [66]. The underground pipe type cable system was represented by a thermal impedance network. A ladder network of resistances and capacitances represents the cable out to the outer surface of the pipe, where the cable parameters were found using Neher-McGrath method. The earth and adjacent pipe type cables as well as cable images were modeled by frequency dependent thermal impedance found by solving the heat transfer differential equation. In the proposed work the only thermal input (source of heat) that was considered is the conductor losses. The authors considered the heat input as a periodic signal, calculated by considering the load curve over a certain period up to 300 hours. A Fast Fourier Transform (FFT) was used to obtain heat input in the frequency domain. The frequency domain thermal input at the conductor was divided by the thermal admittance seen by the conductor and an inverse FFT is used to obtain conductor temperature as a function of time. A similar procedure obtains shield and pipe temperature. Iteration was used to model conductor electrical resistance change with temperature. The ambient temperature and temperature difference due to dielectric loss are added to obtain final values.

A methodology to calculate underground power cable ampacities as well as thermal and electrical cable parameters was presented in reference [67] through the implementation of combined thermal and electrical circuit models in an iterative procedure based on conductor temperature parameter. The author developed a procedure which initializes the conductor temperature in order to calculate the conductor losses using a thermal circuit which, subsequently, will be used to calculate conductor currents. The calculated current with the mutual coupling will be used in the electrical circuit to recalculate the losses and, consequently, the temperatures. This iterative process will stop when conductor temperature converges to specific value. Solutions of both the thermal and electrical circuit models will perform with the iterative procedure until convergence based on conductor temperature occurs. Results from this procedure include not only the calculation of thermal parameters, such as cable ampacities and system temperatures, but also electrical parameters, such as cable voltage drops and open-circuited shield voltages.

By noticing the mathematical similarity between the electrical and thermal circuits, the node voltage method, which is widely used to solve electrical circuit problems, was used to solve the power cable thermal condition in [68]. The node voltage method was applied to calculate the temperature of the power cables conductors in real time based on the polymeric jacket measured temperature of the cable for both steady state and transient state conditions.

Reference [69] introduced a framework for the temperature monitoring of power cables based on real time current measurement in conjunction with cable surface or sheath temperature measurement. The method is based on modeling the temperature response of a cable by summing an appropriate number of exponential functions. These functions are related to a thermal ladder circuit for installations that can be analyzed in such terms, or are mathematically fitted to numerically simulated results for those that cannot. The final conditions are established at each time interval by simple steady state calculations based on the present temperatures. This allows entry into territory that is forbidden for normal superposition methods, namely, a thermally unstable environment. The method provides an alternative method for transient cable rating, is inherently suited for real time implementation, and provides a frame work that accommodates a changing thermal environment.

2.6 MEASUREMENT, LABORATORY SETUP AND LIVE CABLE IMPLEMENTATION

Thermal resistivity depends on the soil type, density and moisture content. The latter can be expected to change as a result of seasonal conditions. The inability to confidently predict values of thermal resistivity, given a particular set of environmental and loading conditions, could lead to uncertainties in the cable current rating estimation. Based on that, references [70] and [71] investigated a probabilistic approach to relating the cable rating with thermal environment studies. The authors aimed at obtaining and analysing actual daily field values of thermal resistivity and diffusivity of the soil around power cables under actual operating condtions, and to correlate these values with rainfall data from weather records. On-line monitoring systems have been developed and installed with a data logger system and buried spheres that use an improved technique to measure thermal resistivity and diffusivity over a short period. Based on the long-term continuous field data for more than four years, a probabilistic approach was developed to establish the correlation between the measured field thermal resistivity values and rainfall data. consequently, a probabilistic cable rating has been established based on monthly probabilistic distribution of thermal resistivity.

Based on field measurements along the cable route, an investigation was presented in reference [72] focusing on the thermal behaviour of critical hot spots of 110 kV underground transmission lines where, during characteristic annual weather periods, the soil surrounding the 110 kV underground transmission lines undergoes a long term process of drying. By measuring different hot spots, the authors noted that, due to the effect of drying out of the soil, temperature increases of the cable surface for several tens of Celsius degrees in relation to other cable rout sections occurs. Authors have described a practical procedure for applying a special manufactured cable backfill material on specific hot spots of 110 kV underground transmission lines in order to reduce the cable operating temperature at these critical spots. Consequently, they suggested correct usage of the backfill material as necessary and sufficient means for removing the negative effects of soil drying on the increase of the operating temperature of 110 kV underground transmission lines.

The transmission capacity of a cable installed in a buried duct was described in reference [73] using a finite element based program, which has the capability to incorporate seasonal changes in air and ground temperature, ground-surface boundary conditions for sunlight and radiation, as well as, it allows transient-current analysis to which daily and seasonal fluctuations are added. In preparing the heat balance model for the proposed underground cable duct configuration, long-term tests were carried out over period of two years in order to measure conductor and cable surface temperatures as well as other quantities including amount of rainfall, wind speed, and soil temperature. The developed analysis was fed by the measured weather and soil data. Then, results were carried out and compared with the soil and cable measured temperatures history collected from the long-term test.

Increasing the possibilities of cable systems beyond their current stationary ampacity limits has been presented in reference [74] using a cable ampacity management algorithm. The authors introduce underground cables in the Netherlands, which have been equipped with integrated optical fibers for temperature measurements where important data about the actual thermal status of the cable circuit can be obtained. Furthermore, a thermal model, based upon a thermal R-C network together with thermodynamic soil heat transfer function, has been developed. The model has the capability to calculate several interesting temperatures and ampacity ratings within the cable system, based upon the type of the cable, the system configuration, soil parameter and the current flowing through the cable system. The model was validated with temperature measurements. In order to use the thermal model for ampacity management, the model has been integrated in a custom-built graphical user interface (GUI). This cable ampacity management system is installed at the cable circuit and performs on-line ampacity calculations. Furthermore, the authors introduced the usage of early warning systems for mechanical stress as an auxiliary factor in improving transport capacity of the cable. They integrated a detection system for severe cable damage and fiber break in the prescribed graphical user interface.

In reference [75], a distributed temperature monitoring system (DTS) was used to monitor the temperature of an optical fiber that installed along a power cable. The DTS injects a sharply-pulsed laser beam into a standard multimode fiber, then, a weak thermally-dependent molecular vibrations produce reflections along the fiber length, which can be detected by a special optical time domain reflectometer (OTDR) and the signals are processed to yield the temperature along the length of the fiber optic cable. The fiber optic can be installed in the power cable construction, inside pipe-type cables, or in ducts alongside the cables. The authors described an algorithm to calculate the maximum allowable current along a cable route, especially at the hot spot locations detected by the temperature monitoring system, using combined Neher-McGarth procedure and DTS temperature profile. The expected temperature at the fiber optic cable location was calculated using the Neher-McGarth interference temperature rise approach. This value was then compared to that measured using DTS, and the effective soil thermal resistivity was adjusted until the calculated temperature matches the measured temperature. Consequently, the ampacity was calculated that would give maximum allowable conductor temperature for those conditions. The authors described an application where a temperature profile combined with method developed to relate optical fiber temperature to cable conductor temperature, plus sophisticated ampacity analyses, permitted one utility to obtain an 8% ampacity increase and defer reinforcing a 69 kV circuit by two years.

References [76, 77] presented an experimental set up around a practical cable duct bank system of four three-phase cable circuits to investigate the transient and steady state thermal behaviour of the system. The values of temperature at different distances from the cable duct bank, cable jacket temperatures, and cable currents were recorded by an underground thermocouple-based data acquisition system. The effect of soil temperatures surrounding the cable depending on distance from the cable duct bank, ambient temperature and cable load was investigated. The transient cable jacket temperature rise corresponding to any step change in cable current was also investigated. Finally, the daily variation of the soil temperatures, cable jacket temperatures and cable current loads was evaluated.

When cables cross external heat sources or cross the areas of high thermal resistivity, the conductor temperature will be higher than the values attained outside of the unfavourable area. For perpendicular and oblique crossings as well as street crossings, these effects are usually ignored for distribution circuits, whereas for transmission cables, corrective actions in physical installation condition are sometimes taken. Almost never are analytical solutions used to determine the effect of external heat sources and high thermal resistivity regions on the ampacity of the rated cable. The main reason no computations are performed is the absence of either derating formulae or derating tables (curves), nor the lack of need. In references [78, 79], analytical solutions for the computation of the derating factors have been developed and sample computational results were presented. The influence of varying ambient soil temperature and presence of high resistivity blocks of soil under roadways were considered using a thermal network model of heat flow in two dimensions.

In reference [80] a derating factor was defined on the basis of the rated ampacity of a direct-buried cable to determine the reduction in ampacity that must be applied if the cable is to remain below acceptable temperatures inside the conduit. A finite element package was used to determine derating factors for typical cable constructions and common installations. The derating factors were provided as a function of conduit length, soil resistivity, burial depth, and number of cables in conduit.

CHAPTER 3

FINITE ELEMENT METHOD AND SOLUTION PROCEDURES

3.1 OVERVIEW

The ampacity computation of a cable buried in multi-layer soil is of significant interest to cable engineers. In conventional analysis using the Neher-McGrath method, the presence of a complex boundary condition or non-uniform soil such as a backfill or duct bank represents significant difficulties and often leads to limiting approximations and the use of correction factors. This may affect the accuracy of the overall results and may force the cable engineer to use higher safety margins with, however, added costs to the cable design. Numerical methods, including the finite difference, finite element, and boundary element methods appear to provide the necessary tools for the solution of the more complex problem of multi-layer soils and non isothermal boundary conditions.

Finite difference and finite element methods for solving the heat conduction differential equation often lead to a very large number of algebraic equations, and their solution is a problem in itself. Large sets would generally be solved iteratively and small sets by direct elimination methods. Iterative methods are more efficient than direct methods in that they take advantage of the large number of zero coefficients in the matrices. There is a vast literature on dealing with sets of linear equations and economy that can be achieved when the matrices are sparse.

The basic difference between finite element and finite difference methods lies in the manner in which approximations are performed. In the finite element method, the temperature is approximated by a discrete model composed of a set of continuous functions defined over a finite number of subdomains. The piecewise continuous functions are defined using values of temperature at a finite number of points in the region of interest. In the finite difference method, the derivatives at a point are approximated by difference quotients over a small interval. Both approximations can be quite accurate if the meshes are made suitably small.

Both methods allow a choice for the multi-nodal elementary subdomains. However, because of the nature of the approximations involved, a rectangular mesh with division lines parallel to the coordinate axes is usually chosen for the finite difference method. This may create difficulty in representing circular boundaries which are quite common in cable representation. This difficulty does not exist in the finite element method because curved boundaries can be well approximated by a suitable selection of elements. In addition, finite difference equations may become very complex when no uniform spacing is used along any of the axes, whereas the finite element method handles differing element sizes quite naturally. Consequently, because of their flexibility in representing the region around the cables and the ease of modeling boundary conditions, finite element methods appear to be more suitable for the numerical solution of the thermal field analysis of underground cable systems.

Unlike domain-type methods (FEM, FDM), the boundary element method focuses attention on the region boundaries rather than on the interior. In the boundary element method, calculations are performed only along the region boundaries which purport to provide sufficient information to compute the desired temperatures everywhere within the region. Consequently, the interior region need not be covered with a grid, and the computational effort associated with the boundary element method is considerably lower than in the domain-type method. The immediate consequence of this approach in that problem dimensions are reduced by one. For example, for a three-dimensional region, the surface enclosing the region is a two dimensional structure, only the surface is discretized and field at any point in the region is found by summing the contributions from boundary elements.

This chapter describes the key aspects of the finite element method used and coded during this research work. The basic formulation of the heat transfer modeling using the finite element method is presented, which will be used as the foundation of the proposed new methodology in the next chapter.

3.2 BASIC FORMULATION

3.2.1 Boundary Value Problem

Boundary value problems arise in the mathematical modeling of physical systems. A typical boundary value problem can be defined by a governing differential equation in a domain, Ω [81]:

$$\ell\varphi = f \tag{3.1}$$

together with the boundary condition on the boundary Γ that encloses the domain. In (3.1) ℓ is a differential operator, f is the exciting function or forcing function, and φ is the unknown quantity. The form of governing differential equation ranges from a simple Poisson equation to complicated wave equation. The boundary conditions also range from simple Dirichlet and Neumann conditions, to complicated radiation conditions.

It is desirable to solve boundary value problems analytically whenever possible. However, this is generally the exception since an analytical solution can be obtained in only a few cases. Many problems of practical importance do not have an analytical solution. To overcome this difficulty, various approximate methods have been developed, among them the Ritz and Galerkin methods have been used most widely.

3.2.2 Solution Using Subdomain Expansion Function

However, to find a trial function defined over the entire solution domain and which is capable of representing, at least approximately, the true solution of the problem, is the first step in the Ritz and Galerkin methods. For many problems this is very difficult, if not impossible, and this is practically true for many two and three-dimension problems. To alleviate this difficulty, we can divide the entire domain into small subdomains and employ the trial functions defined over each subdomain. These trial functions are usually in much simpler forms since the domains are small. Hence the variation of the function φ is less drastic over each subdomain.

3.3 THE FINITE ELEMENT METHOD

3.3.1 Finite Element In Relation to Other Available Techniques

The finite element method consists primarily of replacing a set of differential equations in terms of unknown variables with a corresponding approximate set of algebraic equations where each of the unknown variables is evaluated at a node point. Several approaches may be used in the evaluation of these algebraic equations, and finite element methods are often classified as to the method used. Unfortunately, no one method is suitable for all problems likely to be encountered in engineering today, so several of the methods may have to be examined in order to choose the appropriate one for a particular problem.

In this section we first define boundary value problems and then review two classic methods for their solution. One is the Ritz variational method and the other is Galerkin's method. These two methods form the basis of modern finite element methods. Therefore, to best introduce the finite element method, it is necessary to understand these two methods first.

The Ritz method, also known as the Rayleigh-Ritz method, is a variational method in which the boundary value problem is formulated in terms of a variational expression, referred to as the functional, whose minimum corresponds to the governing differential equation under the given boundary conditions. The approximate solution is then obtained by minimizing the functional with respect to it is variables. On the other hand, Galerkin's method belongs to the family of weighted residual methods, which, as the name indicates, seeks the solution by weighting the residual of differential equation. The procedure that employs the Ritz method is usually referred to as a Ritz finite element method or, better known as the variational finite element method, whereas the one that employs Galerkin's method is usually referred to as the Galerkin finite element method [82].

The finite element method differs from the classical Ritz and Galerkin's methods in the formulation of the trial function. In the classic Ritz-Galerkin's method, the trial function is formulated as a combination of a set of basis functions defined over the entire domain. This combination must be able to represent, at least approximately, the true solution and must also satisfy the boundary conditions. In the finite element method, the trial function is a combination of a set of basis functions defined over the subdomains that comprise the entire domain. Consequently, as the subdomains are small, the basis functions defined over a subdomain can be quite simple. However, in the most practical cases it is very difficult and often impossible to find the required entire domain trial functions, particularly for a problem with irregular boundaries. In the finite element method, the idea of using subdomain basis functions makes it possible to attack complicated boundary value problems, and it is the advent of computer techniques that makes this method practical. For this reason, the finite element method is often categorized as the computer-aided analysis method most widely used in the majority of physical and engineering fields including structure analysis, fluid mechanics, vibration, heat transfer, and electromagnetics.

3.3.2 Basic Steps of the Finite Element Method

The finite element method is a numerical procedure for obtaining solution to boundary value problems. We replace an entire continuous domain by a number of subdomains in which the unknown function is represented by simple interpolation functions with unknown coefficients. Thus the original boundary value problem with an infinite number of degrees of freedom is converted into a problem with a finite number of degrees of freedom, or in other words, the solution of the whole system is approximated by a finite number of unknown coefficients. Then a set of algebraic equations is obtained by applying the Ritz variational or Galerkin procedure. Finally, solution of the boundary value problem is achieved by solving the system of equations. Therefore, a finite element analysis of a boundary value problem should include the following basic steps:

- Discretization or subdivision of the domain
- Selection of the interpolation functions
- Formulation of the system of equations
- Solution of the system of the equations

3.3.2.1 Domain Discretization

The discretization of the domain is the first step and perhaps the most important step in any finite element analysis because the manner in which the domain is discretized will affect the computer storage requirements, the computation time and the accuracy of the numerical results. In this step, the entire domain is subdivided into a number of small domains, denoted Ω^e (e=1,2,3,...E), with E denoting the total number of subdomains. These subdomains are usually referred to as the elements. For a one-dimensional domain which is actually a straight or curved line, the elements are often short line segments interconnected to form the original line. For a two-dimensional domain, the elements are usually small triangles and rectangles. The rectangular elements are, of course, best suited for discretizing rectangular regions, while the triangular ones can be used for irregular regions.

In most finite element solutions, the problem is formulated in terms of the unknown function φ at nodes associated with the elements. For example a linear line element has two nodes, one at each endpoint. A linear triangular element has three nodes, located at its three vertices, whereas a linear tetrahedron has four nodes, located at its four vertices. For implementation purposes, it is necessary to describe these nodes. A complete description of a node contains its coordinate values, local number, and global number. The local number of a node indicates its position in the element, whereas the global number specifies its position in the entire system. Whereas specifying the coordinate values is a rather straightforward job, numbering of nodes and elements requires some strategy. However, a finite element formulation usually results in a band matrix whose bandwidth is determined by the maximum difference between the global numbers of two nodes in an element. Thus, if a banded matrix solution method is employed to solve the final matrix equation, the computer storage and processing cost can be reduced significantly by properly numbering the nodes to minimize the bandwidth.

The discretization of the domain is usually considered a preprocessing task because it can be completely separated from the other steps. Many well-developed finite element program package have the capability of subdividing an arbitrarily shaped line, surface, and volume into corresponding elements and also provide the optimized global numbering.

3.3.2.2 Selecting of Interpolation Function

The second step of the finite element analysis is to select an interpolation function that provides an approximation for the unknown solution within an element. The interpolation is usually selected to be a polynomial of first (linear), second (quadratic), or higher order. Higher-order polynomials, although more accurate, usually result in a more complicated formulation. Hence, the simple and basic linear interpolation is still widely used. Once the order of the polynomial is selected, we can derive an expression for the unknown solution in an element e, in the following form:

$$\varphi^e = \sum_{j=1}^{n} N_j^e \varphi_j^e \tag{3.2}$$

where n is the number of nodes in each particular element, φ^e_j the value of φ at the node j of the element, and N^e_j the interpolation function, which is also known as the expansion or basis function. The highest order of N^e_j is referred to as the order of element. An important feature of the function N^e_j is that the function is nonzero only within element e, and outside this element the function is vanishes.

3.3.2.3 Formulation of the System of Equations

The third step, also a major step in the finite element analysis, is to formulate the system of equations. Both the Ritz variational and Galerkin methods can be used for this purpose.

The Ritz method

The Ritz method concerned with the variations of a quantity called a functional which will be addressed as I. The functional is not dependent upon position or coordinate direction within a physical problem. Generally, the objective of finding the solution to engineering problems using variational methods is to find a stationary value of I.

For simplicity assume that the problem is real valued. The solution of (3.1) can be obtained by minimizing the function [82, 83]

$$I(\tilde{\varphi}) = \tfrac{1}{2} \int_{\Omega} \tilde{\varphi}\, \ell \tilde{\varphi}\, d\Omega - \int_{\Omega} f \tilde{\varphi}\, d\Omega \tag{3.3}$$

with respect to $\tilde{\varphi}$, where $\tilde{\varphi}$ denotes the trial function.

The boundary value problem is formulated in terms of a variational expression, referred to as the functional, whose minimum corresponds to the governing differential equation under the given boundary conditions. The approximate solution is then obtained by minimizing the functional with respect to its variables.

Suppose that $\widetilde{\varphi}$ can be approximated by the expression

$$\widetilde{\varphi} = \sum_{j=1}^{N} c_j v_j = \mathbf{c}^T \mathbf{v} = \mathbf{v}^T \mathbf{c} \tag{3.4}$$

where v_j are the chosen expansion functions defined over the entire domain and c_j are constant coefficients to be determined. Also $\mathbf{c}$ and $\mathbf{v}$ denote column vectors of the elements c_j and v_j respectively. The superscript T denotes the transpose of the vector. Substituting (3.4) in (3.3), we obtain

$$I = \tfrac{1}{2}\mathbf{c}^T \int_{\Omega} \mathbf{v}\ \ell\, \mathbf{v}^T d\Omega\ \mathbf{c} - \mathbf{c}^T \int_{\Omega} \mathbf{v} f \ \ d\Omega \tag{3.5}$$

To minimize I, we let its partial derivatives with respect to c_i vanish. This yields a set of linear algebraic equations. Consequently, an approximation for (3.1) is then obtained by solving the matrix equations.

The Galerkin method

Assume that $\widetilde{\varphi}$ is an approximate solution to (3.1). Substitution of $\widetilde{\varphi}$ for φ in (3.1) would result in a generally non-zero residual

$$r = \ell\widetilde{\phi} - f \neq 0 \tag{3.6}$$

The best approximation for $\tilde{\varphi}$ will be the one that reduces the residual r to the least value at all points of Ω. The weighted residual method enforces the condition

$$R_i = \int_{\Omega} w_i r \, d\Omega = 0 \tag{3.7}$$

where R_i denotes the weighted residual integral and w_i is chosen weighting function.

In the Galerkin method, the weighting function is often selected to be the same as that used for the expansion of the approximate solution. This usually leads to the most accurate solution and is, therefore, popular in developing the finite element equations. To illustrate the method more explicitly, let us assume that the solution is represented as in (3.4). The weighting functions are then selected as $w_i = v_i$, so that (3.7) becomes

$$R_i = \int_{\Omega} (v_i \, \ell \, \mathbf{v}^T \mathbf{c} - v_i \, f) \, d\Omega = 0 \tag{3.8}$$

This leads to a matrix system, although it is not necessarily the same system of equations for the case of a Ritz formulation unless the operator ℓ is self-adjoint.

3.4 FORMULATION OF HEAT TRANSFER IN UNDERGROUND POWER CABLE

3.4.1 Basic Formulation

Ampacity computations of a power cable require the solution of the heat transfer equations which define a functional relationship between the conductor current and the temperature within the cable and in its surroundings. Inevitably, current in the cable conductor generates heat which is dissipated through the insulation, metal sheath, and cable servings into the surrounding medium. The cable ampacity depends mainly upon the efficiency of this dissipation process as well as limits imposed by the insulation temperature. To understand the nature of the heat dissipation process, we need to develop the relevant heat transfer equations.

In the analysis of heat transfer in a cable system, the law of conservation of energy plays an important role. The energy conservation law can be expressed by the following equation [83, 84]

$$Q_{ent} + Q_{int} = Q_{out} + \Delta Q_{st} \tag{3.9}$$

where Q_{ent} is the rate of energy entering the cable. This energy may be generated by other cables located in the vicinity of the given cable or by solar radiation. Q_{int} is the rate of heat generated internally in the cable by joule or dielectric losses, and ΔQ_{st} is the rate of change of energy stored within the cable. The value of Q_{out} corresponds to the rate at which energy is dissipated by conduction, convection and radiation. In other words, this relation says that the amount of energy inflow and generation act to increase the amount of energy stored within the cable, whereas outflow acts to decrease the stored energy. The inflow and outflow terms Q_{int} and Q_{out} are surface phenomena, and these rates are proportional to the surface area. The thermal energy generation rate Q_{int} is associated with the rate of conversion of electrical energy to thermal energy and is proportional to the volume. The energy storage is also a volumetric phenomenon, but it is simply associated with the increase or decrease in the energy of the cable. Under steady-state conditions, there is, of course no change in energy storage.

Let us consider an underground cable located in homogeneous soil. In such a cable, the heat is transferred by conduction through the cable components and the soil. Since the length of the cable is much greater than its diameter, end effects can be disregarded, and the heat transfer problem can be formulated in two dimensions only as shown in Figure 3.1.

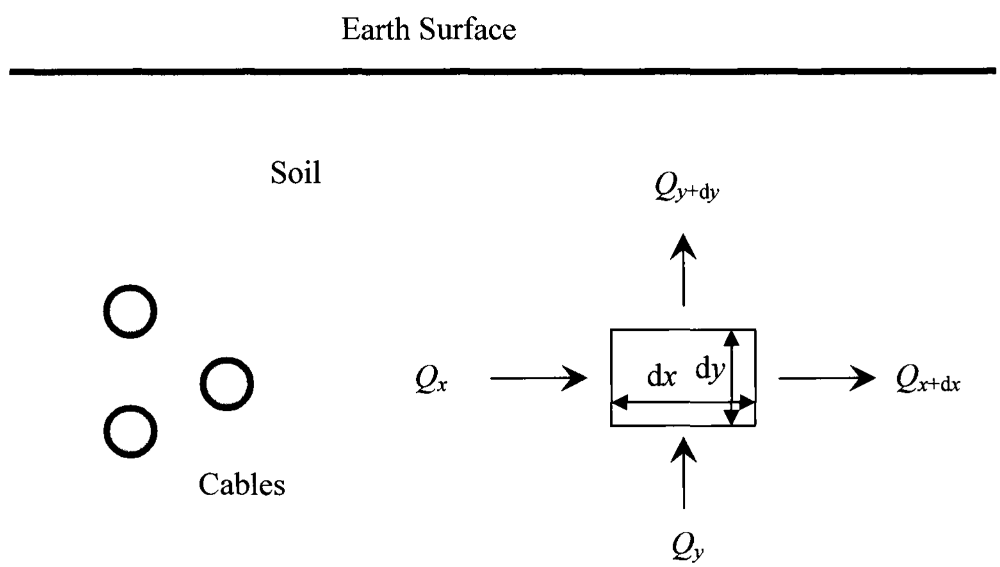

Fig. 3.1 Heat transfer in two dimensions

When heat passes through the body as shown in figure 3.1, it meets a certain thermal resistance. Applying Fourier's law of heat conduction, we have

$$Q_x = \frac{A}{\rho}\frac{\partial T}{\partial x} \tag{3.10}$$

where Q_x is the heat transfer through the area A in the x direction, W

ρ is the thermal resistivity, K.m/W

A is the surface area perpendicular to the heat flow, m^2

T is the temperature at any point.

For underground installation, the cable system will include the surrounding soil. Heat is transferred by conduction through the cable components and the surrounding soil. Consider a small element $dxdy$ in figure 3.1, if there are temperature gradients, the conduction heat rates perpendicular to each of the surfaces at the x and y coordinate locations are indicated by terms Q_x and Q_y, respectively. The conduction heat rates at opposite surfaces can then be expressed as a Taylor expansion where, neglecting higher order terms,

$$\begin{aligned} Q_{x+dx} &= Q_x + \frac{\partial Q_x}{\partial x}\, dx \\ Q_{y+dy} &= Q_y + \frac{\partial Q_y}{\partial y}\, dy \end{aligned} \tag{3.11}$$

Within the element *dxdy*, there may also be an energy source term associated with the rate of thermal energy generation. This term is represented as

$$Q_g = Q_{int}\, dx\, dy \tag{3.12}$$

where Q_{int} is the rate at which energy is generated per unit volume of the body by resistive and capacitive current. In addition, changes in the amount of internal energy stored by material in the small body *dxdy* may be occurred. These changes are related to the capacitive nature of the cable insulation. On the rate basis, we express this energy storage term as

$$\Delta Q_{st} = c\frac{\partial T}{\partial t}\, dx\, dy \tag{3.13}$$

where c is the volumetric thermal capacity of the material. Recognizing that the conduction rate constitutes the energy inflow and outflow, and there are no other energy transfer modes, the energy balance equation (3.9) for this body can be written as

$$Q_x + Q_y + Q_{int}\, dx\, dy - Q_{x+dx} - Q_{y+dy} = c\frac{\partial T}{\partial t}\, dx\, dy \tag{3.14}$$

Observing that, in this case $A=dxdy$, we can rewrite the last equation by substituting from equation (3.10) and (3.11) to obtain

$$\frac{\partial}{\partial x}\left(\frac{1}{\rho}\frac{\partial T}{\partial x}\right)+\frac{\partial}{\partial y}\left(\frac{1}{\rho}\frac{\partial T}{\partial y}\right)+Q_{int}=c\frac{\partial T}{\partial t} \tag{3.15}$$

For the cable buried in the soil, equation (3.15) is solved with the boundary conditions usually specified at the soil surface. For any homogeneous region of given thermal conductivity and heat generation rate, equation (3.15) can be solved for the temperature at any point (x,y) in the region subjected to specific boundary conditions. The power cable thermal circuit includes various regions of complicated shape having different values of thermal conductivity and heat generation. Equation (3.15) should then be solved for the entire cable medium including surroundings.

3.4.2 Two-Dimensional Steady State Problem

The governing partial differential equation for a two-dimensional steady state problem is [83, 85]:

$$k\,\frac{\partial^2 T}{\partial x^2}+k\,\frac{\partial^2 T}{\partial y^2}+Q=0 \tag{3.16}$$

with boundary conditions of the types

$$T(x,y)=T_0 \tag{3.17}$$

$$k\frac{\partial T}{\partial n}=q \tag{3.18}$$

$$k\frac{\partial T}{\partial n}=h(T-T_a) \tag{3.19}$$

$$k\frac{\partial T}{\partial n}=\sigma\varepsilon(T^4-T_a^4) \tag{3.20}$$

where T denotes the temperature at any point, k represents the thermal conductivity (k=1/ρ), Q is the heat generation per unit of area, q is the heat transfer rate crossing a boundary, h is a convective heat transfer coefficient, σ is the Stefan-Boltzmann constant, ε is the surface emissivity, T_0 is a specified surface temperature and T_a is the ambient exchange temperature of convection or radiation.

The variational statement for two dimensional problems involves minimizing a double integral. The idea of variational calculus presented in Appendix A can be extended to the problem of finding a minimum for the integral

$$I = \iint \varphi(x, y, u, u_x, u_y)\, dx\, dy \tag{3.21}$$

The resulting Euler-Lagrange equation for the case of a specified value of u on the boundaries turns out to be

$$\frac{\partial \varphi}{\partial u} - \frac{\partial}{\partial x}\left(\frac{\partial \varphi}{\partial u_x}\right) - \frac{\partial}{\partial y}\left(\frac{\partial \varphi}{\partial u_y}\right) = 0 \tag{3.22}$$

We then work backward from the differential equation (3.16) and find the variational statement for the problem. It can be simply stated that minimizing the function

$$I = \frac{1}{2} \iint_{\Omega} \left[k\left(\frac{\partial T}{\partial x}\right)^2 + k\left(\frac{\partial T}{\partial y}\right)^2 - 2QT \right] dx\, dy \tag{3.23}$$

while requiring that equations (3.17) and (3.18) with $q = 0$ to be satisfied, is equivalent to solving equations (3.16). The expression in equation (3.23) is also applicable to problems with a variable thermal conductivity and generation rate. It is therefore more general than equation (3.16).

It will be more convenient to separate I into two parts and to generalize the problem by considering an arbitrary region of interest Ω. Consequently, equation (3.23) will be rewritten as

$$I = I_k - I_g \tag{3.24}$$

where

$$I_k = \frac{1}{2} \iint_{\Omega} \left[k\left(\frac{\partial T}{\partial x}\right)^2 + k\left(\frac{\partial T}{\partial y}\right)^2 \right] dxdy$$

and

$$I_g = \iint_{\Omega} Q\,T\,dx\,dy$$

The finite element will be used to solve equation (3.16) for the unknown temperature by minimizing the integral function defined by (3.23). The detailed mathematical derivations of such problem are stated in Appendix A that contains the basic formulation of the finite element method. Following the derivation in Appendix A, an expression for the gradient of the integral I with respect to nodal temperature $\mathbf{T}$ is obtained as follows:

$$\frac{dI}{d\mathbf{T}} = \mathbf{K}\ \mathbf{T} - \mathbf{g} = 0 \tag{3.25}$$

which represents a set of linear algebraic equations to be solved for the nodal temperatures $\mathbf{T}$. where $\mathbf{K}$ and $\mathbf{g}$ are referred to as the conduction matrix and the generation vector respectively.

3.4.2.1 Boundary Conditions

Whether a heat transfer solution is implemented using finite element modeling or any other tool, solvable heat conduction problems should also have boundary conditions well defined. The variational statement necessary to handle these boundary conditions is more complicated than equation (3.23), which is valid for boundary conditions of either specified temperature or zero heat flux. A more general variational statement is [85]

$$I = \frac{1}{2}\iint_{\Omega}\left[k\left(\frac{\partial T}{\partial x}\right)^2 + k\left(\frac{\partial T}{\partial y}\right)^2\right]dx\,dy - \iint_{\Omega} QT\;dx\,dy + \frac{1}{2}\int_{B_h} h(T^2 - 2T_a T)\;ds - \int_{B_q} qT\,ds \tag{3.26}$$

The two double integrals are over the region of interest Ω as before. Two new terms have been introduced to handle the two new types of boundary conditions. However, the first of these new terms is an integral along the boundary of the region Ω where a convective heat transfer boundary condition is given and the heat convection loss coefficient (h) is specified. The second term is an integral over that portion of the boundary where the heat flux (q) into the region from the outside has been specified. Minimization of the function I in equation (3.26) will solve the problem pictured in Figure 3.3.

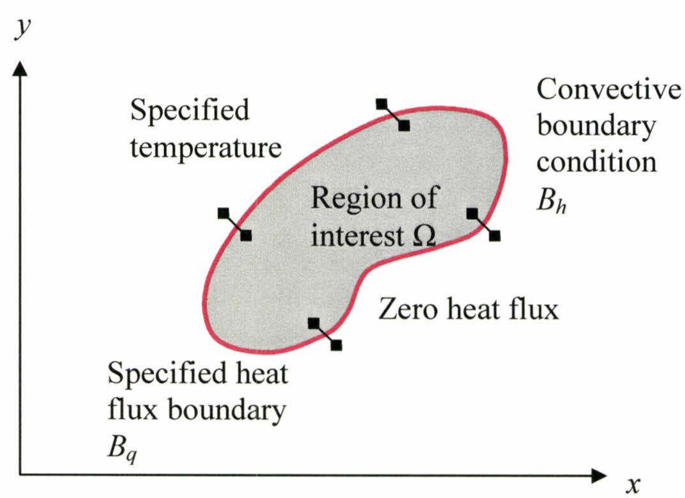

Fig. 3.2 General two-dimensional, steady state conduction problem

Equation (3.26) will be separated into parts each one represents a certain term:

$$I = I_k - I_g + I_h - I_q \tag{3.27}$$

We want to set the derivative of this with respect to the nodal temperatures equal to zero. That is, we want

$$\frac{dI}{d\mathbf{T}} = \frac{dI_k}{d\mathbf{T}} - \frac{dI_g}{d\mathbf{T}} + \frac{dI_h}{d\mathbf{T}} - \frac{dI_q}{d\mathbf{T}} = 0 \tag{3.28}$$

We have already considered the first two terms in appendix A. They are given by equations (A.37) and (A.45). Now we must consider the two new terms that arise from the boundary conditions.

Corresponding to equation (A.25) we can write

$$\frac{dI_h^e}{d\mathbf{T}} = \mathbf{D}_s^e \frac{dI_h^e}{d\mathbf{T}_s^e} \quad \text{or} \quad \frac{dI_q^e}{d\mathbf{T}} = \mathbf{D}_s^e \frac{dI_q^e}{d\mathbf{T}_s^e} \tag{3.29}$$

where $\mathbf{D}_s^e = \begin{array}{c} \begin{bmatrix} 0 & 0 \\ \vdots & \vdots \\ 0 & 0 \\ 1 & 0 \\ 0 & 1 \\ 0 & 0 \\ \vdots & \vdots \\ 0 & 0 \end{bmatrix} \end{array} \begin{array}{l} \\ \\ \\ \leftarrow i\text{th row} \\ \leftarrow j\text{th row} \\ \\ \\ \\ \end{array}$

We have only considered one side of element e, between nodes i and j, to have a convection or specified heat flux boundary condition. If two sides have such boundary conditions, we would have to consider the element twice.

To simplify the integration along the boundary, we will use the coordinate direction s along the boundary as shown in Figure 3.4. The assumed linear temperature distribution then reduces to the following expression along the boundary

$$T_s^e = c_1 + c_2\, s \tag{3.30}$$

or in a matrix form

$$T_s^e = \mathbf{s}^{\mathrm{T}}\, \mathbf{c}^e \tag{3.31}$$

where

$\mathbf{s}^{\mathrm{T}} = [\, 1 \quad s \,]$ and $\mathbf{c}^e = \begin{bmatrix} c_1 \\ c_2 \end{bmatrix}^e$

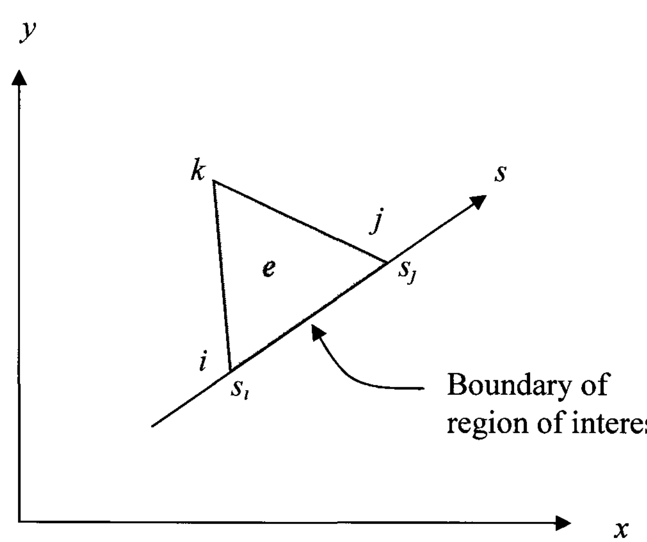

Fig. 3.3 Finite element at surface

Although we have assumed a linear temperature distribution between the two nodes as before, these coefficients are not the same ones we mentioned earlier because we are using a different coordinate system. The coefficients c_1 and c_2 may be evaluated by insisting that T^e be equal to the nodes temperatures T_i and T_j at edges of the segment. Thus we would have

$$\mathbf{T}_s^e = \mathbf{S}^e \, \mathbf{c}^e \tag{3.32}$$

where $\mathbf{T}_s^e = \begin{bmatrix} T_i \\ T_j \end{bmatrix}$ and $\mathbf{S}^e = \begin{bmatrix} 1 & s_i \\ 1 & s_j \end{bmatrix}$

The constants $\mathbf{c}^e$ may then be found by multiplying equation (3.32) by inverse of $\mathbf{S}^e$ which will be assigned as $\mathbf{Z}^e = (\mathbf{S}^e)^{-1}$

$$\mathbf{c}^e = \mathbf{Z}^e \, \mathbf{T}_s^e \tag{3.33}$$

where $\mathbf{Z}^e = \dfrac{1}{s_{ij}} \begin{bmatrix} s_j & -s_i \\ -1 & 1 \end{bmatrix}$ and $s_{ij} = s_i - s_j$

This result may be substituted into equation (3.31) to arrive at the following expression for the temperature distribution within the element

$$T_s^e = \mathbf{s}^{\mathrm{T}} \, \mathbf{Z}^e \, \mathbf{T}_s^e \tag{3.34}$$

Let us first consider the convective boundary condition. For an element with a convective boundary condition along the side of element e between node points i and j, we may write

$$I_h^e = \frac{h^e}{2} \int_{s_i}^{s_j} (T_s^{e\,2} - 2T_a^e \, T_s^e) \, ds \tag{3.35}$$

This assumes the element is small enough so that h^e can be satisfactorily treated as a constant and removed from the integral.

Equation (3.34) may now be substituted for the boundary temperature to give

$$I_h^e = \frac{h^e}{2} \int_{s_i}^{s_j} \left[(\mathbf{s}^{\mathrm{T}} \mathbf{Z}^e \mathbf{T}_s^e)^2 - 2T_a^e (\mathbf{s}^{\mathrm{T}} \mathbf{Z}^e \mathbf{T}_s^e) \right] ds \tag{3.36}$$

Upon differentiating with respect to $\mathbf{T}_s^e$, we get

$$\frac{dI_h^e}{d\mathbf{T}_s^e} = \frac{h^e}{2} \int_{s_i}^{s_j} \left[2(\mathbf{s}^{\mathrm{T}} \mathbf{Z}^e \mathbf{T}_s^e)(\mathbf{s}^{\mathrm{T}} \mathbf{Z}^e)^{\mathrm{T}} - 2T_a^e (\mathbf{s}^{\mathrm{T}} \mathbf{Z}^e)^{\mathrm{T}} \right] ds \tag{3.37}$$

It is more convenient to consider the above as two integrals

$$\frac{dI_h^e}{d\mathbf{T}_s^e} = h^e \int_{s_i}^{s_j} \mathbf{Z}^{e\mathrm{T}} \mathbf{s}\mathbf{s}^{\mathrm{T}} \mathbf{Z}^e \mathbf{T}_s^e \, ds - h^e T_a^e \int_{s_i}^{s_j} \mathbf{Z}^{e\mathrm{T}} \mathbf{s} \; ds \tag{3.38}$$

Since $\mathbf{Z}^e$ and $\mathbf{T}_s^e$ are independent of s, they may be removed from the integral to give

$$\frac{dI_h^e}{d\mathbf{T}_s^e} = h^e \mathbf{Z}^{e\mathrm{T}} \left[\int_{s_i}^{s_j} \mathbf{s}\mathbf{s}^{\mathrm{T}} \, ds \right] \mathbf{Z}^e \mathbf{T}_s^e - h^e T_a^e \mathbf{Z}^{e\mathrm{T}} \int_{s_i}^{s_j} \mathbf{s} \, ds \tag{3.39}$$

The matrix integration can now be carried out to obtain the following result

$$\frac{dI_h^e}{d\mathbf{T}_s^e} = \mathbf{H}_s^e \mathbf{T}_s^e - \mathbf{h}_s^e \tag{3.40}$$

where $\mathbf{H}_s^e = \dfrac{h^e s_{ij}}{6}\begin{bmatrix} 2 & 1 \\ 1 & 2 \end{bmatrix}$ and $\mathbf{h}_s^e = \dfrac{h^e s_{ij} T_a^e}{2}\begin{bmatrix} 1 \\ 1 \end{bmatrix}$

Equation (3.40) can now be substituted into equations (3.29) and the results summed over all the elements that have a convection boundary to give

$$\frac{dI_h}{d\mathbf{T}} = \sum_{e=1}^{E_h} \mathbf{D}_s^e (\mathbf{H}_s^e \mathbf{T}_s^e - \mathbf{h}_s^e) \tag{3.41}$$

The summation may be split into two parts, and the matrix $\mathbf{T}_s^e$ may be replaced by the product of the transpose of $\mathbf{D}_s^e$ and $\mathbf{T}$ as we have done in equation (A.34) of appendix A.

$$\frac{dI_h}{d\mathbf{T}} = \sum_{e=1}^{E_h} \mathbf{D}_s^e \mathbf{H}_s^e \mathbf{D}_s^{e\mathrm{T}} \mathbf{T} - \sum_{e=1}^{E_h} \mathbf{D}_s^e \mathbf{h}_s^e \tag{3.42}$$

It is again convenient to define global matrices to replace the summations in the above equation. Thus we will define

$$\mathbf{H}_s = \sum_{e=1}^{E_h} \mathbf{D}_s^e \mathbf{H}_s^e \mathbf{D}_s^{e\mathrm{T}} \quad \text{and} \quad \mathbf{h}_s = \sum_{e=1}^{E_h} \mathbf{D}_s^e \mathbf{h}_s^e$$

With these definitions, equation (3.42) may simply be stated as

$$\frac{dI_h}{d\mathbf{T}} = \mathbf{H}_s \mathbf{T} - \mathbf{h}_s \tag{3.43}$$

This result will later be substituted into equation (3.28) as the contribution from the convective boundary term.

Now let us consider the specified heat flux boundary conditions. We have defined I_q in equation (3.27) so that, for a specified heat flux into the region along the side of element e between nodal points i and j, we may write

$$I_q^e = q^e \int_i^j T_s^e \, ds \tag{3.44}$$

We are again using surface coordinates to describe the node position. We have also assumed that the element is small enough so that q^e may be treated as a constant and removed from the integral.

Equation (3.34) may now be substituted for the surface temperature in equation (3.44) to give

$$I_q^e = q^e \int_i^j \mathbf{s}^{\mathrm{T}} \, \mathbf{Z}^e \, \mathbf{T}_s^e \, ds \tag{3.45}$$

Differentiating with respect to $\mathbf{T}_s^e$ and moving the constant matrix from the integral, gives

$$\frac{dI_q^e}{d\mathbf{T}_s^e} = q^e \, \mathbf{Z}^{e^{\mathrm{T}}} \int_i^j \mathbf{s} \; ds \tag{3.46}$$

The integration and the matrix multiplication can now be carried out to give

$$\frac{dI_q^e}{d\mathbf{T}_s^e} = \mathbf{q}_s^e \tag{3.47}$$

where the element surface heat flux matrix is given by

$$\mathbf{q}_s^e = \frac{q^e s_{ij}}{2}\begin{bmatrix}1\\1\end{bmatrix}$$

Equation (3.47) can now be substituted in equation (3.29) and the result summed over all the elements that have a specified heat flux boundary condition. This may be written as

$$\frac{dI_q}{d\mathbf{T}} = \sum_{e=1}^{E_q} \mathbf{D}_s^e \mathbf{q}_s^e \tag{3.48}$$

This can be further simplified by defining a global surface heat flux matrix as

$$\mathbf{q}_s = \sum_{e=1}^{E_q} \mathbf{D}_s^e \mathbf{q}_s^e \tag{3.49}$$

With this definition, the equation can be simplified to:

$$\frac{dI_q}{d\mathbf{T}} = \mathbf{q}_s \tag{3.50}$$

The global matrix is constructed by summing up all such element matrices. The complete problem may be formulated by substituting equations (3.25), (3.43) and (3.50) into equation (3.28) to give

$$\frac{dI}{d\mathbf{T}} = \mathbf{KT} - \mathbf{g} + \mathbf{H}_s\mathbf{T} - \mathbf{h}_s - \mathbf{q}_s = 0 \tag{3.51}$$

We arrange equation (3.51) in the form of a set of algebraic equations which are solved for the unknown nodal temperatures **T**.

$$(\mathbf{K} + \mathbf{H}_s)\mathbf{T} = \mathbf{g} + \mathbf{h}_s + \mathbf{q}_s \tag{3.52}$$

It can be observed that the problem of imposing the boundary conditions has the same general form that was obtained earlier. The matrix **K** must now be modified by the addition of $\mathbf{H}_s$, and the matrix **g** must be modified by the addition of $\mathbf{h}_s$ and $\mathbf{q}_s$. The system of equations given by equation (3.52) may be written as

$$\mathbf{A}\,\mathbf{T} = \mathbf{b} \tag{3.53}$$

3.4.2.2 Advanced Problem of Radiation Boundary Condition

In the case of underground cable systems, non-linear boundary conditions were not imposed. Thus, solution of the differential equation reduces to the solution of a linear algebraic system of equations. However, for the problem considered here, boundary radiation will be treated. In the general case, this non-linearity will force an iterative solution. Radiation is hard to handle by exact analytical method because of its dependence on the fourth power of the temperature. Equation (3.20) is considered for the inclusion of the radiation boundary condition. For convenience, we define a radiation heat transfer $h_r(T)$ [36]:

$$h_r(T) = \sigma\varepsilon(T^2 + T_a^2)(T + T_a) \tag{3.54}$$

so that (3.20) can be expressed as

$$k\frac{\partial T}{\partial n} = h_r\,(T - T_a) \tag{3.55}$$

It has the same appearance as (3.19). The radiation boundary condition can be treated as the convectional boundary, as was illustrated in the pervious section. But on the other hand, the radiation heat transfer $h_r(T)$ is not constant, rather, it is a variable since it depends on the unknown boundary temperature. Therefore, a linearization or iteration will be used to overcome the difficulty. The problem may be linearized by assuming that the value of T at the radiation boundary may be close enough to be replaced by the ambient temperature T_a

$$h_r(T) = 4\sigma\varepsilon T_a^3 \tag{3.56}$$

The radiation heat transfer coefficient is now a constant and can be treated exactly as in (3.40) by substituting the value of the radiation coefficient.

For the case in which the boundary temperature is not close to T_a, this linearization will not be adequate and the nonlinear equation must be handled directly. An iterative procedure has to be adopted to find the finite element solution of the problem of (3.52). The solution of (3.52) can be found by applying the Newton-Raphson iteration method as follows:

- For the first iteration n= 0, set $h_r^{(0)} = 4\sigma\varepsilon T_a^3$
- Substitute the value of h_r into (3.40)
- Solve equation (3.52) and find **T**
- Compute the average of two nodal temperatures setting on radiation boundary $T_{av} = (T_i + T_j)/2$
- Find $h_r^{(n)} = \sigma\varepsilon(T_{av}^2 + T_a^2)(T_{av} + T_a)$
- If n>1, test the convergence of the method

  $$\left|\frac{h_r^{(n)} - h_r^{(n-1)}}{h_r^{(n-1)}}\right| \le \delta_1 \quad \text{and} \quad \left\|\mathbf{T}^{(n)} - \mathbf{T}^{(n-1)}\right\| \le \delta_2$$

where δ_1 and δ_2 are specified small numbers. If either of the inequalities are not satisfied, set the new iteration as n= n+1 and repeat the above analysis starting from the second step.

Thermal analysis of cable systems is a topic that has received considerable attention by many researchers. In typical analyses, non-linear boundary conditions resulting from radiation have been addressed. In the cases where the influence of radiative heat exchange at the air-soil interface on the thermal behaviour of the cable can be ignored, noticeably simplified modeling and computation can be obtained. In such cases, the system of algebraic equations becomes linear owing to the domain being discretized. Thermal radiation heat transfer has certainly been considered by various authors but, as it was not the main objective of their research, they considered it in a somewhat approximate manner. This problem has been considered in a more detailed formulation, for steady-state conditions [86]. The evolution of radiative and convective heat transfer was proposed in [40] to study the field of temperature for systems of buried cables. From the results, the authors stated that avoiding radiative heat transfer completely implies minor temperature differences from the ones obtained considering the radiative boundary condition at the air-soil interface. The authors also stated that the magnitudes of these differences are such that the influence of radiative heat exchange at the air-soil interface on the thermal behaviour of the cable can be ignored, this analysis was extended by the authors to the case of a conductor being overloaded and, in this case too, the influence of radiative heat transfer was noticed to be negligible.

3.5 SPECIFIC FEATURE RELATED TO POWER CABLE THERMAL ANALYSIS

The modeling of an underground cable system becomes a very complicated problem due to the involvement of many parameters regarding the cable configuration in the installation, the nature of the soil surrounding the cable trench (multi-soil) and the seasonal variations (temperature, precipitation and solar waves). In modern systems, one trench might include many cables carrying different kinds of signals (electrical, phone, television....etc.) in the vicinity of other trenches with pipes carrying fluids or steam. However, the simple equation used by Neher-McGrath to find the cable ampacity and the temperature distribution around is not appropriate due to the unrealistic assumptions and the complexity of the problem. The numerical approach is more flexible in adapting to the cable system installation.

The proposed finite element model can be used to determine the maximum temperatures to be associated with different cable loadings. Another practical usage will be the investigation of trench dimensions effects, cable diameter and soil properties on the heat dissipated from a buried cable as well as the evaluation of the effects caused by environmental and weather variations on the temperature distribution. Furthermore, in the case of multi-cable systems, the effect of the spacing between the cables can be investigated. Consequently, this will give an insight, in many practical cable systems, into the important parameters that have a great influence on the total ampacity of the system. In this work thermal behaviour is evaluated, considering comprehensive boundary conditions taking into account the mechanism of radiative and convective heat transfer at the soil-air interface.

The maximum cable ampacity is a function of all internal and external cable system components which comprise the thermal circuit of the cable and its boundaries. The parameters of the thermal circuit of power cable are subjected to geographical and seasonal changes which affect the allowable loading level of any particular cable. The proposed perturbed finite element analysis technique provides useful sensitivity information of the cable ampacity, with respect to fluctuations in the cable circuit parameters, to assess the effects on the permissible cable loading caused by these fluctuations without repeating the whole thermal analysis for each possible parameter change. In addition, the technique applies to both the design phase and the operational aspects of power cables buried in complex media of soil, heat sources and skins and variable boundary conditions. Because the simulation procedure for various parameter variations does not involve repeated finite element analyses, the results can be obtained by very fast and compact scheme and displayed in efficient, straightforward manner. Since only one nominal finite element analysis is required, a larger element grid can be employed allowing more accurate modeling. The sensitivity information is useful not only in evaluating the cable ampacity subject to various parameter changes but also in determining the important and non-important parameter variations in terms of their relative effect on the cable temperature and ampacity. The finite element sensitivity technique can be applied to complex cable configurations and boundaries to assess the effect of variations of various soil and boundary parameters.

The design problem of selecting the optimal parameter values of the thermal circuit parameters including the thermal conductivities, boundary conditions and heat generation is formulated using a multi-dimensional gradient optimization method. The technique offers the flexibility of defining the objective functions of interest subjected to upper and lower bounds on the design parameters, linear system of equations constraints, or nonlinear constraints. The technique consideration of sensitivity coefficients associated with various thermal circuit parameters enhances the reliability and security of the developed model. Furthermore, the objective function may contain any of the cable system temperatures of interest, selected cables' ampacity, or any considered thermal circuit parameters (thermal conductivity or boundary conditions). On the other hand, constraints could be designed in order to simulate a certain cable performance and may include node temperatures, cable ampacity, or thermal circuit parameters. This general form optimization model gives the capability of simulating and designing various typical cable system configurations for the purpose of different practical applications. For example, one practical problem would be optimizing the cable system parameters in order to reduce surface cable temperatures which will result in increasing the cable current carrying capacity and enhancing the overall cable performance. In some practical cases, the objective would be minimizing the cost associated with the cable backfill subject to a maximum permissible cable temperature. Another case would be concerned in ampacity maximization by selecting the optimal thermal circuit parameters.

CHAPTER 4

PERTURBED THERMAL FIELD ANALYSIS FOR POWER CABLE SENSITIVITY EVALUATION

4.1 INTRODUCTION

Over the past 25 years, various numerical techniques have been developed to calculate the permissible loading of power cable which is normally limited by a maximum cable system temperature determined by thermal characteristics of its insulation. The maximum cable ampacity is a function of all internal and external cable system components which comprise the thermal circuit of the cable and its boundaries.

In conventional techniques, the cable ampacity is based on assumed fixed values of cable thermal circuit parameters including soil resistivity and heat transfer coefficients at the boundaries. The parameters of the thermal circuit of power cable are subjected to geographical and seasonal changes which affect the allowable loading level of any particular cable. Therefore, sensitivities of the cable ampacity with respect to fluctuations in the cable circuit parameters are needed to assess the effects on the permissible cable loading caused by these fluctuations without repeating the whole thermal analysis for each possible parameter change. The sensitivity information is useful not only in evaluating the cable ampacity subject to various parameter changes but also in determining the important and non-important parameter variations in terms of their relative effect on the cable temperature and ampacity. The finite element sensitivity technique can be applied to complex cable configurations and boundaries to assess the effect of variations of soil and boundary parameters. Unfortunately, the finite element technique does not allow an explicit expression of the cable temperature in terms of cable thermal circuit parameters. However, the sensitivity coefficients associated with various cable parameters of interest provides the cable engineers with important information about relative effects of such parameters variations on the cable performance, which helps in design of a new system and improving the performance of existing systems.

In this chapter, a new approach to cable thermal field and ampacity computations using a proposed concept of perturbed finite element analysis will be formulated. This involves the use of derived sensitivity coefficients associated with various cable parameters of interest, and using such sensitivity coefficients to achieve optimal cable performance. The technique is applied to both the design phase and the operational aspects of power cable buried in a complex media of soils, heat sources and sinks and variable boundary conditions. Because the simulation procedure for various parameter variations does not involve repeated finite element analyses, the results can be obtained by a very fast and compact scheme from which the results may be displayed in an efficient and straightforward manner. Since only one nominal finite element analysis is required, a larger element grid can be employed allowing more accurate modeling.

Also, a new approach to the cable thermal circuit optimization for the purpose of cable ampacity improvement is proposed. The optimization model was developed based generated gradient to ensure secure and reliable algorithm. It allows the selection of thermal circuit parameters as well as the cable temperatures in the objective and constraint functions. The problem of calculating the gradient of an objective function which depends implicitly on the temperature is overcome by engaging the perturbed finite element in the optimization routine. Consequently, at each iteration, an accurate thermal field profile with sensitivity coefficients associated with various cable optimized parameters could be used to calculate the objective function and to ensure descent in the appropriate search direction.

4.2 DESCRIPTION OF THE NOVEL CONCEPT OF PERTURBED THERMAL FIELD ANALYSIS FOR POWER CABLE SENSITIVITY ANALYSIS

4.2.1 Thermal Field Computation

The thermal field in the cable medium is governed by the differential equation as was noted in Chapter 3

$$\nabla \cdot (k\ \nabla T) = -\,Q + c\,\frac{\partial T}{\partial t} \tag{4.1}$$

where T denotes the temperature at any point, k and c represent, respectively, the thermal conductivity and capacity, Q is the heat generation per unit of area and t denotes the time.

In steady state thermal analysis of two-dimensional media, equation (4.1) reduces to

$$\frac{\partial}{\partial x}\left(k\frac{\partial T}{\partial x}\right) + \frac{\partial}{\partial y}\left(k\frac{\partial T}{\partial y}\right) + Q = 0 \tag{4.2}$$

For any homogenous region of given thermal conductivity and heat generation rate, equation (4.2) can be solved for the temperature at any point in the region subjected to specified boundary conditions. The power cable thermal circuit includes various regions of complicated shapes having different values of thermal conductivity and heat generation and equation (4.2) should be solved for the overall cable medium. The formulation of the finite element method was described in Chapter 3 (equation 3.23). It was shown that the solution of equation (4.2) is that which minimizes the function

$$I = \tfrac{1}{2}\iint\left[k_x\left(\frac{\partial T}{\partial x}\right)^2 + k_y\left(\frac{\partial T}{\partial y}\right)^2\right]dx\,dy\ -\ \iint Q\ T\ \ dx\,dy \tag{4.3}$$

The boundary condition on the circumference, Γ_1 of the cable system such as the ground surface may be represented as a convection boundary, where the derivative of the temperature on this boundary in a direction normal to the boundary is proportional to the temperature difference with respect to the ambient temperature:

$$k\frac{\partial T}{\partial n} = h(T - T_a) \tag{4.4}$$

where h is convection loss coefficient and T_a is the ambient temperature.

For another case, consider the circumference, Γ_2 where the heat transfer rate q crossing such boundary has been specified, the boundary condition is given by

$$k\frac{\partial T}{\partial n} = q \tag{4.5}$$

In order to handle the mentioned types of boundary conditions, two new terms have been added to (4.3), as was shown in Chapter 3 (equation 3.26)

$$I = \frac{1}{2}\iint\left[k\left(\frac{\partial T}{\partial x}\right)^2 + k\left(\frac{\partial T}{\partial y}\right)^2\right] dx\,dy - \iint Q\,T\;dx\,dy + \frac{1}{2}\int_{\Gamma_1} h(T^2 - 2T_a\,T)\;d\Gamma_1 - \int_{\Gamma_2} q\,T\,d\Gamma_2 \tag{4.6}$$

The discretization of the domain is the first step in the finite element analysis. In this step, the entire domain is subdivided into a number of small domains, characterized as the element e. The second step of the finite element analysis is to select an interpolation function that provides an approximation of unknown solution within an element. Once the order of the polynomial is selected, the problem is formulated in terms of the unknown function T at nodes associated with the elements. Assume that a triangular element shape was selected, then the nodes associated with the element e are numbered j = 1, 2, 3 and the temperature at any point (x,y) within the element can be expressed linearly in terms of the nodes temperatures as:

$$T^e = \sum_{j=1}^{3} N_j^e T_j^e \tag{4.7}$$

N_j^e are the linear interpolation function of x and y which also known as basis functions.

The minimization of (4.6) is performed over each individual finite element defined by the associated nodes. By assembling these individual approximations, the collection of elements corresponding to (4.6) is usually of the form

$$\sum_{e=1}^{E} \left\{ \begin{aligned} &\sum_{j=1}^{3} T_j^e \iint_{\Omega^e} \left(k \frac{\partial N_i^e}{\partial x} \frac{\partial N_j^e}{\partial x} + k \frac{\partial N_i^e}{\partial y} \frac{\partial N_j^e}{\partial y} \right) dx\, dy - \iint_{\Omega^e} Q\, N_i^e \, dx\, dy \\ &+ \sum_{j=1}^{3} T_j^e \int_{\Gamma_1} h\, N_i^e\, N_j^e \; d\Gamma_1 - T_a \int_{\Gamma_1} h N_i^e \, d\Gamma_1 - \int_{\Gamma_2} q\, N_i^e \, d\Gamma_2 \end{aligned} \right\} = 0 \qquad i = 1,2,3 \tag{4.8}$$

where i and j are the node numbers, Ω^e is the area of the element e, E is the total number of elements.

The above expression may be formulated in a matrix form yielding a set of sparse equations of the form:

$$\mathbf{A}\ \mathbf{T} = \mathbf{b} \tag{4.9}$$

where **T** is a column vector of node temperatures, **A** is a global conductivity matrix and **b** is the global load vector.

For the finite element analysis we specify the following cable parameters:

i. The cable current I (*amperes*).
ii. The ambient temperature T_a at all part of the soil surface (^oC).
iii. The thermal conductivity k of any portion of the cable circuit including backfill and duct bank ($W/(^oC.\ m)$).
iv. Heat generation Q in certain circuit portions (W/m).
v. The heat flux coefficient q at certain circuit boundaries (W/m^2)
vi. The heat convection loss coefficient h at a certain circuit boundaries ($W/(^oC.\ m^2)$).
vii. The emissivity radiation coefficient ε at a certain circuit boundaries.

4.2.2 Sensitivity Analysis

Both the conductivity matrix **A** and load vector **b** are functions of the thermal circuit parameters. Both the matrix **A** and the vector **b** are adjusted to accommodate the boundary conditions of the thermal circuit as it appears in the last three (boundary) terms in (4.8). Consequently, the conductivity matrix and the load vector of equation (4.9) are functions of the cable loading, circuit parameters and boundary conditions.

The sensitivities of the conductivity matrix and the load vector with respect to the individually various thermal circuit parameters can be carried out by differentiating the FEM equations shown in (4.8) with respect to the indicated parameters to give

$$\frac{\partial \mathbf{A}}{\partial k} = \sum_{e=1}^{E} \left\{ \sum_{j=1}^{3} T_j^e \iint_{\Omega^e} \left(\frac{\partial N_i^e}{\partial x} \frac{\partial N_j^e}{\partial x} + \frac{\partial N_i^e}{\partial y} \frac{\partial N_j^e}{\partial y} \right) dx\, dy \right\}$$

$$\frac{\partial \mathbf{A}}{\partial h} = \sum_{e=1}^{E} \left\{ \sum_{j=1}^{3} T_j^e \int_{\Gamma_1} N_i^e N_j^e \, d\Gamma_1 \right\}$$

$$\frac{\partial \mathbf{b}}{\partial Q} = -\sum_{e=1}^{E} \iint_{\Omega^e} N_i^e \, dx\, dy \tag{4.10}$$

$$\frac{\partial \mathbf{b}}{\partial h} = -\sum_{e=1}^{E} T_a \int_{\Gamma_1} N_i^e \, d\Gamma_1$$

$$\frac{\partial \mathbf{b}}{\partial q} = -\sum_{e=1}^{E} \int_{\Gamma_2} N_i^e \, d\Gamma_2$$

$$\frac{\partial \mathbf{A}}{\partial Q} = \frac{\partial \mathbf{A}}{\partial q} = \frac{\partial \mathbf{b}}{\partial k} = 0$$

It is worth mentioning that the formulation above is global and the thermal conductivity, k indicated above may vary from domain to domain to reflect different thermal conductivities in different portions of the thermal circuit. Similarly, other parameters may change from domain to domain due to variation of the material or due other considerations.

The thermal circuit parameters arranged as a column vector $\mathbf{p}$ where m represents the total number of selected parameters and $p_1,..p_k,..p_m$, are the selected parameters of interest such as native soil thermal conductivity, backfill thermal conductivity, heat generation inside the cables and heat convection losses at certain portion of system boundaries.

$$\mathbf{p} = [p_1 \; p_2 \; .... \; p_k \; ....p_m]^T \tag{4.11}$$

The temperature sensitivities can be carried out in the general matrix form by differentiating equation (4.9) with respect to thermal circuit parameters of interest defined in the vector form of (4.11). However, by substituting the sensitivities of the conductivity matrix and the load vector given by (4.10) with respect to each appropriate parameter, the temperature sensitivity would be the only unknown in the following resulting system of equations

$$\mathbf{A(p)}\left(\frac{\partial \mathbf{T(p)}}{\partial \mathbf{p}}\right)=\left(\frac{\partial \mathbf{b(p)}}{\partial \mathbf{p}}\right)-\left(\frac{\partial \mathbf{A(p)}}{\partial \mathbf{p}}\right)\mathbf{T(p)} \tag{4.12}$$

The linear system of equation can now be solved in order to find out the sensitivity matrix ($\partial\mathbf{T}/\partial\mathbf{p}$) of the node temperatures with respect to the selected thermal parameters. The sensitivity matrix, which will be denoted by **S,** has M rows represent the node temperatures and m columns, each one representing the sensitivity vectors associated with a certain parameter [$\partial\mathbf{T}/\partial p_k$].

Unfortunately, in the finite element technique an explicit expression of the cable temperature in terms of cable thermal circuit parameter is not possible. However, using sensitivity coefficients associated with various cable parameters of interest, a reasonably accurate representation of the cable temperature can be accomplished. The change in the temperature vector **T** resulting from a change in some or all parameters is given, to a first order approximation, by

$$\mathbf{T}=\mathbf{T}^{o}+\left(\frac{\partial \mathbf{T}}{\partial \mathbf{p}}\right)_{\mathbf{p}^{o}}\left[\mathbf{p}-\mathbf{p}^{o}\right] \tag{4.13}$$

where $\mathbf{T}^{o}$ denotes the vector of nodes temperatures at base-case (nominal) parameter values $\mathbf{p}^{o}$.

The use of the cable temperature sensitivities with respect to various cable circuit parameters is the key factor in replacing the numerous temperature evaluations for all possible parameters by fewer temperature evaluations which, in conjunction with the temperature sensitivities, are sufficient to describe the cable temperature. The presented novel finite element based sensitivity technique enables cable temperature sensitivity with respect to all parameters to be evaluated in an efficient and fast way. In the finite element sensitivity technique, complex cable, soil and boundary conditions can be simulated accurately in the thermal model leading to a more accurate temperature prediction.

4.3 CONCEPT OF ZONAL SENSITIVITY COEFFICIENTS AND GROUP PARAMETER VARIATION IMPACTS

In practical application, a decomposed form of **A** (by triangular factorization) is calculated only once and stored as basic information for the cable system. Using this decomposed form, the solution of (4.9) is obtained by simple forward and backward substitutions for any defined right hand side vector in equation (4.12) associated with a cable circuit parameter **p**. By examining these sensitivity values for various parameters of the cable circuit, the most important parameters associated with higher sensitivities can be identified and ranked according to their relative effects on cable temperature and, hence, on cable ampacity.

The finite element sensitivity technique can be applied to complex cable configurations and boundaries to asses the effects of variations of various soil and boundary parameters. Some parameters have a great impact on certain considered temperature nodes and, consequently, these parameters can be classified in groups associated with certain zones of the finite element mesh under consideration.

If a set of temperature nodes $\mathbf{T_i}$ represent a considered zone of interest, and $\mathbf{p_j}$ represents a set (group) of parameters which are classified in a number of groups, based on their effects on the chosen zones, then equation (4.13) can be rewritten in the form of zonal sensitivity coefficients and parameters groups as

$$\mathbf{T_i} = \mathbf{T_i^o} + \sum_{j=1}^{n_g} \left(\frac{\partial \mathbf{T_i}}{\partial \mathbf{p_j}} \right)_{\mathbf{p^o}} \left[\mathbf{p_j} - \mathbf{p_j^o} \right] \qquad \mathbf{i} = 1 : n_z \tag{4.14}$$

where n_g represents the number of parameters groups and n_z represents the number of sensitivity coefficient zones. In equation (4.14), a certain zonal sensitivity coefficient $[\partial \mathbf{T_i}/\partial \mathbf{p_j}]$ is set to zero if the correlation between temperatures of zone **i** and impact of parameters group **j** is neglected.

4.4 PARAMETERS DISTRIBUTION EFFECTS ON SENSITIVITY EVALUATION

For a typical triangular element of the finite element mesh whose vertices are *i*, *j* and *m*, the entries of conductivity matrix **A** at rows and columns corresponding to these vertices are a function of the thermal conductivity of the soil portion associated with the element defined by these vertices. More specifically, each diagonal element (*i*,*i*) of the conductivity matrix is a function of the summation of the thermal conductivities of the attached elements connected to the node *i*. These elements may have the same conductivities if they belong to the same medium, but when node *i* is on a border between media, each element will have a value of the thermal conductivity for the medium to which it belongs. On the other hand, each off-diagonal element (*i*,*j*) is a function of the thermal conductivities of the joint elements which have common sides connecting the two elements. Moreover, for any node *n* which does not have a direct contact with node *i* through one of the elements sides, the corresponding conductivity matrix element (*i*,*n*) will vanish. This can be illustrated by the subdomain consisting of a number of elements shown in Figure 4.1, the corresponding contributions of chosen nodes *i*, *j* and *m* is shown.

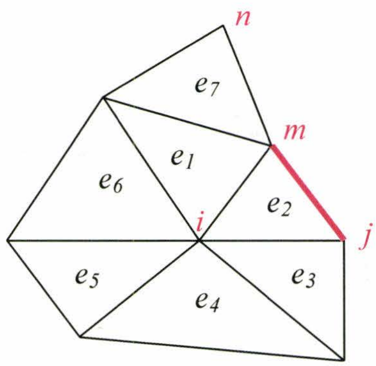

Fig. 4.1 Subdivision of two-dimensional domain

$$
\mathbf{A}=\begin{array}{c} \\ i \\ \\ j \\ \\ m \\ \\ \end{array}
\begin{array}{c}
\begin{array}{ccccccc} i & & j & & m & & \end{array}\\
\begin{bmatrix}
f(k_{e_1}+\cdots+k_{e_6}) & \cdots & f(k_{e_2}+k_{e_3}) & \cdots & f(k_{e_1}+k_{e_2}) & \cdots \\
\vdots & & \vdots & & \vdots & \\
f(k_{e_2}+k_{e_3}) & \cdots & f(k_{e_2}+k_{e_3}+C_\Gamma) & \cdots & f(k_{e_2}+C_\Gamma) & \cdots \\
\vdots & & \vdots & & \vdots & \\
f(k_{e_1}+k_{e_2}) & \cdots & f(k_{e_2}+C_\Gamma) & \cdots & f(k_{e_1}+k_{e_2}+k_{e_7}+C_\Gamma) & \cdots \\
\vdots & & \vdots & & \vdots &
\end{bmatrix}
\end{array},
\quad
\mathbf{b}=\begin{array}{c} i \\ \\ j \\ \\ m \\ \\ \end{array}
\begin{bmatrix}
f(Q_1+\cdots+Q_6) \\ \vdots \\ f(Q_2+Q_3+c_\Gamma) \\ \vdots \\ f(Q_1+Q_2+c_\Gamma) \\ \vdots
\end{bmatrix}
$$

C_Γ: is the boundary contribution in the conductivity matrix

c_Γ: is the boundary contribution in the load vector

f: is the function relate the parameter value to the geometrical data of given element

$$C_\Gamma=\begin{cases} h & \text{convective boundary} \\ 0 & \text{heat flux boundary} \end{cases}$$

$$c_\Gamma=\begin{cases} hT_a & \text{convective boundary} \\ q & \text{heat flux boundary} \end{cases}$$

This demonstrates the nature of the conductivity matrix which thus needs to be considered during solving such linear systems of equations. Also, it shows the effect of node numbering on the conductivity matrix bandwidth, the numbering should be done in an efficient way such that a small semi-bandwidth will be obtained. On the other hand the load vector **b** contains the element internal heat generations. The load vector row (i) is a function of heat generation summation of all elements connected with this node (node is one of the element vertices).

Now let us explore the effect of imposing the boundary condition on the structure of the conductivity matrix and load vector. In the case of a convective boundary condition, the heat convection losses coefficient h will contribute to the conductivity matrix at entries defined by rows and columns corresponding to the nodes set on the boundary, while the ambient temperature will not have any effect on the conductivity matrix. The load vector will be a function of the product of heat convection losses coefficient and ambient temperature at rows corresponding to these boundary nodes. In the case of a heat flux boundary, no effect will arise on the conductivity matrix. This kind of boundary affects the load vector, which will be a function of the heat flux q at rows corresponding to boundary nodes. When a convective boundary or a heat flux boundary is defined on the boundary Γ enclosed by nodes i and j as shown in figure 4.1, the corresponding effect is illustrated for both cases simultaneously as shown above.

It is important to determine the appearance of each parameter of the thermal circuit in the global conductivity matrix and load vector before starting the sensitivity analysis, so as to avoid zero elements in certain portions of **A** and **b**. This step results in a more computationally efficient system if we consider the sparse nature of the conductivity matrix and load vector. After locating the incidence of each parameter of interest in the conductivity matrix and load vector, the evaluation of the sensitivity with respect of each parameter is performed in a straight forward manner as was explained in section 4.2.

4.5 SPECIAL COMPUTATION PROCEDURES TO SPEED UP CALCULATIONS

The importance of determining the location of each parameter in the conductivity matrix and load vector was discussed in the previous section, and the advantage of avoiding dealing with vanished entries was illustrated. Using the same allocation concept, another important advantage can be achieved when dealing with a consecutive sensitivity analysis. As it was mentioned in previous sections, each element in **A** and **b** depends on an interaction of corresponding element geometrical and thermal specifications.

The geometrical specification remains fixed for the same system configuration while the thermal specification is related to associated thermal parameters values, which are affected by the operating and environmental conditions. In this case, for each parameter, associated locations in **A** and **b** are stored in the relevant matrix which also contains the geometrical weight associated with it in **A** and **b**. This matrix is stored once, and when the thermal specification is changed during uncontrolled fluctuation conditions or during extensive optimization procedures, the sensitivity can be performed using the invariant allocation matrix. By substituting the new operating thermal parameter to construct the system defined in (4.12) the computation cost is reduced.

Furthermore, the associated matrix stores only the non-zero elements of the conductivity matrix and load vector, which results in less storage memory. Also the resultant sparse structure of the conductivity matrix itself helps in employing special linear system solvers of sparse linear systems which allow utilization of their advantages in reducing the computational cost.

4.6 OPTIMIZATION FORMULATION

This section introduces the combination of thermal field calculations and the nonlinear optimization into one routine of analysis. The thermal analysis is based on the finite element technique in conjunction with the perturbed sensitivity technique. Consequently, an accurate thermal field profile and sensitivity coefficients associated with various cable optimized parameters, provide the optimization routine, respectively, with temperature values and relative effects of such parameters variations on the temperature variation.

4.6.1 General Form

For a specific underground cable system configuration, it can be anticipated that once the cable construction, installation and loading are determined, the temperature distribution depends only on the thermal properties of the surrounding soil and the ambient temperature. That is, the temperature profile will be a function of the soil parameters, ambient parameters and loading

$$\mathbf{T} = f(\mathbf{p}) = f(p_1, p_2, \ldots\ldots, p_m) \tag{4.15}$$

The mentioned thermal parameters can be considered in the cable system design by appropriate designs of the objective function in order to achieve the desired optimal performance. The temperature which is already a function of these parameters can be implemented in the objective function and constraints to give a more flexible design. The optimization problem can be written in the following form:

$$\begin{array}{ll} \underset{\mathbf{p}}{\text{minimize}} & f(\mathbf{T},\mathbf{p}) \\ \text{subject to} & h(\mathbf{T},\mathbf{p})=0 \\ & g(\mathbf{T},\mathbf{p})\leq 0 \end{array} \tag{4.16}$$

where f: $\Re^m \rightarrow \Re$, h: $\Re^m \rightarrow \Re^v$, g: $\Re^m \rightarrow \Re^l$, m is the number of variables (parameters), v is number of equality constraints, and l is number of inequality constraints.

The objective function (f) has to be minimized subject to the equality and inequality constraints. The objective function is selected according to the design problem. In the form of (NLP) the problem is general, it includes as special cases linear and quadratic programs in which the constraint function, h and g are affine and f is linear or quadratic. The objective function may contain any of the temperatures of interest of the cable system, selected cables ampacity, or any considered thermal circuit parameters (thermal conductivity or boundary conditions). On the other hand, constraints could be designed in order to simulate a certain cable performance and may include node temperatures, cable ampacity, or thermal circuit parameters.

4.6.2 Smooth Nonlinear Optimization (NLP) Problems

A smooth nonlinear programming (NLP) or nonlinear optimization problem is one in which the objective or at least one of the constraints is a smooth nonlinear function of the decision variables. Nonlinear functions may be convex or non-convex. A quadratic programming (QP) problem is a special case of a smooth nonlinear optimization problem, but it is usually solved by specialized, more efficient methods [87, 88].

NLP problems and their solution methods require nonlinear functions that are continuous, and (usually) further require functions that are smooth, which means that derivatives of these functions with respect to each decision variable, i.e. the function gradients, are continuous. An NLP problem where the objective and all constraints are convex functions can be solved efficiently to global optimality, up to very large size, interior point methods are normally very effective on the largest convex problems. But if the objective function or any constraints are non-convex, the problem may have multiple feasible regions and multiple locally optimal points within such regions.

There are a variety of methods for solving NLP problems, and no single method is best for all problems. The most widely used and effective methods are the Generalized Reduced Gradient (GRG) and Sequential Quadratic Programming (SQP) methods, both called active-set methods, and the Interior Point or Barrier methods[88].

NLP solvers generally exploit the smoothness of the problem functions by computing gradient values at various trial solutions, and moving in the direction of the negative gradient. They usually also exploit second derivative information to follow the curvature as well as the direction of the problem functions. To solve constrained problems, NLP solvers must take into account feasibility and the direction and curvature of the constraints as well as the objective [89].

4.6.3 Sensitivity-Optimization

In formulations of many practical problems, the objective function and constraints will be implicit in terms of temperature (ampacity). In this case the calculation of the objective function will not be a straightforward matter, and the rigorous perturbed finite element is needed to provide the optimization routine with the temperature profile required to evaluate the objective function and/or constraints; furthermore, it provides the optimization routine with the gradient of the objective function and/or constraint with respect to the temperature (ampacity).

Given an objective function $f(\mathbf{T},\mathbf{p})$ to be minimized by selecting suitable changes (deviations from a base-case value) $\Delta\mathbf{p}$ which will result in a decrease in objective function, the optimization algorithm is briefly stated as follows:

1. Choose a starting point $\mathbf{p}^{o}$ (where the index counter c=0), calculate the corresponding nominal temperatures $\mathbf{T}^{o}$, and then calculate the corresponding objective function $f^{o}(\mathbf{T}^{o}, \mathbf{p}^{o})$.

2. Use the finite element sensitivity analysis to evaluate the sensitivity matrix $\mathbf{S}^{c}$, which represents the variations of the temperatures with respect to the selected optimized parameters of interest.

3. Compute the search direction by calculating the gradient vector:

$$\frac{df}{d\mathbf{p}^{c}} = \frac{\partial f}{\partial \mathbf{p}^{c}} + (\mathbf{S}^{T})^{c}\,\frac{\partial f}{\partial \mathbf{T}^{c}} \tag{4.17}$$

CHAPTER 5

SIMULATION SOFTWARE CODING

5.1 BACKGROUND

The general structure of the developed software programs is presented in this chapter. The model was based on the proposed perturbed finite element algorithm for the underground cable system thermal analysis. This includes solving the thermal field, performing a sensitivity analysis and optimizing the cable performance for different circumstances. Generality of the developed software and the capability to deal with different kinds of applications was preserved, where different complicated boundary conditions and configurations can be handled easily. The overall model can be classified in several modules as follows:

- User input data preparation
- Generation of the discretization domain mesh
- Processing of the thermal and geometrical specification arrays
- Temperature evaluation
- Sensitivity analysis
- Finite element gradient generation
- Optimization analysis

5.2 UNIQUE FEATURE OF SENSITIVITY-BASED FINITE ELEMENT SIMULATION SOFTWARE DEVELOPMENT CODE

The finite element method is well established as a technique for solving engineering problems, and this may be applied to model heat conduction in non-homogeneous media. The proposed method of the perturbed finite elements was introduced to study the general performance of buried power cable and parameter evaluation procedures for the purpose of advanced thermal analysis and ampacity calculations. In this section, the preprocessing aspects and also typical uses of the method in the assessment of underground cable system thermal fields are presented. This involves solving the thermal field of a cable system. The method needs to handle complex configurations, boundaries, and heat sources, as well as optimizing cable performance and sensitivity analysis under varying loading and environmental conditions. The numerical technique used incorporates a general algorithm, which simulates the real cable installation configuration. The total program structure is divided into several individual modules connected to each other and incorporated in order to construct a comprehensive thermal field model for optimizing the underground power cable performance. All application-specific software modules used were developed during the course of this thesis

5.2.1 Mesh Editing

However, in the finite element method the solution domain must be discretized by means of nodes and elements, also, their geometrical, topological, and property definitions must be specified. The preparation of this input data can be very time consuming and severely impair the ease with which engineers can use the finite element method for tackling cable problems [90]. To overcome this, a preprocessing routine has been developed which, when coupled with the input user file, allows meshes of buried cables to be quickly generated and loaded. The method comprises the following steps:

1. The whole region is first divided into subregions (conductor, insulator, backfill, trench, and mother soil), each one has its associated thermal specifications.

2. The finite element mesh is generated in the specified regions based on the linear triangular elements. The size of generated elements is not fixed, but it varies based on the temperature gradient. Small elements will be located near the conductor where the temperature gradient is high, while the size of elements is increased as we move further away from the conductor, where the temperature gradient is low. Obviously, this general concept of refining the mesh in areas of

high heat transfer helps to maintain optimal accuracy at low computation cost. Material properties can be assigned to the elements and, therefore, separate properties may be specified for the backfill, soil and other media if present.

3. As a result of the meshing process in the specified region, the elements and their nodes will be labeled and the node coordinates are determined. The ordering process will be performed in an efficient way such that a small semi-bandwidth will be obtained for the subsequent finite element calculations.

4. Before initiating the finite element analysis, thermal boundary conditions and loading must be applied to the mesh. The ground surface may be held at constant temperature, or natural convection or radiation conditions may be applied. Conductor, dielectric and sheath losses may be included as heat generation rates in the relevant material regions. These loading and boundary conditions are defined with the associated geometrical definitions in an input user file and then manipulated by the preprocessing routine to indicate the relevant elements or boundary nodes.

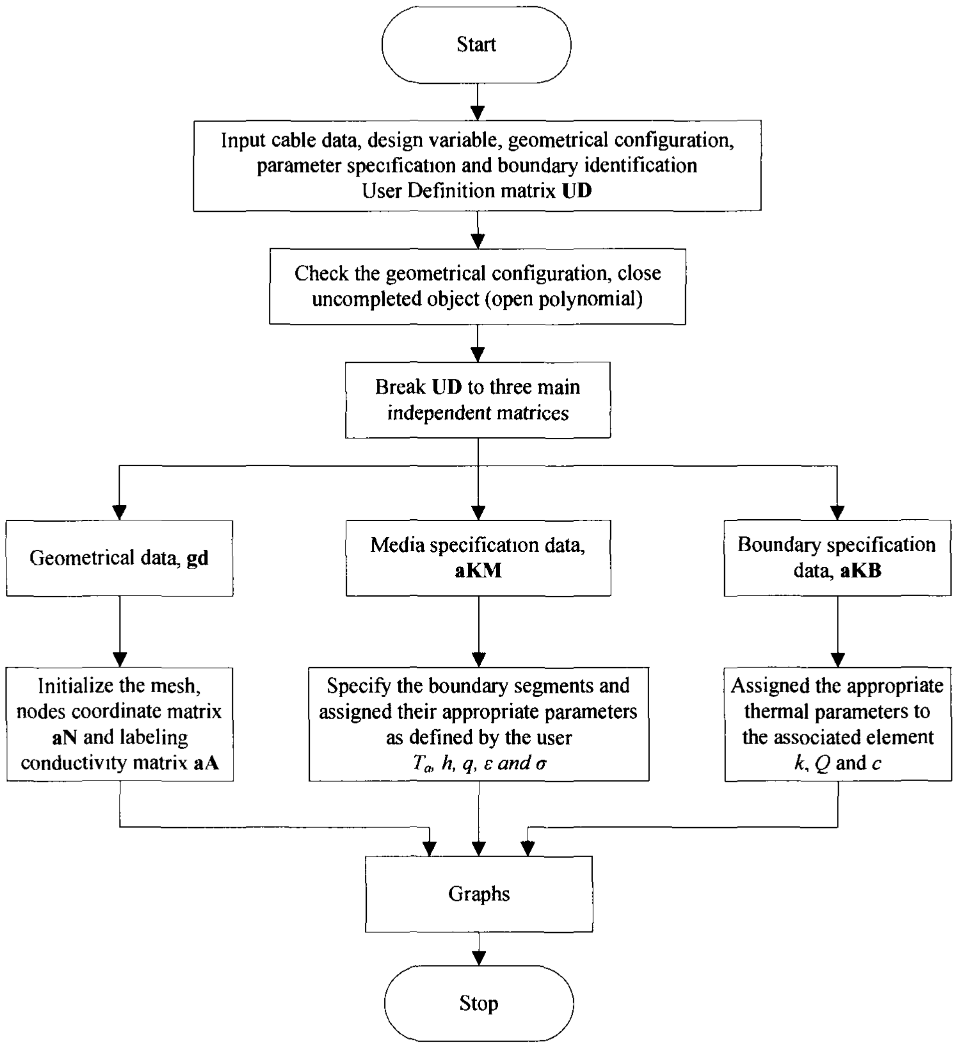

Fig. 5.1 Preprocessing block diagram

5.2.2 Thermal Field Solver

The thermal field solver was constructed to use the mesh, geometrical and properties data provided by the preprocessing routine in order to apply the finite element algorithm and solve the thermal field of the underground cable system. This routine will perform the following tasks:

1. Both the global elements conduction matrix and the global generation vector are constructed based on the algorithm illustrated in chapter three.

2. The user-specified boundary conditions must be imposed on the solution domain. Consequently, both conduction matrix and generation vector will be adjusted to accommodate the boundary conditions of the thermal circuit.

3. The final step in this routine is to solve the linear system of equations comprised by the conduction matrix and generation vector for the unknown node temperatures. Various built-in MATLAB functions are employed in this routine to provide the user with the choice of using the compatible function solver according to the conductivity matrix size and structure.

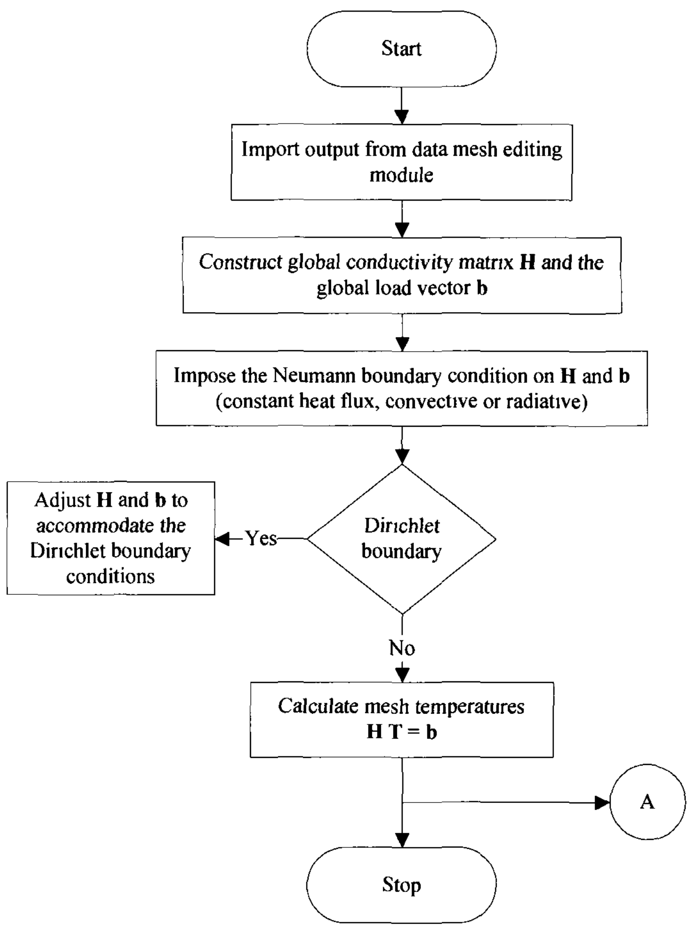

Fig. 5.2 Thermal solver block diagram

5.2.3 Result Display

Two user interactive routines are provided to give the various alternatives choices of the model and field display:

1. The first display routine is constructed to display the system model geometry and discretization, the mesh labeling (nodes and elements numbers, which can be imposed on the mesh) and the system defined boundaries.

2. The second display routine provides the user with the options of displaying the temperature distribution in one of these forms:

    - Temperature contours with auto-set contours, contours with defined number of levels or contours at specified temperature data.
    - Temperature distribution in three dimensions imposed on the model geometry.
    - Syllabic two dimensional displays, where the temperature is displayed with respect to one chosen axis at constant value on the other axis.

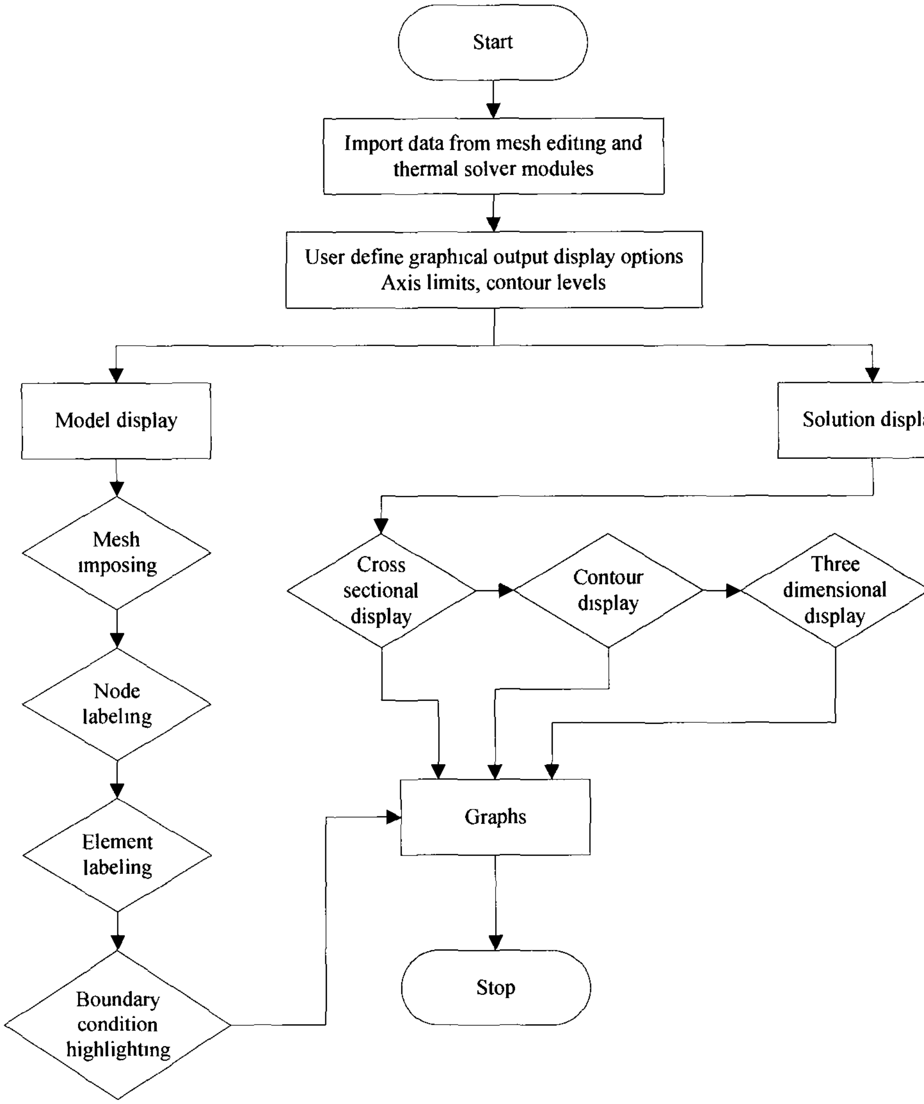

Fig. 5.3 Displayer block diagram

5.2.4 Sensitivity Analysis

A sensitivity methodology based on the finite element model, in which various cable environmental parameters are modeled accurately, was constructed in order to provide the user with temperature sensitivity with respect to fluctuations in the cable circuit parameters. Because of its flexibility, it is possible to consider all the parameters that influence the heat dissipation such as:

- Installation geometry, including the dimensions of the cable components, trench and backfill.
- Thermal and physical properties of the surrounding soil.
- Model parameters associated with all possible types of boundary conditions.

This module task will involve the following:

1. The derivation of the conduction matrix and generation vector are calculated, respectively, and stored in global sparse form with respect to all thermal circuit parameters. Each parameter group is gathered and assigned by index number defined by the user; make it easer to distinguish the related elements of this group. This squeezing out of the nodes which are not in interaction with the given circuit parameter, makes the module more storage efficient and preserves the globalized form of construction. It has to be mentioned that while the two global matrices are geometry dependent, they are independent of the physical properties and boundary condition. In another words, they are not affected by the chosen base-case temperature solution. Consequently, these two general matrices are formulated once and stored in order to carry out the sensitivities at any operating point.

2. The routine extracts the temperature solution from the thermal field solver for a defined base-case thermal field solution. Also the user defines the circuit parameters of interest with respect to which the sensitivity will be calculated.

3. Using the above extracted and derived data, determination of temperatures sensitivities with respect to the specified thermal parameter is carried out by solving a linear system of equations as was illustrated in chapter four.

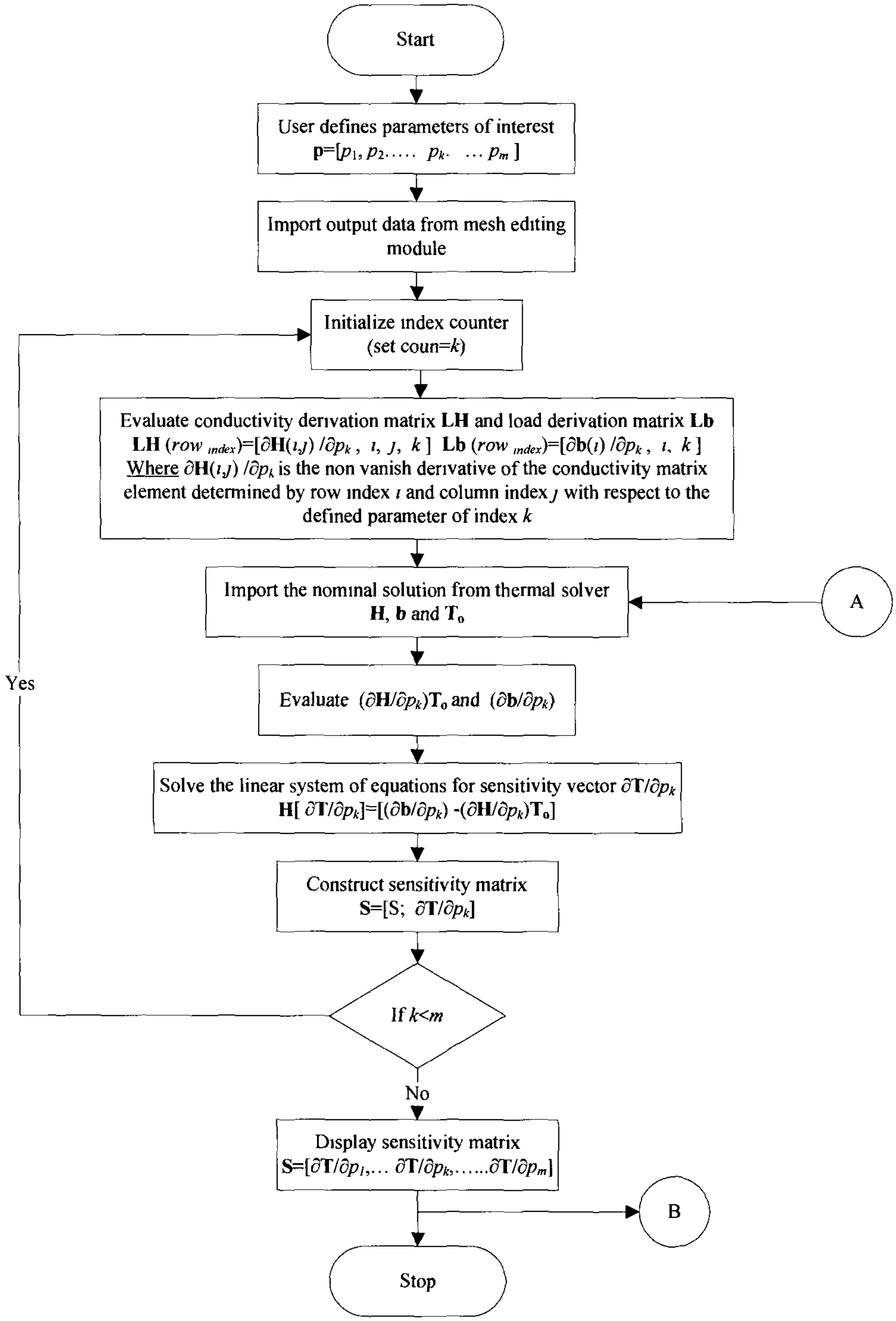

Fig. 5.4 Sensitivity module block diagram

5.2.5 Zonal Sensitivity Analysis

The new concept of the sensitivity methodology can be extended and exploited to cover wide regions of new practical applications. In many practical cases, designers are interested in studying a particular factor in specific range of the complete solution domain. However, this developed module is employed in order to facilitate user interaction in such a way that the desired information can be extracted in a straightforward manner with efficient computation cost. This module involves the following tasks:

1. User defines specific geometries in order to determine the temperatures nodes of interest. In this regard, the user can define a line, rectangle, or circle. Each user-defined geometry will be addressed by an identification number and will be treated as an individual object, where there is no limit on the number of defined objects. However, by defining an object, the user can choose one of these options: nodes inside the object body will be considered, nodes lying on the object boundary will be considered or nodes in proximity to the object boundary will be considered.

2. Usually, multiples of physical properties or boundary parameters are available in the system configuration. However, each physical property parameter will be associated with a certain zone of the whole system mesh defined by their enclosed elements. On the other hand, each boundary parameter will be associated with a portion of the selected system borders defined by their nodes. In this module the user has the capability to define his own zone which may contain one or multiple parameters of interest considered totally or partially, which will be treated as one combined group. Consequently, the sensitivities of the thermal field are considered with respect to a defined group of parameters.

3. User defines specific geometry and address type of the parameter which will be considered in this geometry (thermal conductivity, heat convection losses coefficient, etc.). User has the choice to take all parameters of this kind or just to select one. User can define various shapes including complicated geometry, making it easier to achieve the desired goal. User can define a line, rectangle, circle, ellipse or polynomial of any random shape.

4. The module starts to extract the associated elements in the conduction matrix and generation vector based on the selected parameter group, and then drive the associated derivations with respect to these groups.

5. Based on the user selections, a zonal temperature vector, a derivation of the conduction matrix and generation vector with respect to selected parameter groups are calculated. Consequently, the sensitivity of zonal temperature vector with respect to the selected parameter groups will be calculated by solving the linear system of equations associated with each group as illustrated in chapter four.

5.2.6 Optimization Analysis

The optimal cable design for user defined objective function and constraints is considered in this module. The sensitivity information is extracted and utilized in the optimization routine, this feature opens the scope of user choice to cover completed objective and constraints functions implicit in terms of the temperature and ampacity. This generality will be pursued by using a smooth nonlinear optimization solver. In order to accomplish this mission, the following tasks have to be done:

1. User has to define the desired objective function and constraints (if any) which may be in terms of all the thermal circuits parameters, temperatures or cable ampacities. Furthermore, user has to determine the thermal circuit parameter of

interest which will be optimized as well as the nominal starting values of these parameters.

2. Built-in MATLAB functions are embedded in the routine's core. The user is allowed to choose suitable functions based on the designed problem. This will cover unconstrained optimization, upper and lower limits on controlled parameters, equality and inequality constraints or nonlinear constraints.

3. The routine starts calculating the objective function which has to be minimized and the associated constraints at each iteration starting from the user provided operating point. This task will include solving the thermal field and performing the sensitivity analysis using the finite element solver and sensitivity module, respectively, in case the objective function and/or constraints functions are implicated in temperatures.

4. The sensitivity information is exploited to calculate the gradient values at each iteration and moving in the direction of the negative gradient as illustrated in chapter four.

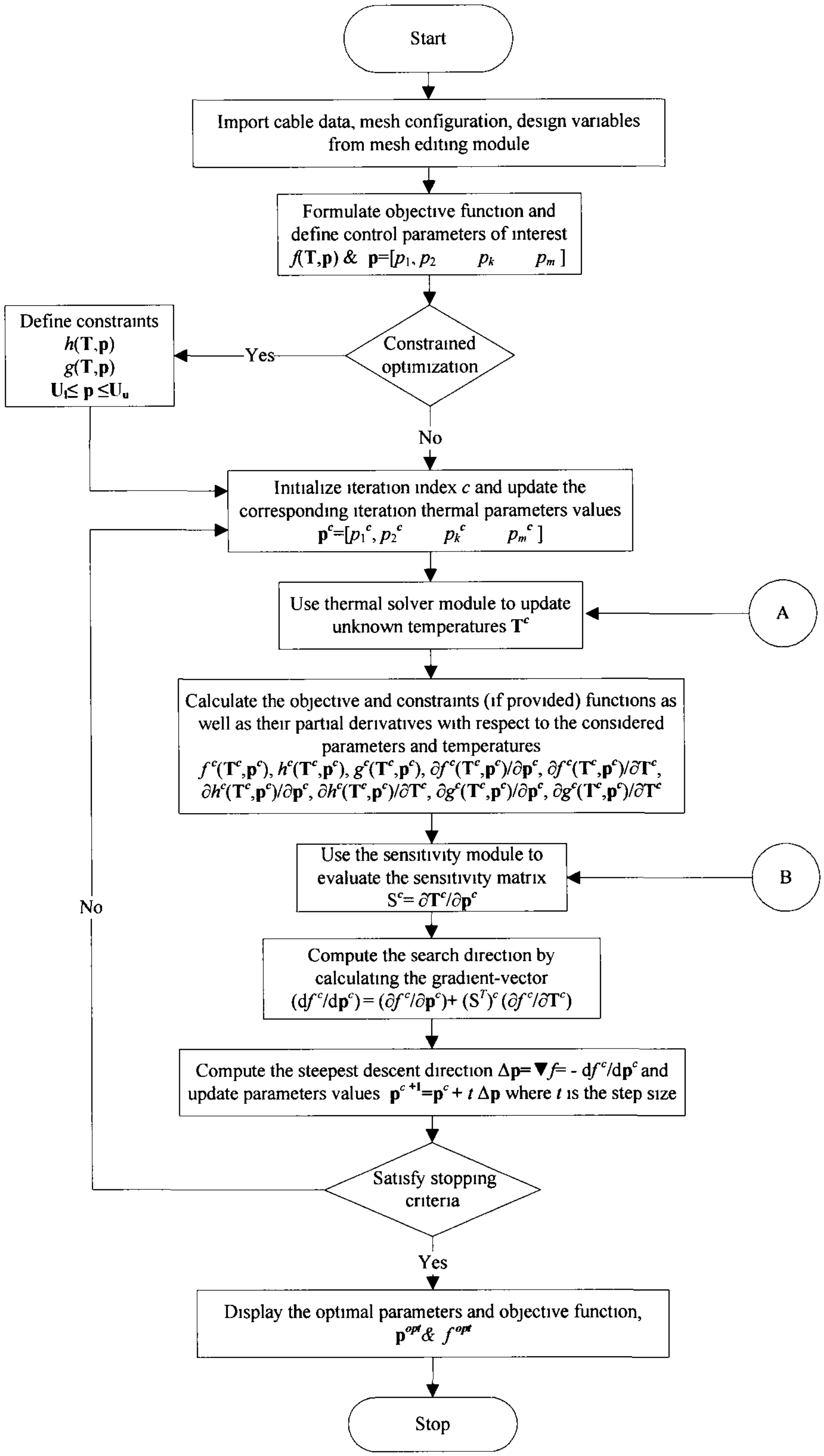

Fig. 5.5 Optimization module block diagram

The following block diagram describes the main structure of the software program developed during the course of study:

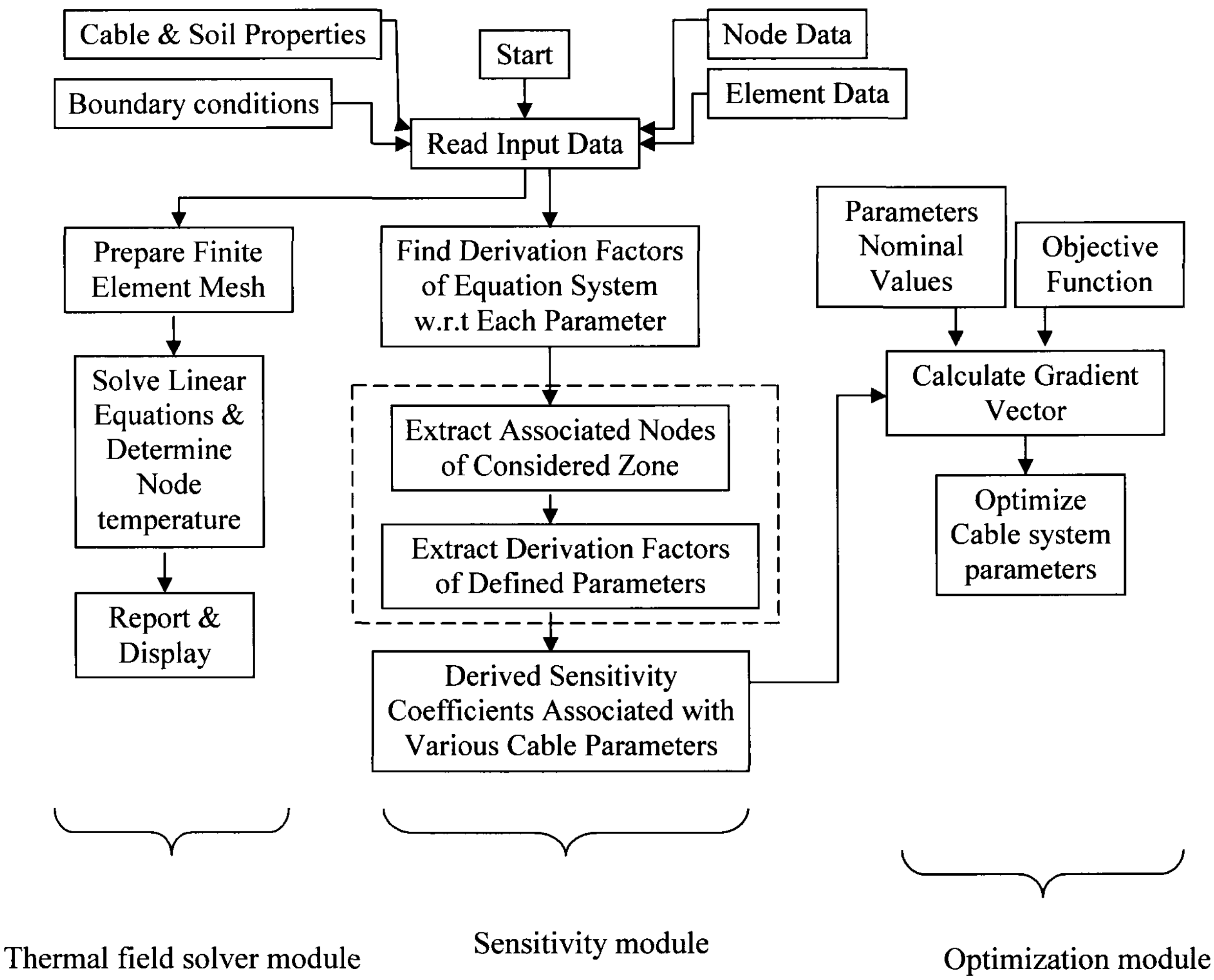

Fig. 5.6 Software-program general structure

CHAPTER 6

LABORATORY EXPERIMENTAL VERIFICATION

6.1 OVERVIEW

The heat transfer and temperature distribution in power cable systems have been studied numerically and experimentally in the present research work. The heat transfer mechanism in cable systems was modeled and solved using the proposed finite element method, which was merged with sensitivity and optimization analysis to introduce the concept of perturbed finite element formulation. As the new concept has been built substantially based on the developed thermal simulation model, this chapter will investigate the thermal behaviour of underground power cable by laboratory experiments and use it for the model validation. The heat transfer analysis of a 15 kV XLPE underground power cable is investigated under different loadings using a full size experimental setup to analyze the behaviour of the underground cables directly buried in sand and soil. The developed experimental model was simulated using proposed thermal finite element tools and the obtained results were compared with the experimental results to validate the developed simulation methodology.

The better the understanding of the thermal parameters' influence on the thermal behaviour, the better the modeling accuracy and substantially, the better the correspondence of the model obtained results with the experimental measurements. The performance of an underground transmission and distribution system is critically influenced by thermal properties of the medium in which it is placed, as well as the thermal properties of the cable it self. Unfortunately, the thermal behaviour of the cable is strongly dependent on the loading conditions, thermal parameters of the cable materials as well as thermal specifications of the surrounding soil, ambient environment and boundary conditions. First, the thermal specification of the used soil was tested by stimulating high temperature gradient along the body of tested sample enclosed by a heat source-heat sink pair facing each other. In the second part, the 15 kV XLPE underground power cable is energized as heat source as in actual case, the thermal field under different spots and loadings was investigated using a full size experimental setup to monitor the thermal behaviour of the underground cables, surrounding soil and boundaries phenomena.

6.2 DESCRIPTION OF EXPERIMENTAL VERIFICATION SETUP

It is necessary to know the temperature distribution around buried cables and situations that can arise during use as accurately as possible. In the field, soil temperature and moisture changes with depth as well as with seasons. Thus, a one time in-site measurement gives a set of parameters true only for that location and time. However, through laboratory analysis of the undisturbed sample one can simulate other conditions and their influences. In this regard, the heat transfer analysis of a 15 kV XLPE underground power cable is investigated under different loadings using a full size experimental setup to analyze the behaviour of the underground cables directly buried in sand and soil. The developed experimental model was also simulated using the proposed thermal finite element tools and the obtained results were compared with the experimental results to validate the simulation methodology.

Unfortunately, soil thermal resistivity is the major parameter affecting the current rating of underground power cable but also least understood [91-94]. An evaluation of the thermal properties of the soil surrounding the underground transmission lines is an important part of the design procedure for underground power cable. In this regard, the thermal properties of the soil sample used in backfilling underground power cables of the Saudi Electricity Company in the central region were investigated using a laboratory setting. Thermal specification of the soil was tested by establishing a high temperature gradient along the body of the sample, enclosed by a heat source-heat sink pair facing each other. An intensive grid of thermocouple probes were used to observe and record the temperature of the tested soil at different selected spots.

Laboratory test facilities were required to simulate the operation of buried electrical transmission cables and to test the thermal behaviour of the tested soil sample using a large scale experimental design:

1. The main unit is the container, which was filled with the soil containing the tested cable. It is a wooden box having approximate dimensions of 154×111×124 cm (W×H×D) placed in the laboratory and designed to be portable, with a removable roof to allow accessibility to the box internal contents, as shown in Figure 6.1, 6.2 and 6.3

2. Thermal specification of the used soil was tested by stimulating high gradient along the container width using heat-source heat-sink provided in the container design.

3. Actual cable samples of XLPE 15 kV were laid in inside the container. Soil surrounded the cable. Then the cable was subjected to a certain load (300A and 600A) in order to examine the thermal behaviour inside the cable and at points surrounding the cable.

4. A high current transformer connected through circuit breakers was used to load the tested cable. The current transformer was used to step up the supply current to the required high current level (300A and 600A) needed to test the cable.

5. Thermocouple probes (50 probes) were used to record the temperature of specific points of the cable (external surface, insulation) as well as the surrounding soil and ambient temperatures. The thermocouple probes were distributed inside the container in three different similar layers each with a different height level. Probes are suspended on the intersections of the shown grid in Figure 6.1.

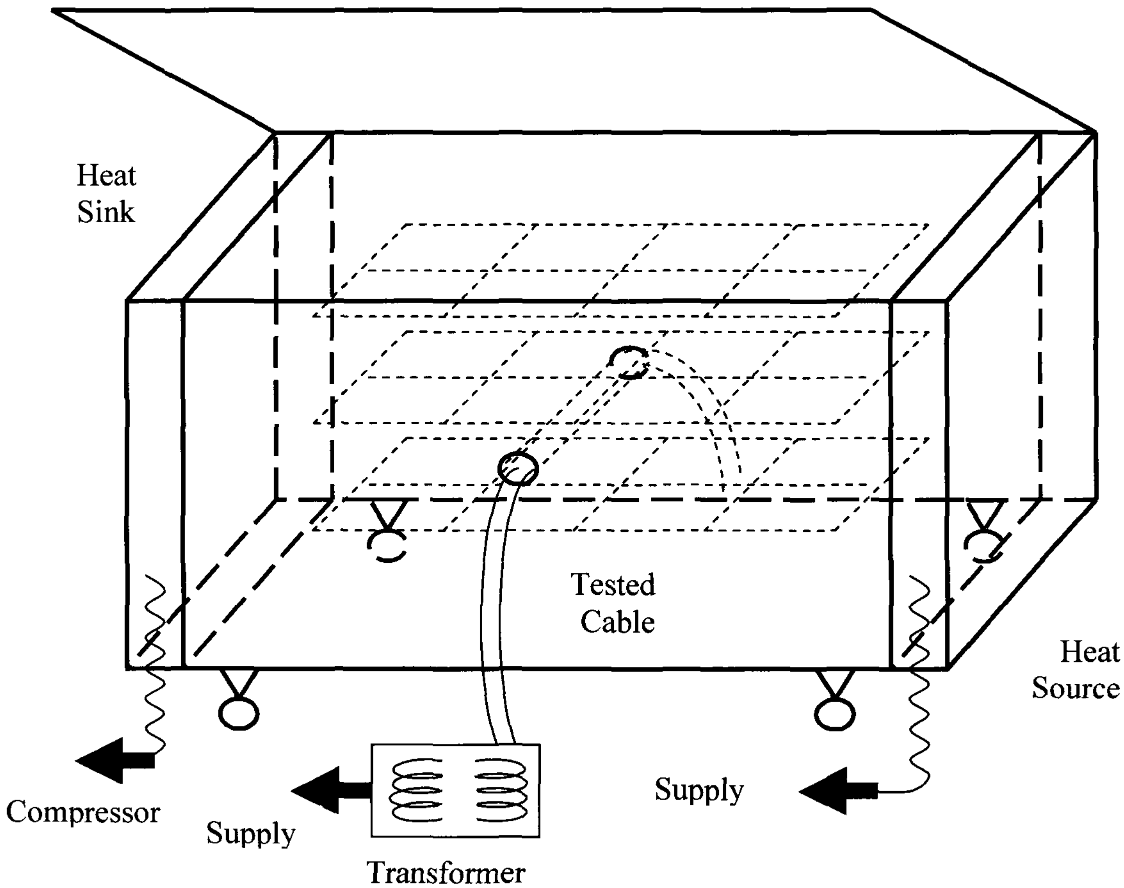

(a) Soil box configuration

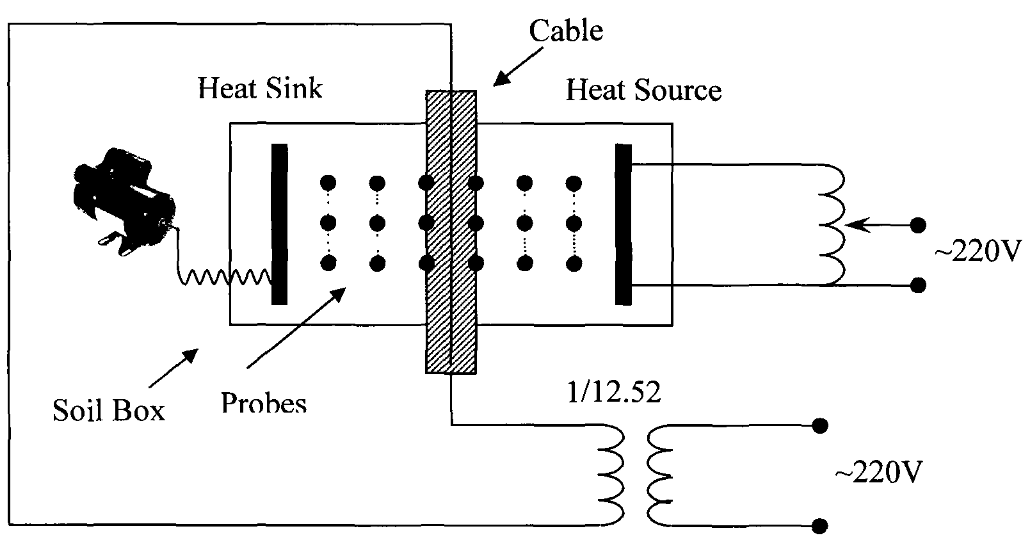

(b) Schematic component diagram

Fig. 6.1 Experiment setup and system configuration

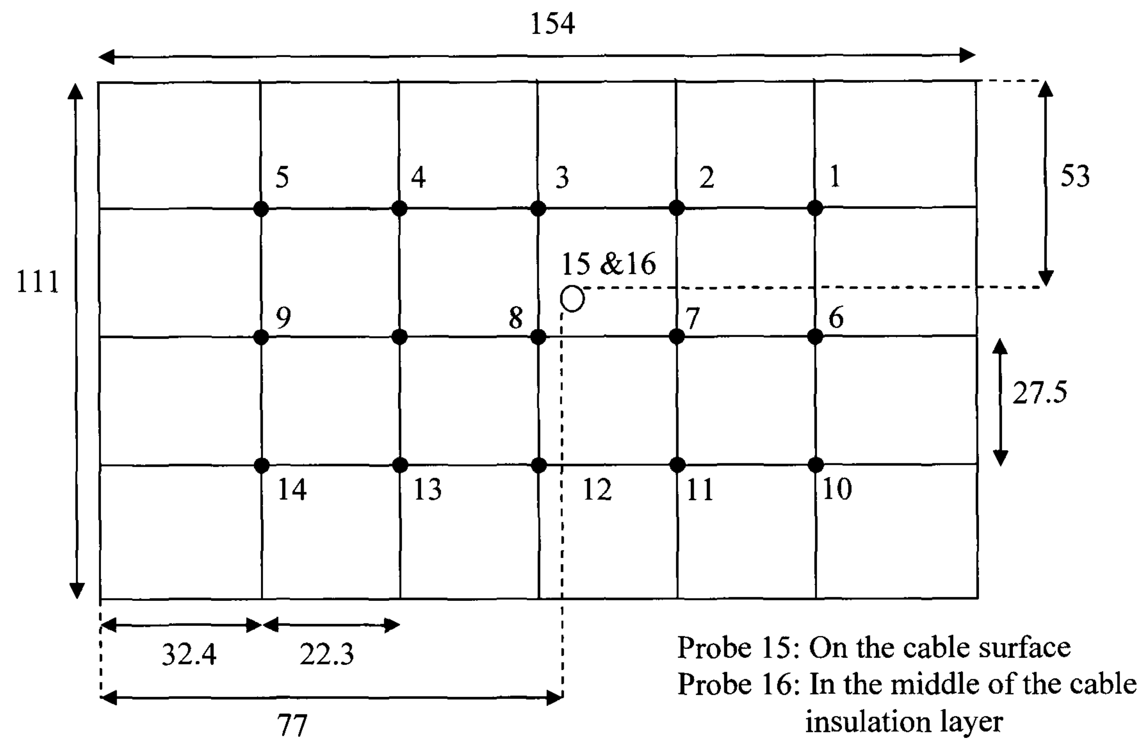

Fig. 6.2 System container front view

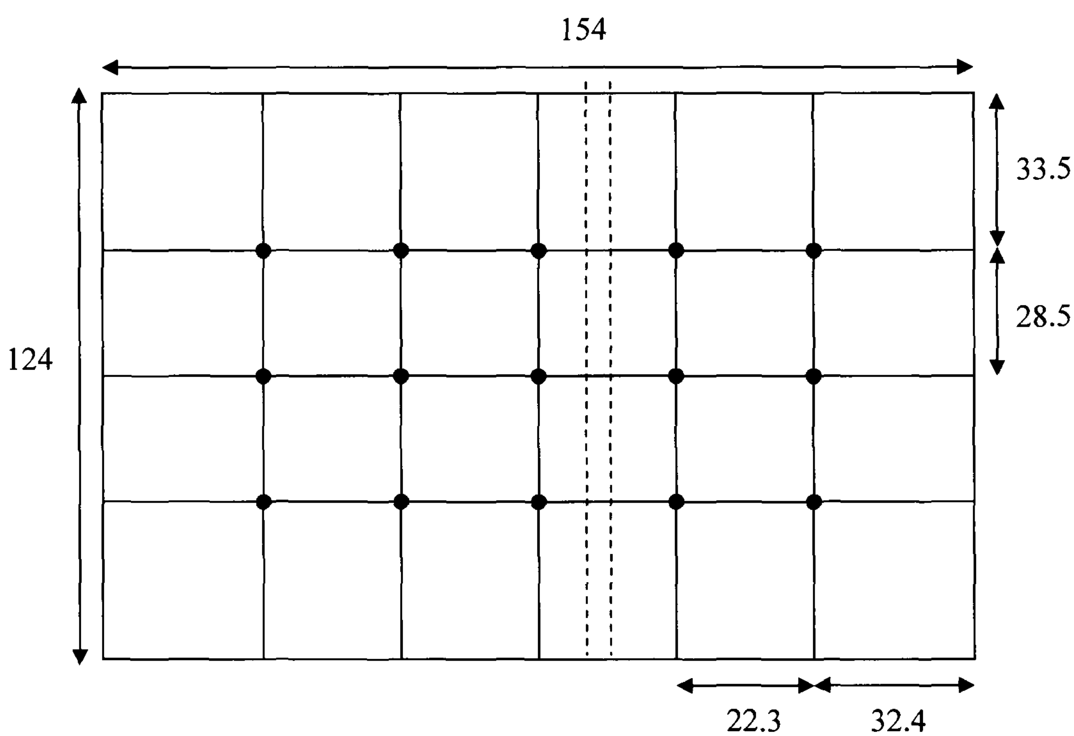

Fig. 6.3 System container top view

6.3 EXPERIMENTAL MODEL

Investigation of the thermal conductivity of the soil surrounding the cable is a critical part of assessment of the underground power cable. In this regard, the first part of the experiment will investigate the soil thermal characteristics used to backfill the tested cable. The second part will include the cable as the heat source, where the measured temperatures in conjunction with the combined finite element- gradient optimization method are used to investigate all operational media and boundary thermal parameters associated with the experimental set, which are needed to simulate the tested cable behaviour. In this regards the boundary losses and convection losses with ambient were tested, as well as the soil thermal conductivity, where the variation of the soil characteristics under high cable loading are of interest.

6.3.1 Soil Specification Test

The container has a heat source along one of its sides and a heat sink along the opposite side face to face with each other (along the box width). The heat source and sink are essential in this part of the experiment. This design allows the heat to flow along the box, and a temperature gradient occurs. The heat source consists of a pure electrical resistance which dissipates heat when connected to the power supply, a potentiometer voltage divider is used to control the amount of heat generation. A compressor is used as a heat sink to absorb the heat generated at the other side. Thermocouple probes are distributed as illustrated in Figure 6.1 and Figure 6.2 to construct a rectangular grid which will record the temperatures at different points and observe temperature gradients along associated segments. The amount of heat generated and transferred through the container's soil is observed and recorded continuously. The recorded temperatures data is used to calculate the temperatures gradients for selective segments with known length which in conjunction with the measured transferred heat will be used to calculate the thermal resistivity of the soil at different spots.

Because the scope of investigation is toward the steady state thermal resistivity, the thermal circuit has to be stabilized at the steady state. The heat is adjusted to maximize the temperature gradient without exceeding the limit of the heat sink capacity to absorb the generated heat, and consequently avoiding the possibility of the heat source overwhelming the capacity to absorb the generated heat. In addition to that, while the heat source is adjusted to achieve the maximum possible gradient, the steady state heat flow has to be maintained at this point of operation. In other words, the tradeoffs among all these factors must be taken into consideration. Figure 6.4 shows the imposed control on the heat source generation achieved by means of current source variation.

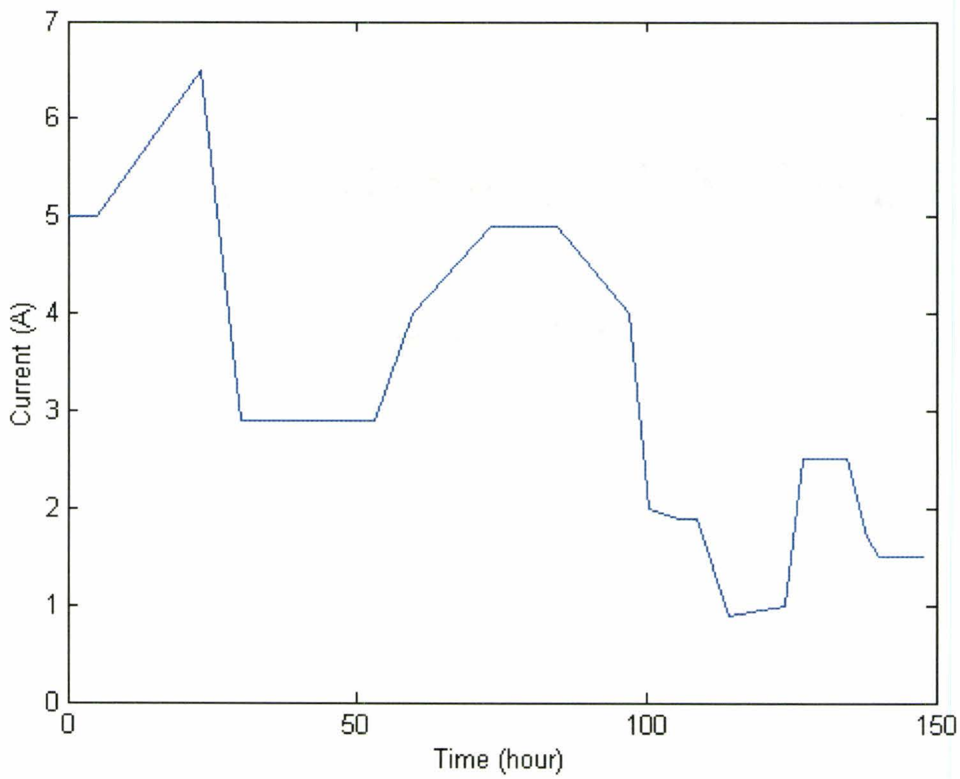

Fig. 6.4 Heat source control via input current adjustment

The amount of heat generation is calculated by measuring the input current flowing through the heat source and the voltage across the heat source resistance

$$Q_s = I_s \; V_s \tag{6.1}$$

Each probe is separated from the adjacent probe by a fixed distance (l) along the box width and fixed distance along the box depth (Figure 6.2). The heat flow mainly in the direction from the heat source toward the heat sink perpendicular to the area of the heat source-heat sink plate, determined by box height. Under this assumption, the thermal resistivity in a segment layer between two adjacent probes along the box width in any of the three layers can be computed by

$$\rho = \frac{A \; (\Delta T)}{l \; Q_e} \tag{6.2}$$

where A is the area perpendicular to the heat flow and defined by the box height and depth, ΔT is the temperature difference between two adjacent probes, l is the segment length between two adjacent probes in the heat flow direction (along the box width), Q_e is the effective heat flow (Q_s-Q_{losses})

Hence, for each layer, we have four segments along three parallel lines in the direction of heat flow; twelve values can be calculated, each associated with a given segment. After the heat flow was stabilized, the average individual thermal resistivity was calculated for each segment based on the mathematical formulation illustrated above. The average thermal resistivity was found to be 1.94 $^oC.m/W$.

6.3.2 Thermal Field Investigation under Cable Energizing

After completing the first part, the heat source-heat heat-sink pair was switched off, the tested soil was allowed to cool down to the ambient temperature. The tested cable, which will be energized to represent the heat source, was inserted inside the container, and shorted (loop configuration) - to be connected on the secondary side of the transformer, which is connected through the primary to the supply- the cable was loaded at 300A and the cable insulation, cable surface, ambient and other grid probe temperatures were recorded continuously several times per day over 570 hours before the steady state was achieved. Then the cable load was increased to 600A and observed daily over 230 hours before the steady state was achieved at the new operating conditions to complete 800 hours of continuous experiment run. Appendix B contains some samples of temperature readings. The cable current and temperature observation of the cable insulation, surface and selected soil probes are shown in Figure 6.5.

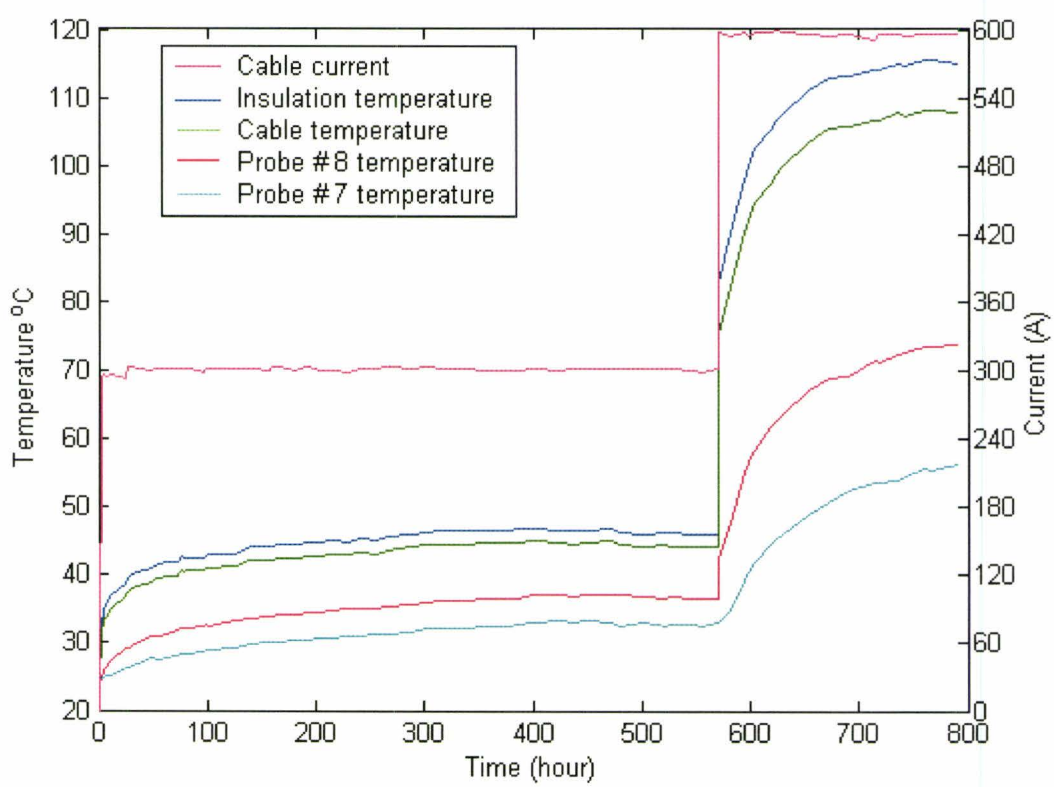

Fig. 6.5 Selected probes temperatures and cable current against time

The proposed finite element algorithm is applied to calculate the thermal field of cable temperatures and the surrounding soil environment, in order to be compared with the recorded experimental readings captured by the intensive grid of the used thermo-couple probes. The experimental setup shown in Figure 6.1 was simulated using a finite element grid consisting of 1,116 nodes which includes the internal cable material portions, used filled soil, and the container boundaries. Figure 6.6 shows the used finite element grid and illustrates positions of the mid layer probes used for the comparison.

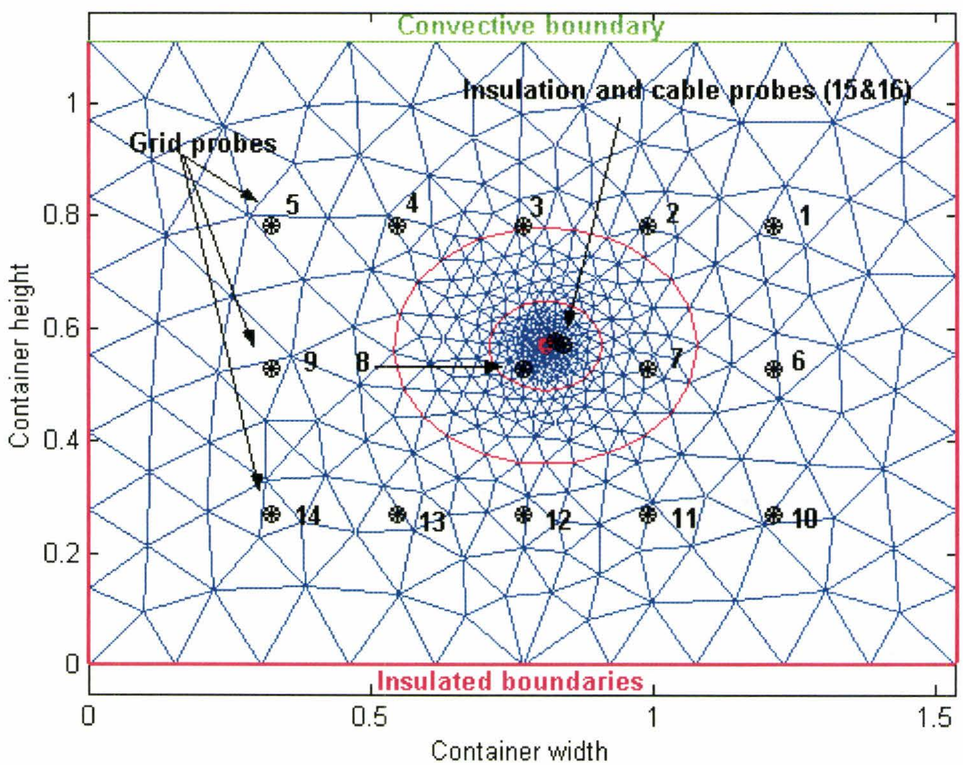

Fig. 6.6 Simulation finite elements grid

As can be noted from Figure 6.1, the container body is constructed to maintain as much as possible the heat generated inside by insulating the body edges. Consequently the sides and lower edges will be simulated as heat flux boundaries. The perfect insulation or a zero heat flux is difficult to implement in the laboratory and a tolerance for minimal heat losses will be allowed through the insulating edges. The upper roof of the container is open to the ambient environment and will be modeled as a convective boundary condition. Unfortunately, the thermal behaviour of the cable is strongly dependent on the loading conditions, the thermal parameters of the cable materials as well as the thermal specifications of the soil surrounding, ambient environment and boundary conditions.

In practice, the cable loading is monitored and observed during the experiment run while the cable specification is provided by manufacturers. The remaining parameters, which are associated with the surroundings, are either difficult to obtain or are subject to variations which may affect the cable thermal field predictions. Soil thermal conductivity is subject to variation under the actual loading due to expected drying of the soil. Consequently, in addition to the soil test in the first experimental part, soil will be reinvestigated again under actual loading in conjunction to other investigated thermal parameters. Under actual cable loading the soil conductivity, heat coefficient losses at the convective boundaries and the heat losses at the isolated boundaries were investigated using the proposed combined finite element- gradient optimization method, which is based on matching the computed thermal field to that obtained from the experimental measurements.

The container soil surrounding the cable is divided into three subregions as can be seen from Figure 6.6, each with a specific thermal resistivity. In practice, when the cable is loaded, the soil around the cable is affected strongly by the intensive thermal field more than the far soils, consequently, more deviation in their thermal resistivity will be expected. Using the proposed algorithm, the estimated values of the thermal resistivities of the sub-divided soils, heat losses at the insulated boundaries and heat convection losses factor are shown in Table 6-1 for the cable loading of 300 A. Using these estimated parameters, the thermal field solution can be carried out using the finite element analysis as shown in Figure 6.7 .

TABLE 6-1: PARAMETER SPECIFICATIONS OF THE EXPERIMENTAL MODEL (300 A LOADING)

Conductor cross section area (mm^2)	185
XLPE insulation thickness (mm)	4.5
Rated voltage (Kv)	15
Conductor losses (W/m)	13.57
Dielectric losses (W/m)	0.0963
Shield losses (W/m)	0.6787
Conductor thermal conductivity W/($^oC.\ m$)	385
Dielectric thermal conductivity W/($^oC.\ m$)	0.2857
Soil cable adjacent thermal conductivity W/($^oC.\ m$)	0.4700
Soil mid layer thermal conductivity W/($^oC.\ m$)	0.4703
Soil outer layer thermal conductivity W/($^oC.\ m$)	0.4952
Ambient temperature ^oC	24.08
Heat convection losses coefficient W/($^oC.\ m^2$)	11.96
Left boundary heat losses (W/m)	-0.8797
Right boundary heat losses (W/m)	-1.667
Bottom boundary heat losses (W/m)	-2.198

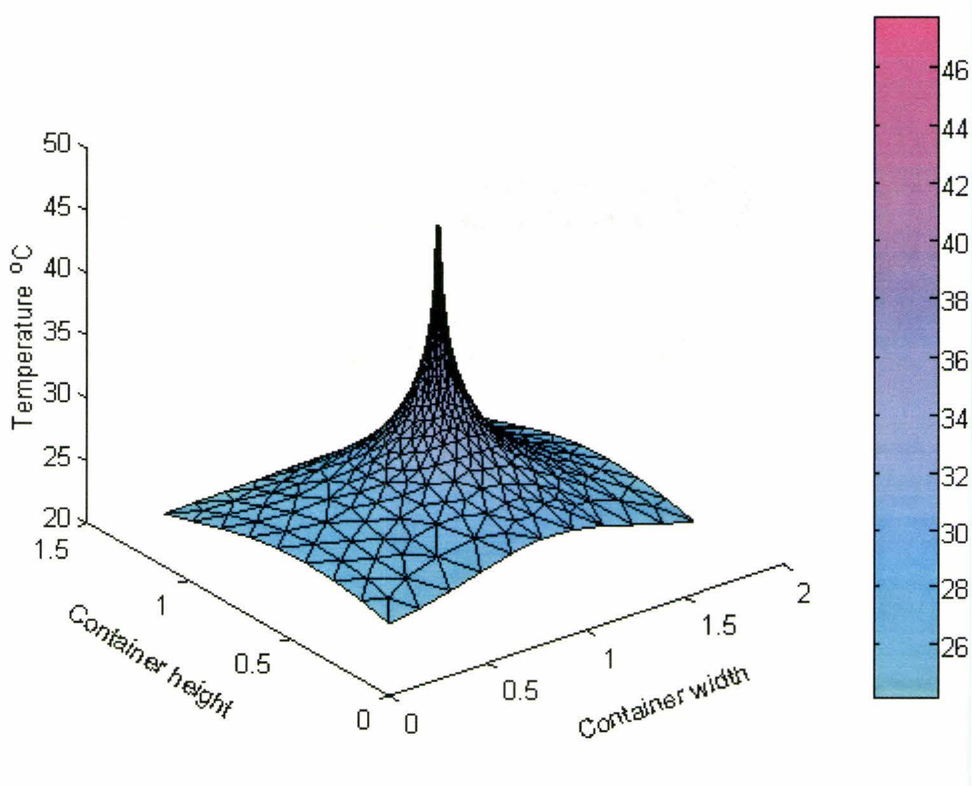

Fig. 6.7 Thermal field solutions (300 A loading)

Table 6-2 shows a comparison between recorded experimental temperatures and calculated values from the simulation. Cable surface and insulation temperatures as well as the other probes reading distributed in the surrounding soil around the cable are shown in Figure 6.8 for both the measured and the computed cases.

TABLE 6-2: COMPARISON OF PROBE EXPERIMENTAL READINGS WITH THE SIMULATION RESULTS (300 A LOADING)

Probe group	Classification	Probe No.	Measured value °C	Calculated value °C	Difference °C	Percentage difference (%)
Grid Probes	Upper layer	1	27.30	27.52	-0.2284	-0.836
		2	29.30	29.39	-0.0928	-0.316
		3	30.20	30.18	0.0158	0.052
		4	28.30	28.37	-0.0767	-0.271
		5	27.20	26.90	0.3039	1.117
	Middle layer	6	28.60	28.86	-0.2645	-0.924
		7	32.60	32.44	0.1631	0.500
		8	36.50	36.22	0.2842	0.778
		9	28.20	27.95	0.2473	0.876
	Lower layer	10	28.30	28.37	-0.0685	-0.242
		11	29.90	29.91	-0.0162	-0.054
		12	30.20	30.40	-0.2021	-0.669
		13	29.10	29.15	-0.0554	-0.190
		14	27.70	27.73	-0.0346	-0.125
Cable Probes	Cable Surface	15	44.10	44.24	-0.1431	-0.324
	Insulation	16	46.0	45.89	0.1146	0.249

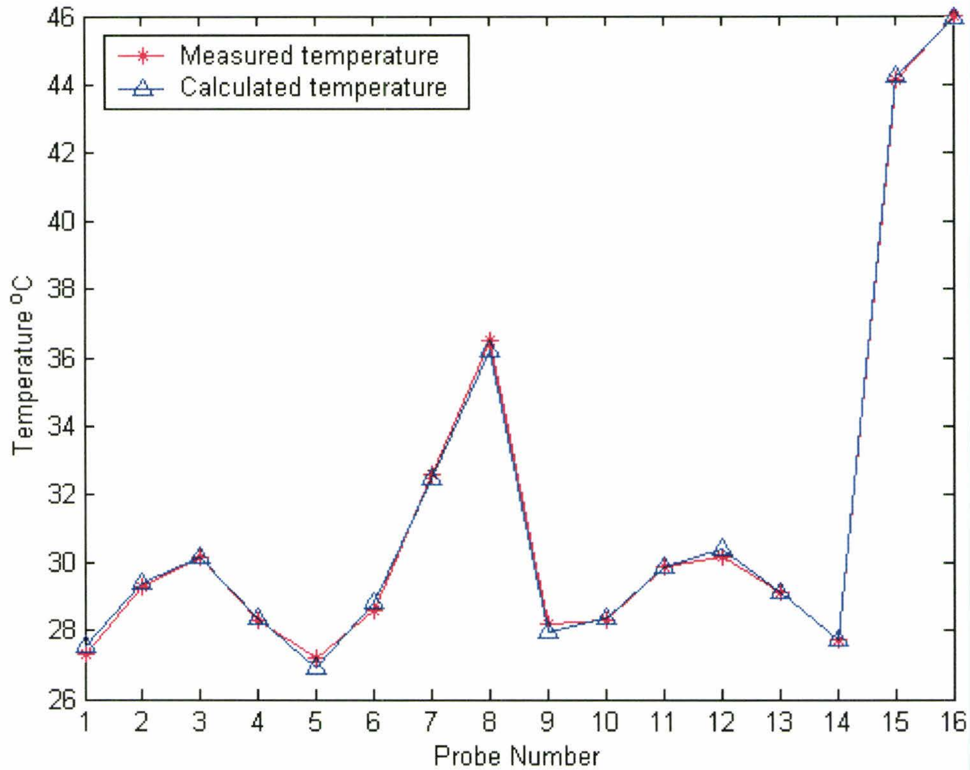

Fig. 6.8 Probe temperatures, measured against calculated (300 A loading)

There is good correspondence between the calculated temperatures and the measured temperatures. Some points have more deviation but with less than 1%, these probes are subjected to movement from their specified coordinates (used in simulation) during the process of filling the container with the soil and may cause such errors.

The cable current was stepped up from the 300A to its maximum current capacity of 600A, in order to investigate the cable thermal behaviour at extensive loading and to test the proposed model capability to handle different circumstances, such overloaded cable. Due to the new heat dissipation value which about four times the previous case, more influence would be expected on the three subdivided soil zones, resulting in lower thermal conductivities. Also more leakage heat transfer would be expected on the insulated boundaries. The new values of the above mentioned parameters, which affected by the 600A loading as well as that which affected by the ambient environment are shown in Table 6-3. Figure 6.9 shows the thermal field temperature solution using the proposed finite element algorithm for the maximum cable loading of 600 A.

TABLE 6-3: PARAMETER SPECIFICATIONS FOR MAXIMUM CABLE LOADING (600 A LOADING)

Conductor losses (W/m)	46.01
Shield losses (W/m)	0.6787
Soil cable adjacent thermal conductivity W/(^oC. m)	0.4426
Soil mid layer thermal conductivity W/(^oC. m)	0.3008
Soil outer layer thermal conductivity W/(^oC. m)	0.3139
Ambient temperature ^oC	22.97
Heat convection losses coefficient W/(^oC. m^2)	13.42
Left boundary heat losses (W/m)	-4.58
Right boundary heat losses (W/m)	-5.99
Bottom boundary heat losses (W/m)	-6.83

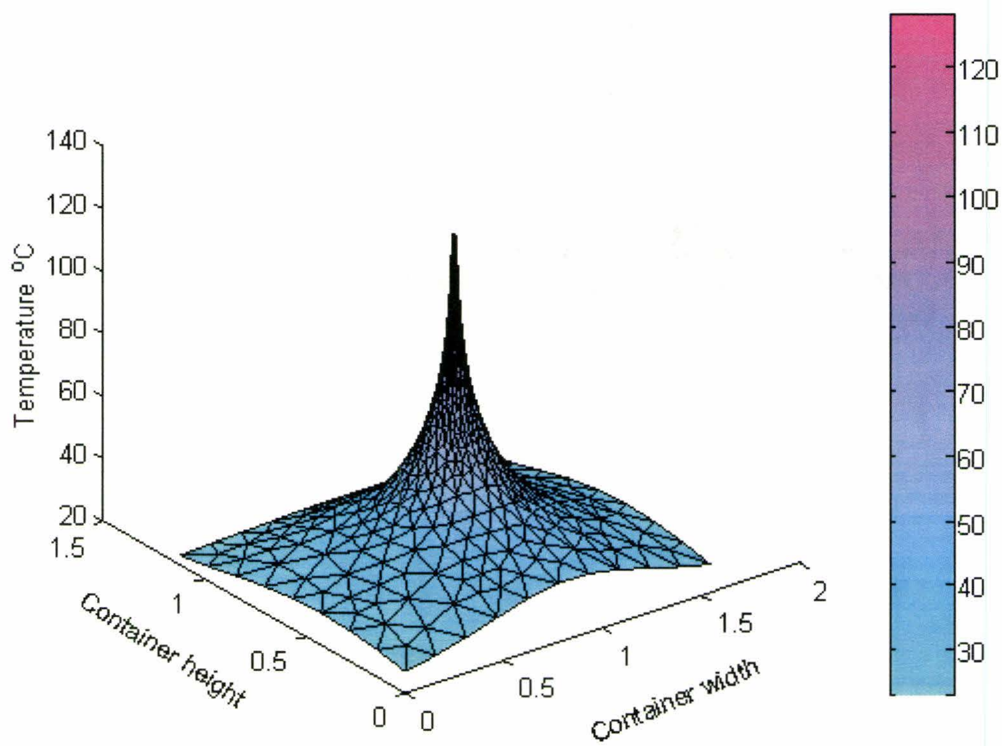

Fig. 6.9 Thermal field solutions at maximum loading (600 A loading)

Table 6-4 shows a comparison between the recorded experimental temperatures and the calculated values using the finite element approach. Cable surface and insulation temperatures as well as the other probes reading distributed in the surrounding soil around the cable are shown in Figure 6.10 for both the measured and the computed cases.

TABLE 6-4: COMPARISON OF THE PROBE EXPERIMENTAL READING WITH THE SIMULATION RESULTS (600 A LOADING)

Probe group	Classification	Probe No.	Measured value ^oC	Calculated value ^oC	Difference ^oC	Percentage difference (%)
Grid Probes	Upper layer	1	33.3	35.04	-1.748	-5.249
		2	42.60	41.83	0.768	1.803
		3	46.40	45.63	0.769	1.657
		4	37.80	37.77	0.032	0.0857
		5	32.60	32.22	0.385	1.183
	Middle layer	6	39.00	39.99	-0.998	-2.559
		7	57.40	57.11	0.290	0.506
		8	76.00	76.01	-0.007	-0.009
		9	37.00	35.85	1.148	3.104
	Lower layer	10	37.80	38.57	-0.771	-2.040
		11	44.70	44.63	0.068	0.152
		12	46.30	46.36	-0.060	-0.130
		13	40.90	41.05	-0.147	-0.359
		14	35.10	35.24	-0.143	-0.408
Cable Probes	Cable Surface	15	116.2	116.3	-0.135	-0.116
	Insulation	16	121.3	121.4	-0.122	-0.100

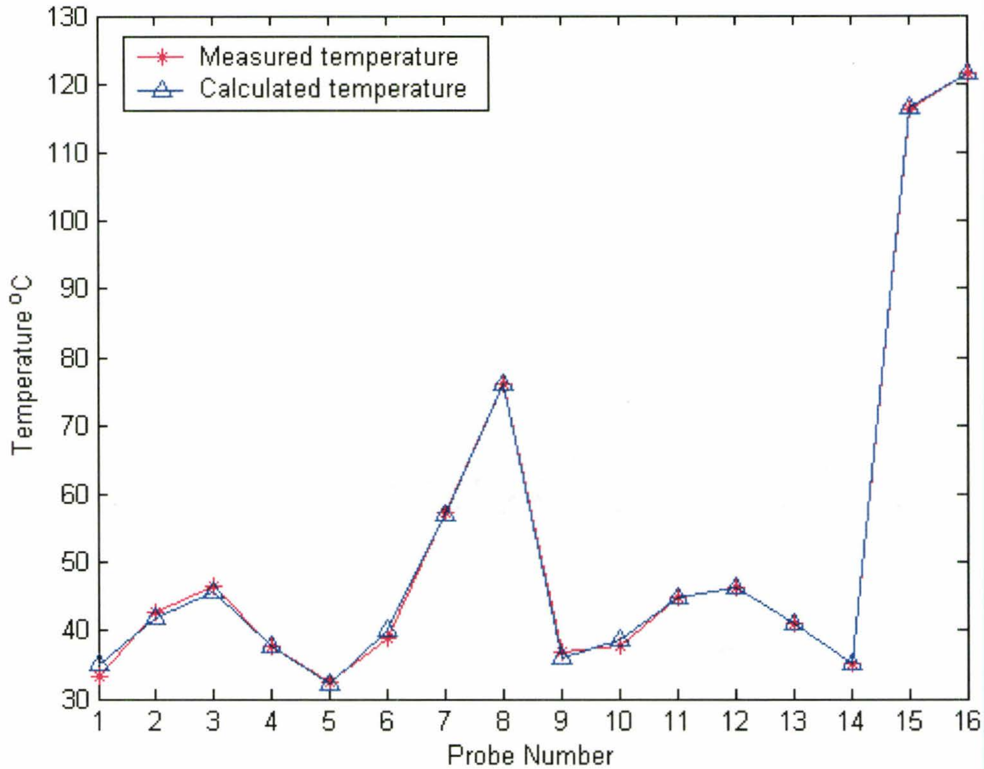

Fig. 6.10 Probe temperatures, measured against calculated (600 A loading)

Now we use the estimated thermal circuit parameter to investigate the thermal field of the tested cable under load variation around the base-case of 600A. The temperature distributions along the cable and surrounding soil for 10%, 20% increasing and decreasing in the cable loading is shown in Figure 6.11 using the achieved thermal parameters. This was performed by both the conventional method of replicating the finite element analysis at various values of heat generation (solid lines) and by the sensitivity analysis of temperatures to the heat generation variation in conjunction with the nominal thermal field solution (Perturbed Finite Element, dots •••). The background and formulation of the sensitivity analysis was discussed in Chapter 4. Figure 6.11 shows the importance of the investigation of the unique thermal parameters characteristics around the interested point of cable operation at the maximum cable loading, which represent a critical point of operation. An accurate parameter evaluation at expected base load leads to a more accurate thermal field representation including the surrounding points with load variation around the base case.

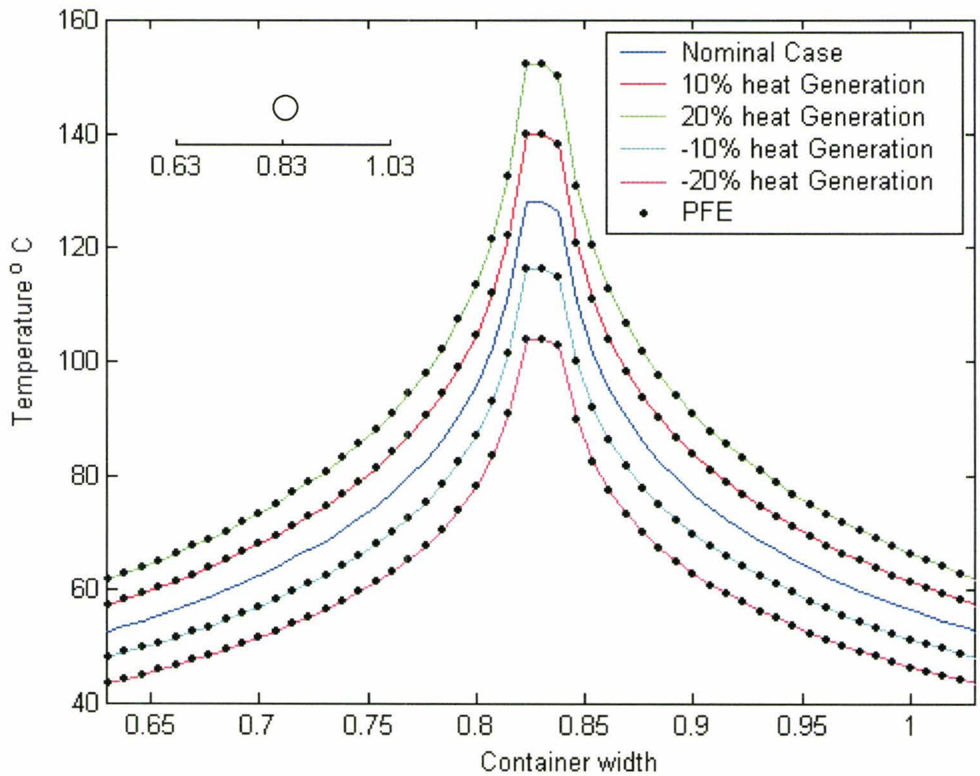

Fig. 6.11 Thermal field across container width at various loading around nominal load using sensitivity analysis

CHAPTER 7

APPLICATION TO DEMONSTRATIVE AND PRACTICAL CABLE CASE SCENARIOS

7.1 INTRODUCTION

The proposed method of the perturbed finite element was introduced to study the general performance of buried power cable and parameter evaluation procedures for the purpose of advanced thermal analysis and ampacity calculations, which involves solving thermal field of cable system which can handle complex configurations, boundaries and heat sources, as well as optimizing cable performance and sensitivity analysis under varying loading and environmental conditions.

The proposed finite element thermal model can be used to determine the maximum temperatures to be associated with different cable loadings. Another practical usage will be the investigation of trench dimensions effect, cable diameter and soil propertied on the heat dissipated from a buried cable as well as the evaluation of the effects caused by environmental and weather variation on the temperature distribution. Consequently, this gives an insight, in many practical applications, into the important parameters that have a great influence on the total ampacity of the system as will be shown in this chapter.

The development of a sensitivity methodology based on the finite element model was accomplished in which various cable environmental parameters are modeled accurately to include the heat transfer mechanisms at boundaries, backfill, duct banks and other media surrounding the cable. The temperature sensitivities with respect to variations in the cable thermal parameters represent the foundation of performance indices of interest to cable designers and operators. The proposed perturbed finite element analysis technique provides useful sensitivity information of the cable ampacity, with respect to fluctuations in the cable circuit parameters, to assess the effects on the permissible cable loading caused by these fluctuations without repeating the whole thermal analysis for each possible parameter change. In addition, the technique applies both to the design phase and the operational aspects of power cables buried in complex media of soil, heat sources and sinks and variable boundary conditions. Because the simulation procedure for various parameter variations does not involve repeated finite element analyses, the results can be obtained by very fast and compact scheme and displayed in efficient, straightforward manner. Since only one nominal finite element analysis is required, larger element grid can be employed allowing even more accurate modeling. The sensitivity information is useful not only in evaluating the cable ampacity subject to various parameter changes but also in determining the important and non-important parameter variations in terms of their relative effect on the cable temperature and ampacity. Unfortunately, in finite element technique an explicit expression of the cable temperature in terms of cable thermal circuit parameters is not possible. However, the sensitivity coefficients associated with various cable parameters of interest provide the cable engineers with important information about relative effects of such parameters variations on the cable performance, which helps in design of a new system and improving performance of existing systems.

The question of how the power cables are optimized for best performance has become of utmost importance, especially under conditions which encourage cost saving and high service quality. Significant design and operating cost reductions could be achieved via optimizing cable performance under various loading, soil parameters and ambient conditions. An optimization model was developed in conjunction with the perturbed finite element in order to achieve optimal desired cable performance. It considers various design parameters and sensitivities associated with these parameters simultaneously and provides the optimal solution subject to user-defined constraints. The design problem of selecting the optimal parameter values of the thermal circuit parameters, including the thermal conductivities, boundary conditions and heat generation, is formulated using a multi-dimensional gradient optimization method. The technique considers all thermal circuit parameters and provides the optimal solution which minimizes the objective function. This model represents a generalization of the nonlinear programming formulation to include practical cases of the cable design objective functions which may include the thermal parameters and the cable temperatures (ampacity) subjected to upper and lower bounds on the design parameters, linear system of equations constraints, or nonlinear constraints. The optimization analysis will include the sensitivities profiles of the temperature (ampacity) with respect to the thermal circuit parameters in case of temperature (ampacity) implicit objective functions or constraint functions so that a secure, reliable cable design may be obtained. Consequently, an accurate thermal field profile and a sensitivity coefficients associated with various cable optimized parameters, provide the optimization routine, respectively, with temperature values and relative effects of such parameters variations on the temperature variation.

The ultimate goal of this work is to develop a methodology for the analysis of heat transfer in electrical power cable systems in order to attain high cable ampacity, and at the same time avoid cable extensive overheating. The main result of this analysis is: temperature distribution in the conductors, sensitivity of the temperature to the thermal circuit parameters variations, and optimizing cable parameters to enhance cable performance by maximizing cable carrying capability. Contrary to previous chapters, where the heat transfer was modeled for power cable systems for advanced thermal analysis, in this chapter the developed methodology will be applied to following applications :

- Application to bench-mark and demonstrative case scenarios.

- Applications to practical transmission level cable systems from North American and/or Saudi systems.

- Applications to practical distribution level cable systems from North American and/or Saudi systems.

7.2 SIX CABLE FLAT ARRANGEMENTS

7.2.1 Overview

Figure 7.1 shows the arrangement of six direct buried 161 kV cables with rating given in Table 7-1, which is extracted from [31]. The trench width is 1.246m and the cable bedding extends 0.12m above and below the cable surface. The cables are buried at a distance of 1.060m between the cable center and the ground surface which is modelled as a convective boundary with a heat convection loss coefficient of 5 $W/(^oC.m^2)$.

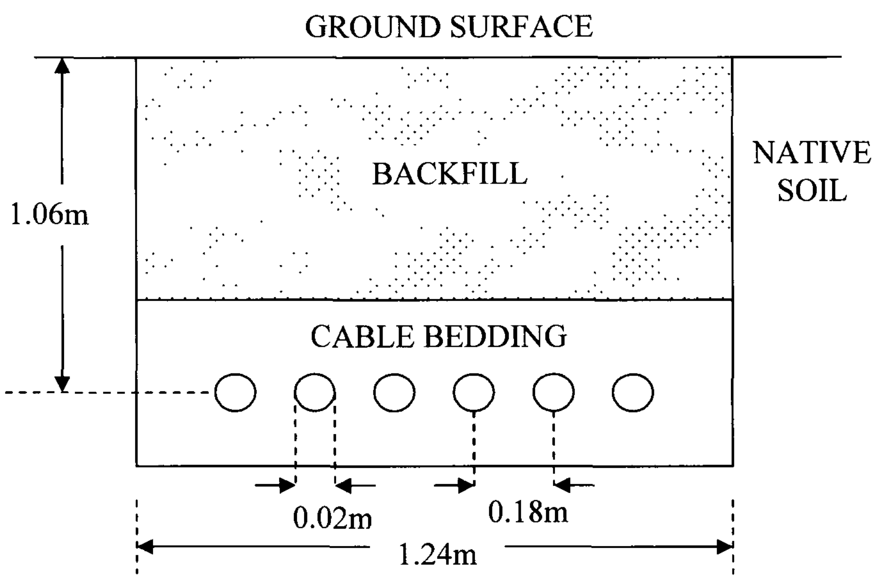

Fig. 7.1 Six direct buried underground cable system

TABLE 7-1: FLAT ARRANGEMENTS CABLE RATINGS

Cable size (mm^2)	400
XLPE insulation (mm)	18
Rated voltage (kV)	161
Rated frequency (Hz)	60
Operating current (A)	650
Conductor losses (W/m)	26.25
Dielectric losses (W/m)	0.424
Shield losses (W/m)	1.968

7.2.2 Thermal Evaluation

The nominal values of the ambient air temperature and the heat convection loss coefficient are 20 ^oC and 5 $W/(^oC.\ m^2)$ respectively. The nominal values of the thermal conductivities of the cable bedding, trench backfill and native soil are, respectively 1.053 $W/(^oC.\ m)$, 1.25 $W/(^oC.\ m)$, 0.833 $W/(^oC.\ m)$ and they are all subjected to variations about their nominal values. For this cable, the temperature distribution profile was evaluated using the finite element grid containing 1520 nodes which is shown in Figure 7.2. Figure 7.3 shows the 3D temperature distribution profile calculated by the finite element technique for the nominal values of the ambient temperature and soil thermal conductivities indicated above and for cable loading of 650A per cable.

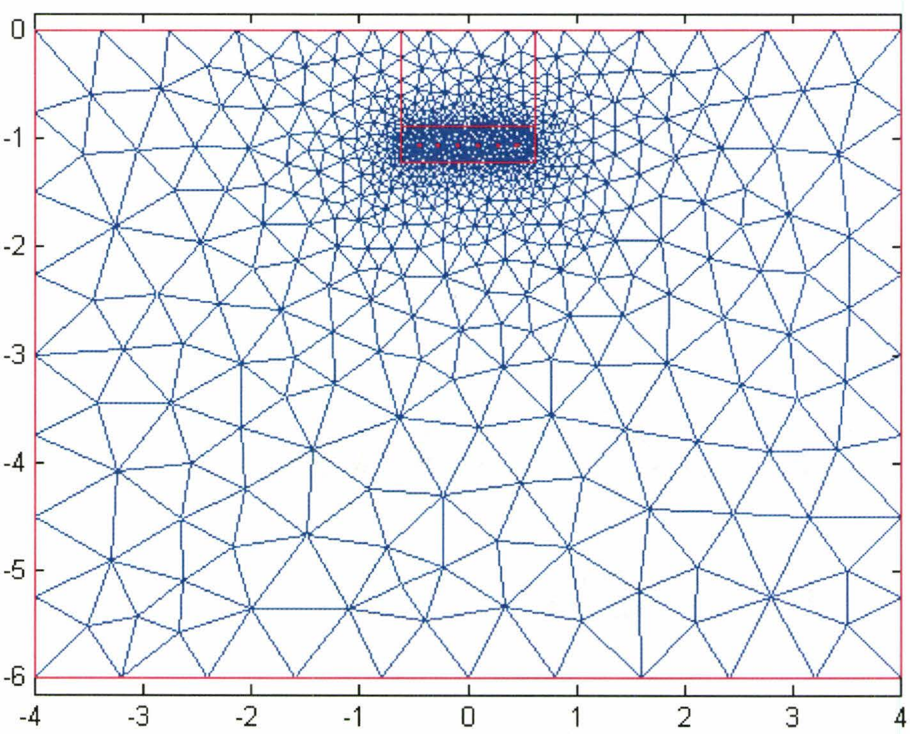

Fig. 7.2 Finite element mesh imposed on the model solution domain of six flat cables arrangement

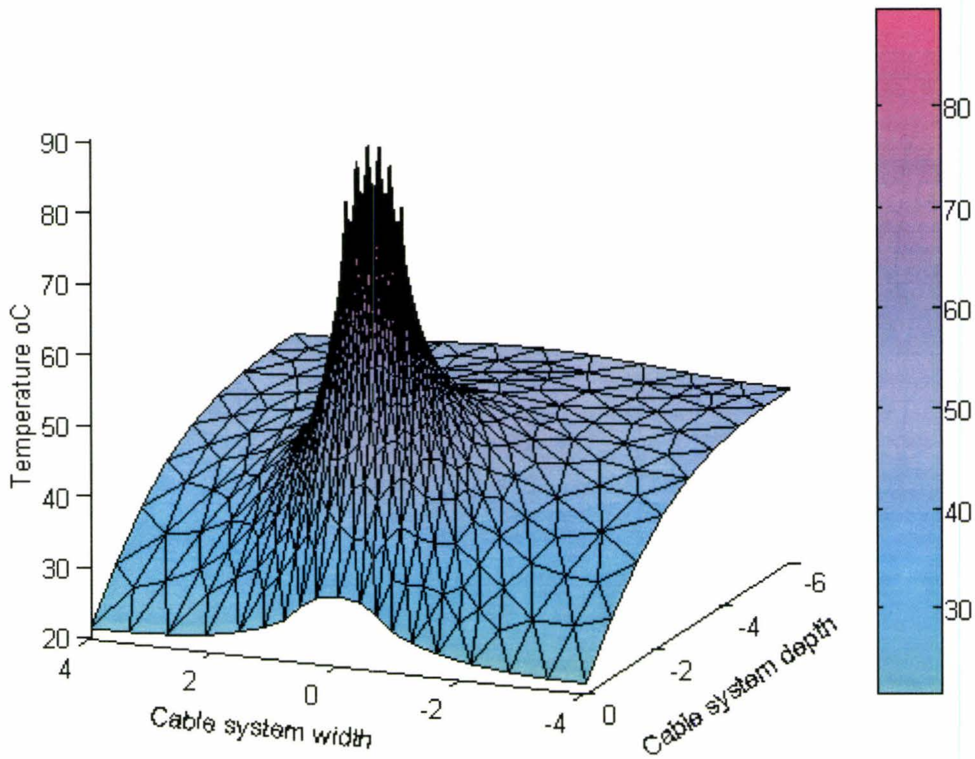

Fig. 7.3 Three-dimensional temperature distribution of six flat cables arrangement

The maximum cable surface temperatures ordered from the left to the right are 81.44, 87.07, 89.48, 89.48, 87.07, and 81.45 respectively.

7.2.3 Sensitivity Calculation

Table 7-2 shows the sensitivities of each cable's maximum surface temperature with respect to various parameters of the thermal circuit. The sensitivity values of Table 7-2 show that the thermal conductivities have the dominant impact on determining the cable temperatures overall other parameters. The heat dissipation increases with an increase of soils conductivities surrounding the cables, and consequently results in markedly temperatures reduction. Furthermore, it can be noted that the mother soil thermal conductivity has the greatest effect among the backfill and the bedding thermal conductivities. This can be demonstrated by considering the large geometrical area occupied by the mother soil. On the other hand, the nearness of a geometrical area specified by such thermal conductivity from the cables plays an important role on determining the sensitivity of the cable temperatures with respect to the thermal conductivity too. Both bedding and backfill are centered in the middle of the cable system, the bedding is containing the cables while the backfill occupying large area, and as result, both associated temperature sensitivities increase in each case due to the mentioned characteristic factor to end up with close sensitivities indicated in table 7-2. Increasing the thermal conductivities and heat convection loss coefficient reduce the cables temperature, both aid in dissipation more heat away from the cables spots. On the other hand, the cable losses increase the amount of heat generation, and cause more temperature rise.

TABLE 7-2: TEMPERATURES SENSITIVITIES OF FLAT ARRANGEMENTS CABLES AT PARAMETRES NOMINAL VALUES

Sensitivity $\partial T/\partial p$ / Parameter(p)	Cable #1	Cable #2	Cable #3	Cable #4	Cable #5	Cable #6
Mother soil thermal conductivity $W/(^oC.\ m)$	-30.48	-30.44	-30.56	-30.56	-30.44	-30.48
Backfill thermal conductivity $W/(^oC.\ m)$	-13.41	-15.21	-16.16	-16.16	-15.21	-13.41
Bedding thermal conductivity $W/(^oC.\ m)$	-12.96	-16.10	-17.12	-17.12	-16.10	-12.97
Ambient temperature ^oC	1	1	1	1	1	1
The heat convection loss coefficient $W/(^oC.\ m^2)$	-1.125	-1.146	-1.157	-1.157	-1.146	-1.125
Generated heat in the cables W/m	2.145	2.342	2.426	2.426	2.342	2.146

However, in addition to the assessment of relative effects of the variations of various parameters, the sensitivity values can be used to estimate the changes in the temperatures profile in the domain of the cable system due to variations of one or more of the parameters. Consequently, the most critical temperatures spots such as cable temperatures can be obtained by this very fast scheme around the nominal operating point in case of fluctuations of cable system parameters without repeating the whole thermal analysis for each possible parameter change. Figure 7.4 shows the difference between the temperature profile using the perturbed finite element sensitivity analysis due to 10 % increase in all the cable system parameters indicated in table 7-2, and the temperature profile from the conventional finite element method at this new operating point. This figure shows a very small difference between the exact conventional method and the proposed approach, which does not exceed $(1\times10^{-7}\,^{o}C)$ according to 10 % of all parameters disturbance from the base-case.

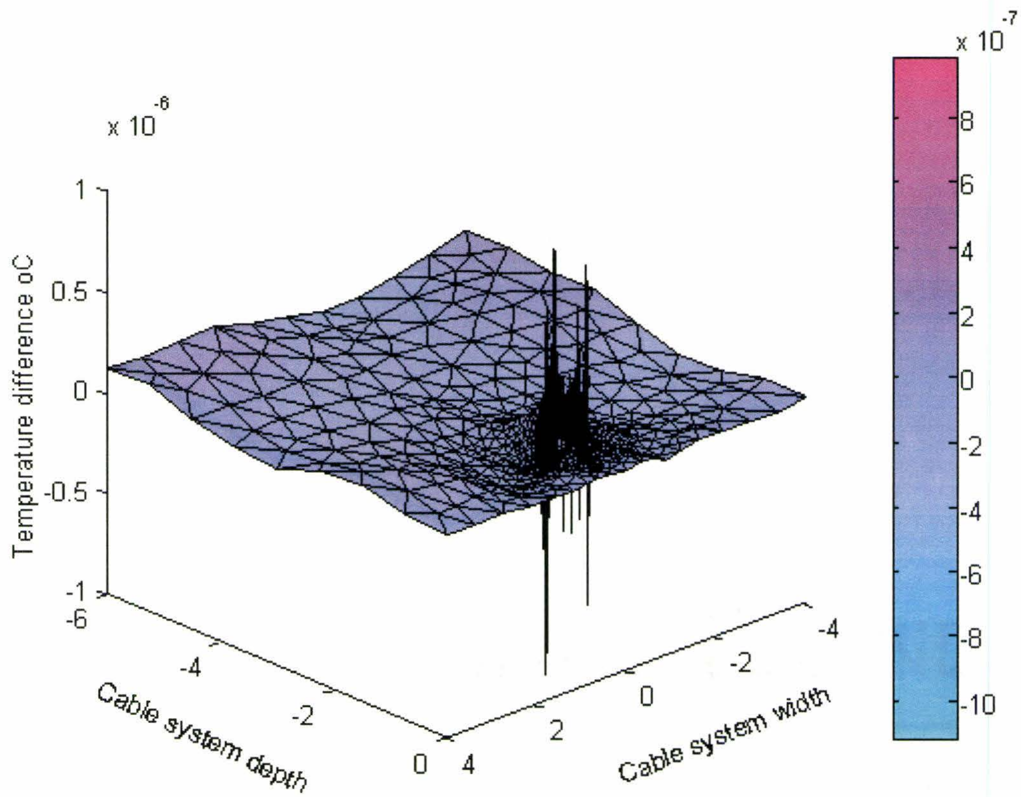

Fig. 7.4 Temperature comparison between the perturbed finite element sensitivity analysis and the conventional finite element analysis of six flat cables arrangement

Table 7-3 shows the cables' hottest temperatures at the nominal case and the new temperatures for the case of 1%, 5%, and 10% increasing in the mother soil thermal conductivity, respectively. Table 7-4 shows the percentage deviation of the cable temperatures calculated using the perturbed finite element sensitivity analysis, from the conventional finite element temperatures illustrated in table 7-3.

TABLE 7-3: CABLES SURFACE TEMPERATURES DUE TO MOTHER SOIL THERMAL CONDUCTIVITY VARIATIONS

Cable Number	Hottest spot cable surface temperature ^oC			
	Nominal value	New values due to parameter variation (conventional finite element)		
		For 1% $k_{\text{mother-soil}}$ increasing	For 5% $k_{\text{mother-soil}}$ increasing	For 10% $k_{\text{mother-soil}}$ increasing
1	81.4390	81.19	80.21	79.05
2	87.0741	86.82	85.84	84.68
3	89.4791	89.23	88.24	87.07
4	89.4834	89.23	88.25	87.08
5	87.0691	86.82	85.84	84.68
6	81.4514	81.20	80.22	79.06

TABLE 7-4: PERCENTAGE DEVIATION BETWEEN THE SENSITIVITY BASE AND CONVENTIONAL FINITE ELEMENT METHODS (MOTHER SOIL)

Cable Number	Temperature percentage deviation (%)		
	For 1% $k_{\text{mother-soil}}$ increasing	For 5% $k_{\text{mother-soil}}$ increasing	For 10% $k_{\text{mother-soil}}$ increasing
1	0.0019	0.0481	0.1893
2	0.0018	0.0433	0.1706
3	0.0017	0.0415	0.1634
4	0.0017	0.0415	0.1634
5	0.0018	0.0433	0.1706
6	0.0019	0.0481	0.1892

It is worth mentioning that these values which are selected at the cables surfaces represent the highest difference between the perturbed finite element sensitivity and the conventional finite element. Less percentage difference was noted at all other temperatures in the solution domain. It is obvious even with a big change in the most effective parameter (mother soil conductivity), we still can achieve a deviation less than 0.2 % in the most sensitive points, and much less in the large scale remaining points.

The effect of changing the backfill thermal conductivity was studied and the temperature deviation of the perturbed finite element sensitivity from the conventional finite element was carried out. Table 7-5 shows the cables surface temperatures calculated using the conventional finite element, while Table 7-6 shows the percentage deviation of the perturbed finite element sensitivity cables surface temperatures from the conventional finite element temperatures, both for the case of changing the backfill thermal conductivity by 5% and10% decreasing and increasing respectively.

TABLE 7-5: CABLES SURFACE TEMPERATURES DUE TO BACKFILL THERMAL CONDUCTIVITY VARIATIONS

Cable Number	Hottest spot cable surface temperature ^oC				
	Nominal Value	New values due to parameter variation (conventional finite element)			
		-5% k_{backfill}	-10% k_{backfill}	5% k_{backfill}	10% k_{backfill}
1	81.44	82.30	83.23	80.63	79.86
2	87.07	88.06	89.10	86.15	85.28
3	89.48	90.52	91.64	88.50	87.58
4	89.48	90.53	91.64	88.50	87.58
5	87.07	88.05	89.10	86.15	85.28
6	81.45	82.32	83.24	80.64	79.87

TABLE 7-6: PERCENTAGE DEVIATION BETWEEN THE SENSITIVITY BASE AND CONVENTIONAL FINITE ELEMENT METHODS (BACKFILL)

Cable Number	Temperature percentage deviation (%)			
	-5% k_{backfill}	-10% k_{backfill}	5% k_{backfill}	10% k_{backfill}
1	0.0325	0.1328	0.0311	0.1217
2	0.0351	0.1437	0.0336	0.1318
3	0.0366	0.1495	0.0350	0.1373
4	0.0366	0.1495	0.0350	0.1373
5	0.0351	0.1436	0.0336	0.1318
6	0.0324	0.1328	0.0311	0.1217

The sensitivity model was used to estimate the new cable temperature values due to -5%, -10%, 5% and 10% changing in the bedding thermal conductivity. The corresponding deviation of the perturbed finite element sensitivity cables surface temperatures from the conventional finite element temperatures is shown in Table 7-7.

TABLE 7-7: PERCENTAGE DEVIATION BETWEEN THE SENSITIVITY BASE AND CONVENTIONAL FINITE ELEMENT METHODS (BEDDING)

Cable Number	Temperature percentage deviation (%)			
	-5% k_{bedding}	-10% k_{bedding}	5% k_{bedding}	10% k_{bedding}
1	0.0431	0.1799	0.0397	0.1526
2	0.0475	0.1979	0.0439	0.1694
3	0.0479	0.1996	0.0444	0.1714
4	0.0479	0.1996	0.0444	0.1714
5	0.0475	0.1978	0.0439	0.1694
6	0.0431	0.1801	0.0397	0.1527

7.2.4 Optimization Performance

The optimization of the thermal circuit parameters for the previous cable system configuration was evaluated and tested using the proposed formulated optimization algorithm, which will provide the optimal set of the backfill design parameters and the associated sensitivity of the cable temperatures (ampacity) with respect to ambient fluctuations. The nominal values of parameters were kept the same as given in the previous section where the ambient air temperature is 20 ^oC and the thermal conductivities of the cable bedding, trench backfill and native soil are, respectively 1.053 $W/(^oC.\ m)$, 1.25 $W/(^oC.\ m)$, 0.833 $W/(^oC.\ m)$. The thermal field analysis for this system was evaluated using finite element analysis at the nominal case in the previous section to give a maximum cable surface temperature of 89.48 ^oC at the inner cables.

In the formulation of a practical problem, the objective function will be formulated to redesign the cable system parameters in order to reduce internal surface cable temperatures by around 15 ^oC, which will result in increasing the cable current carrying capacity and enhancing the overall cable performance. A special focus will be given to the most influential parameters on the cable performance. The mother-soil, bedding and backfill thermal conductivities were chosen to be the controlled parameter which will be constrained using upper and lower limits. The objective function will be defined as the sum of the deviations squared of the chosen cables' temperatures from the desired temperature as can be described mathematically as follows:

$$\begin{aligned} &\text{Minimize} \quad \sum_{i}^{n}(T_i - 75)^2 \\ &\text{st} \qquad 0 \le \ k_{mother\_soil} \le 6 \\ &\qquad\quad\ 0 \le \ k_{bedding} \le 6 \\ &\qquad\quad\ 0 \le \ k_{backfill} \le 6 \end{aligned} \tag{7.1}$$

where T_i are the internal surface temperatures (middle two cables).

The thermal field in the medium of cable and surroundings is solved in terms of design parameters, and the associated chosen cable temperature sensitivities is carried out using the perturbed finite element approach. Consequently these outputs will be utilized by the nonlinear optimization approach in order to achieve the desired objective design in efficient and reliable way.

Using the developed optimization-finite element sensitivity approach, a solution is obtained at $k_{mother\text{-}soil} = 0.6106$ $W/(^oC.\ m)$, $k_{bedding} = 1.8209$ $W/(^oC.\ m)$ and $k_{backfill} = 2.3630$ $W/(^oC.\ m)$, which satisfies the provided constraints for which the objective function has a minimum value of 4.5×10^{-4} $^oC^2$. The thermal field for this system was evaluated at the new optimized parameter using the finite element approach as shown in Figure 7.5.

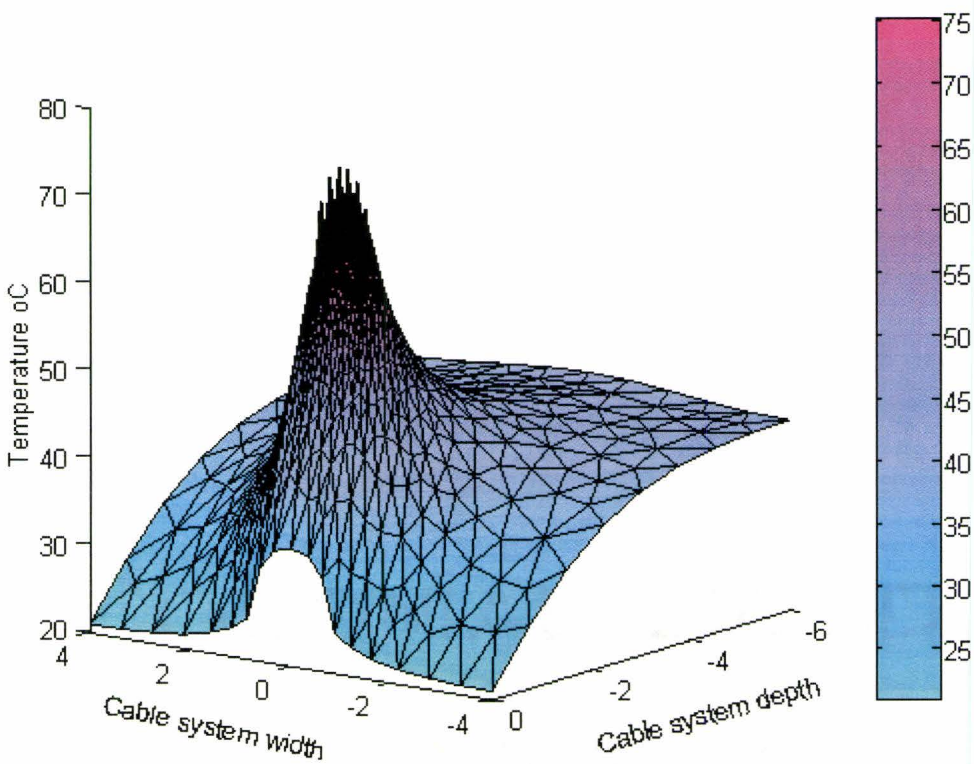

Fig. 7.5 Temperature solution at optimal parameters of six flat cables arrangement (cables surface temperatures reduction)

In order to show the advantage of the proposed optimization-finite element sensitivity approach in terms of reducing the number of iteration required to achieve the optimal solution by means of the objective and constraint gradient, Figure 7.6 shows the number of required iterations against the deviation at each step from the optimal value, it can be noted that only four iterations are sufficient to approach the optimal solution with high accuracy.

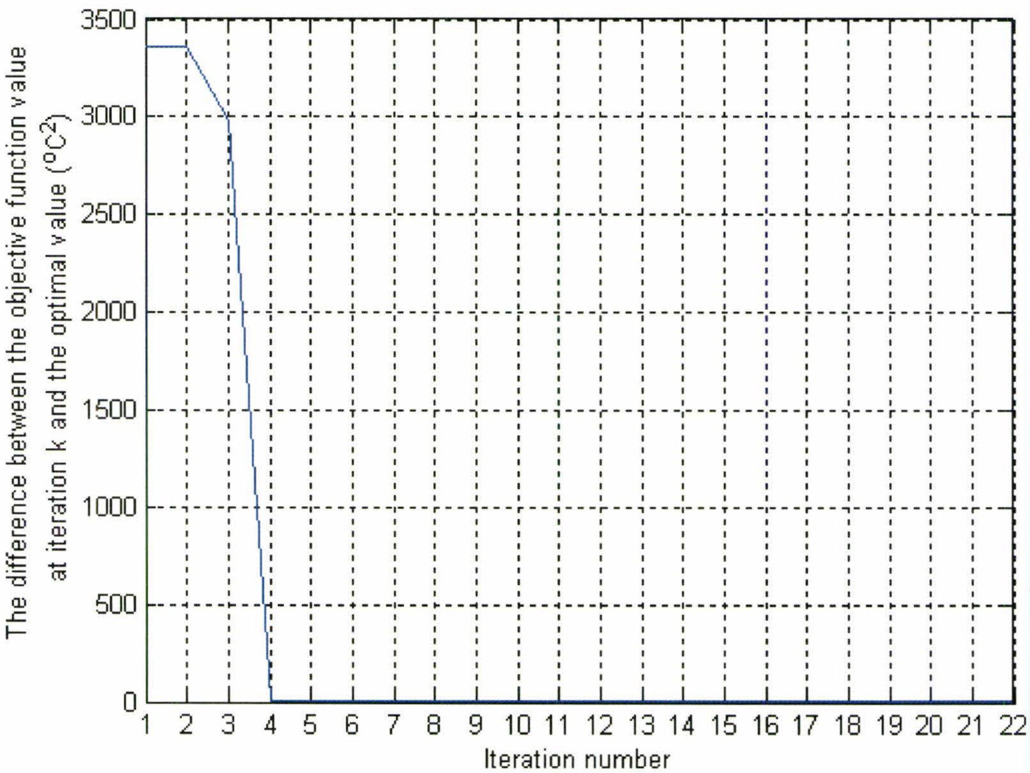

Fig. 7.6 Error versus iteration numbers of optimization process for six flat cables arrangement (cables surface temperatures reduction)

In some practical cases, the objective function represents the cost associated with the cable backfill which is to be minimized, such that the cable temperature does not exceed a specific design value (80 ^oC in this example).

$$
\begin{aligned}
&\text{Minimize} \quad 10\,k_{backfill} \\
&\text{st} \qquad 0 \le k_{backfill} \le 6 \\
&\qquad\quad T_i \le 80
\end{aligned}
\tag{7.2}
$$

where T_i is the internal surface temperatures (middle two cables). The optimal backfill conductivity is found to be 2.0826 $W/(\,^{o}C.\ m)$, it was obtained just after two sequential iterations. The thermal field solution at this optimized parameter is shown in Figure 7.7. As can be expected, the lower the value of the objective function the higher the cables' temperatures as a result of reducing the backfill thermal conductivity, and the iteration will terminate at the nearest possible cable temperatures to the imposed constraint value which does not violate applied constraints and stay within the feasible set of optimized parameter set. The maximum percentage difference of the cable temperature from the imposed constraint value was found to be 0.0127%.

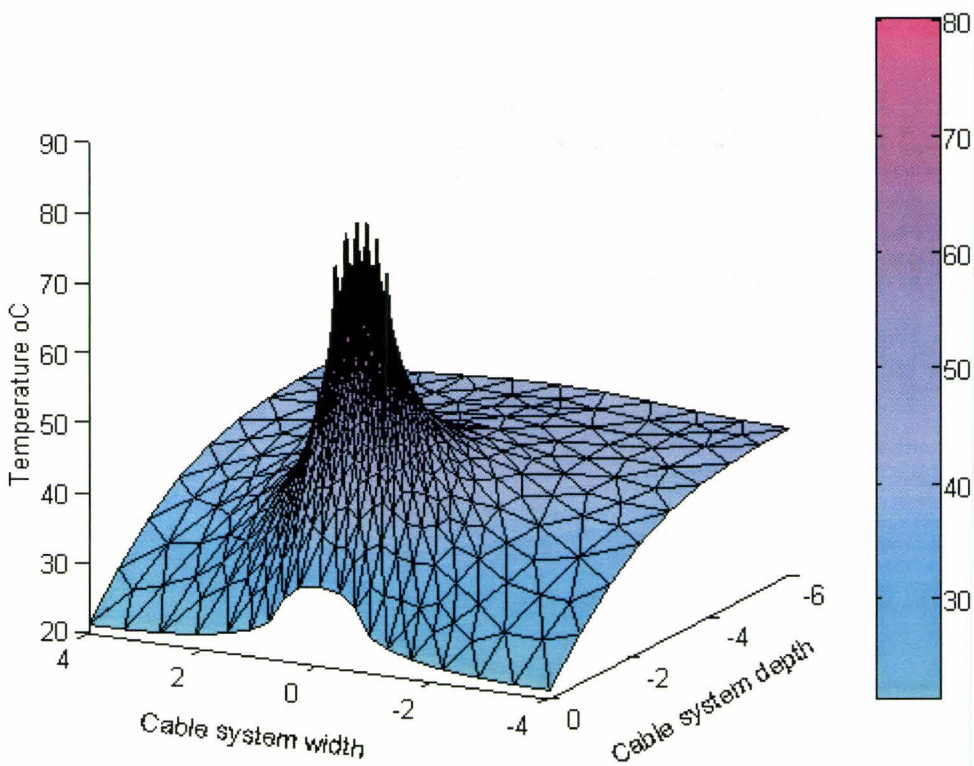

Fig. 7.7 Temperature solution at optimal parameters of six flat cables arrangement (backfill cost reduction)

7.3 SIX DUCT BANK CABLE SYSTEM

7.3.1 Overview

The perturbed finite element sensitivity technique can be applied to any complex cable configurations and boundaries to assess the effect of variations of various cable system parameters. Six 69 kV oil-filled cables laid in fiber and concrete duct bank having the dimensions shown in Figure 7.8 are considered with the nominal values of parameters illustrated in Table 7-8

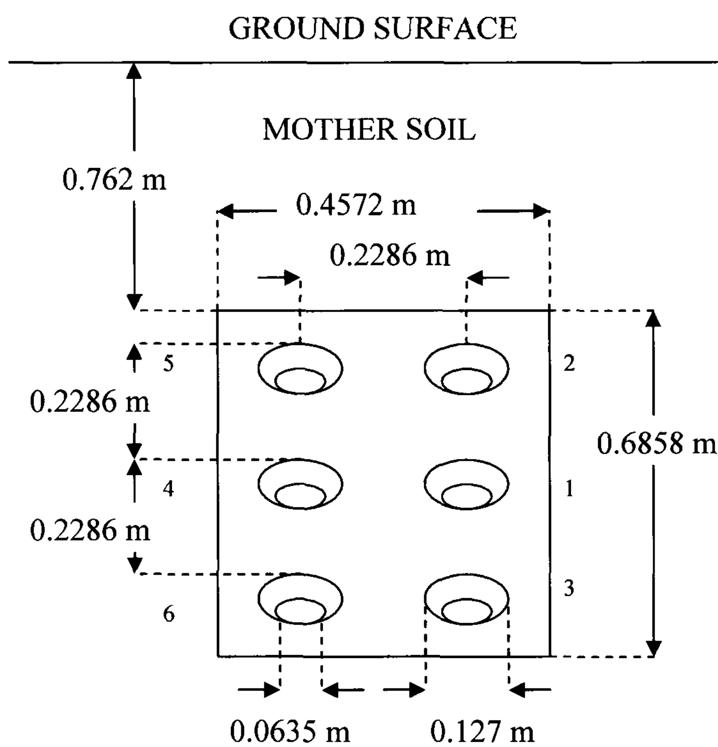

Fig. 7.8 Two identical circuits 69 kV single conductor oil filled cable in fiber and concrete duct bank

TABLE 7-8: DUCT BANK CABLE SYSTEM NOMINAL PARAMETER VALUES

Fiber duct	0.2083 *W/(°C.m)*
Concrete thermal conductivity	1.1764 *W/(°C.m)*
Earth thermal conductivity	0.8333 *W/(°C.m)*
Operating current	696 A
Conductor losses	14.79 *W/m*
Dielectric losses	1.87 *W/m*
Ambient temperature	25 ^oC
Heat convection losses coefficient	5 $W/(^oC.\ m^2)$

7.3.2 Thermal Evaluation

The thermal field for described cable system was evaluated for a convectional boundary condition at the earth surface and generating heat losses inside the cables, with the above mentioned nominal values. The system solution domain and the finite element grids are shown in Figure 7.9, the temperature profile is shown in Figure 7.10.

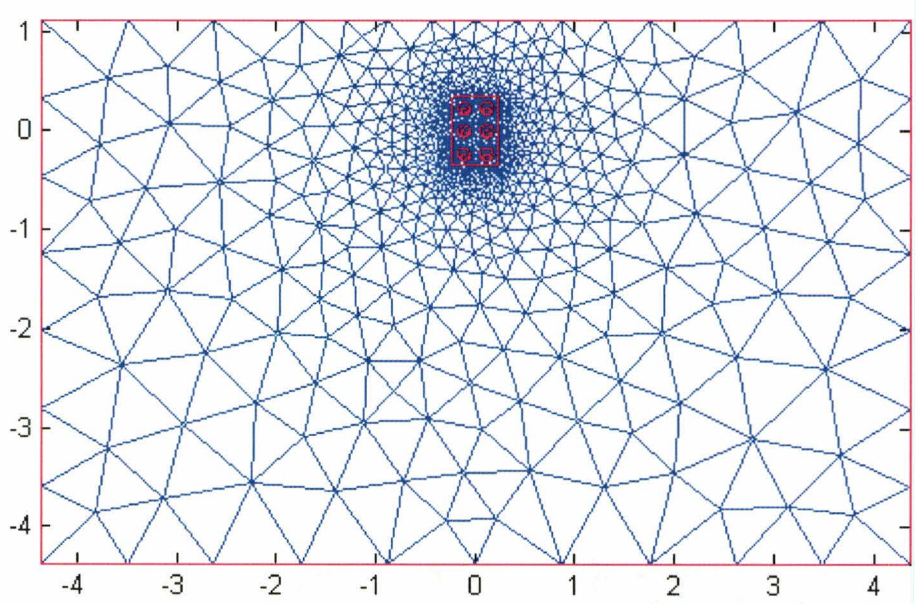

Fig. 7.9 Finite element mesh imposed on the model solution domain of duct bank configuration

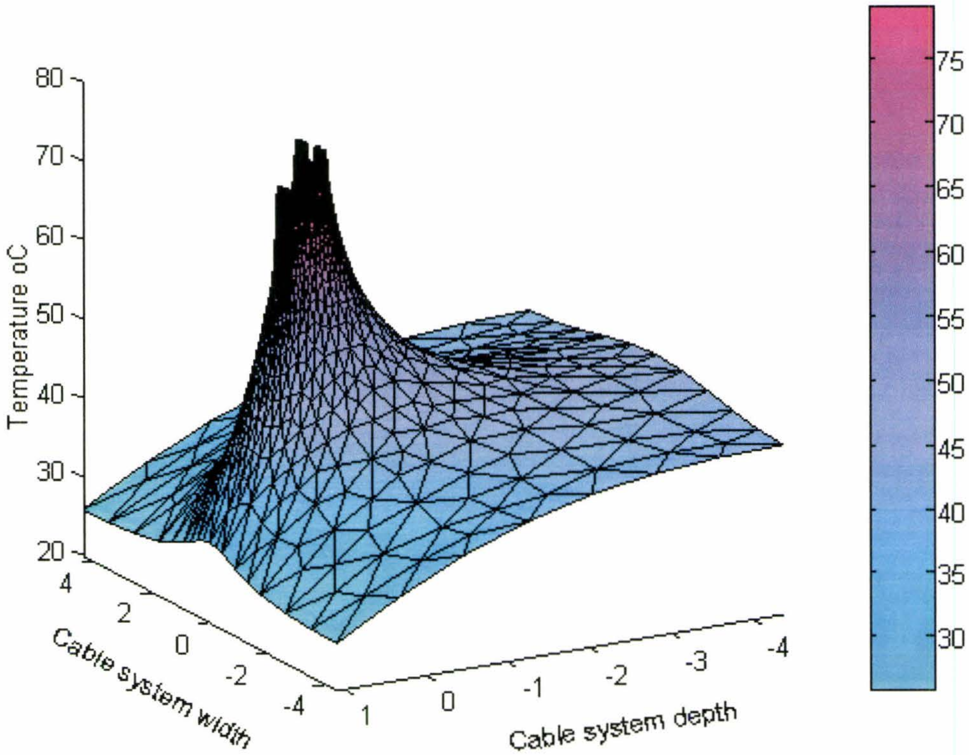

Fig. 7.10 Three dimensional temperature distribution of duct bank configuration

7.3.3 Sensitivity Calculation

Table 7-9 shows the sensitivities of the hottest cables' temperatures (ordered as indicated in figure 7.8) with respect to the system thermal conductivities, boundary condition parameters and generated heat inside the cables.

TABLE 7-9: TEMPERATURES SENSITIVITIES OF DUCT BANK CABLES AT NOMINAL PARAMETRES VALUES

Sensitivity $\partial T/\partial p$ / Parameter(p)	Cable #1	Cable #2	Cable #3	Cable #4	Cable #5	Cable #6
Mother soil thermal conductivity $W/(^oC.\ m)$	-46.71	-43.19	-48.49	-46.71	-43.19	-48.50
Concrete thermal conductivity $W/(^oC.\ m)$	-6.814	-4.930	-4.871	-6.798	-4.978	-4.900
Ambient temperature ^oC	1	1	1	1	1	1
The heat convection loss coefficient $W/(^oC.\ m^2)$	-0.606	-0.640	-0.580	-0.606	-0.640	-0.580
The generated heat in the cables ($W/\ m$)	3.234	2.906	3.157	3.233	2.913	3.161

Table 7-10 shows the new temperature values and the percentage deviation from the cable temperatures calculated using the perturbed finite element sensitivity analysis, due to 10%, increasing in the mother soil and concrete thermal conductivities sequentially.

TABLE 7-10: CABLE SURFACE TEMPERATURES DUE TO MOTHER SOIL AND CONCRETE THERMAL CONDUCTIVITY VARIATIONS

Cable Number	Hottest spot cable surface temperature ^oC			Temperature percentage deviation (%)	
	Nominal value	New values (conventional finite element)			
		10% $k_{\text{mother-soil}}$	10% $k_{\text{concreter}}$	10% $k_{\text{mother-soil}}$	10% $k_{\text{concreter}}$
1	78.88	75.33	78.14	0.4552	0.0697
2	73.41	70.14	72.87	0.4643	0.0576
3	77.59	73.90	77.05	0.4762	0.0448
4	78.85	75.30	78.10	0.4554	0.0695
5	73.53	70.25	72.98	0.4636	0.0580
6	77.66	73.97	77.12	0.4759	0.0450

Table 7-11 shows the cables' hottest temperatures at the nominal case and the new temperatures for the case of 10% and -10% variations in the ambient temperature and the heat convection loss coefficient sequentially. Table 7-12 shows the percentage deviation of the cable temperatures calculated using the perturbed finite element sensitivity analysis from the conventional finite element temperatures.

TABLE 7-11: CABLE SURFACE TEMPERATURES DUE TO AMBIENT TEMPERATURE AND CONVECTION LOSS COEFFICIENT VARIATIONS

Cable Number	Hottest spot cable surface temperature ^oC				
	Nominal Value	New value (conventional finite element)			
		-10% T_{ambient}	10% T_{ambient}	-10% h	10% h
1	78.88	76.38	81.38	79.22	78.61
2	73.41	70.91	75.91	73.77	73.12
3	77.59	75.08	80.09	77.91	77.32
4	78.85	76.35	81.35	79.19	78.57
5	73.53	71.03	76.03	73.88	73.23
6	77.66	75.16	80.16	77.98	77.40

TABLE 7-12: PERCENTAGE DEVIATION BETWEEN THE SENSITIVITY BASE AND CONVENTIONAL FINITE ELEMENT METHODS

Cable Number	Temperature percentage deviation (%)			
	-10% T_{ambient} $\times 10^{-4}$	10% T_{ambient} $\times 10^{-5}$	-10% h	10% h
1	0.0422	-0.9846	0.0410	0.0340
2	0.1446	-0.8249	0.0462	0.0384
3	0.0109	0.5101	0.0401	0.0332
4	-0.0366	0.9331	0.0410	0.0340
5	-0.1323	0.6697	0.0461	0.0383
6	-0.0256	-0.2672	0.0401	0.0332

The sensitivity model was used to estimate the new cable temperatures values due to -10% and +10% changing in the generated heat inside the cables. The disturbed temperatures calculated using the conventional finite element and the corresponding deviation of the perturbed finite element sensitivity of cables temperature from the conventional finite element temperatures is shown in Table 7-13.

TABLE 7-13: CABLE SURFACE TEMPERATURES DUE TO GENERATED HEAT VARIATIONS

Cable Number	Hottest spot cable surface temperature ^oC			Temperature percentage deviation (%)	
	Nominal value	New values (conventional finite element)			
		-10% Q	10% Q	-10% Q $\times 10^{-5}$	10% Q $\times 10^{-5}$
1	78.88	73.50	84.27	-0.0065	-0.0285
2	73.41	68.57	78.25	0.3625	0.9581
3	77.59	72.33	82.85	0.6808	-0.0832
4	78.85	73.47	84.23	-0.0439	0.0748
5	73.53	68.67	78.38	-0.5930	-0.9198
6	77.66	72.39	82.93	-0.2693	0.0566

The cable temperatures were calculated for the case of changing all the mentioned parameters, and were compared with the corresponding values calculated from the sensitivity model. This comparison is shown in Table 7-14 for the case of increasing all parameters by 5% and 10%.

TABLE 7-14: CABLE SURFACE TEMPERATURES DUE TO ALL PARAMETERS VARIATIONS

Cable Number	Hottest spot cable surface temperature ^oC			Temperature percentage deviation (%)	
	Nominal value	New values (conventional finite element)			
		5% *All P*	10% *All P*	5% *All P*	10% *All P*
1	78.88	80.33	81.76	-0.0052	-0.0198
2	73.41	74.83	76.24	-0.0044	-0.0169
3	77.59	79.01	80.43	-0.0046	-0.0176
4	78.85	80.29	81.72	-0.0052	-0.0197
5	73.53	74.95	76.36	-0.0045	-0.0171
6	77.66	79.09	80.50	-0.0046	-0.0177

7.3.4 Optimization Performance

The proposed model in figure 7.8 of six 69 kV oil-filled cables laid in fiber and concrete duct bank is considered. At the parameters nominal values, the maximum cable surface temperature was noted to be 78.88 ^oC, observed at cable 1 and 4. The design problem will be formulated for the maximum desired cable surface temperature to be 65 ^oC. In this case, in addition to the surrounding thermal conductivities, the boundary condition parameters will be optimized. The controlled parameters will be, respectively, mother soil conductivity, concrete thermal conductivity, ambient temperature, and heat convection loss coefficient. This can be described in the following mathematical representation:

$$
\begin{aligned}
\text{Minimize} \quad & \sum_{i}^{n}(T_i - 65)^2 \\
\text{st} \quad & 0 \le k_{mother\_soil} \le 6 \\
& 0 \le k_{concrete} \le 6 \\
& 0 \le T_{ambient} \le 30 \\
& 0 \le h \le 10
\end{aligned}
\tag{7.3}
$$

where T_i are the internal surface temperatures. Using the developed optimization-finite element sensitivity approach, a solution is obtained at $k_{mother\text{-}soil}$ = 1.1260 $W/(\,^oC.\ m)$, $k_{concrete}$=1.6063 $W/(\,^oC.\ m)$, $T_{ambient}$=23.7122 ^oC and h=5.1527 $W/(\,^oC.\ m^2)$, which satisfy the provided constraints for which the objective function has the minimum value of 1.3172 $^oC^{\ 2}$. The thermal field for this system was evaluated at the new optimized parameter using the finite element approach as shown in Figure 7.11. Four iterations are sufficient to approach the optimal solution with high accuracy as can be noted from Figure 7.12.

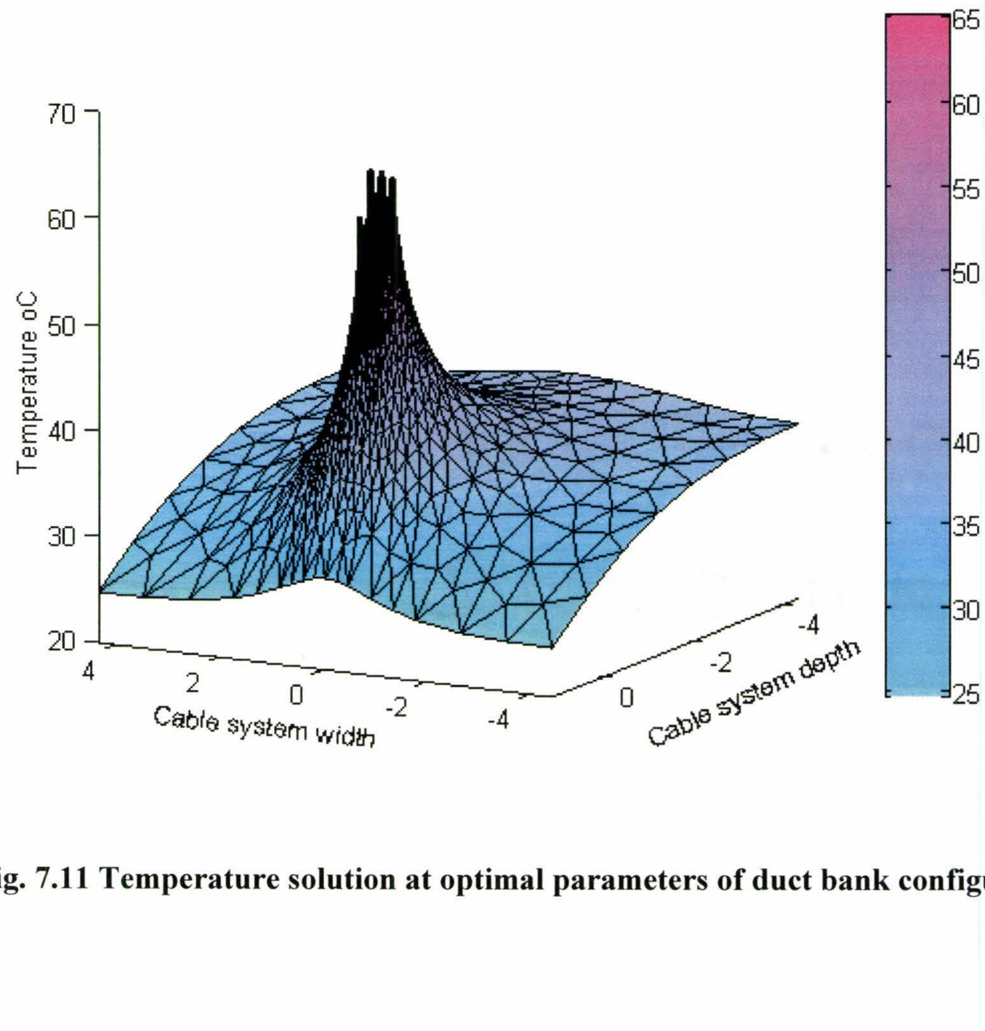

Fig. 7.11 Temperature solution at optimal parameters of duct bank configuration

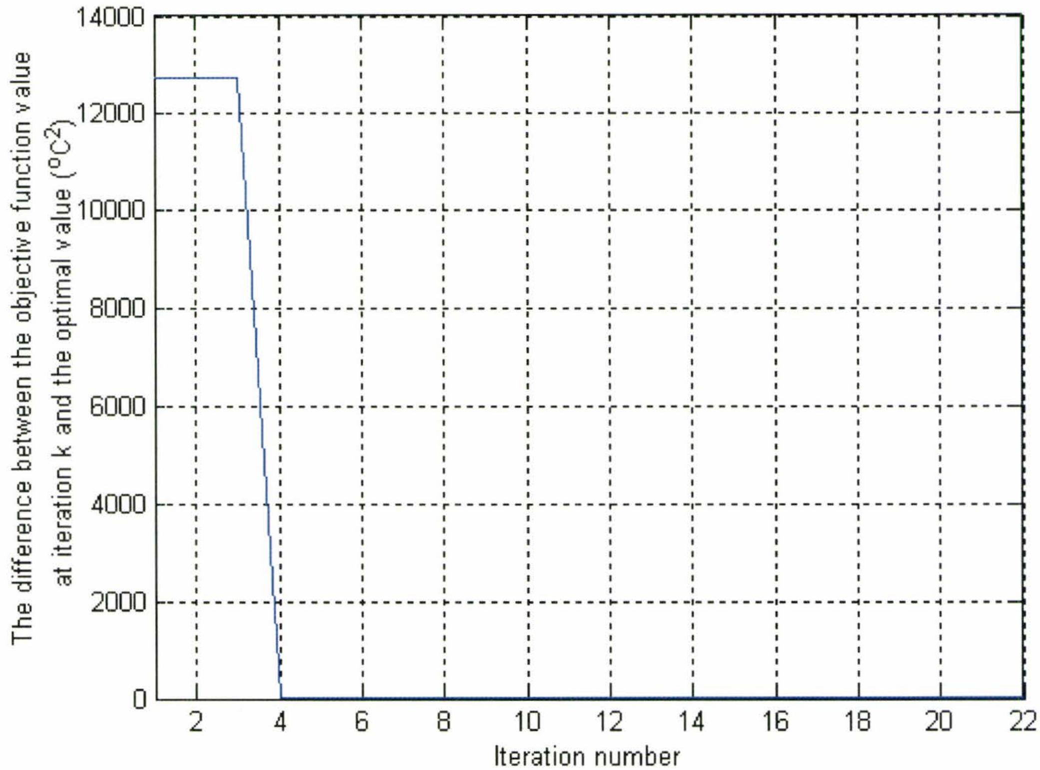

Fig. 7.12 Error versus iteration numbers of optimization process for duct bank configuration

7.4 THREE 132 kV XLPE CABLE SYSTEM

7.4.1 Overview

A benchmark system of three 132 kV XLPE underground cables in multilayered non-homogenous soil is modeled using perturbed finite element sensitivity analysis in order to optimize the cable performance. The effect of multilayered thermal conductivities and boundary parameters variations on the actual cable system ampacity is investigated, using the introduced sensitivity model. Also, a comparison is held of the obtained results with the conventional finite element approach in order to show the applicability and usefulness of the developed methodology for the purpose of exploring the operating parameter variations effect in straight sensitivity manner without repeating the thermal field analysis for such parameter changes. Furthermore, optimization of the cable system parameters is performed for a desired objective performance.

Figure 7.13 shows the configuration of a 132 kV XLPE cable system of the Saudi Electricity Company, which is still in service (Appendix C). The three cables are directly buried in a trench and covered by a backfilled layer, both layers are surrounded by the native soil. The technical data for the cable and associated surrounding material are given in Table 7-15.

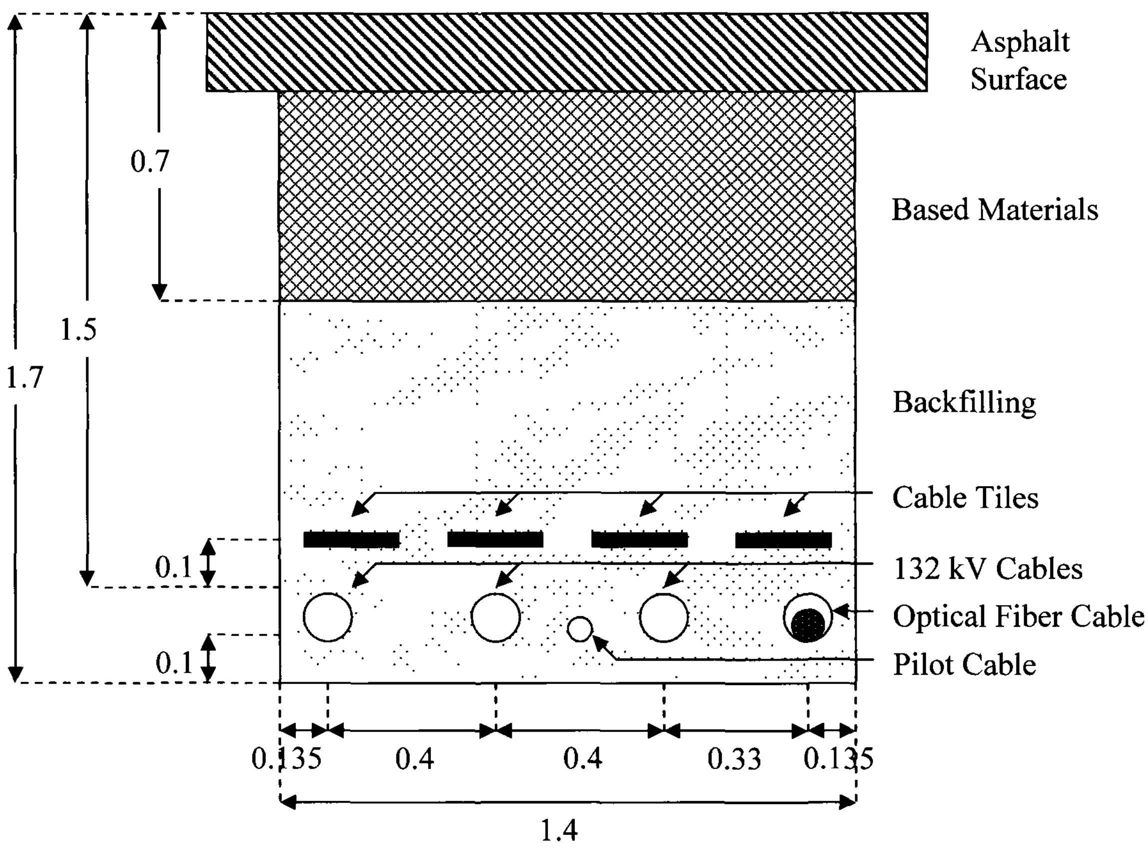

Fig. 7.13 Three 132 kV XLPE buried underground cable system

TABLE 7-15 TECHNICAL DATA FOR 132 kV 1000 mm^2 COPPER XLPE CABLE

Max. temperature on insulation	90 °C
Ground temperature	30 °C
Heat convection loss	5 W/(°C. m^2)
Max. dielectric losses of 3-phase circuit	1.6 W/m
Sheath loss of 3-phase circuit	3.7 W/m
Total losses when cable loaded	53.8 W/m
Ground thermal resistivity	166 °C. cm/W
Bedding thermal resistivity	95 °C. cm/W
Backfill thermal resistivity	80 °C. cm/W
Conductor thermal resistivity	0.26 °C. cm/W
Tape thermal resistivity	2 °C. cm/W
XLPE insulation thermal resistivity	350 °C. cm/W
Sheath thermal resistivity	2.9 °C. cm/W
Cement thermal resistivity	91 °C. cm/W

7.4.2 Thermal Evaluation

The ground surface is modeled as a convective boundary with an ambient temperature and heat convection loss coefficient provided in table 7-15. However, in the finite element method the solution domain must be discretized by means of nodes and elements. Also, their geometrical, topological, and property definitions must be specified. Consequently, as a result of meshing process, the elements and their nodes will be labeled and the node coordinates will be determined. Figure 7.14 shows a sample of the discretized field region of the proposed model.

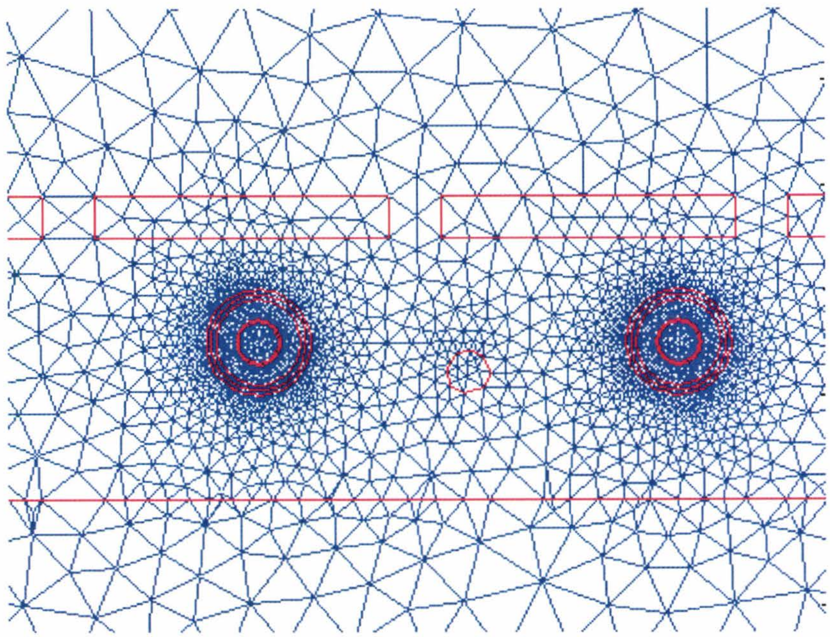

Fig. 7.14 Portion of the discretized region shows middle and right cables of 132 kV cable system

7.4.3 Thermal Parameter Variation Investigation Using Sensitivity Model

In this section, the sensitivity model is used to investigate the variations effects of the native soil, bedding and backfill thermal conductivities as well as the conductors current and heat convection loss on the three cable maximum temperatures.

7.4.3.1 Effect of Native Soil Thermal Conductivity on the Cable Temperatures

Soil thermal resistivity can easily vary by a factor of 5 over the length of the circuit, and it can vary by a factor of 2 or more at a specific location over time because of a change in moisture content [64]. In the proposed model, the thermal conductivity of the native soil is varied over a specified range while the all other parameters, including thermal conductivities of the bedding, backfill and cable contents as well as boundary condition parameters, are kept at the nominal values described in table 7-15. The effect of variation of the native soil thermal conductivity on the three cables maximum temperatures using both perturbed and conventional finite elements is shown in Figure 7.15. Note the close correspondence between the results. In order to show the impact of such conductivity variation, sensitivity curves of cables temperature at different parameter values are shown in Figure 7.16.

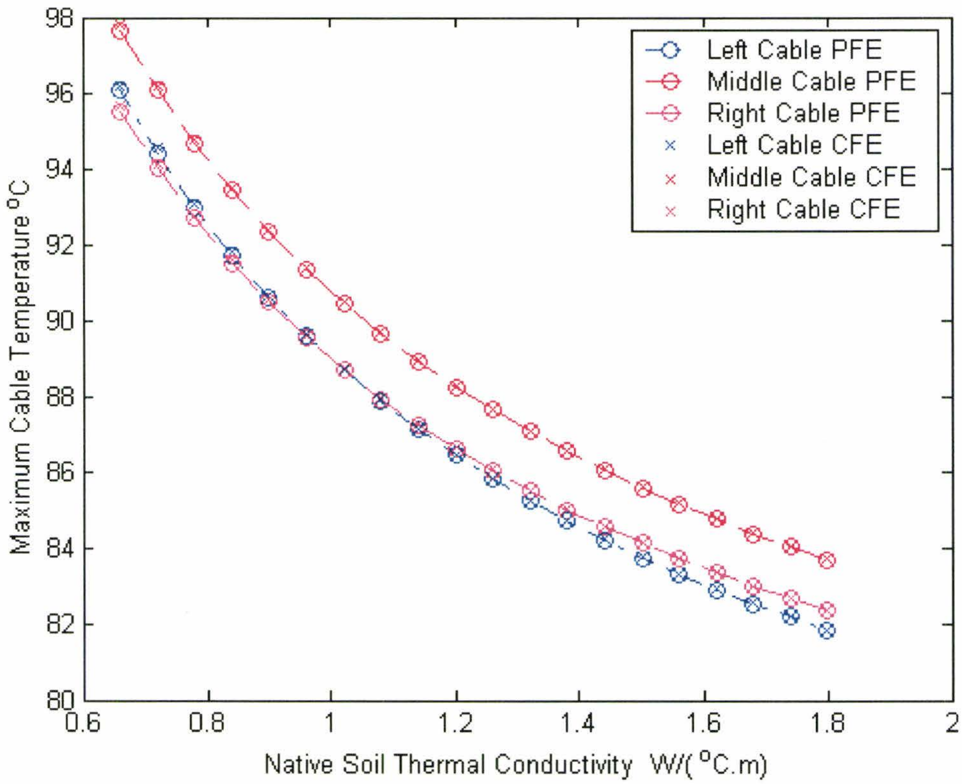

Fig. 7.15 Effect of variation of the native soil thermal conductivity (132 kV cable system)

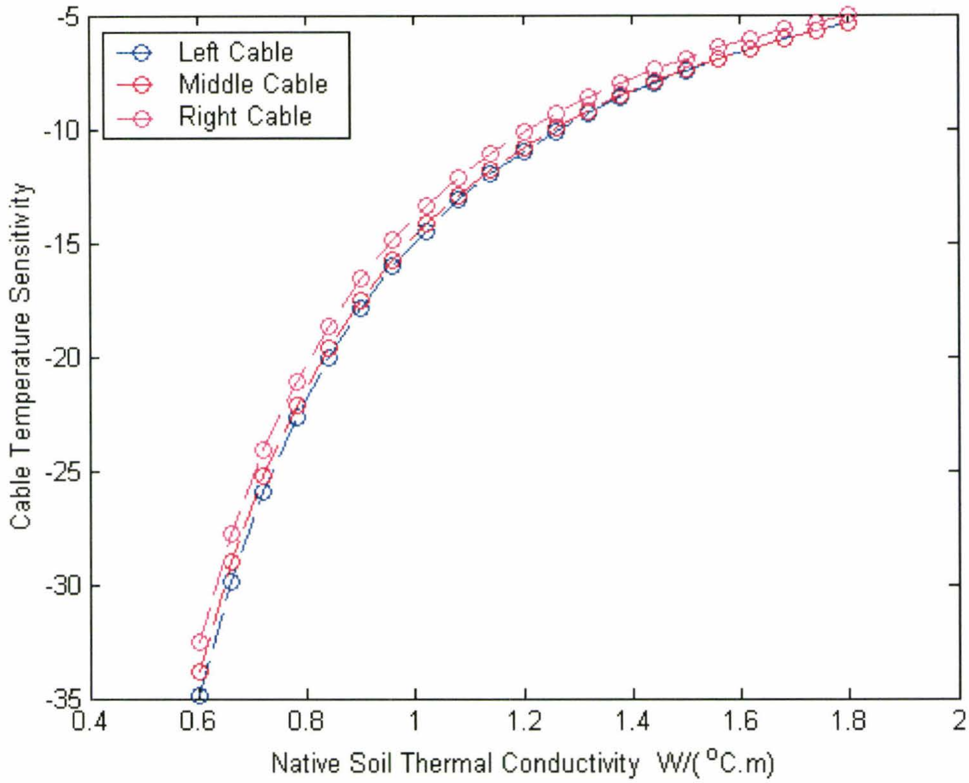

Fig. 7.16 Cables temperature sensitivity curves at different native soil thermal conductivity values (132 kV cable system)

7.4.3.2 Effect of Bedding and Backfill Conductivities on the Cable Temperatures

The corrective trench envelope has to be made up of the specific material and placed at specific conditions (density and moisture). Any variations from the design specifications can lead to conditions that will adversely affect the performance. In the proposed model the trench is divided into two zones under the protective layer, namely the backfill and bedding. The thermal conductivity of both bedding and backfill are varied simultaneously to illustrate the effect on the cables temperature and shown in Figure 7.17 and Figure 7.18 respectively. A comparison between both perturbed finite element and conventional finite element shows high matching between both results. The advantage of the PFE is due to flexibility and low computation analysis. As well, the additional information for the temperature sensitivity with parameter changes is illustrated in Figure 7.19 and Figure 7.20 for both bedding and backfill respectively. The cable temperatures decrease while soil thermal conductivities increase. The rate of temperature reduction due to bedding thermal conductivity increasing is much than that achieved by increasing backfill thermal conductivity. For example, the increase of the bedding conductivity from its nominal value by 40% results in a temperature reduction on the middle cable by 2.8°C. On the other hand, the same percentage increase of the backfill from its nominal value results in just a 0.34°C temperature reduction on the same cable. This can be noted by comparing the two sensitivity curves associated with each of the two parameters. The improvement in the bedding soil allows more heat dissipation from the cable than the improvement in the backfill.

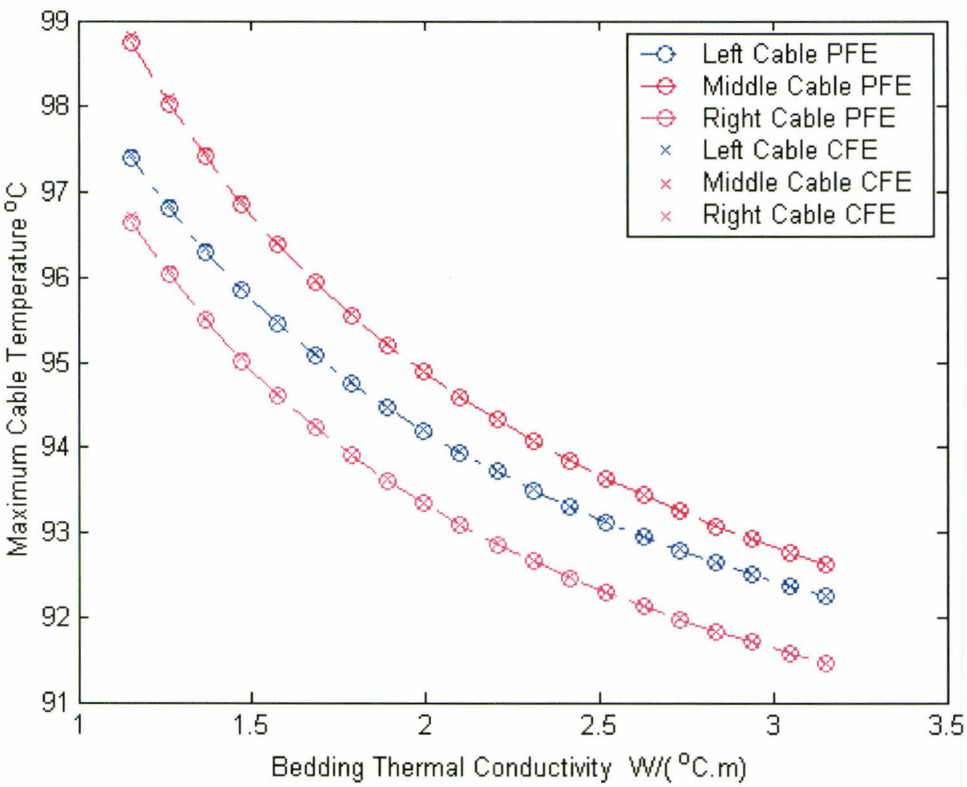

Fig. 7.17 Effect of variations in bedding conductivity on the cable temperatures (132 kV cable system)

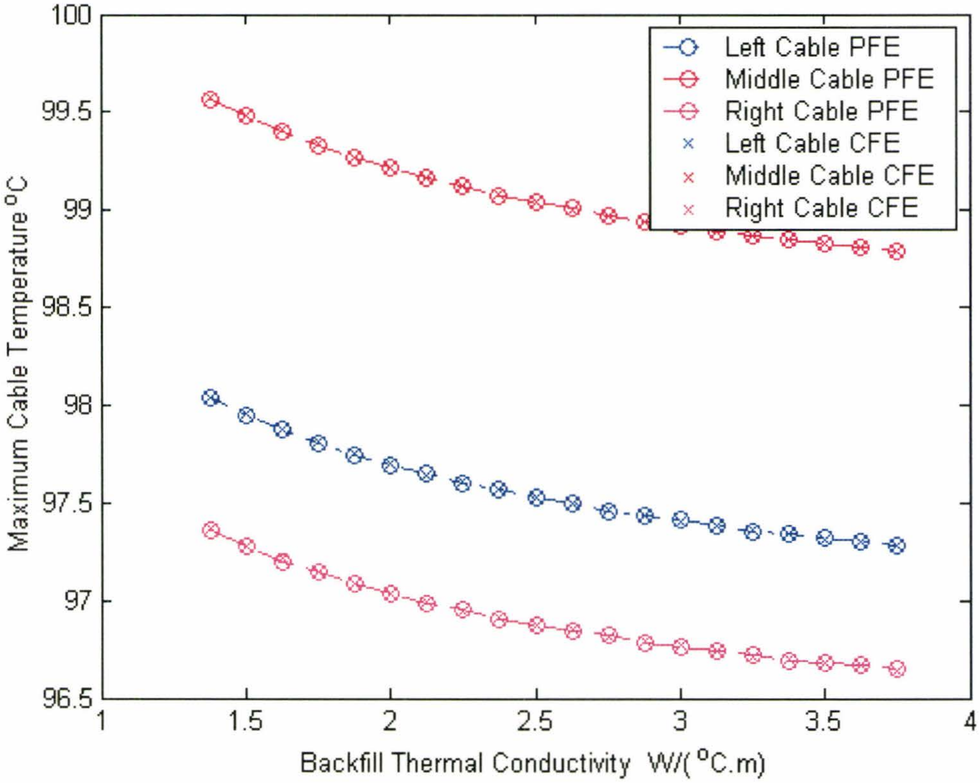

Fig. 7.18 Effect of variations in backfill conductivity on the cable temperatures (132 kV cable system)

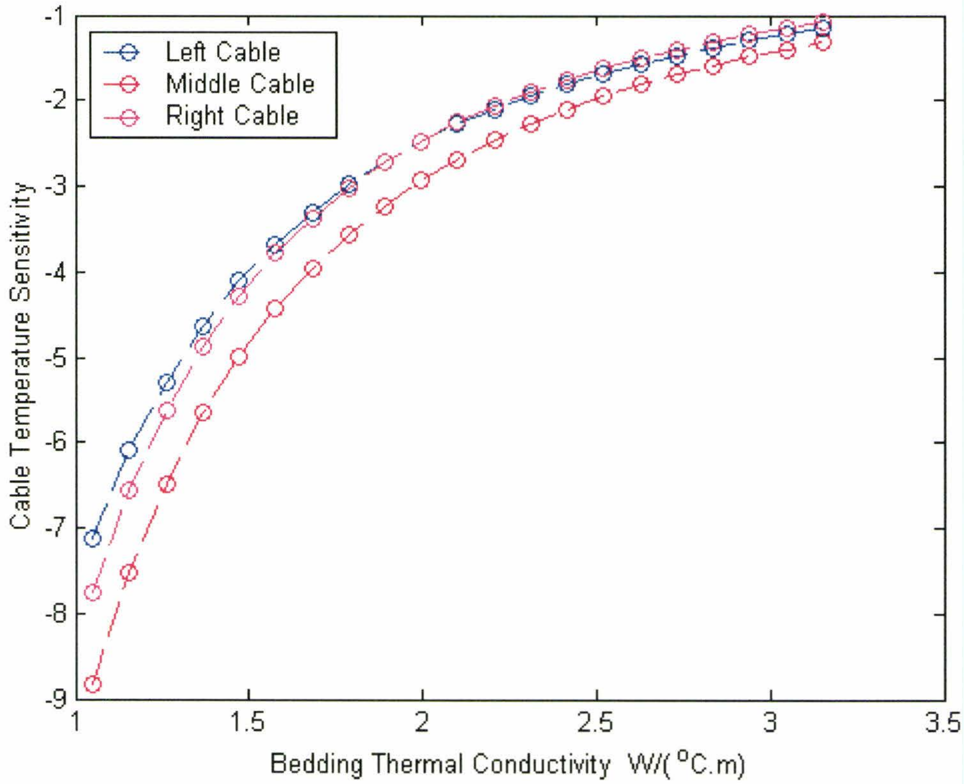

Fig. 7.19 Cables temperature sensitivity curves at different bedding thermal conductivity values (132 kV cable system)

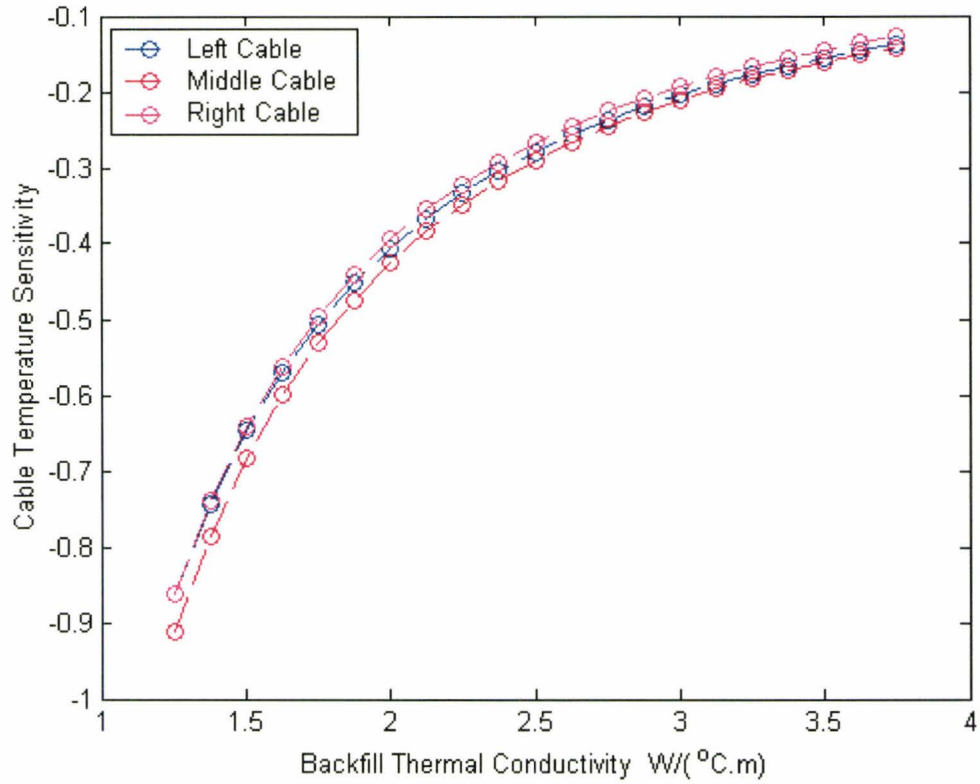

Fig. 7.20 Cables temperature sensitivity curves at different backfill thermal conductivity values (132 kV cable system)

7.4.3.3 Effect of Heat Generation on the Cable Temperatures

The allowable heat input increase is directly proportional to the maximum allowable steady state cable temperatures as can be noted from Figure 7.21 and from the flat lines of the sensitivity curves shown in Figure 7.22. The rates of temperature increase due to the increase in the heat dissipation on right, middle and left cables are 4.06, 4.15 and 4.02 ($W/^oC.m^2$) respectively. However, this study was performed to study the effect of variation of each parameter simultaneously where remaining parameters are assumed to be unchanged. This will provide operators with pure role of each parameter change on the overall cable performance. However, some parameters can appear highly correlated with each other. For example, the bedding soil is highly moisture dependent which will be affected by the amount of heat dissipation depending on the initial moisture content.

Consequently, in high moisture content the bedding conductivity will not stay constant due to migration of moisture caused by heat generation in side the cable.

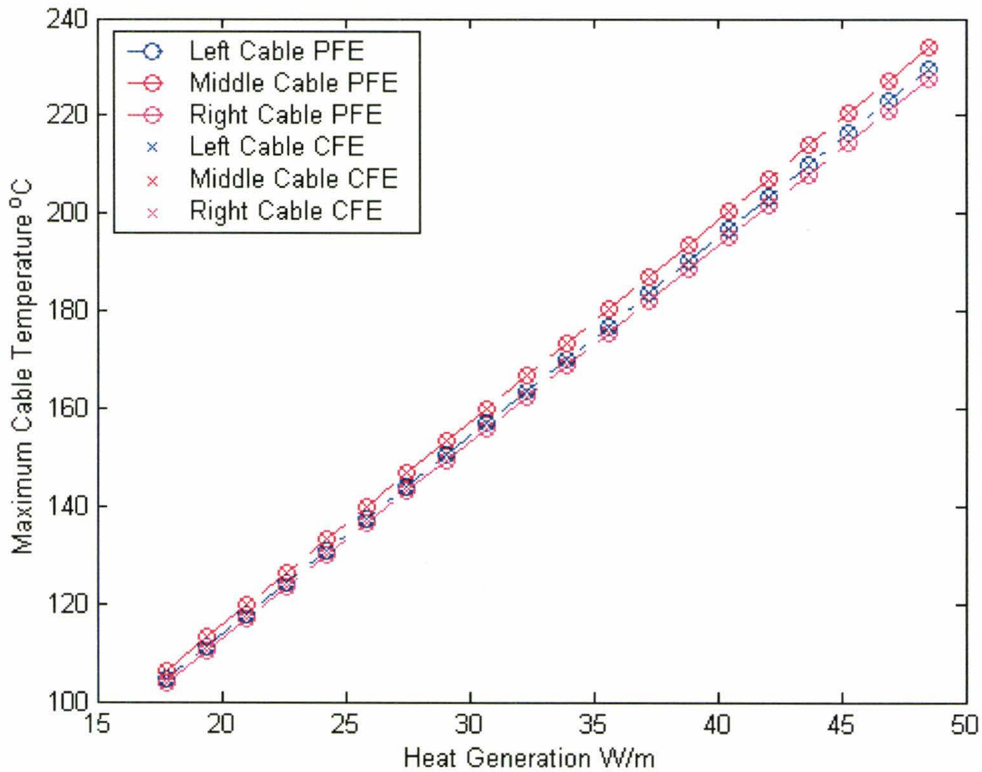

Fig. 7.21 Effect of heat generation on the cable temperatures (132 kV cable system)

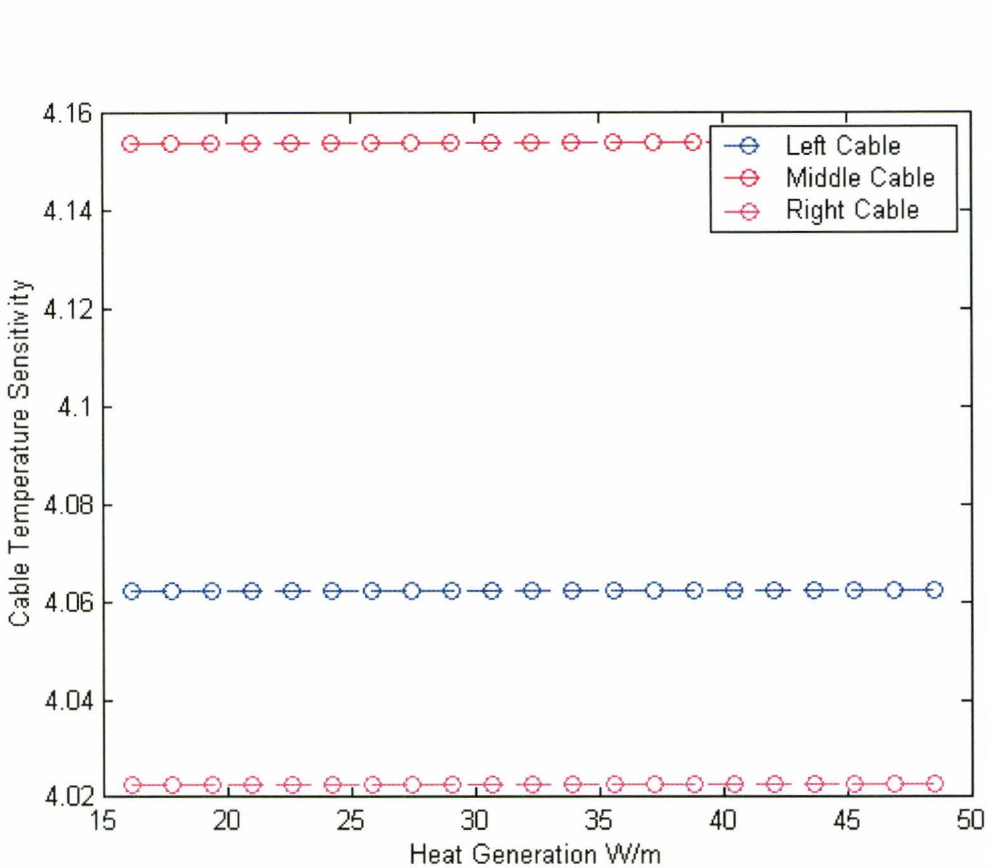

Fig. 7.22 Sensitivities of cables temperature to heat generation (132 kV cable system)

7.4.3.4 Effect of Heat Convection Losses Variation

The effect of heat convection losses coefficient on the cable temperatures is considered. The heat transfer coefficient is directly related to wind velocity which is influenced by seasonal changes and environmental conditions. Consequently, in such a highly environmental dependent parameter, uncertainty is expected when determining its value. The effect of the heat convection losses on the cables temperature is shown in Figure 7.23, increasing this coefficient value increases the amount of heat dissipation and results in cables temperature reduction. However, this reduction is noticeable up to 10 W/^{o}C.m^2 and after that the reduction is insignificant. Similarly, from an associated sensitivity curve as shown in Figure 7.24, the sensitivity curves start to flatten. Furthermore, it can be noted from this figure that the three cables sensitivity curves overlap each other which means that the effect due to the heat convection parameter is equal on all three cables and results in identical temperature increases.

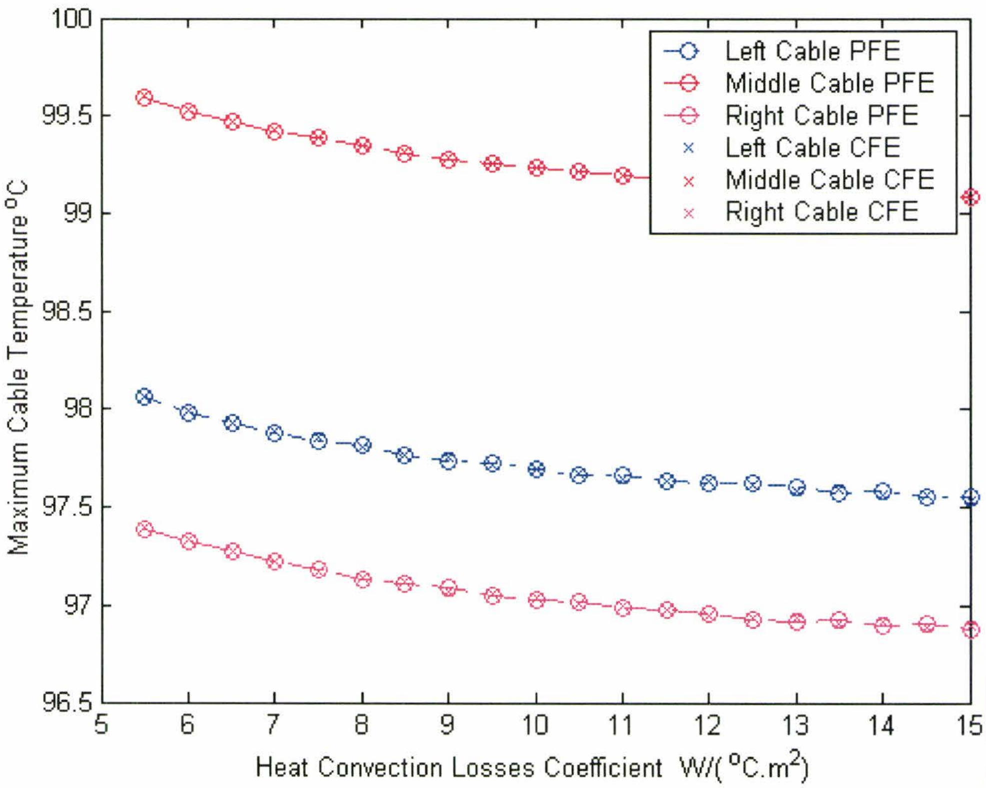

Fig. 7.23 Effect of the heat convection losses on the cable temperatures (132 kV cable system)

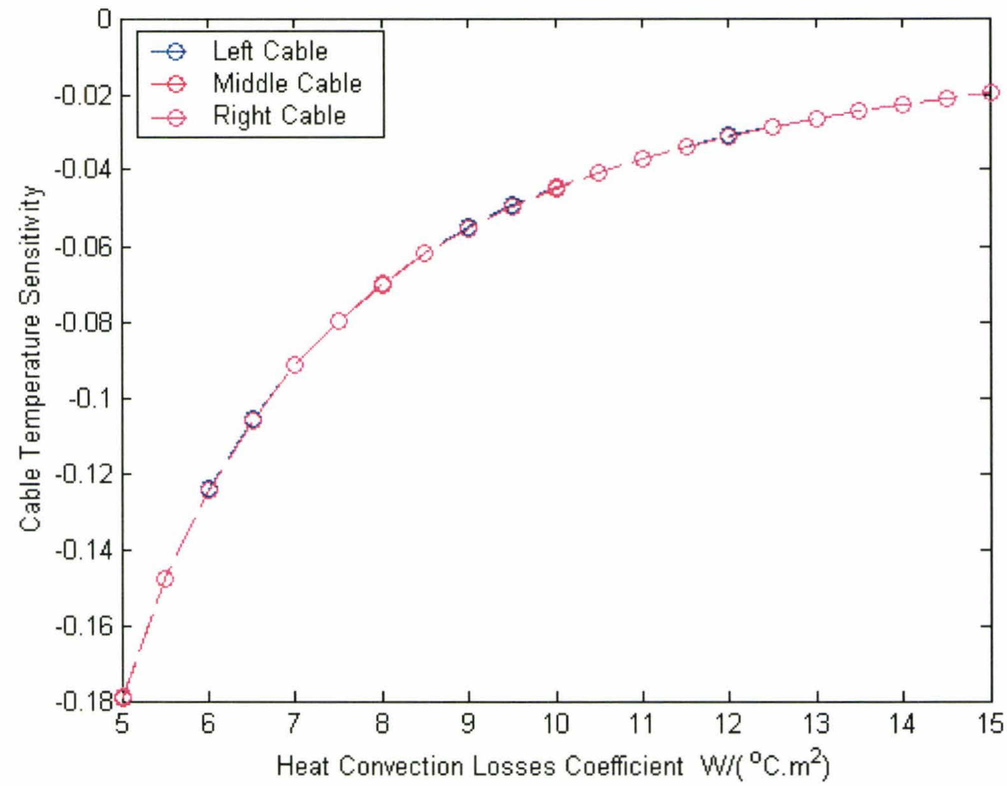

Fig. 7.24 Sensitivities of the cables temperature to heat convection losses (132 kV cable system)

7.4.4 Optimization Performance

In the formulation of a practical problem, the objective function is formulated to redesign the cable system parameters in order to reduce cables temperature of their high operating temperature to a desired temperature of 75 ^{o}C, which would result in increasing the cable current carrying capacity and enhancing the overall cable performance. The mother-soil, bedding and backfill thermal conductivities were chosen to be the controlled parameter as they have a big impact on determining the cables temperature. Theses parameters are constrained using upper and lower limits. The objective function is defined as the sum of the deviations squared of the three maximum cables temperature from the desired temperature as can be described mathematically as follows:

$$\text{Minimize} \quad \sum_{i}^{n} (T_i - 75)^2 \tag{7.4}$$

$$\begin{aligned} \text{st} \quad & 0 \leq k_{\_mother\,soil} \leq 6 \\ & 0 \leq k_{\_bedding} \leq 6 \\ & 0 \leq k_{\_backfill} \leq 6 \end{aligned}$$

where T_i is the internal conductor temperature of the cable i, i=1,2,3

The thermal field in the medium of cable and surrounding is solved in terms of design parameters, and the associated chosen cable temperature sensitivities are carried out using the perturbed finite element approach. Consequently, these outputs are utilized by the nonlinear optimization approach in order to achieve the desired objective design in an efficient and reliable way. Using the developed optimization-finite element sensitivity approach, solution is obtained at $k_{mother\text{-}soil}$ = $5.86 W/(^oC.m)$, $k_{bedding}$ =$5.16 W/(^oC.m)$ and $k_{backfill}$ =$5.99 W/(\ ^oC.\ m)$, which satisfy the provided constraints for which the objective function has the minimum value of $0.1165\ {}^oC^{\ 2}$. The thermal field for this system was evaluated at the new optimized parameters using the finite element approach as shown in Figure 7.25.

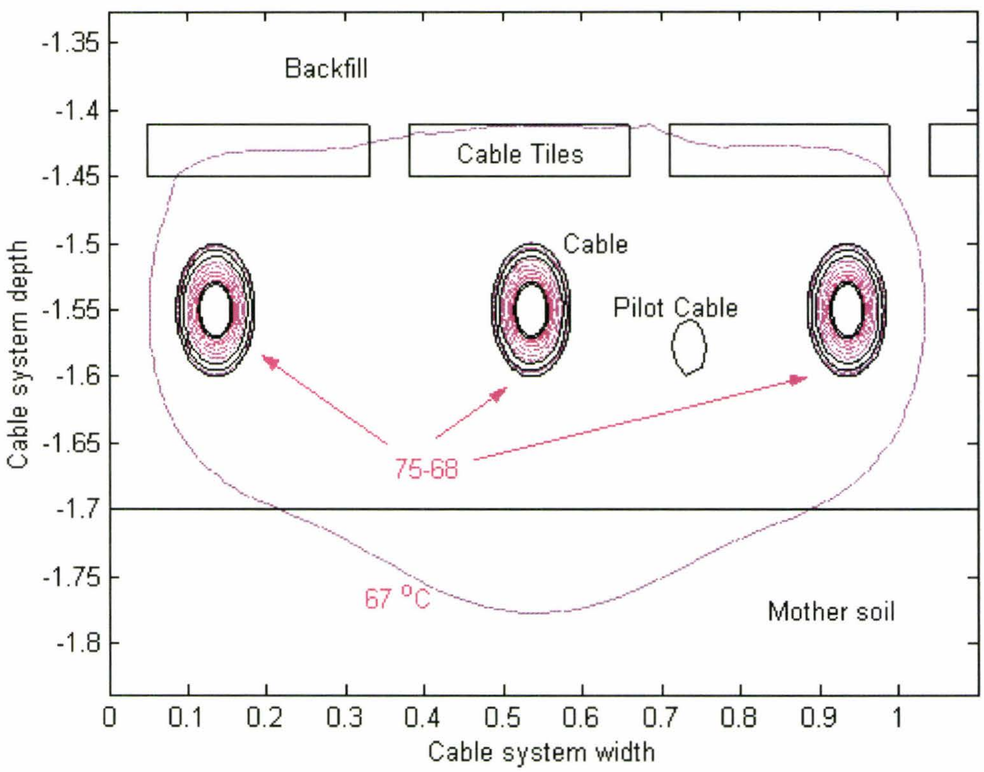

Fig. 7.25 Temperature solution at optimal parameters for the cable temperature reduction (132 kV cable system)

In order to show the advantage of the proposed optimization- finite element sensitivity approach in terms of reducing the number of iterations required by means of the objective and constraint gradient, Figure 7.26 shows the number of required iterations against the deviation at each step from the optimal value. A dramatic reduction in the minimized objective function can be noted in the second iteration, and at the sixth iteration the desired objective was almost achieved with high accuracy.

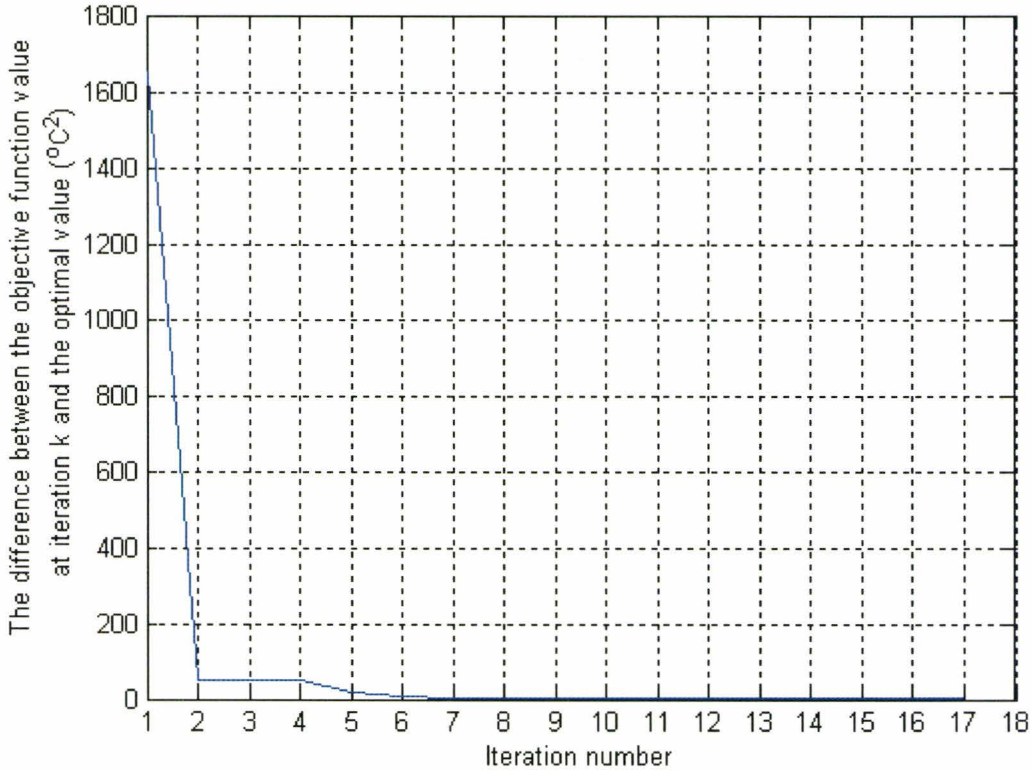

Fig. 7.26 Error versus iteration numbers (132 kV cable system)

One of the desired objectives by power utilities is to increase the maximum allowable load that cable can carry without exceeding the permissible temperature. This practical design was applied on the same cable system, where the summation of the three cables loading is used to define the objective function, the cable temperatures are used to define the nonlinear constraints in terms of the thermal circuit parameters as described mathematically by:

$$\begin{aligned} &\text{Minimize} \quad -\sum_{i}^{n} Q_i \\ &\text{st} \qquad T_i \leq 100 \\ &\qquad\quad k_{backfill} \leq 6 \end{aligned} \tag{7.5}$$

where Q_i are the heat losses inside cable i, n is the total number of cables and T_i the internal conductor temperature on cable i.

In addition to the three controlled parameters defined in the objective function (Q_1,Q_2,Q_3), the backfill can be improved to enhance such objective, and this parameter is defined as additional controlled parameter with upper and lower limits bounds. As was expected, the backfill value was driven up to its maximum allowable value defined in constraint 6 $W/(^oC.\ m)$, as the increasing of the backfill thermal conductivity allows more heat dissipation from the cables to the surrounding and, therefore, aid in reducing the cables temperature and allowing high internal cable heat generation without violating the imposed temperature in constraints as can be noted from the thermal field solution shown in Figure 7.27 and Figure 7.28, where the maximum cable temperatures are almost equal to the upper limit constraints. The maximum allowable heat generation was found to be 17.33 W, 15.14 W and 18.04 W for left, middle and right cables respectively.

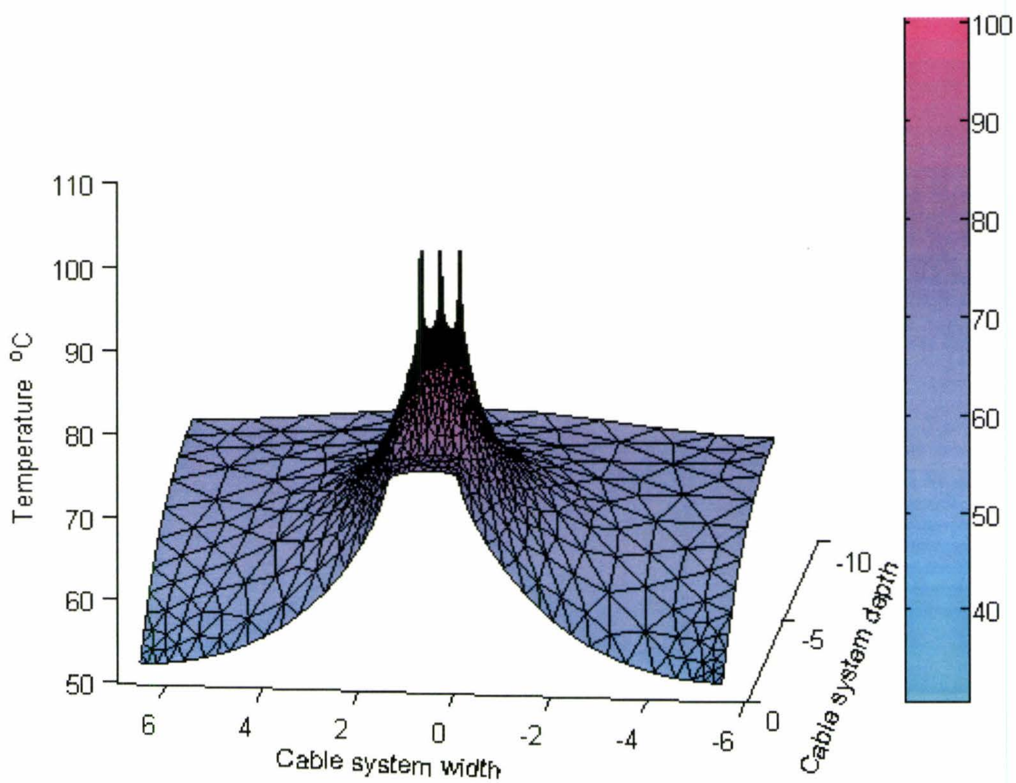

Fig. 7.27 Temperature solution at optimal parameters for ampacity improvement (132 kV cable system)

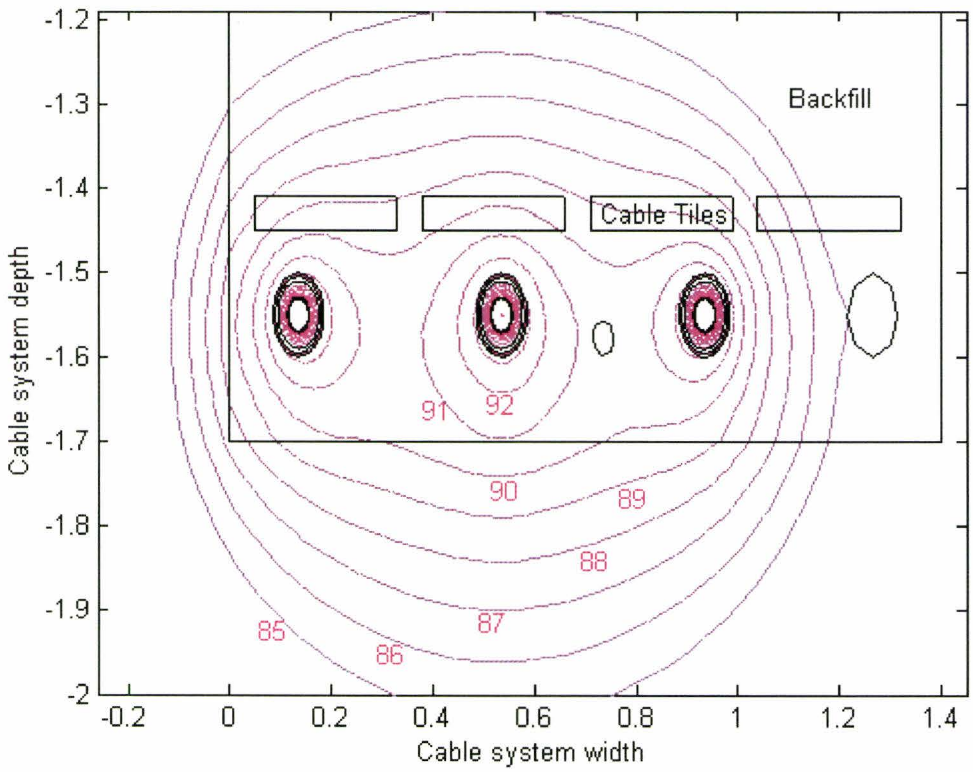

Fig. 7.28 Temperature contours at optimal parameters for ampacity improvement (132 kV cable system)

7.5 380 kV OIL-FILLED CABLE SYSTEM

7.5.1 Overview

In order to show the capability of the proposed algorithm to various complex cable configurations and boundaries, a double circuit of six cables at 380 kV, oil-filled and paper insulated (Appendix C), is considered with the technical specifications listed in Table 7-16, having the configuration shown in Figure 7.29.

TABLE 7-16: TECHNICAL DATA FOR 380 kV OIL FILLED CABLE

Rated voltage between phases	380 kV
Conductor radius	26.65 *mm*
Insulation thickness	20 *mm*
Ground temperature	30 ^oC
Heat convection loss	5 $W/(^oC.\ m^2)$
Total losses when cable loaded	49.8 *W/m*
Mother soil thermal conductivity	0.6 $W/(^oC.\ m)$
Trench thermal conductivity	1.05 $W/(^oC.m)$
Backfill thermal conductivity	1.25 $W/(^oC.\ m)$
Concrete raft thermal conductivity	1.1 $W/(^oC.\ m)$
Conductor thermal conductivity	385 $W/(^oC.\ m)$
Oil thermal conductivity	0.02 $W/(^oC.\ m)$
Jacket thermal conductivity	0.2 $W/(^oC.\ m)$
Paper insulation thermal conductivity	0.28 $W/(^oC.\ m)$

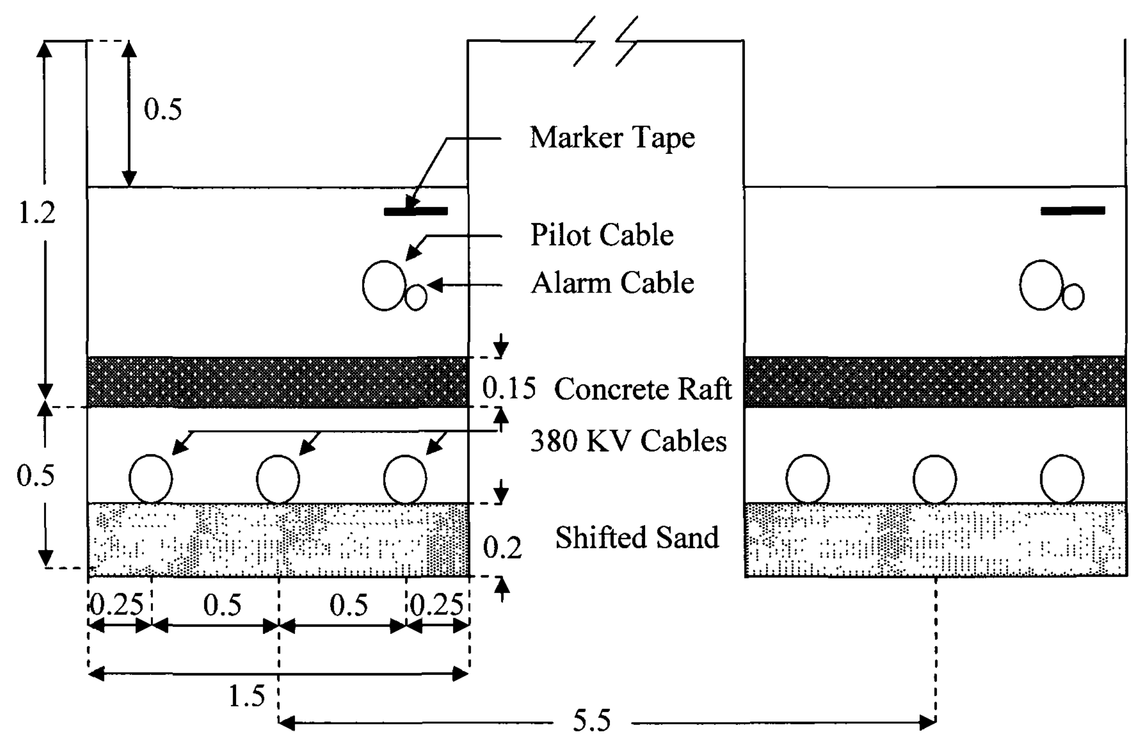

Fig. 7.29 Two identical circuits 380 kV single conductor oil filled cable

7.5.2 Thermal Evaluation

The maximum conductor temperatures were carried out using finite element analysis to be 93.02 ^oC, 96.33 ^oC, 94.05 ^oC, 93.94 ^oC, 96.42 ^oC and 93.46 ^oC for the cables from right to left respectively. The finite element grid of the system solution domain is shown in Figure7.30.

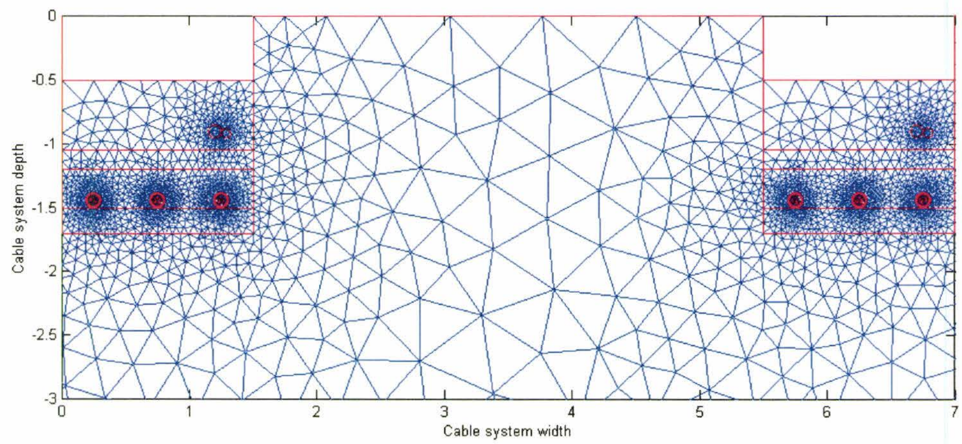

Fig. 7.30a Finite element mesh imposed on solution domain (both trench side)

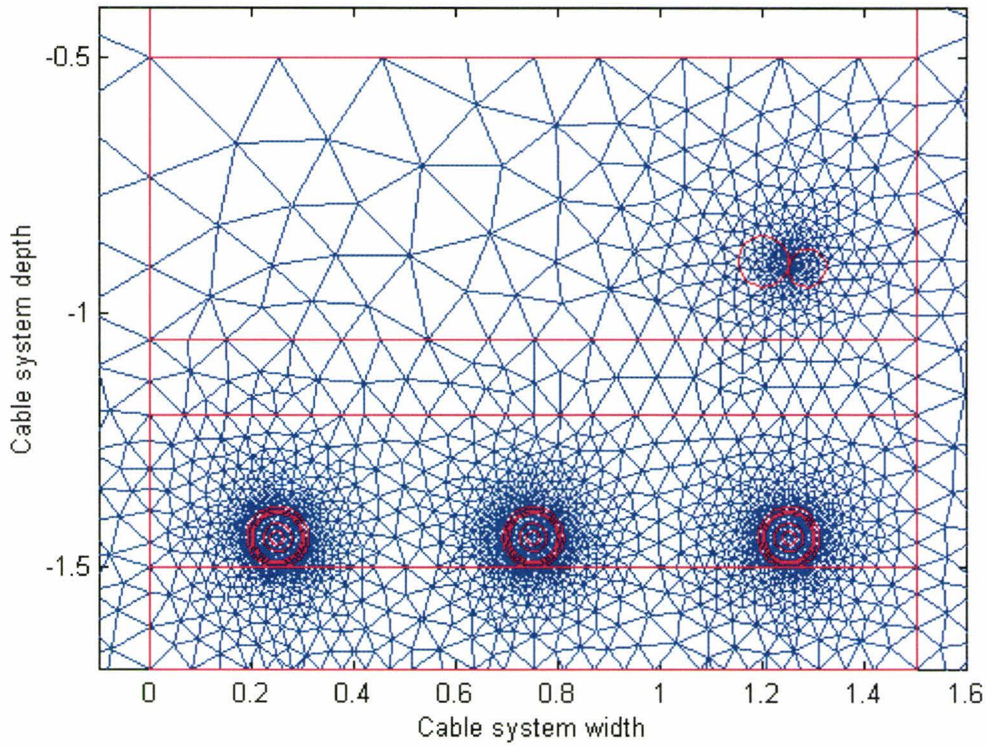

Fig. 7.30b Finite element mesh imposed on solution domain (one trench side)

7.5.3 Thermal Parameter Variation Investigation Using Sensitivity Model

In this regard, another advantage of the developed finite element sensitivity analysis is, the low computation required for the analysis which merits further investigation. On the other hand, a comparison between the conventional and perturbed finite element algorithms was proposed to show the flexibility and accuracy of the sensitivity based approach.

7.5.3.1 Effect of Native Soil Thermal Conductivity on the Cable Temperatures

The variation effect of the native soil thermal conductivity on the three cables maximum temperatures of the left circuit is shown in Figure 7.31 using both perturbed and conventional finite elements. Cables temperature sensitivity curves at different parameter values are shown in Figure 7.32.

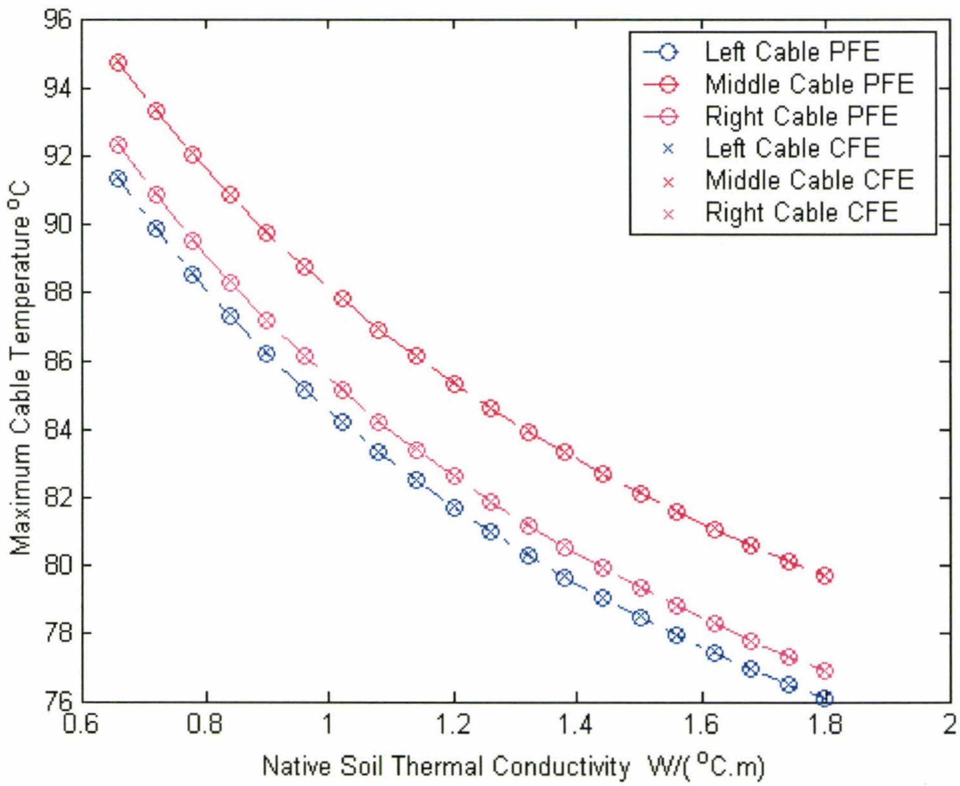

Fig. 7.31 Effect of variation of the native soil thermal conductivity (380 kV cable system)

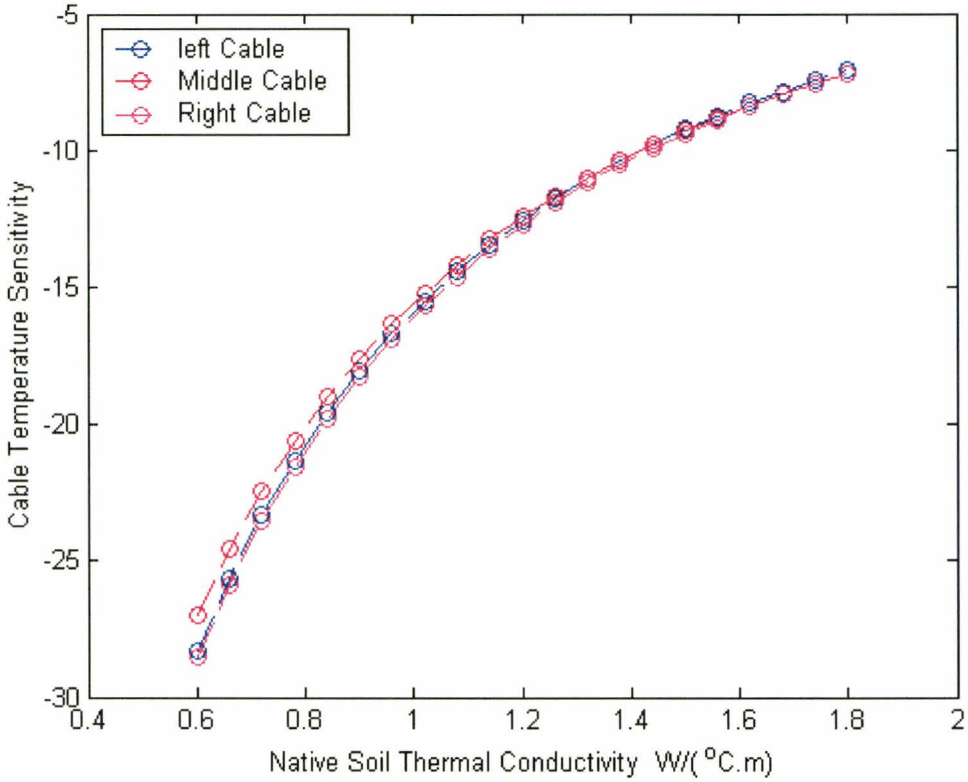

Fig. 7.32 Cables temperature sensitivity curves at different native soil thermal conductivity values (380 kV cable system)

7.5.3.2 Effect of Bedding and Backfill Conductivities on the Cable Temperatures

Bedding and backfill thermal conductivities variation effects on left circuit cables temperature using both perturbed and conventional finite elements are shown in Figure 7.33 and Figure 7.34. A comparison between both PFE and CFE in all cases shows high matching between both results, with the gained advantage of PFE due to its flexibility and low computation analysis as well as the additional information of the temperature sensitivity. From the shown results, it can be stated that the soil has a dominant impact on the cable temperatures among all other parameters. The rate of temperature reduction due to bedding thermal conductivity increase is much more than that achieved by increasing backfill thermal conductivity. The sensitivity curves for both conductivity parameters are shown in Figure 7.35 and Figure 7.36.

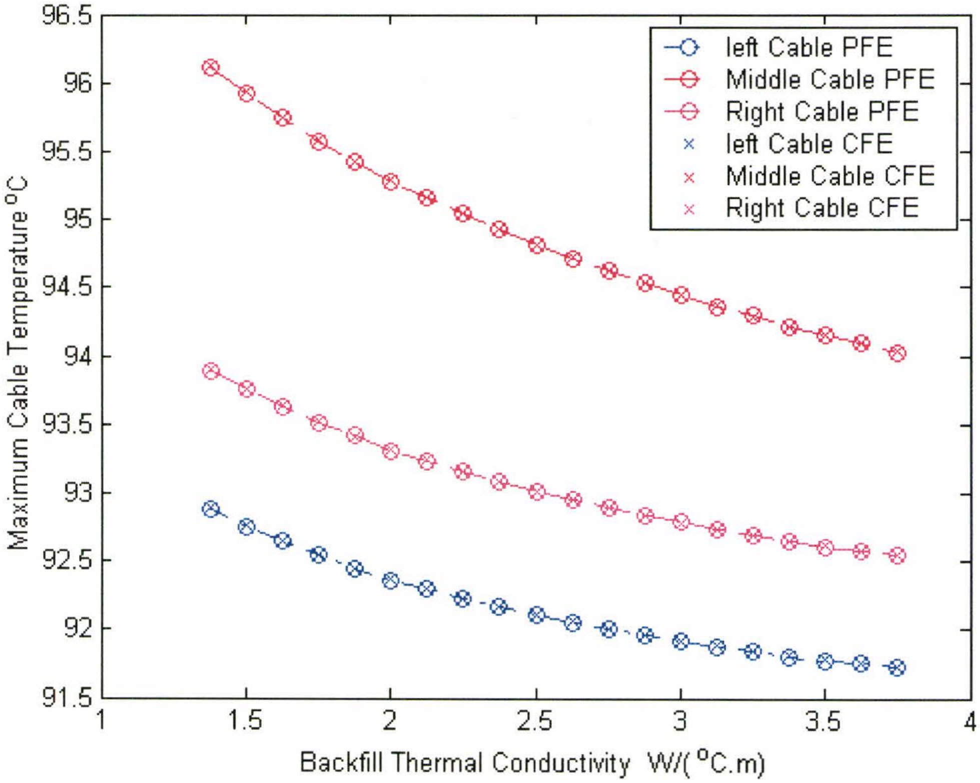

Fig. 7.33 Effect of variations in backfill conductivity on the cable temperatures (380 kV cable system)

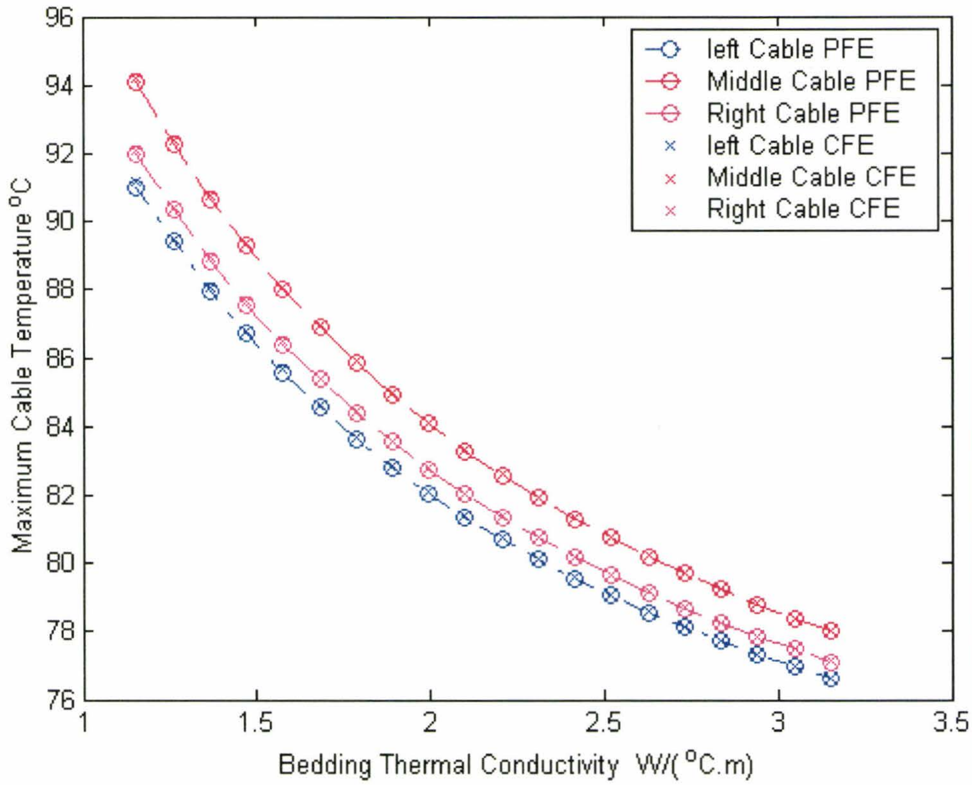

Fig. 7.34 Effect of variations in bedding conductivity on the cable temperatures (380 kV cable system)

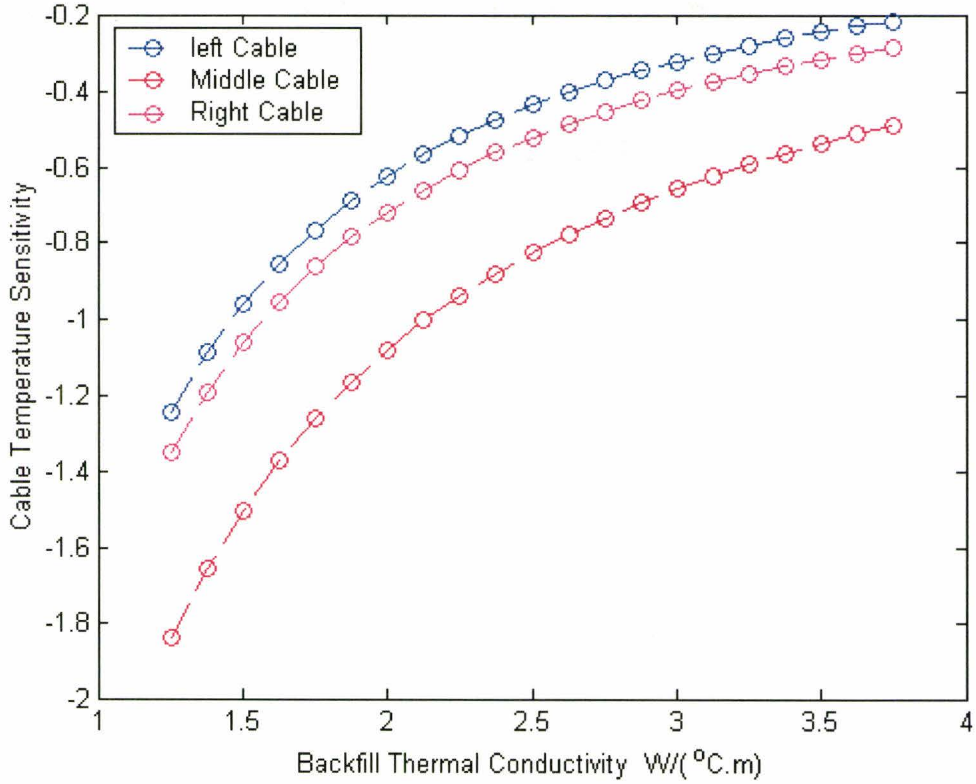

Fig. 7.35 Cables temperature sensitivity curves at different backfill thermal conductivity values (380 kV cable system)

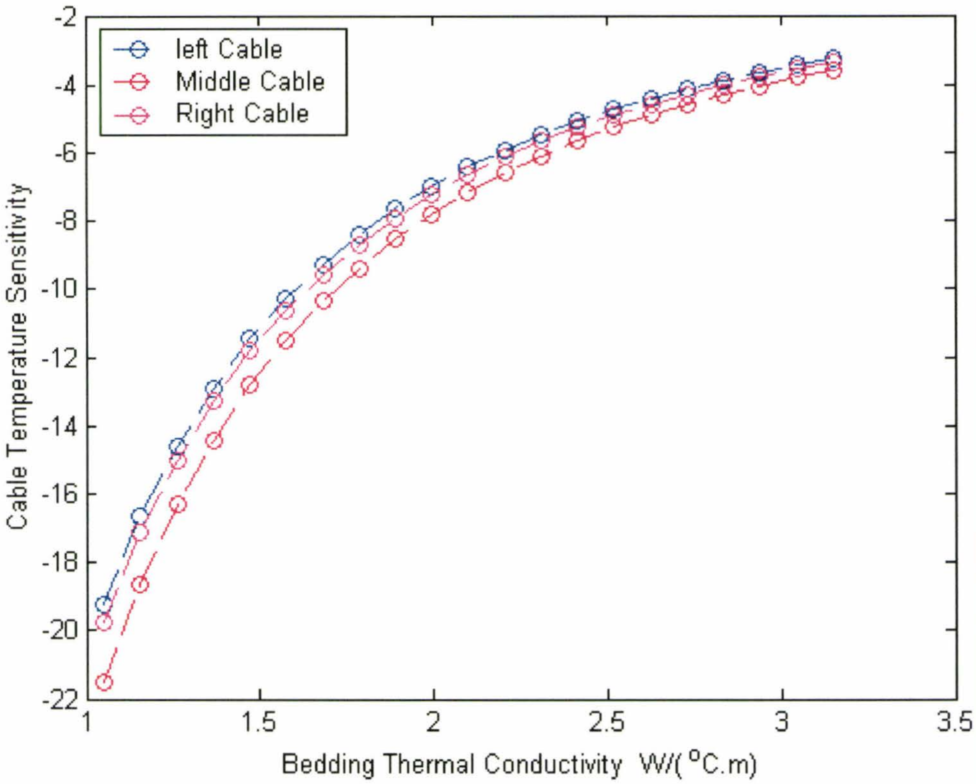

Fig. 7.36 Cables temperature sensitivity curves at different bedding thermal conductivity values (380 kV cable system)

7.5.3.3 Effect of Heat Generation on the Cable Temperatures

The allowable heat input increase is directly proportional to the maximum allowable steady state cable temperatures as can be noted from Figure 7.37 and Figure 7.38. The same characteristic was noticed in the previous case system. The rates of temperature increase due to the increase in the heat dissipation on right, middle and left cables are 1.287, 1.332 and 1.265 (W/^{o}C.m^2) respectively.

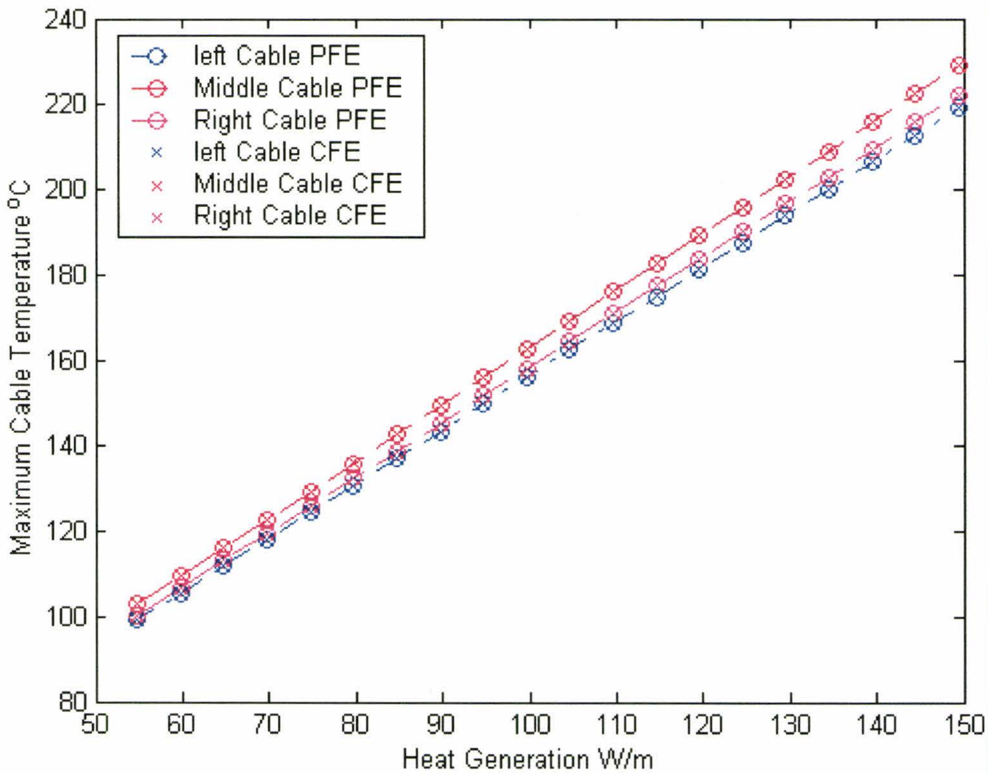

Fig. 7.37 Effect of heat generation on the cable temperatures (380 kV cable system)

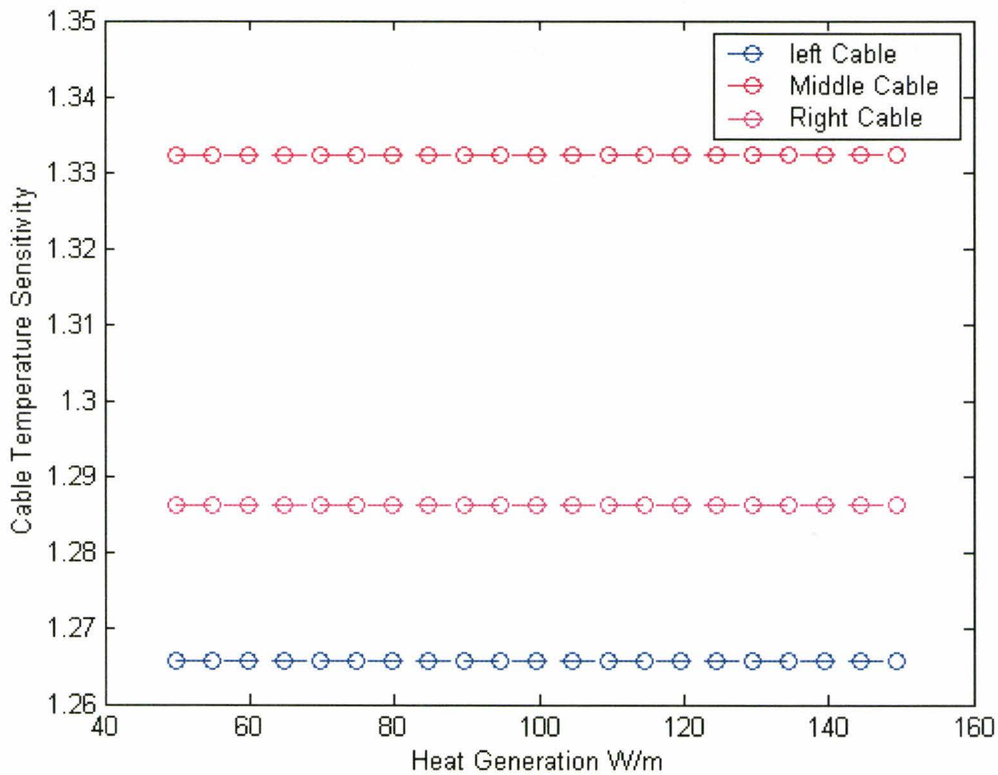

Fig. 7.38 Sensitivities of cables temperature to heat generation (380 kV cable system)

The cables on the sides of a particular circuit do not have like temperatures. By looking to the side cables of the left circuit, the right cable has a higher temperature than the left cable, as can be noted from the previous figures of all cases. This is due to the effect of mutual heating with the adjacent circuit, where the right cable that belongs to the left circuit is the closest cable to the other circuit, and will be the most effectible by such circuit mutual heating. On the other hand, the cable in the middle has the highest temperature due to the mutual heating of the individual cables in the circuit.

7.5.4 Optimization Performance

The thermal parameters of the 380 kV oil filled cable system will be optimized for the same objective function formulated in the pervious cable system, where the conductor temperatures of the six cables are aimed to be reduced to the desired temperature of 80 ^oC. In this case, the controlled parameters will be, respectively, the mother soil conductivity, the two backfills thermal conductivities of the right and left circuits and the trenches pairs thermal conductivities of both circuits. This can be described in the following mathematical representation:

$$\begin{aligned} &\text{Minimize} \quad \sum_{i}^{n}(T_i - 80)^2 \\ &\text{st} \qquad 0 \le \; k_{mother\_soil} \le 6 \\ &\qquad\quad\; 0 \le \; k_{backfill} \le 6 \\ &\qquad\quad\; 0 \le \; k_{ternch} \le 6 \end{aligned} \tag{7.6}$$

where T_i is the internal conductor temperature of the cable i, i=1, 2, 3, 4, 5, 6.

Using the developed optimization-finite element sensitivity approach, the optimized parameters are given in Table 7-17. These values satisfy the defined constraints for which the objective function has the minimum value of 3.4914 $^oC^2$. The thermal field for this system was evaluated at the new optimized parameters using the finite element approach as shown in Figure 7.39 where the temperature reduction toward the desired temperature can be noted. The cable temperatures were noted to be 79.15 ^oC, 81.06 ^oC, 79.79 ^oC, 79.66 ^oC, 81.02 ^oC and 79.33 ^oC for the cables from right to left respectively. The iteration numbers required to reach the objective point are shown in Figure 7.40, where a dramatic reduction in the objective function can be noted in the first couple of iterations.

TABLE 7-17: OPTIMIZED PARAMETERS FOR 380 kV, CABLE TEMPERATURES REDUCTION

Parameter	Layer Description	Circuit Description	Optimal Thermal Conductivity $W/^oC.\ m$
Mother Soil	N/A	N/A	0.734
Backfill	N/A	Left	2.360
		Right	2.312
Trench	Lower	Left	1.863
	Upper	Left	2.143
	Lower	Right	1.850
	Upper	Right	2.195

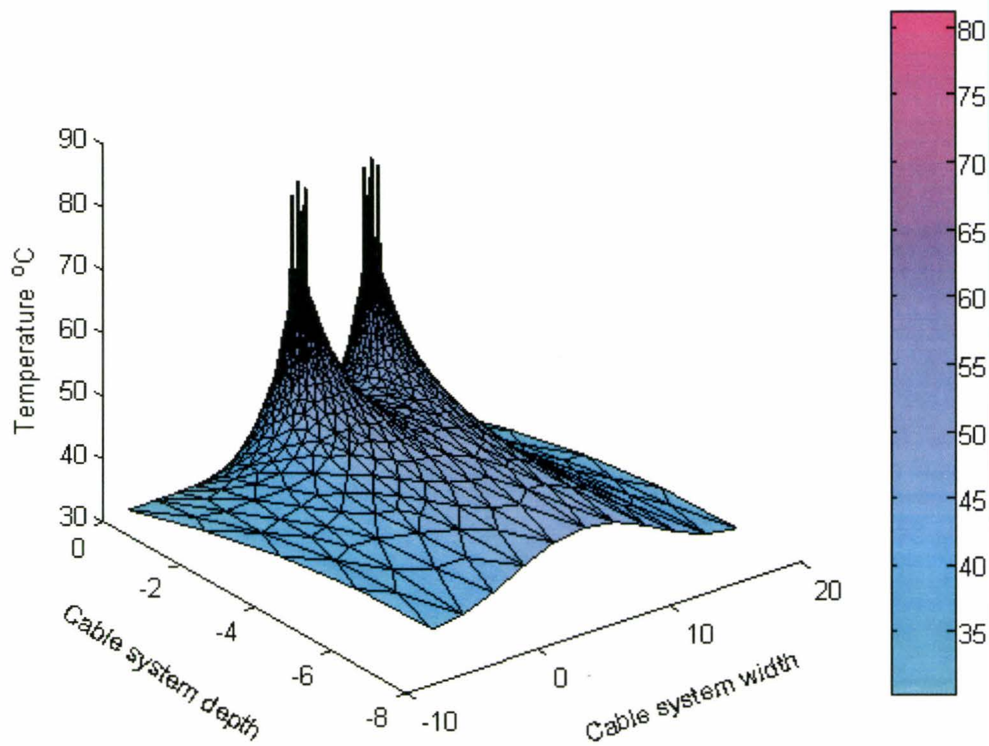

Fig. 7.39 Temperature solution at optimal parameters for temperature reduction (380 kV cable system)

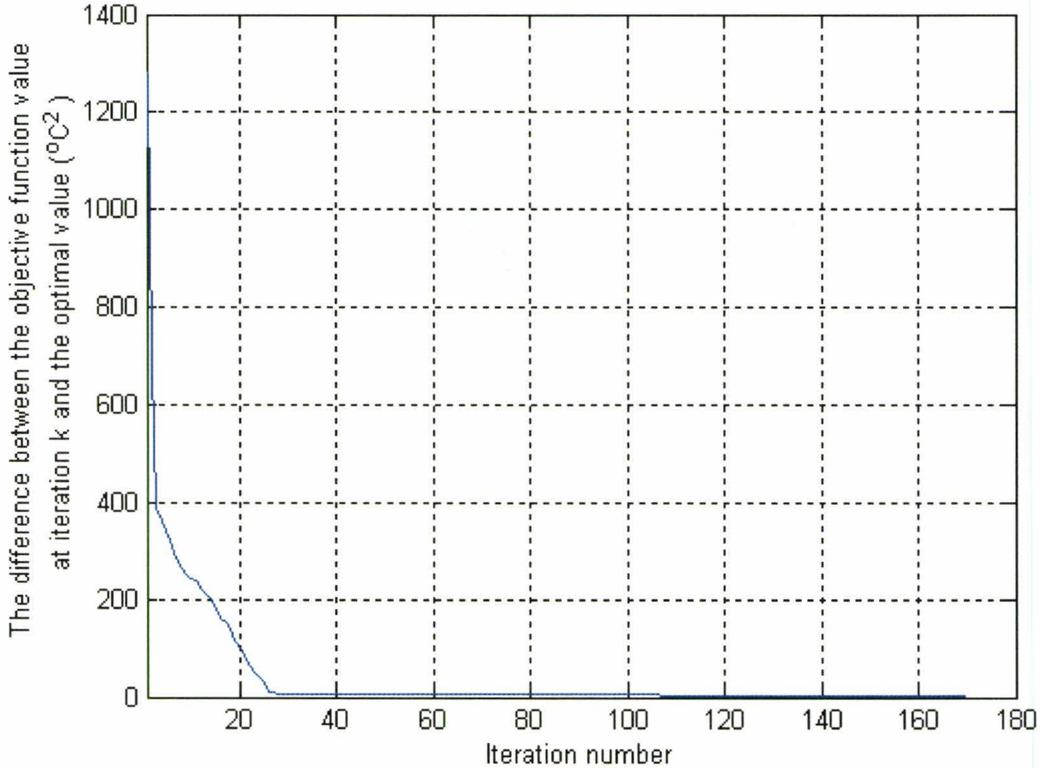

Fig. 7.40 Error versus iteration numbers (380 kV cable system)

In another practical formulation, the objective function will be designed for the purpose of increasing the cable carrying capacity of the 380 kV cable systems by controlling the cables loading and the two backfills thermal conductivities. This can be described in the following mathematical representation:

$$\text{Minimize} \quad -\sum_{i}^{n} Q_i$$

$$\begin{aligned} \text{st} \qquad & T_i \leq 90 \\ & k_{backfill} \leq 6 \end{aligned} \tag{7.7}$$

where Q_i is the heat losses inside cable i , n is the total number of cables and T_i is the internal conductor temperature on cable i.

Using the developed optimization-finite element sensitivity approach, the optimized parameters are given in Table 7-18. The same conclusion can be drawn as in the previous cable system, where the backfill values were driven up to their maximum allowable value, as the increasing of the backfill thermal conductivity allows more heat dissipation from cables to the surrounding and, therefore, aid in reducing the cables temperature and allowing high internal cable heat generation.

TABLE 7-18: OPTIMIZED PARAMETERS FOR 380 kV, CABLE AMPACITY IMPROVEMENT

Parameter	Description	Circuit Description	Optimal Parameter Value
Backfill Conductivity *W/(°C. m)*	N/A	Left	6.000
		Right	6.000
Cable Losses *W/m*	Left cable	Left	55.45
	Mid cable	Left	51.43
	Right cable	Left	54.08
	Left cable	Right	54.32
	Mid cable	Right	51.43
	Right cable	Right	54.86

On the other hand, conductor temperatures of the cables are expected to be driven to their maximum allowable temperature as cables heat dissipations are maximized, but should not violate the imposed temperature in constraint, this can be noted by looking to the associated conductor temperatures at these optimized parameters which were found to be 89.9999 ^oC, 89.9999 ^oC, 89.9999 ^oC, 90 ^oC, 90 ^oC, 90 ^oC for the cables from right to left respectively. The thermal field solution at these optimized parameters is shown in Figure 7.41.

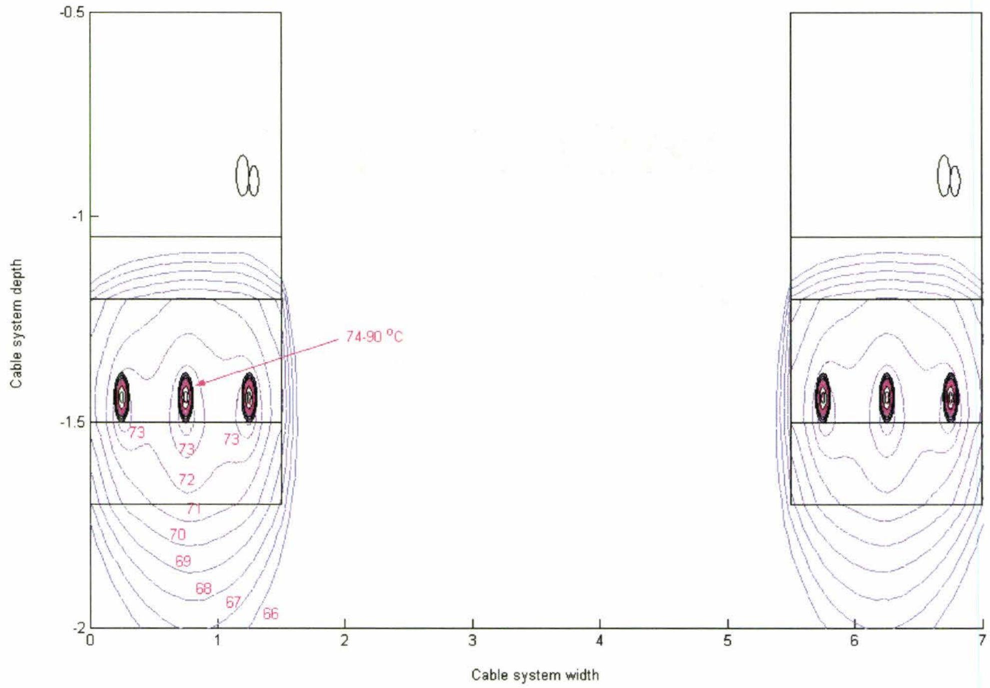

Fig. 7.41 Temperature contours at optimal parameters for ampacity improvement (380 kV cable system)

7.6 15 kV CABLE SYSTEM

7.6.1 Overview

In this application, the new finite element sensitivity algorithm is applied to a 15 kV, 3×300 mm^2 CU/XLPE/SWA/PVC cable system, where the performance of the cable is optimized using the gradient information supplied by the sensitivity calculations. In such cable systems of three cores, as shown in Figure 7.42, an intensive grid will be required to model the cable system. The developed algorithm shows high potential in adapting intensive complicated typical cable-trench arrangements due to its flexibility and low required computation efforts as will be shown in results of such system. The three of 15 kV cables described above are directly buried in the soil with the actual practical configuration shown in Figure 7.43. The nominal values of the cable parameters as well as the soil thermal specification are considered in Table 7-19.

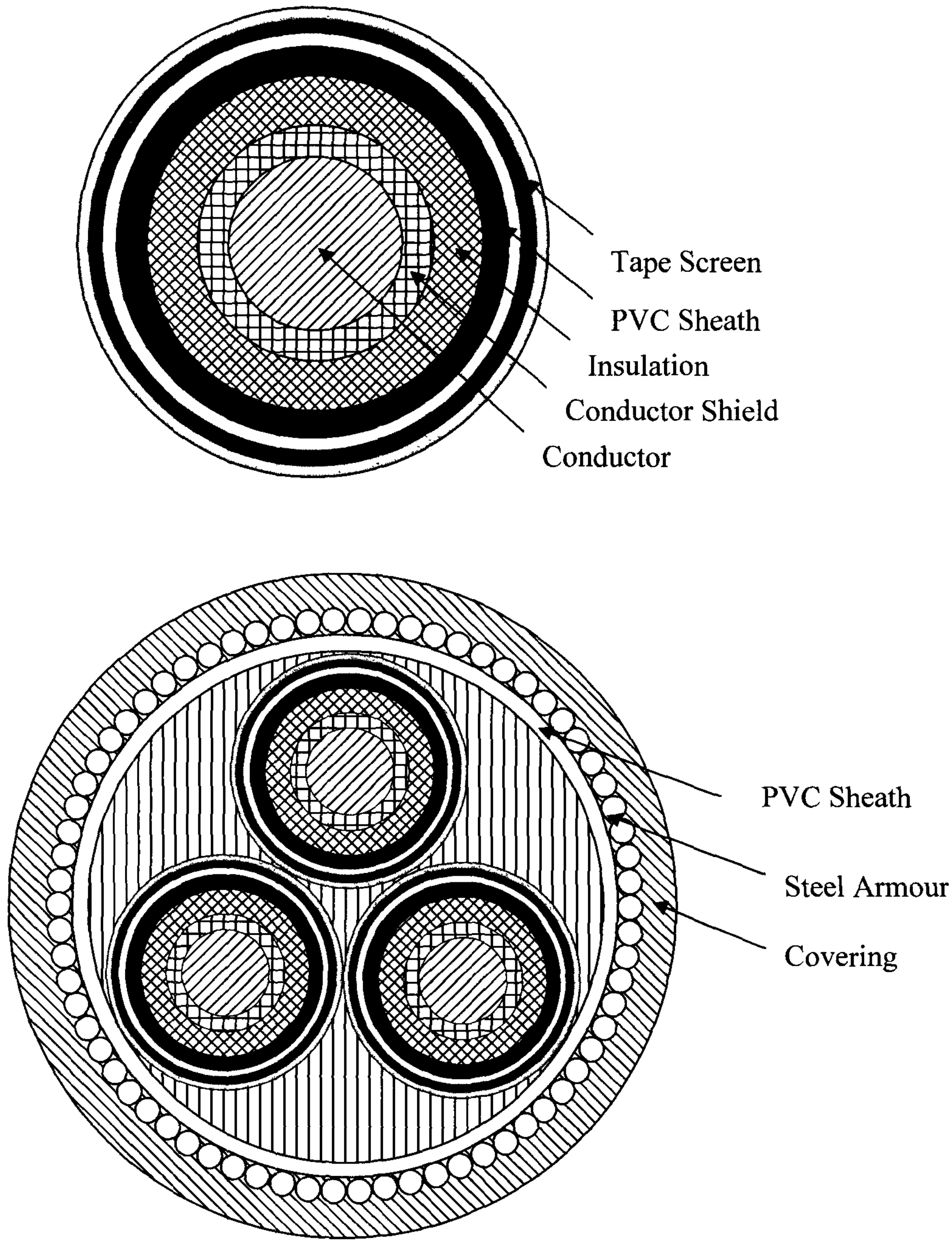

Fig. 7.42 A 15 kV cable system

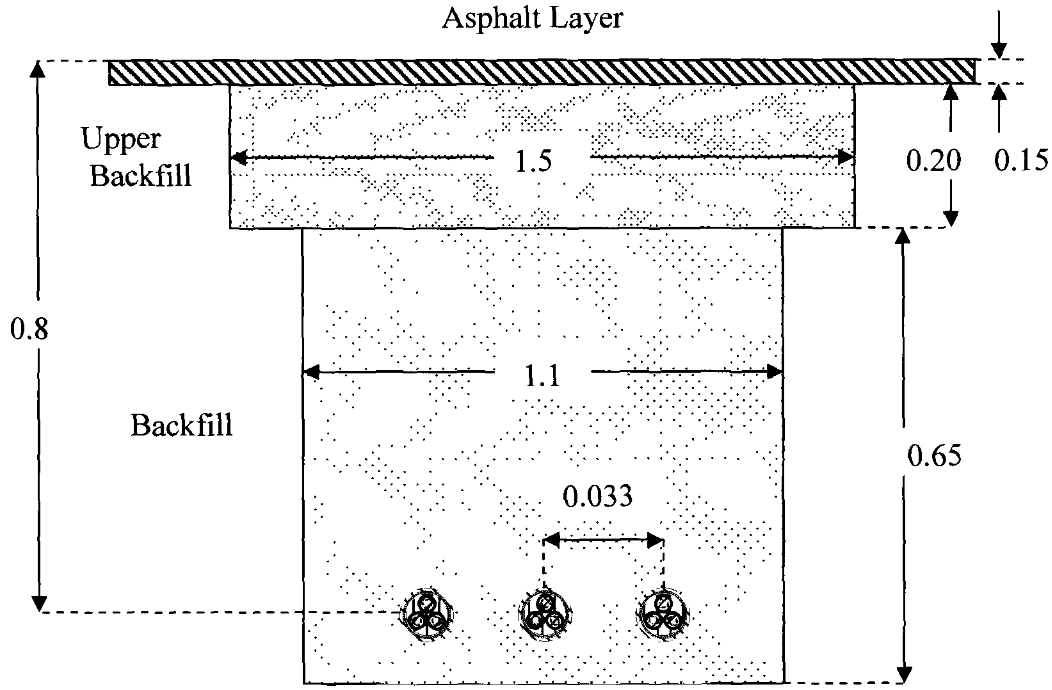

Fig. 7.43 Trench configuration of 15 kV cable system

TABLE 7-19: TECHNICAL DATA FOR 15 kV CABLE SYSTEM

Rated voltage	15 kV
Number of cores	3
Nominal cross section area of conductor	300 mm^2
Diameter over conductor	20.4 *mm*
Nominal thickness of insulation	4.5 mm
Diameter over insulation	31 *mm*
Diameter over insulation shield	33.4 *mm*
Diameter over copper tape screen	33.8 *mm*
Diameter over Assembled cores	73 *mm*
Nominal thickness of PVC separation sheath	2 *mm*
Diameter over steel wire armour	83.8 *mm*
Ground temperature	35 ^oC
Heat convection loss	5 $W/(^oC.\ m^2)$
Actual conductor current	281 A
Mother soil thermal conductivity	0.5 $W/(^oC.\ m)$
Bedding thermal conductivity	1.05 $W/(^oC.m)$
Upper backfill thermal conductivity	1.25 $W/(^oC.\ m)$
Conductor thermal conductivity	385 $W/(^oC.\ m)$
Jacket thermal conductivity	0.2 $W/(^oC.\ m)$
XLPE insulation thermal resistivity	0.002 $W/(^oC.\ m)$

7.6.2 Thermal Evaluation

The thermal field for the described cable system was evaluated for a convection boundary condition at the earth surface, with the previously mentioned nominal values. The finite element grid and the temperature profile are shown in Figure 7.44 and Figure 4.45 respectively.

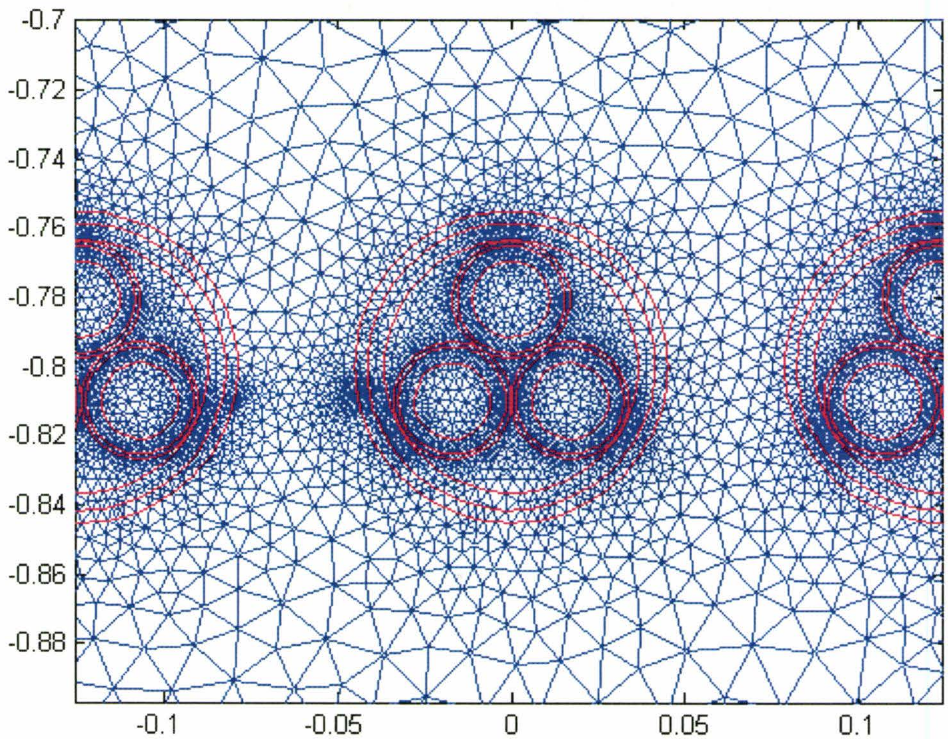

Fig. 7.44 Finite element mesh (15 kV cable system)

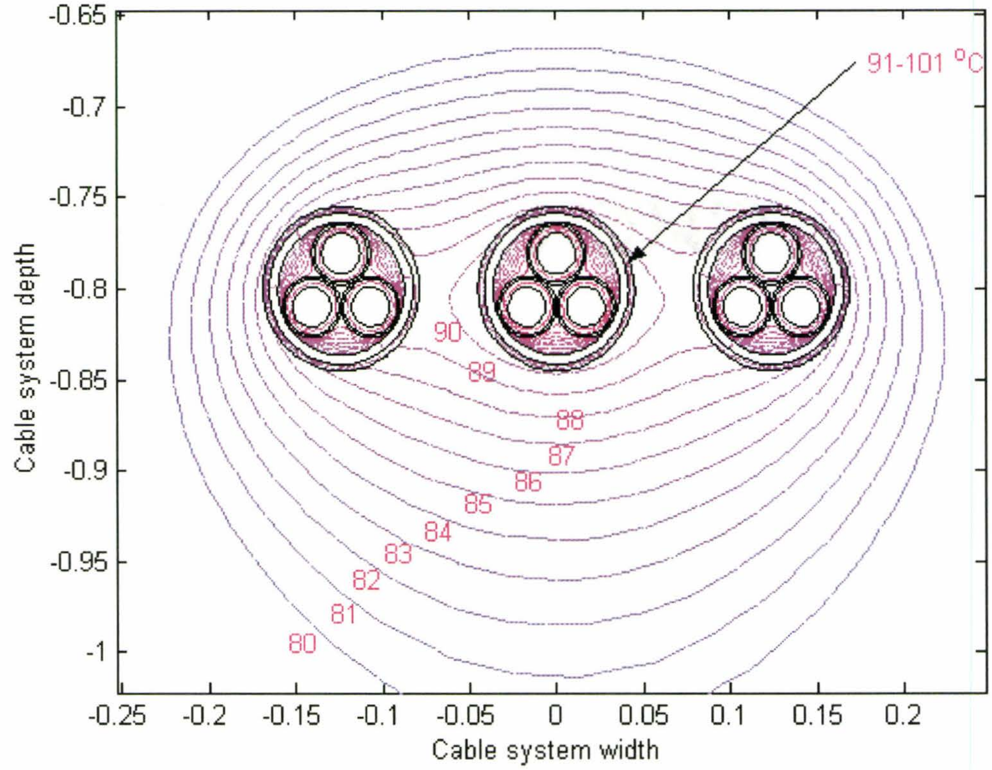

Fig. 7.45 Temperature solution at nominal parameters (15 kV cable system)

7.6.3 Thermal Parameter Variation Investigation Using Sensitivity Model

7.6.3.1 Effect of Native Soil Thermal Conductivity on the Cable Temperatures

The variation effect of the native soil thermal conductivity is shown in Figure 7.46. The sensitivity curves of each cable are shown in Figure 7.47. It can be noted that all cables have almost the same temperature sensitivity to the mother soil thermal conductivity variation, as the three cables are close to each other.

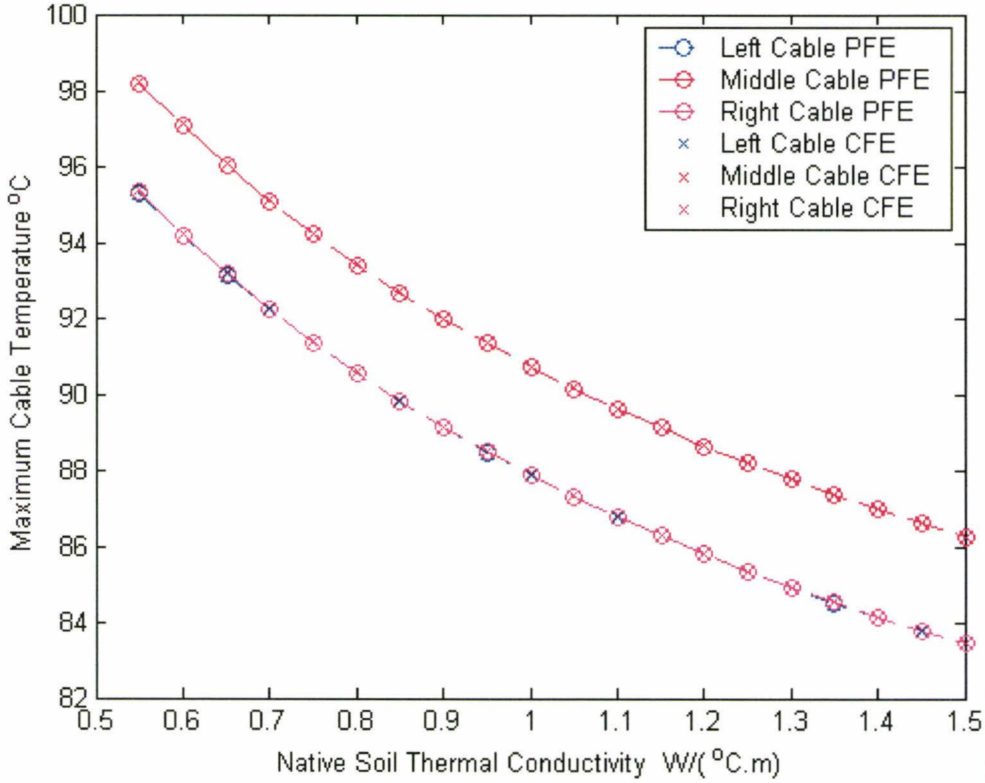

Fig. 7.46 Effect of variation of the native soil thermal conductivity (15 kV cable system)

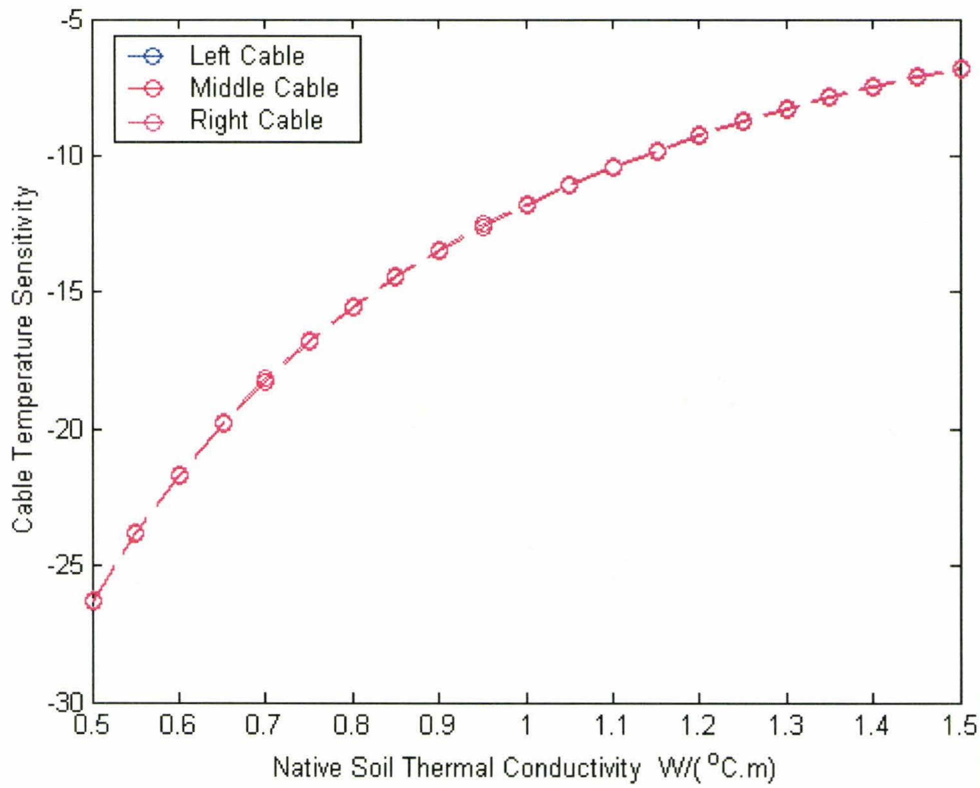

Fig. 7.47 Cables temperature sensitivity curves at different native soil thermal conductivity values (15 kV cable system)

7.6.3.2 Effect of Bedding and Backfill Conductivities on the Cable Temperatures

Bedding and upper backfill thermal conductivities variation effects on three cables temperature using both perturbed and conventional finite elements are shown in Figure 7.48 and Figure 7.49. Sensitivity curves associated with bedding and backfill conductivity variation are shown in Figure 7.50 and Figure 7.51 respectively.

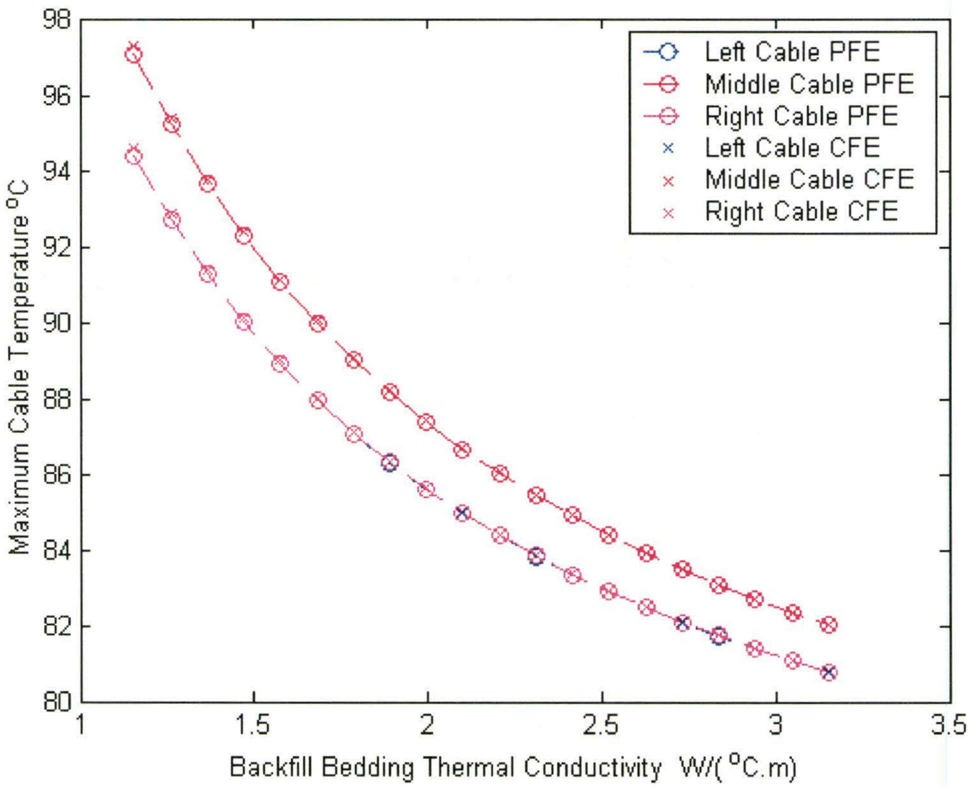

Fig. 7.48 Effect of variations in bedding conductivity on the cable temperatures (15 kV cable system)

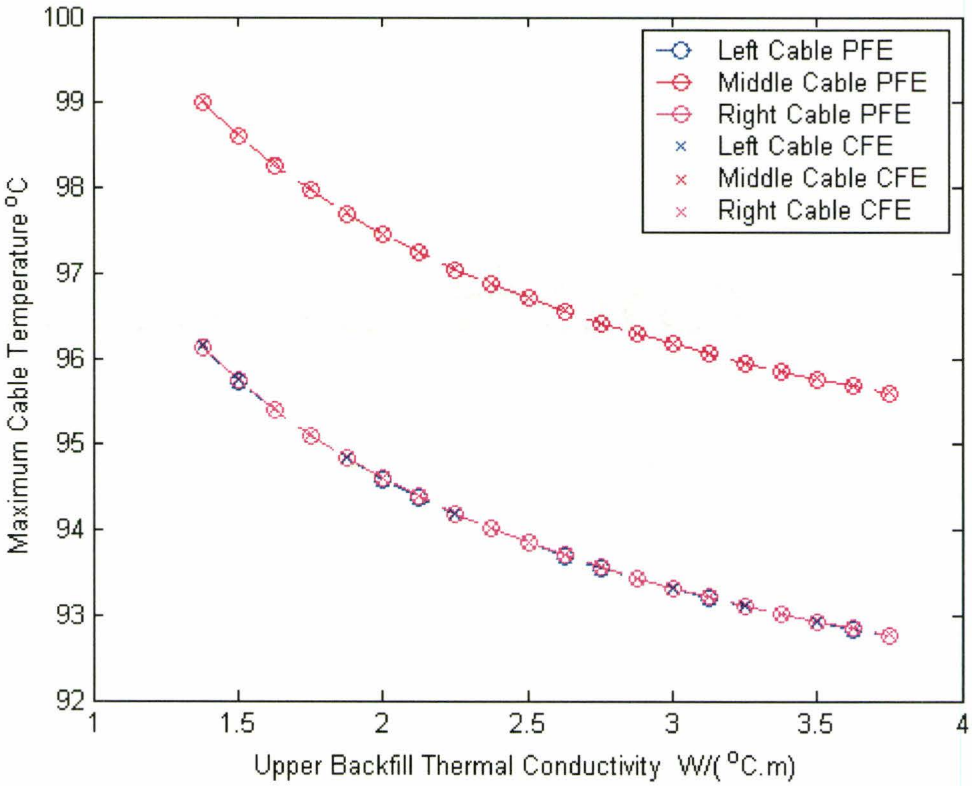

Fig. 7.49 Effect of variations in upper backfill conductivity on the cable temperatures (15 kV cable system)

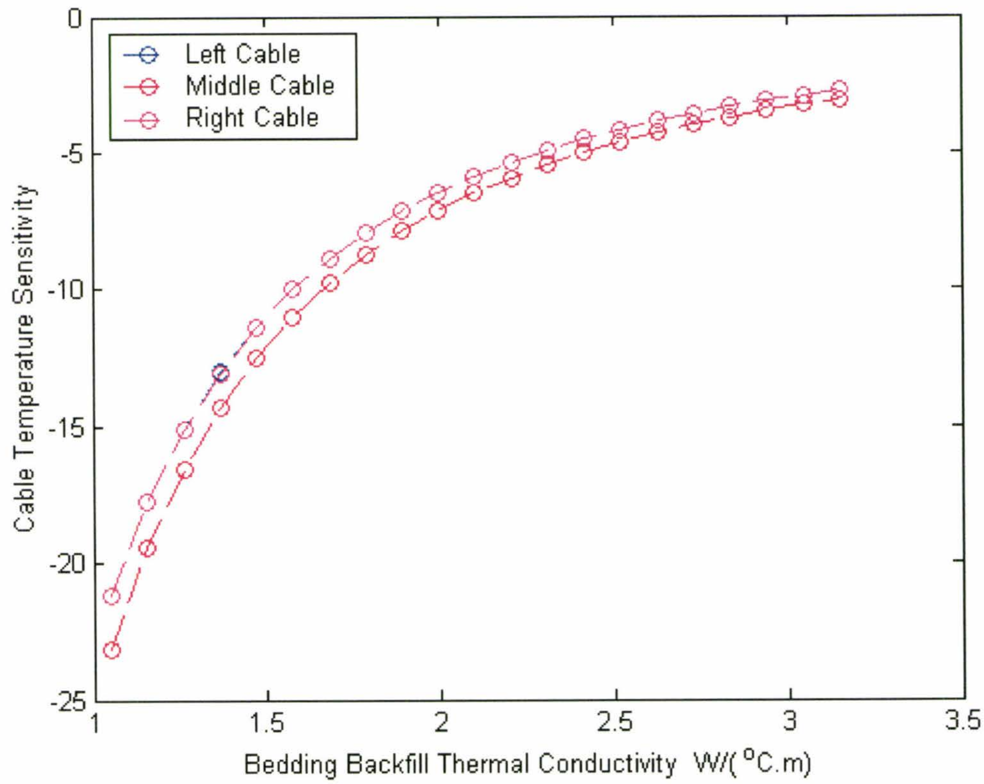

Fig. 7.50 Cables temperature sensitivity curves at different bedding thermal conductivity values (15 kV cable system)

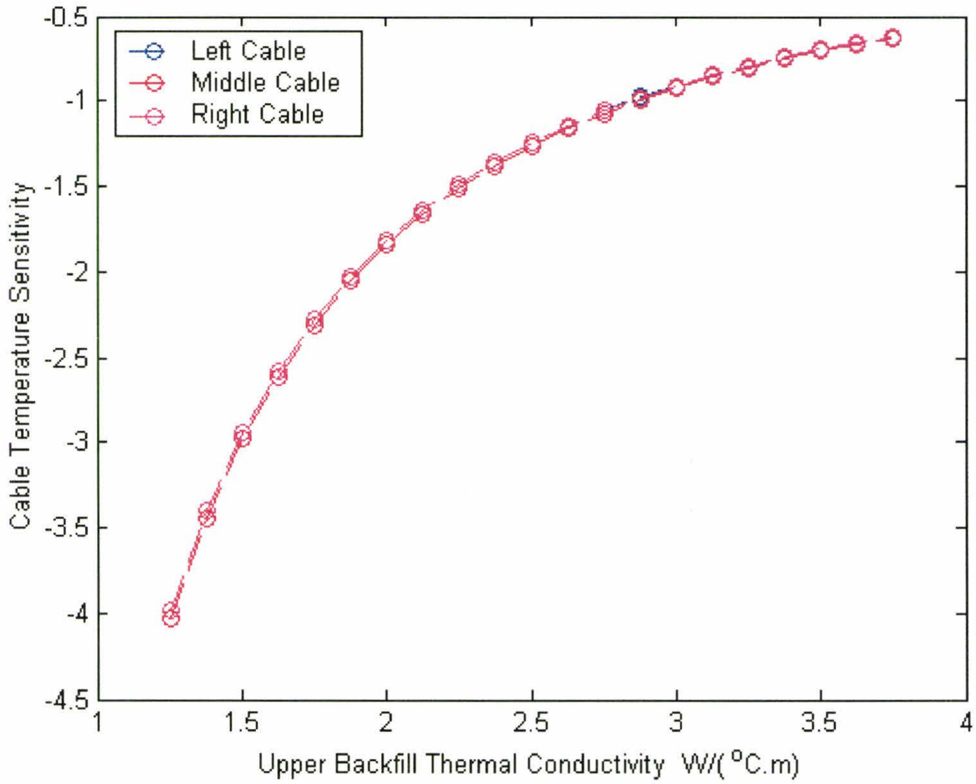

Fig. 7.51 Cables temperature sensitivity curves at different upper backfill thermal conductivity values (15 kV cable system)

7.6.3.3 Effect of Heat Generation on the Cable Temperatures

The allowable heat input increase is directly proportional to the maximum allowable steady state cable temperatures as can be noted from Figure 7.52 and Figure 7.53. This is consistent with previously shown cable systems, which had the same relation of heat generation with cable temperatures. The effect on the side cables is almost the same, which was found to be 6.26 (W/°C.m^2). This rate is higher on the middle cable which is about 6.56 (W/°C.m^2).

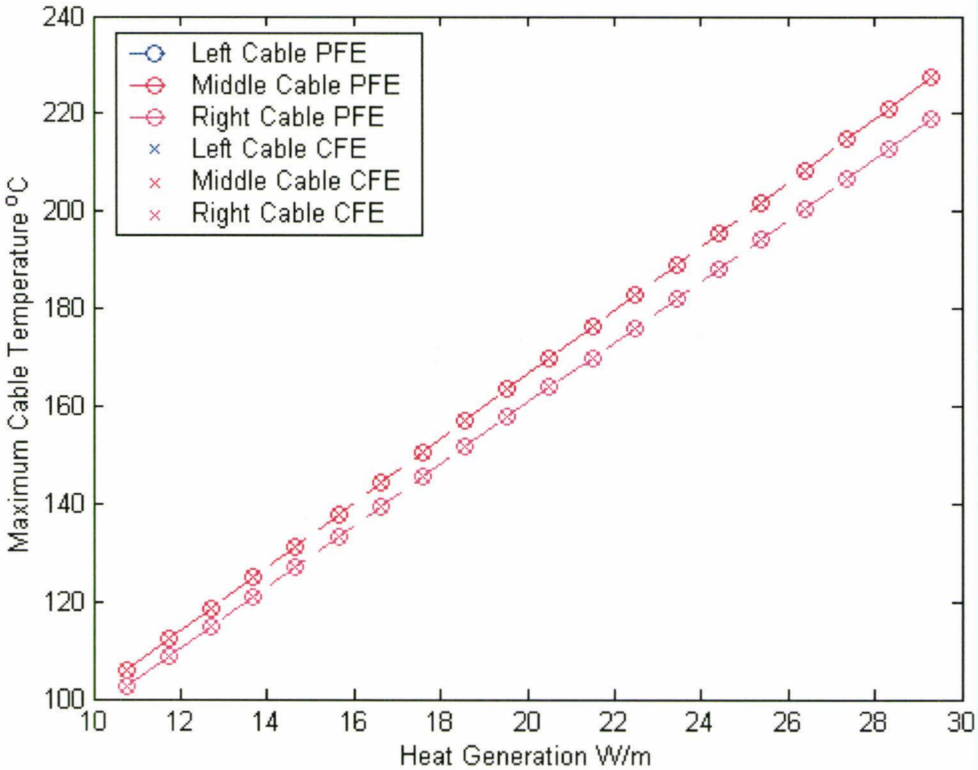

Fig. 7.52 Effect of heat generation on the cable temperatures (15 kV cable system)

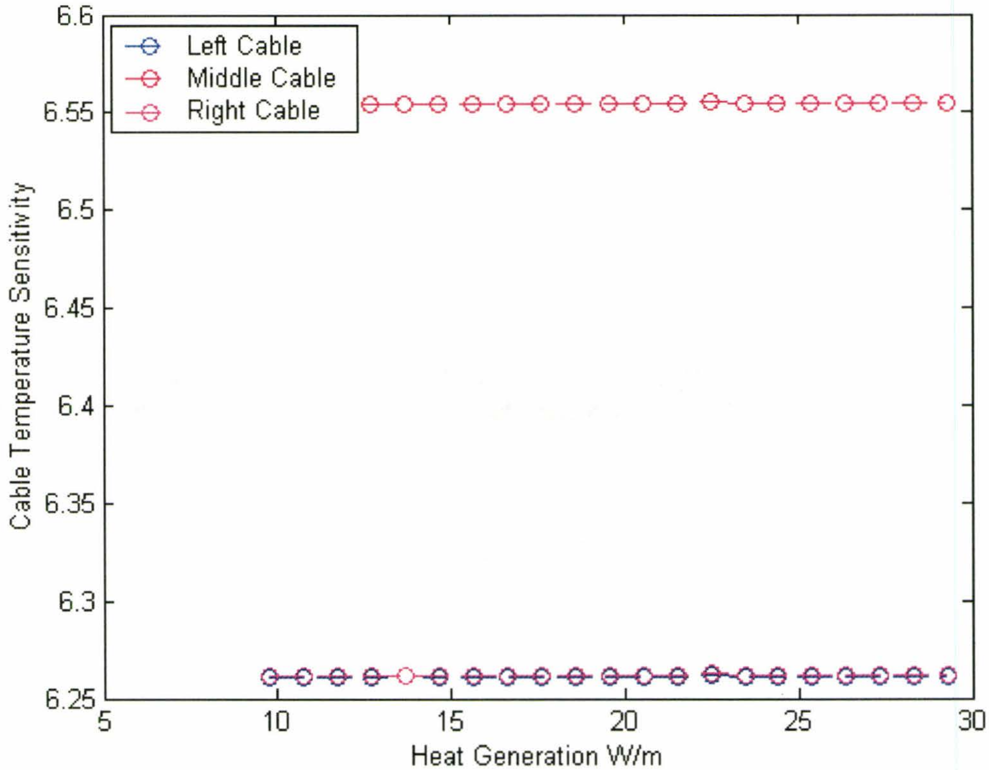

Fig. 7.53 Sensitivities of cables temperature to heat generation (15 kV cable system)

A comparison between both PFE and CFE in all cases shows high matching between both results, with the advantage of PFE due to its flexibility and low computation time as well as the additional information of the temperature sensitivity. From the shown results, it can be stated that the soil has a dominant impact on the cable temperatures among all other parameters. The rate of temperature reduction due to bedding thermal conductivity increase is much more than that achieved by increasing backfill thermal conductivity. Because the simulation procedure for various parameter variations does not involve repeated finite element analyses, the results can be obtained very quickly, and displayed in an efficient, straightforward manner. Since only one nominal finite element analysis is required, a larger element grid can be employed, allowing even more accurate modeling. In the proposed cable system, 13851 nodes are implemented in the solution domain discretization, where a computation cost reduction was effected for this configuration design assessment.

7.6.4 Optimization Performance

The developed optimization generated gradient model will be used to optimize the cable parameters of the previously demonstrated cable systems. For this cable system, the high cable operating temperatures found to be 101 ^oC, will be reduced to a more reasonable temperature of 75 ^oC. The same shape of objective used in the previous cable systems for the purpose is used in this case, and the objective function can be described mathematically as follows:

$$\text{Minimize} \sum_{i}^{n}(T_i - 75)^2$$

$$\begin{aligned} \text{st} \quad & 0 \le k_{mother\_soil} \le 6 \\ & 0 \le k_{bedding\ bf} \le 6 \\ & 0 \le h_{upper\ bf} \le 6 \end{aligned} \tag{7.8}$$

where T_i is the internal conductor temperature of the cable i.

Using the developed optimization-finite element sensitivity approach, a solution is obtained at $k_{mother\text{-}soil}$ = 1.0087 $W/(^oC.\ m)$, $k_{bedding}$ =2.5914 W/($^oC.\ m$), $k_{Upper\ backfill}$ = 3.0996 $W/(^oC.\ m)$, which satisfies the provided constraints for which the objective function has the minimum value of 1.35867 $^oC^2$. The thermal field for this system was evaluated at the new optimized parameter using the finite element approach as shown in Figure 7.54. The iteration numbers required to reach the objective point are shown in Figure 7.55 where it can be noted that at the sixth iteration the desired objective was almost achieved with relatively high accuracy. In this complicated configuration that employed a very large intensive grid, the great advantage of the develop model is clearly detected. In this case, at each single iteration, a linear system of equations with 13851 unknowns needs to be solved.

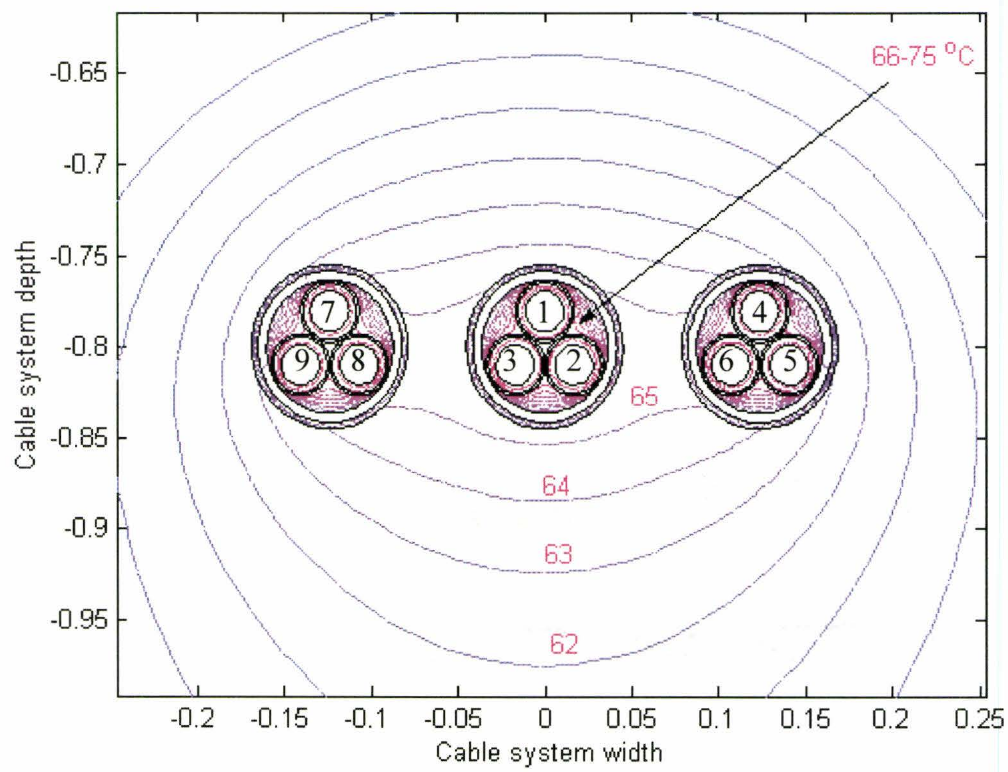

Fig. 7.54 Temperature solution at optimal parameters for temperature reduction (15 kV cable system)

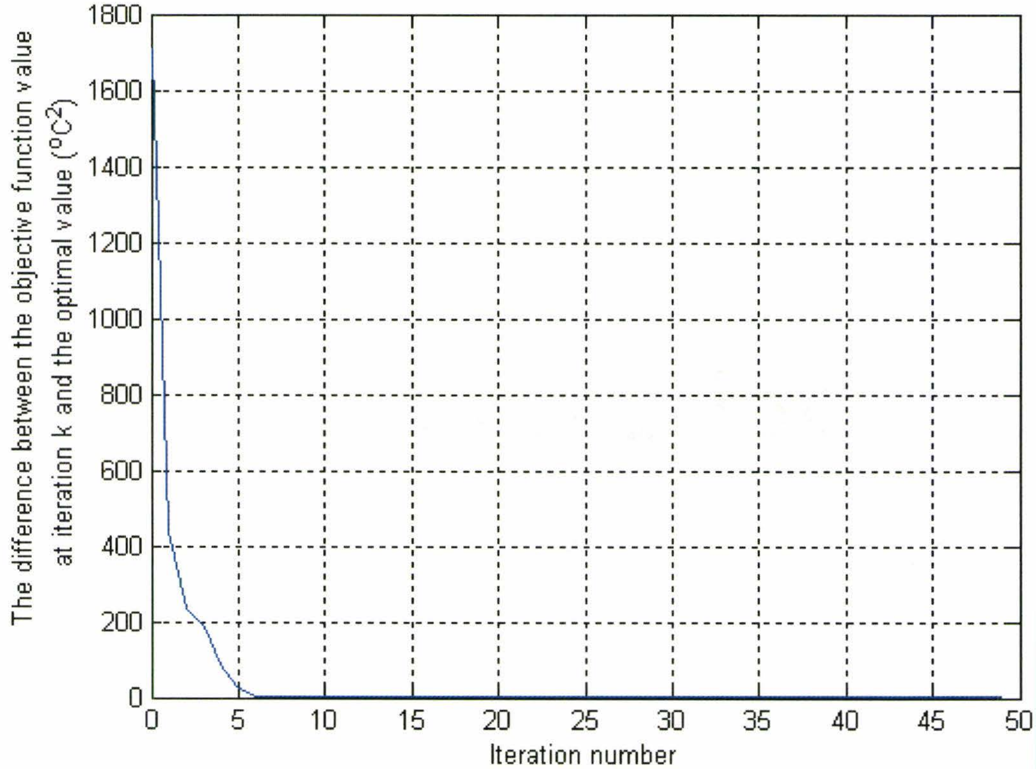

Fig. 7.55 Error versus iteration numbers (15 kV cable system)

Maximizing the allowable load that a cable can carry for a maximum permissible temperature on the cable conductors is again addressed in this case. This can be described mathematically by:

$$\begin{aligned} &\text{Minimize} \quad -\sum_{i}^{n} Q_i \\ &\text{st} \qquad T_i \le 90 \\ &\qquad\quad k_{bedding\ bf} \le 6 \end{aligned} \tag{7.9}$$

where Q_i is the heat loss inside conductor i, n is the total number of conductors and T_i the internal conductor temperature.

Bounding the cable temperatures to not exceeding a certain allowable temperature, imposes nonlinear constraints on the thermal circuit parameters which are to be optimized. The gradient of the nonlinear constraint functions is considered. Heat generations are controlled in the nine conductors which are defined in the objective function ($Q_1,\ldots,Q_9$), and the trench thermal conductivity that represents the medium contains all three cables. As was expected, the trench thermal conductivity value was driven up to its maximum allowable value as defined at 6 $W/(^oC.\ m)$, as increasing the trench thermal conductivity allows more heat dissipation and helps in maximizing the allowable generated heat. The maximum allowable heat generation associated with each conductor numbered as labeled in figure 7.54 is shown in Table 7-20. These values are consistent with the effect of the mutual heating between conductors. For example, cables 2 and 3 have the least allowable heat generation since they are the most affected conductors by mutual heating. Then cables 6 and 8 are affected, and finally cables 5 and 9. The thermal field solution at the optimized parameter is shown in Figure 7.56, where the maximum cable temperatures are almost equal to the upper limit constraints.

TABLE 7-20: OPTIMIZED PARAMETERS FOR 15 kV, CABLE AMPACITY IMPROVEMENT

Parameter	Cable No.	Optimal Parameter Value	Cable Temperature ^oC
Backfill Conductivity $W/(^oC.\ m)$	N/A	6.0000	N/A
Cable Losses W/m	1	12.05	90.0000
	2	11.92	90.0000
	3	11.92	90.0000
	4	12.85	89.9999
	5	12.88	89.9999
	6	12.58	89.9999
	7	12.85	90.0000
	8	12.59	90.0000
	9	12.89	90.0000

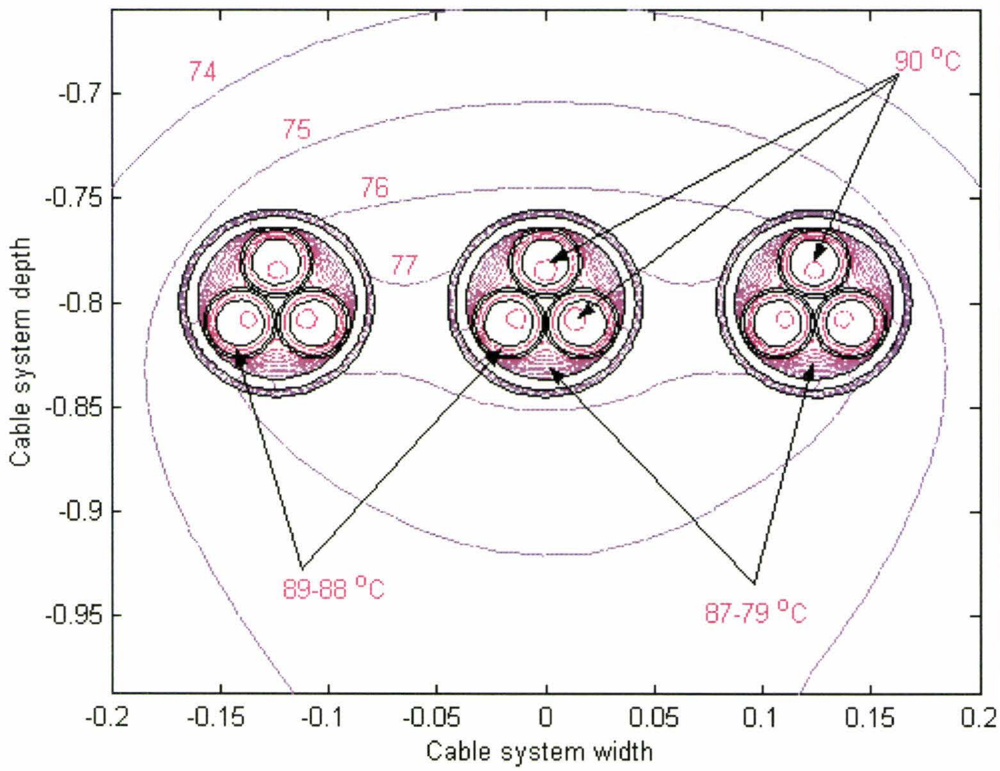

Fig. 7.56 Temperature solution at optimal parameters for ampacity improvement (15 kV cable system)

CHAPTER 8

CONCLUSIONS

8.1 OVERVIEW

The proposed perturbed finite element analysis provides a fast sensitivity methodology, based on the finite element model, to assess the cable thermal performance subjected to variations in the cable thermal circuit parameters. In this regard, the finite element sensitivity analysis method was used successfully to predict the thermal field under varying soil specifications and loading for a practical underground cable system in a multilayered soil. Furthermore, the model was used to investigate the cable performance indices of interest with respect to variations in the cable thermal parameters, where it accommodates most of the thermal parameters and the ambient conditions. The sensitivity information is useful not only in evaluating the cable ampacity subject to various parameter changes but also in determining the important and non-important parameter variations in term of their relative effect on the cable temperature and ampacity. The sensitivity information of the proposed technique is not limited to the cable temperatures only. In fact, the proposed model solves the thermal field at the nominal point and provides the associated sensitivity values for each node on the solution domain.

The sensitivity technique is general and can be applied to any cable system configuration. The work presented in this thesis was intended to show the capability of the perturbed finite element sensitivity technique to deal with complex system configurations. In this regard, various applications of practical cable systems were presented with diverse specifications (single core and three core), installations (directly buried and laid in a duct bank) and applications (transmission level and distribution level). The technique reduces significantly the amount of analysis and computation, and avoids numerous finite element analyses required to simulate various parameter changes. Because the simulation procedure for various parameter variations does not involve repeated finite element analyses, the results can be obtained by a very fast and compact scheme and displayed in an efficient, straightforward manner. Since only one nominal finite element analysis is required, a larger element grid can be employed allowing even more accurate modeling. As it was shown in the body of this thesis, 13851 nodes were implemented in the solution domain of the 15 kV, CU/XLPE/SWA/PVC cable system, and a tangible computation cost reduction was utilized for a complicated configuration design.

A comparison between both perturbed finite element and conventional finite element solutions was performed to show high matching between both results, where the perturbed finite element method was distinguished by its flexibility and low computational cost. The maximum deviation was noted to be less that 0.2% for a 10% increasing in the soil thermal conductivity. This shows the capability of the proposed perturbed finite element sensitivity analysis on capturing the trend of the cables temperature with respect to the thermal parameters variations, even in the case of a complicated cable system and boundary conditions. Consequently, the perturbed finite sensitivity method solves the thermal field just once (at the nominal case) and uses the derived sensitivities to calculate the new thermal fields over various sets of circuit parameters changes within $\pm 10\%$ from the nominal values. It is worth mentioning that this range is based on the most sensitive parameters such as thermal conductivities.

The applications of the technique to a variety of cable systems have shown that the sensitivity values have a different characteristic associated with each parameter. One of the important findings is that the heat generation has a direct relation with the cable temperature (constant sensitivity). Nevertheless, for each group of parameters (i.e. thermal conductivity, heat generation), the individual parameters belonging to the same group have a common sensitivity characteristic which is governed by the heat equation. The behaviour of each individual parameter is governed by the tradeoff among the parameter associated configuration and the nominal value of the parameters. The sensitivity results have shown that the variations of the thermal conductivity of the soil would affect the cable temperatures more than variations of other parameters. As would be anticipated, the lower the thermal resistivity of the mother soil, the greater the allowable heat input from the cable. Manipulation of the mother soil thermal conductivity by means of the backfilling soil will result in a big reduction of cable temperatures. The influence of the backfilling soil was illustrated for different configurations including multilayer backfilling soils. The potential benefits to be achieved, through development of backfill and bedding materials with low thermal resistivity, were shown.

Also, this thesis has demonstrated the use of nonlinear optimization, in conjunction with finite element thermal field analysis, as well as sensitivities of the cable temperatures to thermal circuit parameters. This optimization procedure combines the conventional finite element method with sensitivity analysis in one interactive simulation approach to attain an optimal design of selected cable thermal parameters. The technique offers flexibility in defining objective functions of interest subjected to upper and lower bounds on the design parameters, linear system of equations constraints, or nonlinear constraints. The technique allows the selection of thermal circuit parameters as well as the cable temperatures in the objective function and constraints. It implements the proposed finite element thermal analysis to evaluate the cable temperature and its sensitivity with respect to optimized thermal parameters at each iteration. Therefore, the objective and constraint functions and their gradients respectively could be accurately evaluated, so that a secure and reliable design could be achieved based on accurate gradient search direction. The generality of the developed model algorithm and its capability of handling complicated problems, from both a configuration point of view as well as objective function shape, were demonstrated by analyzing different practical cable systems covering a wide span of practical applications, as demanded by power utilities.

The developed optimization generated gradient model was used to improve the cable thermal circuit design of various practical cable system configurations. The obtained results showed that we were able to reduce cables temperature by more than 25% of their high operating temperatures. Also, we were able to increase the maximum allowable load that the cable could carry without exceeding the permissible temperature. This would increase the cable current carrying capacity and enhance the overall cable performance. The model was also applied for economical purposes, where the cost of the backfill was minimized subject to a temperature constraint.

Allowing the objective function and constraints to be implicit in terms of temperature, as encountered in many practical problems formulation, opens the door for more design flexibility. But on the other hand, it causes the problem to be a nonlinear optimization where the objective and constraint functions are related to the parameters, which have to be optimized by a partial differential equation. In order to avoid sacrificing model accuracy by simplifying the parameter-temperature relationship, the accurate finite element method is used to calculate the objective function value. In such circumstances, where the finite element is part of iteration procedure, the calculation cost in each iteration step toward the optimal parameters is considerable. The efficient finite element sensitivity method employs an accurate search algorithm in order to ensure a secure optimization procedure. This will also result in reduction of overall computation costs by reducing the number of iteration steps required to achieve the optimal parameters.

In addition to the numerical investigation, the thermal behaviour of the underground cables directly buried in soil was investigated experimentally. A full size experimental setup was constructed and instrumented in order to analyze the behaviour of 15 kV XLPE underground power cable. The existing underground thermal behaviour experiments focus on monitoring the cable temperatures, for which we have investigated a large scale experiment set including cable backfilling with intensive thermocouple probes grid. The probes are not only mounted on the cable, but distributed in the surrounding soil, in order to investigate the effect of each parameter on the cable thermal field. This will ensure a highly accurate representation of the cable thermal model. The developed experimental model was simulated using the proposed thermal finite element tools and the obtained results were compared with the experimental results to validate the developed simulation methodology. A good correspondence between both experimental and simulation results was obtained. The thermal field was observed at different loading scenarios (300A and 600A). The effects of load overheating on the adjacent soil and on boundary losses were highlighted, and parameters investigation was performed for each case loading.

The thermal resistivity of the backfill is one of the important parameters that can influence the cable system thermal behaviour. The results showed a high dependency of thermal resistivity on the operating conditions. It was shown that the laboratory measurement, in the absence of intensive load heating, is not sufficient. Investigation for cases under intensive thermal fields is strongly recommended. When the cable is loaded, the soil around the cable is affected strongly by the intensive thermal field more than the far soils. Consequently, more deviation in their thermal resistivity will be expected. Moreover, in this experimental work, sensitivity analysis was presented to predict the thermal field of the tested cable due to load variation around the maximum loading. The obtained results revealed that the finite element method is quite suitable as numerical solution for thermal field analysis of underground cable systems. Sufficient investigations of the thermal parameters supported by experimental measurements, as was shown in this work, could lead to better analytical modeling, and therefore more accurate results.

8.2 KEY CONTRIBUTIONS

1. Unlike the conventional methods of power cable thermal analysis based on the Neher/McGrath method and the subsequent more detailed methods that have appeared in the literature, including those using the traditional finite element technique, the work of this thesis takes the concept of finite elements one step further by perturbing the finite element formation and, hence, deriving sensitivity coefficients directly from within the finite element numerical solution structure. Therefore, these sensitivities are both very fast in computations and general in nature as they encompass all known parameters of cable, soil, trench and atmospheric conditions representing complex boundaries and non-uniform media around the cable.

2. The successful derivation of the finite element sensitivities opened the door for subsequent utilization of such sensitivities as gradients of an objective function in a general framework of power cable performance optimization. Therefore, based on the work of this thesis, it is now possible to perform non-linear optimization of cable performance indices using the more accurate finite element method, without sacrificing the modeling accuracy.

3. Some computational and software programming aspects of the present work are also considered new. For example, the derivation and use of the so-called zonal sensitivities allows lumping specific groups of media patches around the cable, that are of interest to the power cable engineer, for the derivation of the associated sensitivity information. Also, the linear nature of the sensitivity expressions allows very fast computations to predict the resulting impact on cable performance indices (including its ampacity) due to combined, relatively small, variations of several cable design and/or operating parameters without repeating the finite element analysis.

8.3 IDEAS FOR FUTURE RESEARCH

The proposed sensitivity model is based on first order sensitivity. In spite of the high achieved accuracy using first order sensitivity a higher order sensitivity could have benefits.

The proposed model provides a fast sensitivity methodology, based on the finite element model, to assess the cable thermal performance subjected to variations in the cable thermal circuit parameters. An extension to this developed model to include the variations of geometrical parameters is an interesting possibility for future work. It may involve an assessment of other practical cases that of interest to power utilities such as the effect of the spacing between the cables.

The same line of research may also be applied to other numerical solvers such as finite difference, finite volume and boundary element methods. In this regard, the added sensitivity and optimization features could be very promising where different unique advantages related to the nature of each method may be gained.

List of References

[1] M. A. El-Kady, "Optimization of power cable and thermal backfill configurations," *IEEE Transactions on Power Apparatus and Systems*, vol. PAS-101, pp. 4681-4688, 1982.

[2] M. A. El-Kady, J. Motlis, and K. MacKay, "A knowledge base system for power cable design, " *IEEE Transactions on Power Delivery*, vol. 5, pp. 449-455, 1990.

[3] G. J. Anders, M. A. El-Kady, R. W. Ganton, D. J. Horrocks, and J. Motlis, "FICAG A user oriented utility program for ampacity calculation of power cables on a desktop computer," *IEEE Transactions on Power Apparatus and Systems*, vol. PWRD -2, pp. 289-295, 1987.

[4] C. Garrido, A. F. Otero, and J. Cidras, "Theoretical model to calculate steady-state and transient ampacity and temperature in buried cables," *IEEE Transactions on Power Delivery*, vol. 18, pp. 667-678, 2003.

[5] J. H. Neher and M. H. McGrath, "The calculation of the temperature rise and load capability of cable systems," *AIEE Trans. (power apparatus and systems)*, vol. 76, 1957, pp. 752-772.

[6] I. Kocar and A. Ertas, "Thermal analysis for determination of current carrying capacity of PE and XLPE insulated power cables using finite element method," presented at Electrotechnical Conference, 2004. Proceedings of the 12th IEEE Mediterranean, 2004.

[7] "Calculation of the continuous current rating of cables (100% load factor)," IEC standard, publication 287, 1982, 2nd edition.

[8] "Determination of rating for underground and aerial Cables," NELA publication 28, March, 1932.

[9] "Current carrying capacity of impregnated paper-insulated cable," EEI publication A-14, 1933.

[10] "Guide for wartime conductor temperatures for power cables in service," IPCEA, January, 1943.

[11] D.M. Simmons, "Cable geometry and the calculation of current-carrying capacity," *AIEE Trans.*, Vol. 42, pp. 600-615, 1923.

[12] D.M. Simmons, "Calculation of the electrical problems of underground cables," *The Electric Journal,* Vol. 29, No. 9. pp. 395-426, 1932.

[13] H. Goldenberg, "The calculation of cyclic rating factors for cables laid direct or in ducts," *Proc. IEE,* Vol. 104, Pt. C, pp. 154-166, 1957.

[14] H. Goldenberg, "The calculation of cyclic rating factors and emergency loading for one or more cables laid direct or in ducts," *Proc. IEE,* Vol. 105, Pt. C, pp. 46-54, 1958.

[15] "IEEE standard-Power cable ampacity tables," IEEE (1994) Standard 835.

[16] M. S. Al-Saud, M. A. El-Kady, and R.D. Findlay, "Accurate assessment of thermal field and ampacity of underground power cables," Proceedings of IEEE Canadian Conference on Electrical and Computer Engineering, Ottawa, Canada May, 2006, pp. 651-654.

[17] M. S. Al-Saud, M. A. El-Kady, and R.D. Findlay, "Application of finite-element sensitivities to power cable thermal field analysis," Proceedings of Sixth IASTED International Conference on European Power and Energy Systems (EuroPES 2006), Rhodes, Greece 2006, pp. 149-154.

[18] M. S. Al-Saud, M. A. El-Kady, and R.D. Findlay, "Power cable thermal field sensitivities using finite-elements," Proceedings of IASTED International Conference on Power, Energy and Applications (PEA 2006), Gaborone, Botswana, September 2006, pp. 159-163.

[19] M. S. Al-Saud, M. A. El-Kady, and R.D. Findlay, "Optimization of power cable thermal performance using finite-element generated gradient," Proceedings of Ninth IASTED International Conference on Power and Energy Systems, Clearwater, Florida, USA, January 2007, pp. 63-68.

[20] M. S. Al-Saud, M. A. El-Kady, and R.D. Findlay, "Advanced thermal field sensitivity analysis of power cables," Proceedings of IEEE Canadian Conference on Electrical and Computer Engineering, Vancouver, Canada, April 2007, pp. 133-136.

[21] M. S. Al-Saud, M. A. El-Kady, and R.D. Findlay, "Experimental investigation of power cable performance," Proceedings of International Conference on Power Engineering, Energy and Electrical Drives, April 12-14, 2007, Setubal, Portugal, pp. 595-599.

[22] M. S. Al-Saud, M. A. El-Kady, and R.D. Findlay, "Preparation of Future Practical Engineers - Case Study: Laboratory Experiments on Power Cables," Proceedings of 7th Saudi Engineering Conference (SEC7), 26-28 November, 2007, Riyadh, Saudi Arabia (accepted).

[23] M. S. Al-Saud, M. A. El-Kady, and R.D. Findlay, "A novel finite-element optimization algorithm with applications to power cable thermal circuit design," IEEE Power Engineering Society, 2007 General Meeting, 24-28 June 2007, Tampa, Florida USA, Paper# 07GM0891.

[24] M.S. Al-Saud, M.A. El-Kady and R.D. Findlay, "Combined simulation-experimental approach to power cable thermal loading assessment," *IEE Proceedings-Generation, Transmission and Distribution* (accepted for publication, revision is underway).

[25] M.S. Al-Saud, M.A. El-Kady and R.D. Findlay, "Finite-element sensitivity analysis for power cable thermal performance optimization," *IEEE Transaction on Power Delivery* (T-PWRD) (submitted).

[26] M.S. Al-Saud, M.A. El-Kady and R.D. Findlay, "A new approach to underground cable performance assessment," *Electric Power System Research* (accepted for publication, revision is underway).

[27] M. S. Al-Saud, M. A. El-Kady, and R.D. Findlay, "Simulation of finite-element sensitivities for power cables in complex media," Proceedings of 18th IASTED International Conference on Modelling and Simulation (MS-2007), May 30 – June 1, 2007, Montreal, Quebec, Canada, pp. 84-89.

[28] N. Flatabo, "Transient heat conduction problem in power cables solved by the finite element method," *IEEE Transactions on Power Apparatus and Systems*, vol. PAS-92, pp. 56-63, 1973.

[29] J. K. Mitchell and O. N. Abdel-hadi, "Temperature distribution around buried cables," *IEEE Transactions on Power Apparatus and Systems*, vol. PAS-98, pp. 1158-1166, 1979.

[30] E. Tarasiewicz, E. Kuffel, and S. Grzybowski, "Calculation of temperature distribution within cable trench backfill and the surrounding soil," *IEEE Transactions on Power Apparatus and Systems*, vol. PAS-104, pp. 1973-1978, August 1985.

[31] M. A. El-Kady, "Calculation of the sensitivity of power cable ampacity to variations of design and environment parameters," *IEEE Transaction on power apparatus and Systems*, vol. PAS-103, August 1984, pp. 2043-2050.

[32] M. A. El-Kady and D. J. Horrocks, "Extended values for geometric factor of external thermal resistance of cables in duct banks," *IEEE Transactions on Power Apparatus and Systems*, vol. PAS-104, pp. 1958-1962, Agust 1985.

[33] M. A. El-Kady, G. A. Anders, J. Motlis, and D. J. Horrocks, "Modified values for geometric factor of external thermal resistance of cables in duct banks," *IEEE Transactions on Power Delivery*, vol. 3, pp. 1303-1309, 1988.

[34] G. J. Anders and H. S. Radhakrishna, "Computation of temperature field and moisture content in the vicinity of current carrying underground power cables," *IEE Proceedings-Generation, Transmission and Distribution*, vol. 135, pp. 51-62, 1988.

[35] C. C. Hwang, "Calculation of thermal fields of underground cable systems with consideration of structural steels constructed in a duct bank," *IEE Proceedings-Generation, Transmission and Distribution*, vol. 144, pp. 541-545, 1997.

[36] C. Hwang and J. Yi-Hsuan, "Extensions to the finite element method for thermal analysis of underground cable systems," *Electric Power Systems Research* Volume: 64, Issue: 2, February, 2003, pp. 159-164.

[37] M. Moallem and R. Jafari, "Transformation method in the coupled FE magneto-thermal field analysis," *IEEE Transactions on Magnetics*, vol. 34, pp. 3126-3129, 1998.

[38] M. A. El-Kady, F. Y. Chu, H. S. Radkrishna, D. J. Horrcks, and R. W. D. Ganton, "A probabilistic approach to power cable thermal analysis and ampacity evaluation," *IEEE Transactions on Power Apparatus and Systems*, vol. PAS-103, pp. 2735 2740, 1984.

[39] Foty, M.S.; Anders, G.J.; Croall, S.C., "Cable environment analysis and the probabilistic approach to cable rating," *IEEE Transactions on Power Delivery*, vol.5, no.3pp.1628-1633, Jul 1990.

[40] G. Buonanno, A. Carotenuto, M. Dell'Isola, and D. Villacci, "Effect of radiative and convective heat transfer on thermal transients in power cables," *IEE Proceedings-Generation, Transmission and Distribution*, vol. 142, pp. 436-444, 1995.

[41] J. Nahman and M. Tanaskovic, "Determination of the current carrying capacity of cables using the finite element method," *Electric Power Systems Research* Volume: 61, Issue: 2, March 28, 2002, pp. 109 – 117.

[42] J. Desmet, D. Putman, F. D'hulster, and R. Belmans, "Thermal analysis of the influence of nonlinear, unbalanced and asymmetric loads on current conducting capacity of LV-cables," presented at Power Tech Conference Proceedings, IEEE Bologna, 2003.

[43] J. J. Desmet, D. J. Putman, G. M. Vanalme, and R. J. Belmans, "Modelling and sensitivity analysis of the thermal behaviour of cables for different current conditions," presented at 11th International Conference on Harmonics and Quality of Power, 2004.

[44] S. W. Kim, H. H. Kim, S. C. Hahn, B. Y. Lee, K. Y. Park, Y. J. Shin, W. P. Song, J. B. Kim, and I. H. Shin, "Coupled finite-element-analytic technique for prediction of temperature rise in power apparatus," *IEEE Transactions on Magnetics*, vol. 38, pp. 921-924, 2002.

[45] G. J. Anders, A. K. T. Napieralski, and W. Zamojski, "Calculation of the internal thermal resistance and ampacity of 3-core unscreened cables with fillers," *IEEE Transactions on Power Delivery*, vol. 13, pp. 699-705, 1998.

[46] G. J. Anders, A. Napieralski, and Z. Kulesza, "Calculation of the internal thermal resistance and ampacity of 3-core screened cables with fillers," *IEEE Transactions on Power Delivery*, vol. 14, 1999, pp. 729-734

[47] H. J. Li, "Estimation of thermal parameters and prediction of temperature rise in crane power cables," *IEE Proceedings-Generation, Transmission and Distribution*, vol. 151, pp. 355-360, 2004.

[48] H. J. Li, "Estimation of soil thermal parameters from surface temperature of underground cables and prediction of cable rating," *IEE Proceedings-Generation, Transmission and Distribution*, vol.152, no.6pp. 849- 854, 4 Nov. 2005

[49] H. J. Li, K. C. Tan and Q. Su, "Assessment of Underground Cable Ratings Based on Distributed Temperature Sensing," *IEEE Transactions on Power Delivery*, Accepted for future publication.

[50] Q. Su, H. J. Li and K. C. Tan, "Hotspot location and mitigation for underground power cables," *IEE Proceedings-Generation, Transmission and Distribution*, vol.152, no.6pp. 934- 938, 4 Nov. 2005

[51] N. Kovac, I. Sarajcev and D. Poljak, "Nonlinear-coupled electric-thermal modeling of underground cable systems," *IEEE Transactions on Power Delivery*, vol.21, no.1pp. 4- 14, Jan. 2006

[52] N. Kovac, I. Sarajcev and D. Poljak, "A numerical-stochastic technique for underground cable system design," *IEE Proceedings-Generation, Transmission and Distribution*, vol.153, no.2pp. 181- 186, 16 March 2006.

[53] M. A. Hanna, A. Y. Chikhani, and M. M. A. Salama, "Modelling of underground cable systems in non-homogeneous soils," presented at 35th Midwest Symposium on Circuits and Systems, Washington, DC, pp. 381-384, 1992.

[54] M. A. Hanna, A. Y. Chikhani, and M. M. A. Salama, "Thermal analysis of power cables in multi-layered soil. I. Theoretical model," *IEEE Transactions on Power Delivery*, vol. 8, pp. 761-771, 1993.

[55] M. A. Hanna, A. Y. Chikhani, and M. M. A. Salama, "Thermal analysis of power cables in multi-layered soil. II. Practical considerations," *IEEE Transactions on Power Delivery*, vol. 8, pp. 772-778, 1993.

[56] M. A. Hanna, A. Y. Chikhani, and M. M. A. Salama, "Thermal analysis of power cables in multi-layered soil. III. Case of two cables in a trench," *IEEE Transactions on Power Delivery*, vol. 9, pp. 572-578, 1994.

[57] M. A. Hanna, A. Y. Chikhani, and M. M. A. Salama, "Thermal analysis of power cable systems in a trench in multi-layered soil," *IEEE Transactions on Power Delivery*, vol. 13, pp. 304-309, 1998.

[58] G. Gela and J. J. Dai, "Calculation of thermal fields of underground cables using the boundary element method," *IEEE Transactions on Power Delivery*, vol. 3, pp. 1341-1347, 1988.

[59] J. Lyall, "Two dimensional modelling of three core cable transient temperature rise," *IEEE Transactions on Power Delivery*, vol. 5, pp. 21-25, 1990.

[60] D. S. Freitas, A. T. Prata, and A. J. de Lima, "Thermal performance of underground power cables with constant and cyclic currents in presence of moisture migration in the surrounding soil," *IEEE Transactions on Power Delivery*, vol. 11, pp. 1159-1170, 1996.

[61] G. Bontempi, A. Vaccaro, and D. Villacci, "Power cables thermal protection by interval simulation of imprecise dynamical systems," *IEE Proceedings-Generation, Transmission and Distribution*, vol. 151, pp. 673-680, 2004.

[62] G. J. Anders and M. A. El-Kady, "Transient ratings of buried power cables. I. Historical perspective and mathematical model," *IEEE Transactions on Power Delivery*, vol. 7, pp. 1724-1734, 1992.

[63] M. Sakata and S. Iwamoto, "Genetic algorithm based real-time rating for short-time thermal capacity of duct installed power cables," presented at International Conference on Intelligent Systems Applications to Power Systems, Proceedings ISAP, Orlando, Florida, 1996.

[64] J. A. Williams, D. Parmar, and M. W. Conroy, "Controlled backfill optimization to achieve high ampacities on transmission cables," *IEEE Transactions on Power Delivery*, vol. 9, pp. 544-552, 1994.

[65] P. Slaninka and V. T. Morgan, "External thermal resistance of power cable in nonuniform soil," *IEE Proceedings- Science, Measurement and Technology*, vol. 139, pp. 117-124, 1992.

[66] G. C. Thomann, T. Aabo, E. C. Bascom, Jr., A. R. Ghafurian, and T. McKernan, "A Fourier transform technique for calculating cable and pipe temperatures for periodic and transient conditions," *IEEE Transactions on Power Delivery*, vol. 6, pp. 1345-1351, 1991.

[67] T. L. Jones, "The calculation of cable parameters using combined thermal and electrical circuit models," *IEEE Transactions on Power Delivery*, vol. 4, pp. 1529-1540, 1989.

[68] J. Luo; Y. Liu and Y. Luo, "Temperature calculation of power cable conductor in real time," Proceedings of Electrical Insulation Conference and Electrical Manufacturing Expo, 2005, Indianapolis, IN, USA, 23-26 Oct. 2005, pp. 26- 29.

[69] R. J. Millar and M. Lehtonen, "A robust framework for cable rating and temperature monitoring," *IEEE Transactions on Power Delivery*, vol.21, no.1pp. 313- 321, Jan. 2006

[70] H. C. Zhao, J. S. Lyall, and G. Nourbakhsh, "Probabilistic cable rating based on cable thermal environment studying," presented at International Conference on Power System Technology, (PowerCon 2000).

[71] J. S. Lyall, G. Nourbakhsh, and H. C. Zhao, "Underground power cable environment on-line monitoring and analysis," presented at Power Engineering Society Summer Meeting, 2000, IEEE, 2000.

[72] M. R. Sredojevic, R. M. Naumov, D. P. Popovic, and M. D. Simie, "Long term investigation of thermal behaviour of 110 kV underground transmission lines in the Belgrade area," presented at 14th International Conference and Exhibition on Electricity Distribution (IEE Conf. Publ. No. 438), 1997.

[73] T. Saito, M. Nakade, T. Kano, and T. Ishikawa, "Development of a new program to estimate the conductor temperature of underground transmission cables in the buried ducts," presented at Transmission and Distribution Conference and Exhibition 2002: Asia Pacific, IEEE/PES, 2002.

[74] B. J. Grotenhuis, J. E. Jaspers, A. H. van der Wey, F. H. de Wild, and A. Kerstens, "Increasing the capacity of cable systems using cable asset management based on thermal and mechanical properties," presented at 16th International Conference and Exhibition on Electricity Distribution, CIRED 2001, (IEE Conf. Publ No. 482).

[75] J. A. Williams, J. H. Cooper, T. J. Rodenbaugh, G. L. Smith, and F. Rorabaugh, "Increasing cable rating by distributed fiber optic temperature monitoring and ampacity analysis," presented at Transmission and Distribution Conference, 1999 IEEE, 1999.

[76] M. Sankaran, C. Cooper, M. L. Dyer, and G. Karady, "Investigation of the heat distribution around cable ducts in a desert climate," presented at Power Engineering Society General Meeting, 2004. IEEE, 2004.

[77] C. L. Cooper, M. L. Dyer, and G. G. Karady, "Investigation of the seasonal variation of ground thermal conductivity on high voltage cable ampacity," presented at Large Engineering Systems Conference on Power Engineering, 2004, (LESCOPE-04).

[78] H. Brakelmann and G. Anders, "Ampacity reduction factors for cables crossing thermally unfavorable regions," *IEEE Transactions on Power Delivery*, vol. 16, pp. 444-448, 2001.

[79] G. Anders, J. M. Braun, M. Vainberg, S. Rizzetto, and H. Brakelmann, "Rating of cables in a nonuniform thermal environment," presented at Transmission and Distribution Conference, 1999 IEEE, 1999.

[80] P. Vaucheret, R. A. Hartlein, and W. Z. Black, "Ampacity derating factors for cables buried in short segments of conduit," *IEEE Transactions on Power Delivery*, vol. 20, pp. 560-565, 2005.

[81] O.C Zienkiewicz, "The finite element method in engineering science," McGraw-Hill, London 1971.

[82] Jianming Jin, "The finite element method in electromagnetics," 2nd edition, John Wiley & Sons, Inc.

[83] P. E. Allaire, "Basic of the finite element method, solid mechanics, heat transfer, and fluid mechanics," Brown publisher 1985.

[84] G. J.Anders, "Rating of electrical power cables; ampacity computation for transmission, distribution and industrial applications," IEEE Press.

[85] G. Myers, "Analytical method in conduction heat transfer," McGraw-Hill.

[86] R. Haskew, R.F. Carwile and L.L. Grigsby, "An algorithm for steady-state thermal analysis of electrical cables with radiation by reduced Newton-Raphson techniques," *IEEE Transactions on Power Delivery*, Vol. 9. No. 1, pp. 526-533, January 1994.

[87] J. Nocedal and S. Wright, "Numerical Optimization," Springer, New York, 1999.

[88] D. P. Bertsekas, "Nonlinear Programming," Second Edition, Athena Scientific, Belmont, MA, 1999.

[89] P.E. Gill, W. Murry and M.H Wright, "Practical Optimization," Academic Press, London, 1986.

[90] D. Mushamalirwa, N. Germay, and J. C. Steffens, "A 2-D finite element mesh generator for thermal analysis of underground power cables," *IEEE Transactions on Power Delivery*, vol. 3, pp. 62-68, 1988.

[91] j. E. Steinmanis, "Thermal property measurement using a thermal probe," symposium on underground cable thermal backfill, Toronto, Ontario, Canada, September 17-18, 1981, pp. 72–85.

[92] H. C. Reader, R. Savo, S. Lorentz, and N. Iecler, "Time domain methods for soil moisture determination," presented at Ninth International Conference on Antennas and Propagation (ICAP '95), 1995, (Conf. Publ. No. 407).

[93] D. Parmar; J. Steinmanis, "Underground cables need a proper burial," *Transmission & Distribution World;* Apr 2003; 55, 4; ABI/INFORM Global, pp 44-51

[94] S. Milun, T. Kilic and O. Bego, "Measurement of soil thermal properties by spherical probe," *IEEE Transactions on Instrumentation and Measurement*, Vol.54, Iss.3, pp. 1219- 1226, June 2005.

APPENDICES

APPENDIX A

Variational Calculus

The calculus of variations provides the bridge between what we are already familiar with and the statement of the problem that is required for the finite element formulation.

A simple problem in the theory of the calculus of variations seeks to find a function $u(x)$ that minimizes the integral

$$I = \int_{x=0}^{L} \varphi(x, u(x), u'(x))\, dx \qquad \text{(A.1)}$$

In this section the prime on u' will denote differentiation with respect to x. Observe that φ is a function of both $u(x)$ and $u'(x)$. In this simple problem we will also specify the value of $u(x)$ at $x = 0$ and at $x = L$. That is, we will require that

$$u(0) = u_0 \qquad \text{and} \qquad u(L) = u_L \qquad \text{(A.2)}$$

To find $u(x)$ we are going to consider every function that satisfies equation (A.2). From all these possible functions we will be seeking the one that gives I its minimum value. This set of possible functions may be represented simply by $\tilde{u}(x, \varepsilon)$, where

$$\tilde{u}(x, \varepsilon) = u(x) + \varepsilon\, \eta(x) \qquad \text{(A.3)}$$

The function $u(x)$ is the desired function that will minimize I and $\varepsilon\eta(x)$ is called variation of this function. The function $\tilde{u}$ and u are shown in Figure (A.1). The function $\eta(x)$ is completely arbitrary but smooth function of x except that we must insist that

$$\eta(0) = 0 \qquad \text{and} \qquad \eta(L) = 0 \tag{A.4}$$

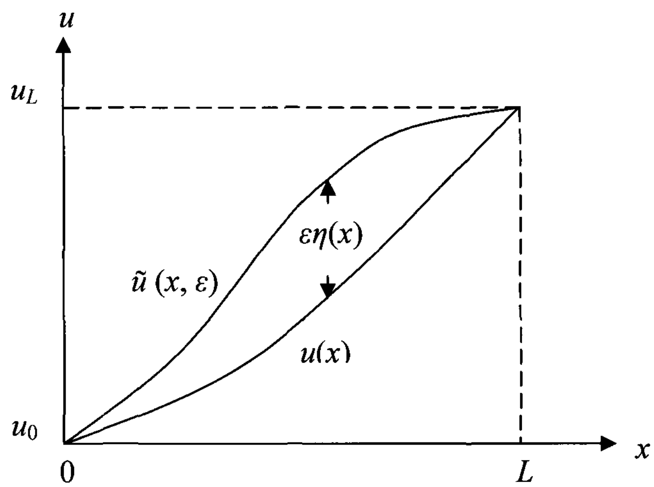

Figure A.1 Desired vocational solution *u(x)* and trial function $\tilde{u}$ *(x, ε)*

to ensure that all the $\tilde{u}$ will have the correct value at $x = 0$ and $x = L$. That is, we want

$$\tilde{u}(0,\varepsilon) = u(0) \quad \text{and} \qquad \tilde{u}(L,\varepsilon) = u(L) \tag{A.5}$$

so that equation (A.2) will be satisfied.

Notice that the function we are seeking is included in the complete set of possible functions given by equation (A.3). The desired function $u(x)$ is the one in the complete set which has $\varepsilon = 0$. That is, from equation (A.3)

$$\tilde{u}(x,0) = u(x) \tag{A.6}$$

We will also need to consider the derivative $\tilde{u}$ (x, ε) with respect to x. This may be obtained by differentiating equation (A.3) to give

$$\tilde{u}'(x,0) = u'(x) + \varepsilon\eta'(x) \tag{A.7}$$

Now let us consider the integral that is obtained by replacing $u(x)$ and $u'(x)$ in equation (A.1) with $\tilde{u}\,(x, \varepsilon)$ and $\tilde{u}'(x, \varepsilon)$. That is, let us consider

$$I(\varepsilon) = \int_{x=0}^{L} \varphi(x, \tilde{u}(x), \tilde{u}'(x))\; dx \tag{A.8}$$

Observe that this integral is a function of ε since it will still appear as a parameter after the integration over x is carried out. Also notice that when $\varepsilon = 0$ the integral in equation (A.8) reduces to the integral we started with in equation (A.1) because $\tilde{u}\,(x, \varepsilon) = \tilde{u}\,(x)$ when $\varepsilon = 0$ as given by equation (A.6). This means that we want $I(\varepsilon)$ to have a minimum when $\varepsilon = 0$.

To find minimum of $I(\varepsilon)$ we must first differentiate it with respect to ε. Since the limits of integration are not functions of ε, we may use Leibnitz's rule to write

$$\frac{dI(\varepsilon)}{d\varepsilon} = \int_{x=0}^{L} \frac{\partial}{\partial\varepsilon}\; \varphi(x, \tilde{u}(x), \tilde{u}'(x))\; dx \tag{A.9}$$

The chain rule of calculus may now be employed to give

$$\frac{dI(\varepsilon)}{d\varepsilon} = \int_{x=0}^{L} \left[\frac{\partial\varphi}{\partial\tilde{u}}\frac{\partial\tilde{u}}{\partial\varepsilon} + \frac{\partial\varphi}{\partial\tilde{u}'}\frac{\partial\tilde{u}'}{\partial\varepsilon} \right] dx \tag{A.10}$$

From equation (A.3) and (A.7) it follows that

$$\frac{\partial \tilde{u}}{\partial \varepsilon} = \eta(x) \qquad \text{and} \qquad \frac{\partial \tilde{u}'}{\partial \varepsilon} = \eta'(x) = \frac{d\eta(x)}{dx}$$

There for equation (A.10) may be written as

$$\frac{dI(\varepsilon)}{d\varepsilon} = \int_{x=0}^{L} \left[\frac{\partial \varphi}{\partial \tilde{u}} \eta(x) + \frac{\partial \varphi}{\partial \tilde{u}'} \frac{d\eta(x)}{dx} \right] dx \tag{A.11}$$

The second term may be integrated by parts to give

$$\frac{dI(\varepsilon)}{d\varepsilon} = \int_{x=0}^{L} \frac{\partial \varphi}{\partial \tilde{u}} \eta(x)\ dx + \left[\frac{\partial \varphi}{\partial \tilde{u}'} \eta(x) \right]_{x=0}^{L} - \int_{x=0}^{L} \eta(x) \frac{d}{dx}\left[\frac{\partial \varphi}{\partial \tilde{u}'} \right] dx \tag{A.12}$$

From equation (A.4) we see that the integration term vanishes at both its upper and lower limits. Thus, upon recombining the two integrals, equation (A.12) reduces to

$$\frac{dI(\varepsilon)}{d\varepsilon} = \int_{x=0}^{L} \eta(x) \left[\frac{\partial \varphi}{\partial \tilde{u}} - \frac{d}{dx}\left(\frac{\partial \varphi}{\partial \tilde{u}'} \right) \right] dx \tag{A.13}$$

We will now insist that this be equal to zero when $\varepsilon = 0$ so that $I(0)$ may be a minimum. Thus

$$\left.\frac{dI(\varepsilon)}{d\varepsilon}\right|_{\varepsilon=0} = \int_{x=0}^{L} \eta(x) \left[\frac{\partial \varphi}{\partial u} - \frac{d}{dx}\left(\frac{\partial \varphi}{\partial u'} \right) \right] dx = 0 \tag{A.14}$$

Observe, from equation (A.1) that $\tilde{u}$ has become u because ε has been set equal to zero.

Since $\eta(x)$ is arbitrary, the term in brackets must be zero to ensure that this integration will be zero. Therefore, for I to be a minimum

$$\frac{\partial \varphi}{\partial u} - \frac{d}{dx}\left(\frac{\partial \varphi}{\partial u'}\right) = 0 \tag{A.15}$$

This differential equation is called Euler-Lagrange equation. Its boundary conditions in this simple problem are given by equation (A.2). The solution $u(x)$ to this differential equation will be the function that minimizes the original integral in equation (A.1). Consequently, in the finite element method the problem will be cast as integral to be minimized, and we will use a numerical approximation of integral to obtain a solution.

Finite Element Formulations

The first step is to break up the region of interest Ω into E elements, each element specify by nodal points as shown in Figure A.2.

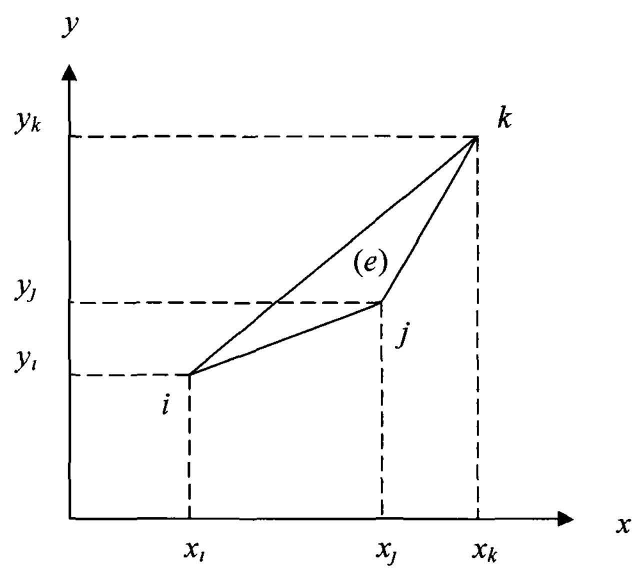

Fig. A.2 Finite element triangular for two-dimensional grid

To evaluate the integral in equation (3.23), it will be broken into E sub-integrals over each of the E elements. That is, we will consider

$$I = I^{(1)} + I^{(2)} + \cdots\cdots I^{(e)} \cdots\cdots + I^{(E)} = \sum_{e=1}^{E} I^{(e)} \tag{A.16}$$

In order to evaluate the elemental $I^{(e)}$, the temperature T within each element will be approximated using unknown node temperatures. If linear triangular elements are used, the temperature T within each element varies linearly in the region defined by the three corner temperatures. This may be expressed as

$$T^e(x,y) = c_1^e + c_2^e\, x + c_3^e\, y \tag{A.17}$$

or in a matrix form

$$T^e = \mathbf{p}^{\mathrm{T}}\, \mathbf{c}^e \tag{A.18}$$

where

$$\mathbf{p}^{\mathrm{T}} = \begin{bmatrix} 1 & x & y \end{bmatrix} \quad \text{and} \quad \mathbf{c}^e = \begin{bmatrix} c_1 \\ c_2 \\ c_3 \end{bmatrix}^e$$

consequently, the integral $I^{(e)}$ over a typical finite element e is given by

$$I^e(T^e) = I_k^e - I_g^e = \frac{1}{2}\iint_{\Omega^e} \left[k\left(\frac{\partial T^e}{\partial x}\right)^2 + k\left(\frac{\partial T^e}{\partial y}\right)^2 \right] dx\,dy - \iint_{\Omega^e} Q^e\, T^e\, dx\,dy \tag{A.19}$$

The coefficients c_1,c_2 and c_3 may be evaluated by insisting that T^e be equal to the node temperatures T_i, T_j and T_k at the vertices of the element. Thus we would have

$$\mathbf{T}^e = \mathbf{P}^e\,\mathbf{c}^e \tag{A.20}$$

where $\mathbf{T}^e = \begin{bmatrix} T_i \\ T_j \\ T_k \end{bmatrix}$ and $\mathbf{P}^e = \begin{bmatrix} 1 & x_i & y_i \\ 1 & x_j & y_j \\ 1 & x_k & y_k \end{bmatrix}$

The constants $\mathbf{c}^e$ may then be found by multiplying equation (A.20) by the inverse of $\mathbf{P}^e$ which will be assigned as $\mathbf{R}^e = (\mathbf{P}^e)^{-1}$

$$\mathbf{c}^e = \mathbf{R}^e\,\mathbf{T}^e \tag{A.21}$$

where $$\mathbf{R}^e = \frac{1}{x_{ij}y_{jk} - x_{jk}y_{ij}} \begin{bmatrix} x_j y_k - x_k y_j & x_k y_i - x_i y_k & x_i y_j - x_j y_i \\ -y_{jk} & y_{ik} & -y_{ij} \\ x_{jk} & -x_{ik} & x_{ij} \end{bmatrix}$$

where we have adopted the shorthand notation that $x_{ij} = x_i - x_j$.

This result may be substituted into equation (A.18) to arrive at the following expression for the temperature distribution within the element

$$T^e = \mathbf{p}^{\mathrm{T}}\,\mathbf{R}^e\,\mathbf{T}^e \tag{A.22}$$

It can be observed from equations (A.16) and (A.19) that the integral I which has to be minimized is a function of nodal temperature. Consequently, to minimize I we have to set its derivative with respect to each of the nodal temperatures to zero:

$$\frac{dI}{d\mathbf{T}} = \frac{dI_k}{d\mathbf{T}} - \frac{dI_g}{d\mathbf{T}} = 0 \tag{A.23}$$

where $\mathbf{T}$ represents a vector of M node temperatures, that is

$$\mathbf{T} = \begin{bmatrix} T_1 \\ \vdots \\ T_i \\ T_j \\ T_k \\ \vdots \\ T_M \end{bmatrix} \qquad \text{and} \qquad \frac{dI}{d\mathbf{T}} = \begin{bmatrix} \frac{dI}{dT_1} \\ \vdots \\ \frac{dI}{dT_i} \\ \frac{dI}{dT_j} \\ \frac{dI}{dT_k} \\ \vdots \\ \frac{dI}{dT_M} \end{bmatrix}$$

From equation (A.16) the integral I can be computed as a sum over the small elements, and could be written as

$$\frac{dI}{d\mathbf{T}} = \sum_{e=1}^{E} \frac{dI^e}{d\mathbf{T}} = \sum_{e=1}^{E} \frac{dI_k^e}{d\mathbf{T}} - \sum_{e=1}^{E} \frac{dI_g^e}{d\mathbf{T}} \tag{A.24}$$

where $$\frac{dI^e}{d\mathbf{T}} = \begin{bmatrix} 0 \\ \vdots \\ 0 \\ \frac{dI^e}{dT_i} \\ \frac{dI^e}{dT_j} \\ \frac{dI^e}{dT_k} \\ 0 \\ \vdots \\ 0 \end{bmatrix}$$

For a particular element specified by nodes i, j and k, it can be deduced that I_k^e and I_g^e will be functions of the three corresponding temperatures T_i, T_j and T_k. Consequently, the partial derivatives of I_k^e and I_g^e with respect to all other nodal temperatures will be zero, and to avoid working with all these zeros we will consider an $M\times 3$ displacement matrix and a 3×1 column matrix containing only the particular element nodal temperatures.

$$\mathbf{D}^e = \begin{bmatrix} 0 & 0 & 0 \\ \vdots & \vdots & \vdots \\ 0 & 0 & 0 \\ 1 & 0 & 0 \\ 0 & 1 & 0 \\ 0 & 0 & 1 \\ 0 & 0 & 0 \\ \vdots & \vdots & \vdots \\ 0 & 0 & 0 \end{bmatrix} \begin{array}{l} \\ \\ \\ \leftarrow i\text{th row} \\ \leftarrow j\text{th row} \\ \leftarrow k\text{th row} \\ \\ \\ \\ \end{array} \qquad \text{and} \qquad \frac{dI^e}{d\mathbf{T}^e} = \begin{bmatrix} \frac{dI^e}{dT_i} \\ \frac{dI^e}{dT_j} \\ \frac{dI^e}{dT_k} \end{bmatrix}$$

We can then write

$$\frac{dI^e}{d\mathbf{T}} = \mathbf{D}^e \frac{dI^e}{d\mathbf{T}^e} \tag{A.25}$$

and equation (A.24) can be rewritten as:

$$\frac{dI}{d\mathbf{T}} = \sum_{e=1}^{E} \mathbf{D}^e \frac{dI^e}{d\mathbf{T}^e} = \sum_{e=1}^{E} \mathbf{D}^e \frac{dI_k^e}{d\mathbf{T}^e} - \sum_{e=1}^{E} \mathbf{D}^e \frac{dI_g^e}{d\mathbf{T}^e} \tag{A.26}$$

Each term in equation (A.26) will be computed separately and substituted again into equation (A.26). We are now ready to rewrite the function I_k^e defined in equation (A.19) by assuming the element is small enough so that the thermal conductivity can be taken to be a constant over the element

$$I_k^e = \frac{k^e}{2} \iint_{\Omega^e} \left[\left(\frac{\partial T^e}{\partial x} \right)^2 + \left(\frac{\partial T^e}{\partial y} \right)^2 \right] dx\, dy \tag{A.27}$$

Equation (A.22) may be differentiated with respect to space and then substituted into equation (A.27). The matrix $\mathbf{p}$ is the only matrix in equation (A.22) that depends upon location within the element

$$I_k^e = \frac{k^e}{2} \iint_{\Omega^e} \left[\left(\mathbf{p}_x^{\mathrm{T}} \mathbf{R}^e \mathbf{T}^e\right)^2 + \left(\mathbf{p}_y^{\mathrm{T}} \mathbf{R}^e \mathbf{T}^e\right)^2 \right] dx\, dy \tag{A.28}$$

where $\mathbf{p}_x^{\mathrm{T}} = \dfrac{d\mathbf{p}^{\mathrm{T}}}{dx} = \begin{bmatrix} 0 & 1 & 0 \end{bmatrix}$ and $\mathbf{p}_y^{\mathrm{T}} = \dfrac{d\mathbf{p}^{\mathrm{T}}}{dy} = \begin{bmatrix} 0 & 0 & 1 \end{bmatrix}$

This can be differentiated with respect to each of the three corner temperatures

$$\frac{dI_k^e}{d\mathbf{T}^e} = \frac{k^e}{2} \iint_{\Omega^e} \left[2\left(\mathbf{p}_x^{\mathrm{T}} \mathbf{R}^e \mathbf{T}^e\right)\left(\mathbf{p}_x^{\mathrm{T}} \mathbf{R}^e\right)^{\mathrm{T}} + 2\left(\mathbf{p}_y^{\mathrm{T}} \mathbf{R}^e \mathbf{T}^e\right)\left(\mathbf{p}_y^{\mathrm{T}} \mathbf{R}^e\right)^{\mathrm{T}} \right] dx\, dy \tag{A.29}$$

We may interchange the order of multiplication in equation (A.29) and then take the transposes of $\mathbf{p}_x^{\mathrm{T}} \mathbf{R}^e$ and $\mathbf{p}_y^{\mathrm{T}} \mathbf{R}^e$ to arrive at

$$\frac{dI_k^e}{d\mathbf{T}^e} = k^e \iint_{\Omega^e} \left[\mathbf{R}^{e\mathrm{T}} \mathbf{p}_x \mathbf{p}_x^{\mathrm{T}} \mathbf{R}^e \mathbf{T}^e + \mathbf{R}^{e\mathrm{T}} \mathbf{p}_y \mathbf{p}_y^{\mathrm{T}} \mathbf{R}^e \mathbf{T}^e \right] dx\, dy \tag{A.30}$$

In equation (A.30), $\mathbf{R}^e$ and $\mathbf{T}^e$ are independent of the space. Therefore they may be factored out of the integral to give

$$\frac{dI_k^e}{d\mathbf{T}^e} = k^e\ \mathbf{R}^{e^{\mathrm{T}}} \left(\iint_{\Omega^e} \left(\mathbf{p}_x \mathbf{p}_x^{\mathrm{T}} + \mathbf{p}_y \mathbf{p}_y^{\mathrm{T}}\right) dx\, dy \right) \mathbf{R}^e\, \mathbf{T}^e \tag{A.31}$$

where $\iint_{\Omega^e} \left(\mathbf{p}_x \mathbf{p}_x^{\mathrm{T}} + \mathbf{p}_y \mathbf{p}_y^{\mathrm{T}}\right) dx\, dy = \iint_{\Omega^e} \begin{bmatrix} 0 & 0 & 0 \\ 0 & 1 & 0 \\ 0 & 0 & 1 \end{bmatrix} dx\, dy = \Omega^e \begin{bmatrix} 0 & 0 & 0 \\ 0 & 1 & 0 \\ 0 & 0 & 1 \end{bmatrix}$

and Ω^e represents the element area.

This integral can be multiplied by $\mathbf{R}^{e\mathrm{T}}$ and postmultiplied by $\mathbf{R}^e$ to give

$$\frac{dI_k^e}{d\mathbf{T}^e} = \mathbf{K}^e\, \mathbf{T}^e \tag{A.32}$$

where the element conduction matrix is given by

$$\mathbf{K}^e = \frac{k^e\, A^e}{(x_{ij}\, y_{jk} - x_{jk} y_{ij})^2} \begin{bmatrix} x_{jk}^2 + y_{jk}^2 & -(x_{ik}x_{jk} + y_{ik}y_{jk}) & x_{ij}x_{jk} + y_{ij}y_{jk} \\ & x_{ik}^2 + y_{ik}^2 & -(x_{ij}x_{ik} + y_{ij}y_{ik}) \\ \text{symmetric} & & x_{ij}^2 + y_{ij}^2 \end{bmatrix}$$

Equation (A.32) can now be substituted into the first term of (A.26) to give

$$\frac{dI_k}{d\mathbf{T}} = \sum_{e=1}^{E} \mathbf{D}^e \mathbf{K}^e\, \mathbf{T}^e \tag{A.33}$$

It will be helpful if we relate the nodal temperature of the element, $\mathbf{T}^e$, to the entire set of nodal temperatures $\mathbf{T}$. This can be done by using the displacement matrix $\mathbf{D}^e$

$$\mathbf{T}^e = \mathbf{D}^{e^{\mathrm{T}}}\, \mathbf{T} \tag{A.34}$$

and by substituting (A.34) into(A.33) we get

$$\frac{dI_k}{d\mathbf{T}} = \sum_{e=1}^{E} \mathbf{D}^e \mathbf{K}^e \ \mathbf{D}^{e^{\mathrm{T}}} \ \mathbf{T} \tag{A.35}$$

It is now convenient to define a global conduction matrix as

$$\mathbf{K} = \sum_{e=1}^{E} \mathbf{D}^e \mathbf{K}^e \ \mathbf{D}^{e^{\mathrm{T}}} \tag{A.36}$$

Then equation (A.35) may be simplified to

$$\frac{dI_k}{d\mathbf{T}} = \mathbf{K} \ \mathbf{T} \tag{A.37}$$

This is the final result that we need for equation (A.23). Now let us consider I_g which may be written for element e from (A.19)

$$I_g^e = Q^e \iint_{\Omega^e} T^e \, dx \, dy \tag{A.38}$$

In writing this we have assumed that the element is small enough so that the generation rate may be taken to be uniform and moved outside the integral. However, substituting equation (A.22) into (A.38) gives

$$I_g^e = Q^e \iint_{\Omega^e} \mathbf{p}^{\mathrm{T}} \, \mathbf{R}^e \, \mathbf{T}^e \, dx \, dy \tag{A.39}$$

This can be differentiated with respect to each of element nodal temperatures $\mathbf{T}^e$

$$\frac{dI_g^e}{d\mathbf{T}^e} = Q^e \iint_{\Omega^e} (\mathbf{p}^{\mathrm{T}} \mathbf{R}^e)^{\mathrm{T}} \, dx\, dy \tag{A.40}$$

Transposing $\mathbf{p}^{\mathrm{T}} \mathbf{R}^e$ and recognizing that $\mathbf{R}^e$ is independent of the space, the following is obtained:

$$\frac{dI_g^e}{d\mathbf{T}^e} = Q^e \, \mathbf{R}^{e^{\mathrm{T}}} \iint_{\Omega^e} \mathbf{p} \; dx\, dy = Q^e A^e \, \mathbf{R}^{e^{\mathrm{T}}} \mathbf{p}_c^e \tag{A.41}$$

where $\mathbf{p}_c^e = \begin{bmatrix} 1 & \dfrac{x_i + x_j + x_k}{3} & \dfrac{y_i + y_j + y_k}{3} \end{bmatrix}^{\mathrm{T}}$

The matrix multiplication in equation (A.41) is carried out to give

$$\frac{dI_g^e}{d\mathbf{T}^e} = \mathbf{g}^{e^{\mathrm{T}}} \tag{A.42}$$

where $\mathbf{g}^e = \dfrac{Q^e A^e}{3} \begin{bmatrix} 1 \\ 1 \\ 1 \end{bmatrix}$

Equation (A.42) may now be substituted into the equivalent second term of (A.26)

$$\frac{dI_g}{d\mathbf{T}} = \sum_{e=1}^{E} \mathbf{D}^e \mathbf{g}^e \tag{A.43}$$

If we now define a global generation vector as

$$\mathbf{g} = \sum_{e=1}^{E} \mathbf{D}^e \mathbf{g}^e \tag{A.44}$$

equation (A.43) reduces to

$$\frac{dI_g}{d\mathbf{T}} = \mathbf{g} \tag{A.45}$$

Finally equations (A.37) and (A.45) may be substituted into equation (A.23) to give

$$\frac{dI}{d\mathbf{T}} = \mathbf{K}\ \mathbf{T} - \mathbf{g} = 0 \tag{A.46}$$

This is a set of algebraic equations which has to be solved for the nodal temperatures **T**.

APPENDIX B
Sample of experimental results sheets

Experiment #4
Filled container /loaded cable

Figure:

Notes

(1) step (1)

$I_{sec} = 293.8$ A ? switch on at 8:30 am

$I_p = 23.6$ A saturday

$V_p = 14.08$ V

Prop number	Depth level	300.5A 24.0A Temp 12:45	302.7A 24.2A Temp pm 9:30	299.8A 23.9A Temp 8:15	298.4A 23.8A Temp 7:20	297.5A 23.8A Temp am 9:20	301.6A 24.1A Temp pm 9:00	301.2A 24.0A Temp am 10:00	303.1A 24.2A Temp pm 10:00	301.2A 24.1 pm 7:20	302.1A 24.1A pm 8:30
9	A	26.0	26.1	26.1	26.4	26.6	26.6	26.9	27.0	27.3	27.5
	B	26.5	26.7	26.7	26.9	27.0	27.3	27.3	27.6	27.8	28.1
	C	26.2	26.3	26.3	26.5	26.6	26.7	26.9	27.1	27.3	27.6
10	A	27.3	27.4	27.6	27.8	28.0	28.1	28.3	28.5	28.8	29.1
	B	30.1	30.2	30.2	30.5	30.6	30.8	30.9	31.0	31.3	31.8
	C	27.3	27.4	27.5	27.7	27.9	28.0	28.2	28.3	28.5	28.9
11	A	28.1	28.3	28.4	28.6	28.8	28.8	29.1	29.2	29.5	29.9
	B	24.1	34.2	34.4	34.6	34.7	34.8	34.9	35.1	35.5	35.9
	C	27.6	27.8	27.9	28.1	28.2	28.4	28.5	28.5	28.9	29.3
12	A	26.4	26.6	26.6	26.8	26.9	27.2	27.4	27.5	27.8	28.2
	B	27.3	27.6	27.7	27.9	28.0	28.2	28.4	28.4	28.6	29.1
	C	26.2	26.5	26.6	26.8	27.0	26.9	27.2	27.3	27.7	28.0
13	A	25.0	25.5	25.6	25.8	26.0	26.1	26.3	26.5	26.7	27.0
	B	25.7	25.9	26.0	26.2	26.3	26.3	26.6	26.8	27.0	27.4
	C	25.3	25.5	25.7	25.7	25.9	26.0	26.3	26.4	26.6	27.0
20	A	25.5	25.6	25.9	25.9	26.2	26.2	26.5	26.6	26.8	27.1
	B	25.9	25.9	26.3	26.3	26.5	26.6	26.8	26.9	27.2	27.5
	C	25.5	25.6	25.9	25.9	26.1	26.3	26.5	26.6	26.8	27.1
27	A	25.5	25.7	25.8	25.8	26.2	26.3	26.4	26.7	26.9	27.3
	B	25.7	25.9	26.0	26.1	26.3	26.3	26.5	26.8	27.1	27.3
	C	25.4	25.4	25.7	25.8	26.0	26.1	26.2	26.3	26.7	27.0
26	A	26.7	26.8	27.0	27.1	27.3	27.4	27.7	27.8	28.0	28.4
	B	27.8	27.9	28.1	28.2	28.4	28.5	28.7	28.9	29.2	29.5
	C	26.4	26.6	26.8	26.9	27.0	27.1	27.3	27.5	27.7	28.0
25	A	28.3	28.4	28.5	28.7	28.9	29.0	29.2	29.3	29.6	30.0
	B	35.3	35.4	35.6	35.7	35.9	35.9	36.0	36.4	36.8	37.1
	C	27.7	27.8	28.0	28.1	28.3	28.3	28.6	28.7	29.0	29.3
24	A	27.3	27.5	27.6	27.8	28.0	28.1	28.3	28.4	28.7	29.0
	B	29.9	30.0	30.2	30.2	30.5	30.6	30.8	30.9	31.1	31.6
	C	27.3	27.3	27.6	27.7	27.9	28.0	28.2	28.3	28.6	28.9
23	A	26.0	26.2	26.3	26.4	26.6	26.8	27.0	27.1	27.3	27.7
	B	26.6	26.8	27.0	27.0	27.2	27.3	27.5	27.6	27.9	28.2
	C	26.1	26.2	26.5	26.5	26.7	26.8	27.0	27.1	27.3	27.7
16	A	25.9	26.1	26.2	26.3	26.6	26.7	26.9	27.0	27.3	27.6
	B	26.6	26.8	27.0	27.0	27.2	27.3	27.5	27.6	27.9	28.2
	C	26.2	26.3	26.5	26.5	26.8	26.9	27.1	27.2	27.4	27.8

17	A	27.8	27.9	28.1	28.2	28.3	28.5	28.8	28.9	29.1	29.5
	B	30.3	30.4	30.7	30.7	31.0	31.0	31.3	31.3	31.6	32.0
	C	27.5	27.6	27.8	27.9	28.0	28.2	28.4	28.5	28.8	29.0
19	A	26.5	26.8	26.9	27.0	27.3	27.4	27.5	27.7	28.0	28.3
	B										
	C	26.6	26.7	26.9	27.0	27.2	27.3	27.5	27.6	27.9	28.2
18	A	28.4	28.6	28.8	28.9	29.2	29.3	29.5	29.6	29.9	30.1
	B	34.3	34.5	34.6	34.7	35.0	35.0	35.2	35.3	35.7	36.0
	C	27.8	27.9	28.0	28.2	28.5	28.5	28.7	28.9	29.0	29.3
B-near wall		26.5	26.5	26.7	26.9	27.1	27.2	27.3	27.4	27.7	28.0
B-inside		26.5	26.5	26.7	26.9	27.1	27.2	27.3	27.5	27.8	28.0
Cable surface		42.5	42.7	42.7	42.9	43.0	43.3	43.0	43.6	44.0	44.4
Cable insulation		44.5	44.7	44.7	44.9	44.8	45.3	45.0	45.6	46.0	46.3
		25.7	25.5	25.7	26.5	26.2	26.6	26.0	26.8	27.0	27.4

Prop number	Depth level	Temp am 8:10	293A 23.4A Temp am 10:30	296 A 23.7A Temp pm 12:30	293.6 A 23.5 A Temp pm 2:30	295.3A 23.7A Temp pm 7:30	291.5A 23.2A Temp am 8:30	301.8A 24.2A Temp am 10:30	301.8A 24.2A Temp pm 12:30	301.9A 24.2A pm 2:30	301.7A 24.1A pm 8:00
9	A	24.2	24.3	24.2	24.2	24.0	24.0	23.9	23.9	23.9	23.9
	B	24.6	24.7	24.7	24.6	24.4	24.3	24.3	24.3	24.3	24.3
	C	24.8	24.6	24.8	24.6	24.5	24.3	24.4	24.3	24.4	24.4
10	A	24.1	24.0	24.0	23.8	23.9	24.3	24.2	24.1	24.3	24.5
	B	24.4	24.5	24.4	24.2	24.8	25.8	26.0	26.2	26.3	26.6
	C	24.5	24.4	24.5	24.1	24.3	24.5	24.5	24.5	24.5	24.7
11	A	23.7	23.7	23.8	23.4	23.3	24.3	24.4	24.4	24.5	24.8
	B	23.8	24.6	25.4	26.0	27.3	29.2	29.2	29.4	29.5	30.0
	C	24.0	23.9	24.0	23.6	23.8	24.2	24.3	24.4	24.3	24.6
12	A	23.5	23.5	23.5	23.5	23.3	23.5	23.5	23.2	23.4	23.8
	B	23.5	23.5	23.6	23.5	23.3	23.7	22.9	23.8	24.0	24.2
	C	23.5	23.6	23.6	22.3	23.5	23.6	23.5	23.6	23.5	23.6
13	A	23.2	23.3	23.3	23.2	23.0	23.1	23.1	23.1	23.1	23.0
	B	23.3	23.3	23.3	23.4	23.2	23.3	23.3	23.3	23.3	23.3
	C	23.3	23.3	23.3	23.1	22.8	23.3	23.3	23.2	23.2	23.2
20	A	23.2	23.2	23.3	23.2	23.2	23.2	23.2	23.1	23.1	23.2
	B	23.2	23.3	23.3	23.3	23.1	23.3	23.2	23.3	23.3	23.3
	C	23.3	23.3	23.3	23.3	23.1	23.3	23.3	23.3	23.3	23.4
27	A	23.3	23.2	23.4	23.4	23.1	23.2	23.2	23.2	23.2	23.3
	B	23.2	23.3	23.3	23.2	23.2	23.3	23.3	23.3	23.3	23.5
	C	23.3	23.2	23.3	23.4	23.1	23.2	23.2	23.2	23.1	23.3
26	A	23.5	23.5	23.6	23.6	23.4	23.6	23.6	23.6	23.6	23.9
	B	23.6	23.6	23.5	23.6	23.5	24.1	24.1	24.1	24.2	24.6
	C	23.6	23.6	23.5	23.6	23.5	23.6	23.6	23.6	23.6	24.0
25	A	23.8	23.7	23.8	23.9	23.9	24.5	24.6	24.5	24.5	25.1
	B	23.9	25.1	26.3	27.2	28.3	30.0	30.1	30.5	30.7	31.2
	C	23.9	23.9	24.0	24.1	23.9	24.3	24.3	24.3	24.2	24.7
24	A	24.1	24.2	24.2	24.2	24.0	24.2	24.3	24.3	24.3	24.6
	B	24.5	24.5	24.5	24.6	25.0	25.8	25.9	26.0	26.1	26.5
	C	24.5	24.5	24.6	24.5	24.4	24.5	24.5	24.5	24.5	24.8
23	A	24.2	24.2	24.3	24.3	24.1	24.0	24.0	23.9	23.9	24.0
	B	24.8	24.7	24.8	24.8	24.6	24.6	24.6	24.5	24.5	24.6
	C	24.8	24.6	24.8	24.8	24.6	24.5	24.5	24.4	24.4	24.5
16	A	24.3	24.3	24.3	24.4	24.2	24.0	24.0	23.9	23.9	24.1
	B	24.8	24.9	24.9	24.8	24.7	24.6	24.6	24.5	24.5	24.8
	C	24.9	24.9	24.9	24.9	24.7	24.6	24.6	24.5	24.5	24.6

Experiment #4 Filled contai...

17	A	24.0	24.2	24.2	24.3	24.1	24.5	24.5	24.5	24.5	24.9
	B	24.6	24.7	24.7	25.0	25.1	26.3	26.3	26.3	26.5	27.0
	C	24.6	24.6	24.6	24.6	24.5	24.6	24.7	24.6	24.6	25.0
19	A	23.6	23.6	23.7	23.8	23.5	23.6	23.6	23.7	23.6	24.0
	B										
	C	23.8	23.9	23.8	23.9	23.6	23.6	23.8	23.8	23.8	24.0
18	A	24.0	24.0	24.0	24.0	24.0	24.5	24.6	24.8	24.7	25.2
	B	24.0	24.8	25.6	26.3	27.5	29.1	29.2	29.3	29.5	30.2
	C	24.1	24.1	24.2	24.3	24.1	24.4	24.4	24.5	24.5	24.9
B-near wall		23.6	23.6	23.6	23.6	23.5	23.5	23.6	23.6	23.6	23.9
B-inside		23.5	23.6	23.6	23.6	23.5	23.6	23.6	23.6	23.6	23.9
Cable surface		24.2	31.0	32.7	33.7	35.1	36.8	37.3	37.8	38.0	38.3
Cable insulation		24.2	32.9	34.6	35.8	37.0	38.6	39.3	39.8	40.0	40.4
		22.2	22.2	22.5	22.0	22.6	21.8	23.6	23.6	24.5	22.3

Experiment #4 Filled container /loaded cable

Experiment #3

Filled container /unloaded cable/Thermal gradient driven by heat source and heat sink

Figure:

Notes

9cm from the soil surface
up to the end refrence (111cm)
∴ from button to soil surface = 111-9 = 102cm

Experiment #3 Filled container /unloaded cable/Thermal gradient driven by heat source and heat sink

Prop number	Depth level	Temp	Temp	Temp	Temp	Temp	Temp	Temp	Temp	
9	A	23.5	24.1	24.3	24.6	25.0	24.4	24.3	24.3	24.5
	B	27.6	26.4	26.6	26.8	27.0	26.5	26.5	26.5	26.4
	C	27.6	26.6	26.9	27.1	27.3	27.0	26.9	27.0	27.0
10	A	23.6	24.1	24.3	24.5	24.5	24.3	24.4	24.3	24.0
	B	28.0	26.5	27.0	27.2	27.1	27.0	26.9	26.9	26.8
	C	27.4	26.7	26.9	27.0	27.0	26.6	26.8	26.9	26.8
11	A	23.8	24.3	24.4	24.6	24.7	24.5	24.4	24.2	24.3
	B	27.9	26.5	26.8	27.0	27.2	26.8	26.6	26.7	26.8
	C	27.3	26.6	26.8	27.0	27.0	26.8	26.8	26.3	26.8
12	A	23.8	24.2	24.2	24.6	24.7	24.5	24.5	24.5	24.5
	B	28.5	27.1	27.2	27.3	27.2	27.2	27.2	26.9	26.9
	C	27.1	26.6	26.6	26.9	26.9	26.8	26.8	26.6	26.5
13	A	23.7	24.2	24.4	24.5	24.5	24.5	24.4	24.3	24.3
	B	28.5	26.8	27.0	27.2	27.2	26.8	27.0	26.7	26.7
	C	26.8	26.7	26.5	26.7	26.6	26.5	26.5	26.4	26.4
20	A	23.5	24.2	24.5	24.5	24.6	24.5	24.5	24.3	24.3
	B	28.3	26.9	27.0	27.1	27.1	26.7	26.9	26.8	26.7
	C	26.2	26.1	26.3	26.3	26.3	26.1	26.2	26.1	25.6
27	A	24.1	24.5	24.6	24.7	24.8	24.6	24.6	24.5	24.5
	B	28.1	26.6	26.8	26.8	26.9	26.7	26.6	26.5	26.3
	C	25.9	25.8	26.0	25.9	26.1	26.0	25.9	25.8	25.7
26	A	24.2	24.5	24.6	24.7	24.8	24.8	24.7	24.6	24.5
	B	27.8	26.7	26.8	26.8	26.9	26.7	26.6	26.5	266
	C	25.6	25.8	26.0	26.0	26.1	25.9	25.9	25.9	25.9
25	A	23.9	24.3	24.5	24.4	24.5	24.5	24.5	24.4	24.5
	B	27.2	26.2	26.5	26.4	26.5	26.4	26.5	26.2	26.3
	C	25.5	25.9	26.0	26.0	26.0	26.0	26.0	25.8	25.9
24	A	23.5	24.2	24.4	24.3	24.4	24.4	24.5	24.3	24.3
	B	27.6	26.6	26.8	26.8	26.8	26.6	26.6	26.5	26.5
	C	25.8	25.7	26.0	26.2	26.3	26.1	26.2	25.9	26.0
23	A	23.1	24.0	24.2	24.2	24.4	24.1	24.4	24.0	24.2
	B	27.9	26.7	26.8	26.9	27.0	26.7	26.9	26.6	26.6
	C	26.5	26.2	26.4	26.4	26.5	26.3	26.5	26.1	26.2
16	A	23.3	24.3	24.4	24.5	24.3	24.4	24.8	24.1	24.4
	B	27.9	26.9	27.2	27.2	26.9	26.8	26.9	26.7	26.7
	C	27.1	26.8	26.9	27.0	27.0	26.9	26.9	26.8	26.6

Experiment #3 Filled container /unloaded cable/Thermal gradient driven by heat source

17	A	23.7	24.2	24.6	24.6	24.6	24.7	24.6	24.6	24.5
	B	28.0	26.8	27.1	27.3	27.2	27.3	27.2	26.9	26.9
	C	26.6	26.6	26.9	27.0	26.8	27.0	26.6	26.8	26.6
19	A	23.9	24.4	24.7	24.7	24.8	24.8	24.7	24.7	24.6
	B	X								
	C	26.3	26.5	26.8	26.5	26.6	26.4	26.6	26.4	26.3
18	A	24.0	24.5	24.8	24.8	24.9	24.8	24.9	24.8	24.7
	B	27.9	27.0	27.1	27.0	27.1	27.0	27.0	26.9	26.8
	C	26.3	26.5	26.6	26.6	26.7	26.5	26.6	26.5	26.4
B-near wall		25.2	25.2	25.6	25.3	25.5	25.5	25.4	25.3	25.3
		X								
		X								
B-inside		25.3	25.3	25.6	25.3	25.5	25.5	25.4	25.3	25.3
Cable surface		27.3	26.6	26.6	26.6	26.6	26.6	26.5	26.4	26.3
Cable insulation		27.3	26.6	26.6	26.6	26.6	26.5	26.5	26.3	26.3

Experiment #3 Filled container /unloaded cable/Thermal gradient driven by heat source

Laboratory Setup Photos

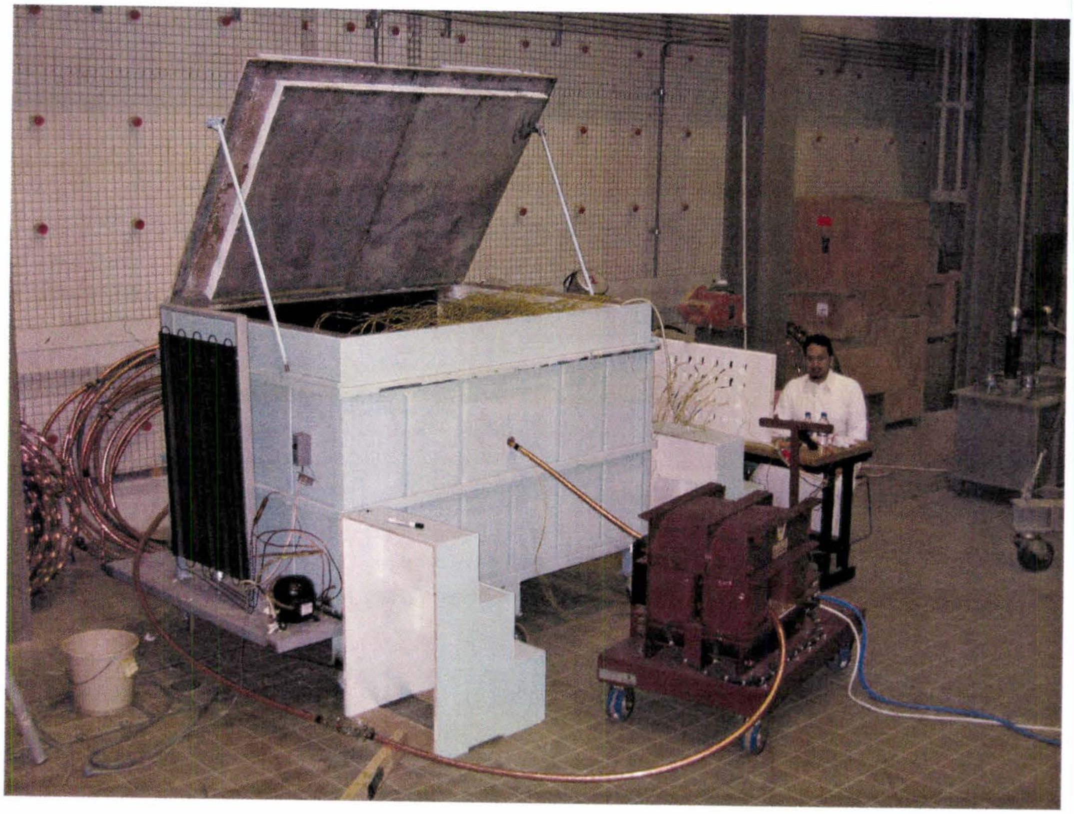

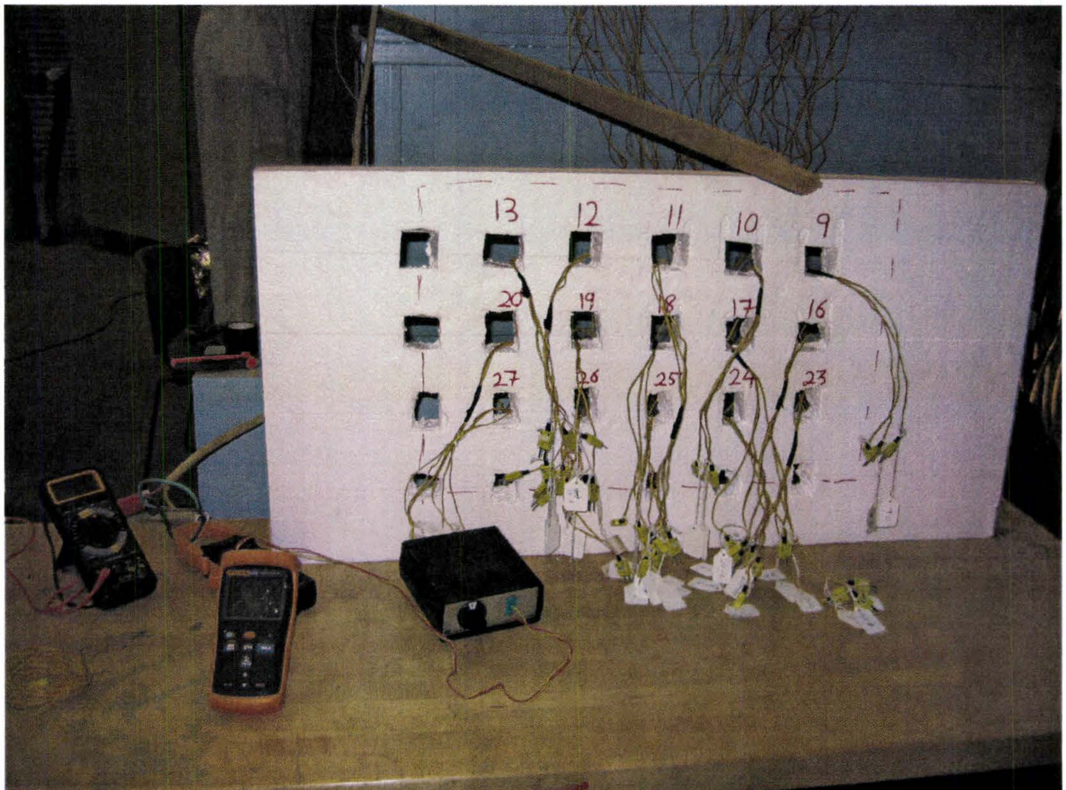
13
12
11
10
9
20
19
18
17
16
27
26
25
24
23


1
2

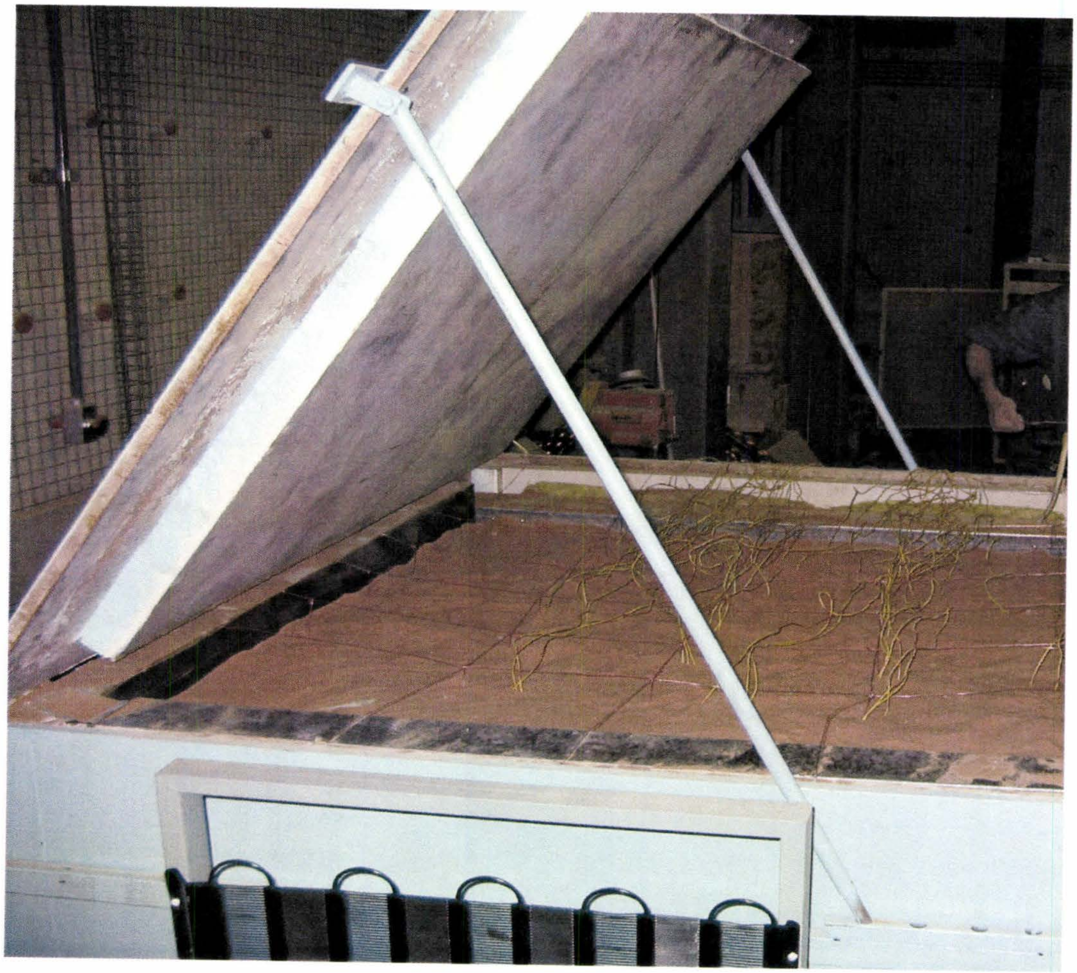

APPENDIX C

Saudi Electricity Company Data Sheet /Riyadh cable 132 kV

FROM : PHONE NO. : Aug. 15 2000 02:22AM P1

Spec -5/16 717-4-S-0312

TECHNICAL DATA FOR
132kV 1000mm² XLPE CABLE

Item No.	Description	Unit	SCECO Requirement	Technical Data
1	Current carrying capacity under following installation and operating conditions;			
	- Max temperature on insulation	°C	90	90
	- Ground temperature	°C	35	35
	- Ground resistivity	°C cm/W	200	200
	- Depth to top of cable	cm	150	150
	- Cable spacing (axis to axis)	cm	Max.40	40
	- Load factor		100%	100%
	- Backfill resistivity	°C.cm/W	200	200
2	Maximum d.c resistance of conductor per 1000m of completed cable			
	- at 20°C 1000mm²	Ω	0 0177	0.0177
	- at 90°C 1000mm²	Ω	0.0227	0.0227
3	Minimum a.c resistance of contuctor per 1000m of completed cable at 90°C	Ω		0.0235
4	Inductance when laid in close trefoil formation	mH/km		0.39
	Inductance when laid in flat formation spacing as per no.1	mH/km		0.70
5.	Equivalent star reactance per m of three phase circuit at 60Hz	μΩ		147
6	Nominal electrostatic capacitance to neutral per 1000m of completed cable at 90oC	F		2.4×10^{-7}
7.	Maximum charging current per 1 conductor per 1000m of completed cable at nominal voltage	A		6.9
8	Maximum dielectric loss of cable per m of 3-phase circuit when laid direct in the ground at nominal voltage, nominal frequency at 90°C	W		1 6
9	Sheath loss of completed cable per m of 3-phase circuit at nominal voltage, nominal frequency at current rating given in Item 1 above	W		3 7

PHONE NO. : Aug. 15 2000 02:23AM P2

Spec -5/16

717-4-S-0312

2

Item No	Description	Unit	SCECO Requirement	Technical Data
10.	Total losses when cable loaded as in item.1 above	kW/km		53.8
11	Maximum value of tagent of dielectric loss angle of cable at nominal frequency of 60Hz - at 20°C at nominal voltage - at 90°C at nominal voltage - at 20°C at 200% of nominal voltage			 0 1% 0.1% 0.1%
12.	Maximum change in tangent of dielectric loss angle between nominal voltage and 200% Nominal voltage at 20°C			0.05%
13.	Relative dielectric constant at 20°C			2.5
14	Average electric stress	kV/km		4.3
15.	Conductor short circuit current carrying capacity for 1 second when cable loaded as in Item 1 before short circuit, and final conductor temperature of 250°C	kA	Min.40	144
16	Minimum insulation resistance at 20°C	MΩ/km		2650
17	Minimum insulation resistance at 90°C	MΩ/km		1.06
18.	Volume resistivity at 20°C	Ω.cm		2.5×10^{15}
19.	Volume resistivity at 90°C	Ω.cm		1.0×10^{12}
20.	A.C withstand test on finished cable length	kV/min.		190/30
21.	Measured discharge level on finished cable length	pC		less than 5
22.	A.C breakdown voltage on test sample	kV/min.		400kV/1sec
23	Impulse breakdown voltage on test sample	kV/no.		980kV/1st
24.	Metallic screen short circuit current carrying capacity for 1 sec cable loaded as in Item. 1 before short circuit, and final sheath temperature of 250°C	kA	Min 40	41.6
25.	Cable embossing - Manufacturer's name - Year of manufacture - "Electric Cable 132,000V" - Maximum size of characters	 mm	 13	 Yes Yes Yes 13

PHONE NO. : Aug. 15 2000 02:24AM P1

Spec -5/16 717-4-S 0313

3

CONSTRUCTION DATA FOR 132kV 1000mm² XLPE CABLE

Item No	Description	Unit	SCECO Requirement	Technical Data
1.	Nominal voltage, phase to phase	kV	132	132
2.	Conductor			
	- Matenal		Copper	Copper
	- Cross section area	mm^2	1000	1000
	- Form and shape			Compacted Segment
	- Outside diameter	mm		Nom. 38.5
3.	Minimum thickness of conductor screen	mm		1.2
4.	Minimum thickness of XLPE insulation	mm	17.0	17.0
5.	Minimum thickness of insulation screen	mm		1.2
6.1	Swellable conductive tape			
	- Material			Swellable Polyester Tape
	- Thickness	mm		0 5
6 2	Metallic screen			
	- No. of wires			65
	- Dia. of wire			2.3
	- Material			Copper
	- Cross section	mm^2		270
6.3	Swellable conductive tape			
	- Material			Swellable Polyester Tape
	- Thickness	mm		0.5
6.4	Aluminium foil barrier [*1]			
	- Thickness	mm		0.2
	- Cross section	mm^2		Approx.60
	- DC resistance at 20°C	Ω/km		0.473
7.	Nominal thickness of oversheath	mm		4.5
8.	Overall diameter of cable	mm	17.0	Approx.105
9.	Nett weight of cable	kg/m		Approx.18.0
10.	Nominal drum length	m		500[*2]
11.	Minimum radius of bend			
	- Laid direct or in air	m		2 0
	- Laid in ducts	m		2.0

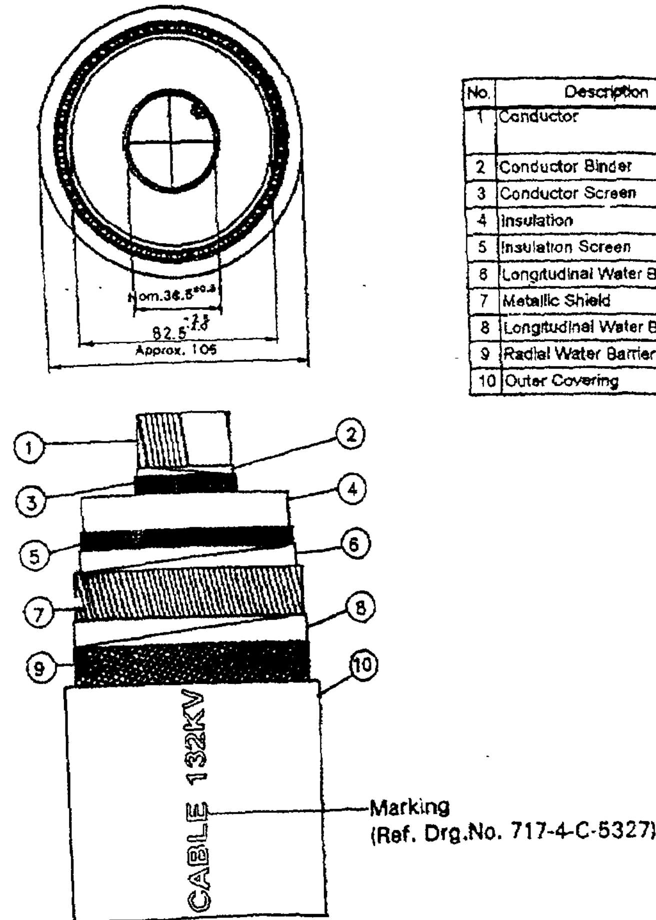

No.	Description	Material	Thickness(mm)
1	Conductor	Annealed Copper Wires (4 Segmental Compacted Round)	Nom 38 5
2	Conductor Binder	Semi-Conductive Tape	0.5
3	Conductor Screen	Semi-Conductive XLPE	Nom 1.5
4	Insulation	XLPE	Nom.19 0
5	Insulation Screen	Semi-Conductive XLPE	Nom.1.5
6	Longitudinal Water Barrier	Swellable Polyester Tape	0.5
7	Metallic Shield	Copper Wires(2.3f x 65)	Nom.2 3
8	Longitudinal Water Barrier	Swellable Polyester Tape	0.5
9	Radial Water Barrier	Bothside PE coated AL.Foil	0 35
10	Outer Covering	HDPE(Black) with Graphite Coating	Nom.4 5

4

FROM : PHONE NO. : Aug. 15 2000 02:27AM P1

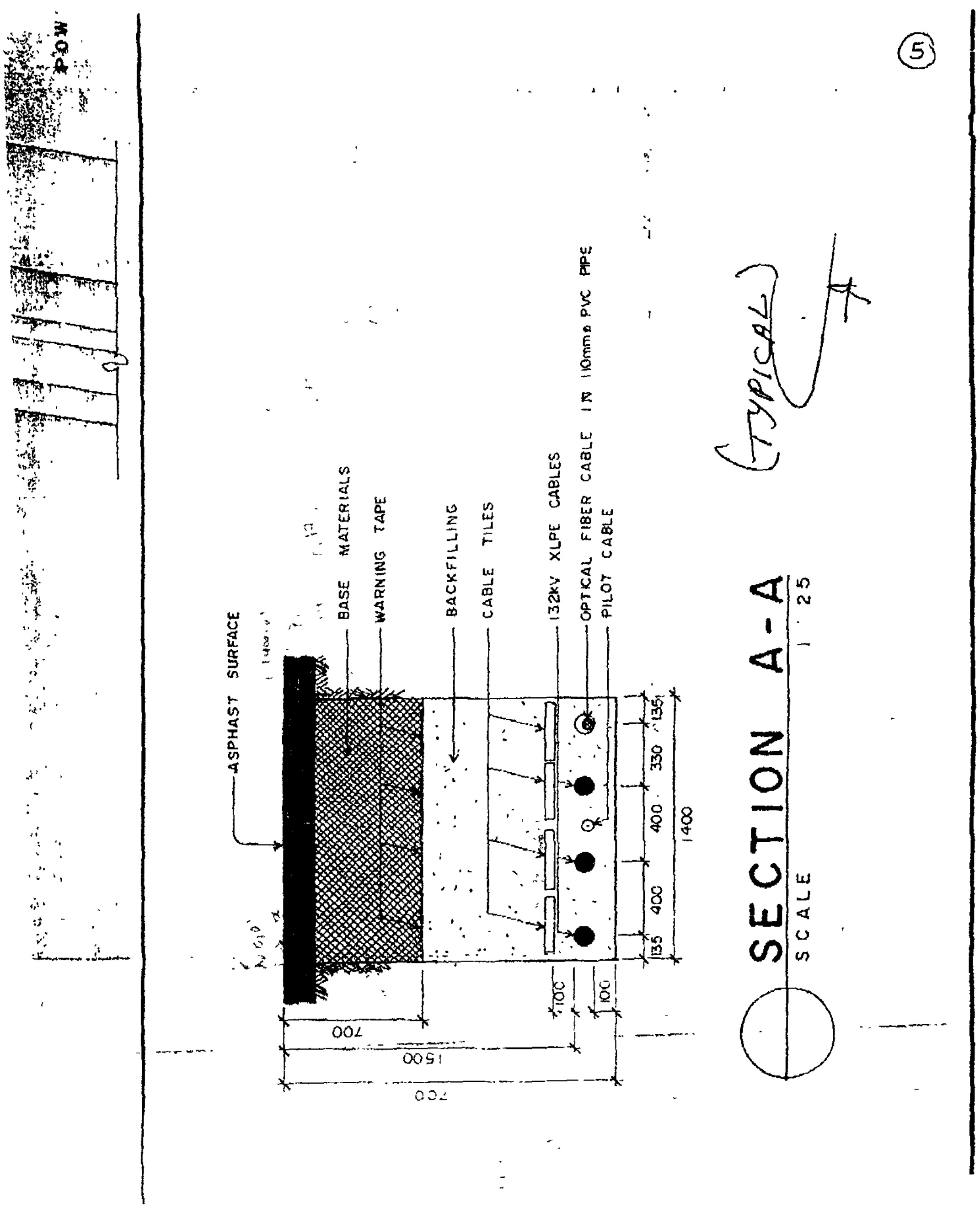

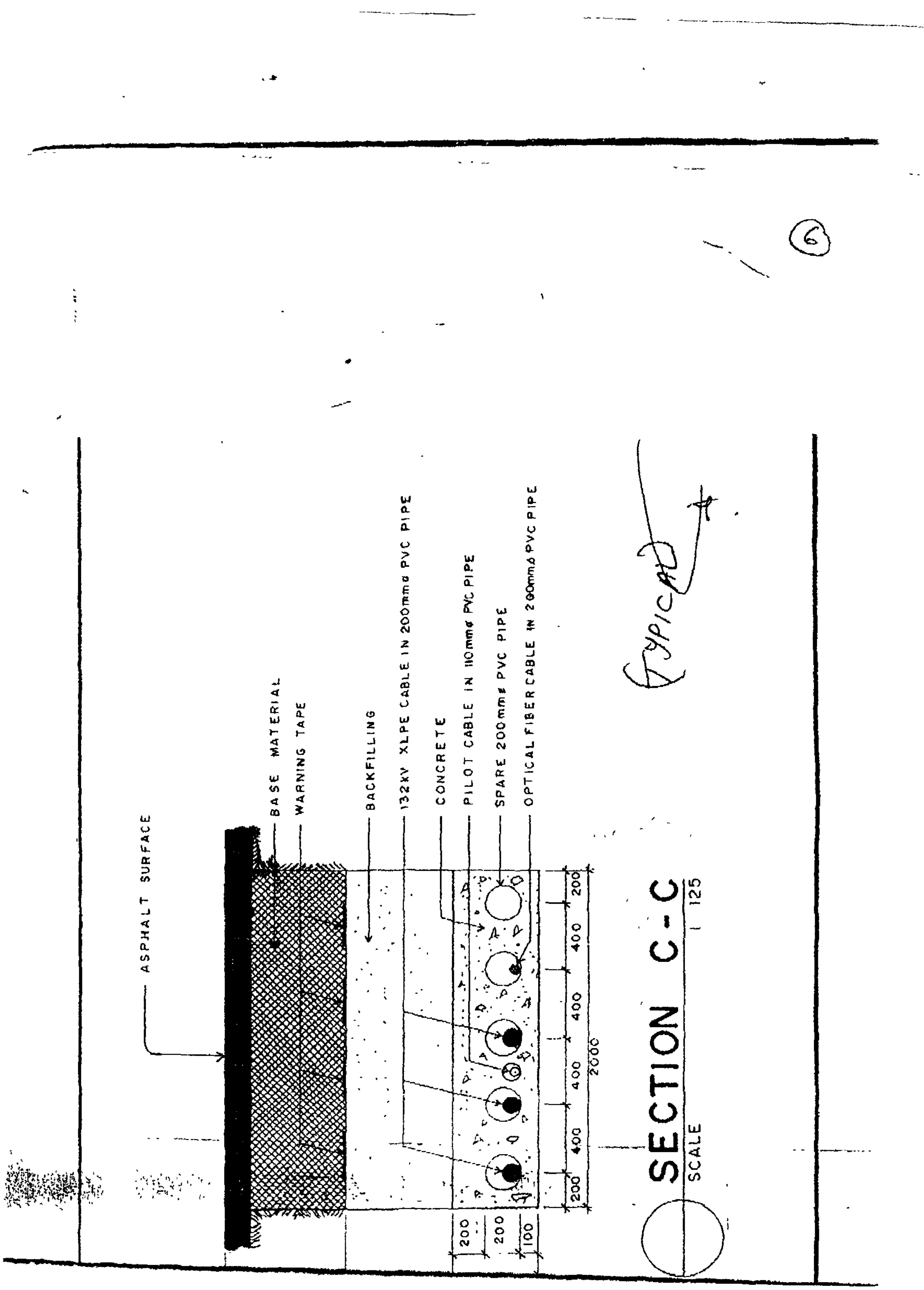
ASPHALT SURFACE
BASE MATERIAL
WARNING TAPE
BACKFILLING
132kV XLPE CABLE IN 200mmø PVC PIPE
CONCRETE
PILOT CABLE IN 110mmø PVC PIPE
SPARE 200mmø PVC PIPE
OPTICAL FIBER CABLE IN 200mmø PVC PIPE
200 400 400 400 400 200
2000
200
200
100
SECTION C-C
SCALE 1:25
TYPICAL
6

Saudi Electricity Company Data Sheet /Jeddah cable 380 kV

Page 5/6

No A-7723D

TABLE
FOR
CONSTRUCTION DATA FOR 380 kV OIL-FILLED POWER CABLE

Rated Voltage between phases		kV	380
Number of core			1
Sectional area of conductor		sq mm	1600
Conductor details	Material		Plain annealed copper
	Shape		6-segmental with hollow
	Diameter of conductor	(nom.)mm	53 3
Conductor binder	Material		Stainless steel tape and carbon black paper
	Thickness	(nom.)mm	Stainless steel tape : 0.10x1 Carbon black paper . 0 15x1
Conductor screen	Thickness	(nom)mm	Carbon black paper 0 15x1 0 1x1
Insulation	Thickness	(min.)mm	20
	Number of papers	(approx.)	144
Insulation screen	Thickness	(nom)mm	Carbon black paper 0.1 Metallized paper 0.1 Carbon black paper : 0.15 Copper-woven fabric tape · 0 5
Metal Sheath	Material		Lead-alloy sheath
	Thickness	(min.)mm	3 7
	Diameter over sheath	(nom)mm	106
Reinforce-ment	Material		Stainless steel tape
	Bedding material		Non-woven fabric tape
	Thickness	(nom)mm	Stainless steel tape 0 15x2
Anti-corrosion jacket	Material		PVC
	Thickness	(min.)mm	3 1
Diameter of completed cable		(nom)mm	119
Weight of completed cable		(approx)kg/m	41
D C. resistance of conductor at 20°C		(max)Ω/km	0 01'2
Capacitance at 20°C		(max)μF/km	0 3564

Per core

SECTION A – A

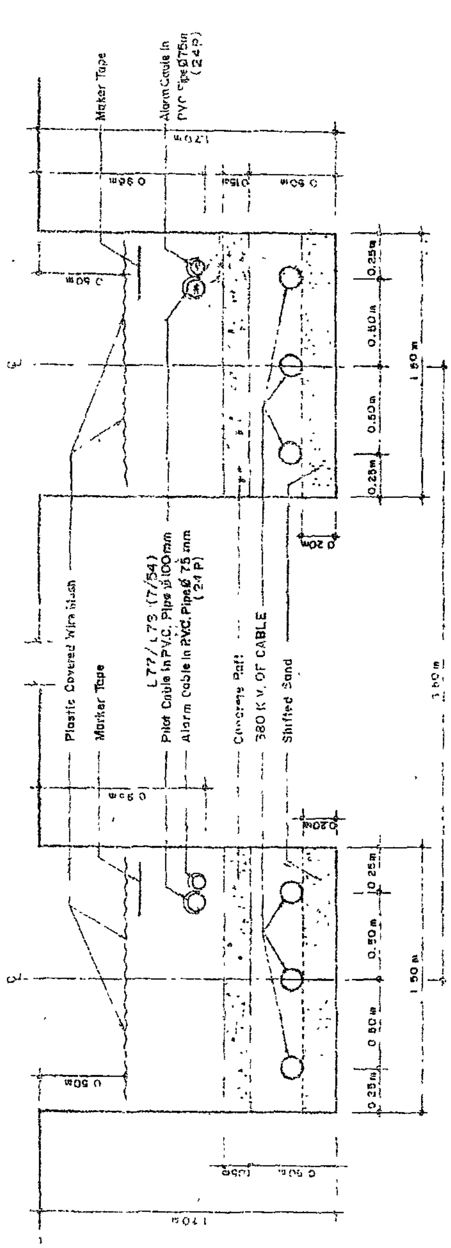
Plastic Covered Wire Mesh
Marker Tape
L77/L73 (7/54)
Pilot Cable in PVC Pipe Ø100mm
Alarm Cable in PVC Pipe Ø 75 mm (24 P)
380 K.V. OF CABLE
Shifted Sand
0.25m
0.50m
1.50m
0.20m

FUJIKURA

380kV 1×1600mm², COPPER-CONDUCTOR, PAPER-INSULATED,
LEAD-ALLOY SHEATHED AND PVC JACKETED OIL-FILLED CABLE